Artificial Small RNAs in Plants: Characterization of Systemic Activity, and Engineering Minimal Precursors for Transgene-Free, Virus-Based Expression

Adriana E. González Cisneros

Advisor: Dr. Alberto Tomás Carbonell Olivares

València, October 2024

UNIVERSITAT POLITÈCNICA DE VALÈNCIA

UNIVERSITAT POLITÈCNICA DE VALÈNCIA

Biotechnology program

Artificial Small RNAs in Plants: Characterization of Systemic Activity, and Engineering Minimal Precursors for Transgene-Free, Virus-Based Expression

Adriana E. González Cisneros

Advisor:

Dr. Alberto Tomás Carbonell Olivares

València, October 2024

Acknowledgements | Agradecimientos

Como no podía ser de otra forma, esta sección la encabeza mi madre. Frases como "sin ti no habría llegado hasta aquí" o "gracias por apoyarme siempre" son un cliché, pero no por ello son menos ciertas. Gracias, mamá, por estar siempre a mi lado y por seguir haciéndolo, por darme un empujón cuando me atasco y por decirme las cosas que no quiero escuchar. He aprendido de ti a poner amor en todo lo que hago, a seguir adelante cuando las cosas se complican y a ser honesta conmigo misma y con las demás. Te aseguro que, sin todos estos aprendizajes, y muchos más, no habría podido continuar. Te dedico cada palabra que he escrito, junto con todo el esfuerzo que he puesto en intentar cumplir con las exigencias propias y externas. Pero, sobre todo, te dedico cada momento en el que, durante estos cuatro años, he aprendido, me he reído, he compartido alegrías y desilusiones, me he atrevido y he encontrado mi camino, aunque me haya caído y haya tenido que volverlo a intentar. En definitiva, te dedico todo lo que he vivido en este tiempo y lo que está por venir. Te quiero ma.

Querría también dedicarle este trabajo a mi abu. A pesar de que no soy médica ni maestra, como me temo que preferirías, creo que ser doctora en biotecnología no está nada mal para fardar de nieta. Gracias por seguir acompañándome, por hacerlo siempre a tu manera y por hacer que no me olvide de dónde vengo ni de quién soy. Gracias también a mi padre por su interés, que le llevó a coger un avión de doce horas nada menos.

Quiero agradecer los momentos, las quedadas, la risa y la desconexión que consigo con Irene y Javi. Gracias por ayudarme (a veces a la fuerza) a reírme de mi misma y a relativizar lo que a mí se me hace un mundo. Como cuarto elemento de este grupito que tanta alegría me da, está Rosa. Amiga, gracias por seguir siendo una de las personas más cercanas a mí, estemos donde estemos. Gracias por no darte nunca por vencida conmigo y por acompañarme siempre. Has sufrido mi “yo de tesis”, que no es poco, y cada día haces méritos para seguir formando parte de esto y de mí. Gracias. No me quiero olvidar de mis amigas de León, tanto las de la uni como las de toda la vida. A pesar de que para algunas soy ya “la valenciana”, os puedo asegurar que allí donde voy saben de dónde soy y qué catedral es la más bonita de España. A mis amigas del rugby, Mer, Clau, Soni y Jani, gracias a las cuatro por haberme acompañado este tiempo y por darme tan buenos momentos dentro y fuera del campo. Después de todo, creo que hemos mejorado en aquello de recibir golpes con estilo (en sentido figurado y literal). Especialmente a Mer, quiero agradecerte tu generosidad y tu cariño, que creas tanto en mí y sigas recordándome de lo que soy capaz cuando a mí se me olvida. Gracias por sostenerme y dejar que yo también lo haga.

No me quiero olvidar de hacer una pequeña, pero importante mención, a mi psicóloga Carol. Gracias por ayudarme a mantener lo más parecido posible a una estabilidad emocional y por darme las herramientas para enfrentarme a la movida que es vivir y hacer una tesis. Igualmente quiero acordarme de mis compis del grupo, en particular de Carla, por muchísimos años más contándonos las penas y haciéndonos reír.

A nivel de lab, tengo que decir que yo soy 0.09, y como tal me siento agradecida de haber tenido a Sonia y Maite como compis de lab. A Sonia por ser tan cercana, amable, risueña y guasona, y al mismo tiempo tan inteligente. Creo que he aprendido mucho de ti y me has ayudado a sentirme más segura de mí misma como científica. Gracias por cuidar de mí estos años. A Maite tengo que agradecerle sus particularidades que no dejan a nadie indiferente. Admiro esa combinación de inteligencia y excentricidad que reside en ti, haciendo que la misma persona cierre el lab todos los días y de pronto se suba a una silla a bailar. Sin duda referente del IBMCP. También quiero agradecerte la presión que has hecho para tomarnos las cervecitas del lab, todos sabemos que sin ti no hubieran existido. A Pavel por tu ironía certera y por tu honestidad, me ha gustado mucho compartir lab contigo.

Durante estos años ha habido mucha gente que ha pasado por el lab, sin los cuales acabar todo el trabajo que contiene esta tesis hubiera sido **completamente impensable**. A todos ellos les quiero agradecer su contribución y compromiso con el proyecto. Especialmente a Tamara, una científica muy brillante a la par que agorera. Eres increíblemente trabajadora y perseverante, con un humor muy particular. Gracias por hacerme sentir tan cómoda el tiempo que pasamos juntas. También le quiero agradecer a Iván esa ironía que tanta gracia me hace y todos los momentos de chismorreo compartidos.

Quiero agradecerle al ministerio que le concediera otra FPI a Alberto, y al destino que quiso que fuera para Juanjo. Como le dije una vez a Sonia, me has salvado el doctorado. Gracias por tu ironía, por bajarme a tierra tantas veces y por ser tan auténtico. Solo puedo decir que ojalá hubieses llegado antes. A Ana por ser una persona tan maja, tan amable y cariñosa y tan resolutiva. Muchas gracias porque tenerte es tener seguridad y cariño a partes iguales. Ariel, gracias por tu apoyo y por la ayuda que me has brindado en tantas ocasiones. Me gusta mucho la actitud que tienes frente a todo, tu positividad y tus recontra- lo que sea. A Sara por su templanza y humor, creo que tienes muchisimo talento, y donde vayas triunfarás. Quiero agradecer también a Markita Landry por permitirme pasar unos meses en su laboratorio y a Sophie por su amabilidad, cercanía y humor, que me hizo sentir más cerca de casa.

Por último, quiero agradecerle a Alberto que depositase en mí su confianza para llevar a cabo todo este trabajo y que me hiciera partícipe de todos los proyectos que han ido surgiendo.


ABSTRACTS

Resumen

Los pequeños ARNs artificiales (art-sRNAs) son moléculas de ARN de simple cadena, de 21 nucleótidos (nt), diseñados computacionalmente para silenciar genes de la planta con alta eficacia y especificidad. Los art-sRNAs se clasifican en dos grupos: micro ARNs artificiales (amiRNAs) y pequeños ARNs interferentes sintéticos que actúan en trans (syn-tasiRNAs). A pesar de que los art-sRNAs se usan frecuentemente para silenciar genes endógenos y exógenos en plantas, todavía hay algunos aspectos desconocidos que limitan sus aplicaciones. Uno de ellos es su capacidad de movimiento, dado que se desconoce si son capaces de moverse y silenciar genes endógenos en tejidos distintos a los de origen. Por tanto, el uso de art-sRNAs para inducir silenciamiento génico a nivel de toda la planta, habitualmente implica la generación de plantas transgénicas que expresen los precursores completos de art-sRNAs, limitando su versatilidad como herramienta biotecnológica para genómica funcional y mejora de cultivos. En esta tesis, hemos investigado en primer lugar la capacidad de silenciamiento sistémico de los art-sRNAs y, posteriormente, hemos diseñado precursores mínimos de art-sRNAs para facilitar su expresión no transgénica a partir de virus y en toda la planta.

En primer lugar, estudiamos la capacidad de silenciamiento local y sistémico de art-sRNAs dirigidos contra la subunidad CHLI de la quelatasa de magnesio, codificada por el gen *SULPHUR* (*NbSu*), mediante ensayos de expresión transitoria en *Nicotiana benthamiana*. Tanto amiRNAs como syn-tasiRNAs indujeron el silenciamiento sistémico de *NbSu*, para lo cual se requieren altos niveles de expresión cerca del peciolo. Esta actividad sistémica está facilitada por el movimiento vascular de art-sRNAs de doble cadena y 21 nt a través de la planta, permitiendo silenciar genes en tejidos distintos a los de origen. Este resultado pone de manifiesto el potencial biotecnológico de expresar localmente art-sRNAs que sean capaces de moverse a tejidos distales de la planta y desencadenar un silenciamiento génico altamente específico.

En segundo lugar, nos centramos en diseñar precursores de tamaño mínimo derivados de las moléculas precursoras endógenas de *Arabidopsis thaliana* (Arabidopsis): *MIR390a* (521 nt) y *TAS1c* (1011 nt). Evaluamos la eficacia de silenciamiento de una colección de construcciones que contenían versiones acortadas de los precursores *AtMIR390a* y *AtTAS1c* mediante expresión transitoria y estable en *N. benthamiana* y Arabidopsis, respectivamente. Observamos que, tanto amiRNAs como syn-tasiRNAs, son altamente eficientes y se procesan de forma precisa cuando se producen a partir de precursores mínimos de solo 89 y 54 nt

respectivamente. Además, comprobamos que cuando se expresan a partir de un vector viral de ARN, como el virus X de la patata, solo se producen art-sRNAs auténticos a partir de precursores mínimos, y no de los de longitud completa, lo que da lugar al silenciamiento eficiente de genes endógenos en *N. benthamiana*. Asimismo, pudimos inducir silenciamiento génico mediante art-sRNAs expresados a partir de un virus, de forma no transgénica y escalable, mediante la pulverización sobre plantas de extractos infecciosos que contenían los vectores modificados. Estos resultados muestran que la longitud de los precursores de art-sRNAs puede ser acortada de forma significativa sin comprometer la eficacia del silenciamiento inducido, y que los precursores mínimos ofrecen una ventaja biotecnológica sobre los precursores de longitud completa cuando se expresan a partir de vectores virales.

Resum

Els xicotets ARNs artificials (art-sRNAs) són molècules d'ARN de simple cadena de 21 nucleòtids (nt), dissenyats computacionalment per a silenciar gens de plantes amb alta eficàcia i especificitat. Els art-sRNAs es classifiquen en dos tipus: microARNs artificials (amiRNAs) i xicotets ARNs interferents sintètics que actuen en trans (syn-tasiRNAs). Encara que els art-sRNAs són àmpliament utilitzats per a silenciar tant gens endògens com exògens en plantes, hi ha alguns aspectes desconeguts que limiten les seues aplicacions. Un d'ells és la seua capacitat de moviment, ja que encara no s´ha establit si poden desplaçar-se i silenciar gens endògens en teixits diferents del d'origen. Conseqüentment, aconseguir un silenciament gènic en tota la planta mediat per art-sRNAs normalment requereix la producció de plantes transgèniques que expressen els precursors complets dels art-sRNAs, la qual cosa restringeix el seu ús versàtil com a eina biotecnològica per a la genòmica funcional i la millora de cultius. En aquesta tesi, primer vam investigar la capacitat de silenciament sistèmic dels art-sRNAs, i després vam dissenyar precursors mínims d'art-sRNAs per a facilitar la seua aplicació de manera no transgènica a tota la planta, expressant els art-sRNAs a partir de vectors virals.

Primer, vam estudiar la capacitat de silenciament local i sistèmic dels art-sRNAs, dirigits contra el gen *SULPHUR (NbSu)* ,que codifica per a una subunitat de la quelatasa de magnesi, assajada en *Nicotiana benthamiana* mitjançant l'expressió transitòria. Tant amiRNAs com syn-tasiRNAs van produir silenciament sistèmic de *NbSu*, amb una alta expressió d'art-sRNAs prop del pecíol de la fulla. El moviment vascular dels dúplexs d'art-sRNAs de 21 nt va facilitar aquesta activitat sistèmica a través de la planta, permetent el silenciament d'aquest gen en teixits distals als quals els art-sRNAs han sigut produïts. Aquest resultat destaca el gran potencial biotecnològic dels art-sRNAs expressats localment, capaços de moure's a grans distancies i amb molta especificitat, desencadenant el silenciament gènic a tota la planta.

En segon lloc, ens vam centrar en dissenyar precursors d'amiRNAs i syn-tasiRNAs del mínim tamany possible, derivats dels precursors endògens *MIR390a* (521 nt) i *TAS1c* (1011 nt) d' *Arabidopsis thaliana*, respectivament. Vam avaluar l'eficàcia de silenciament d'una col·lecció de construccions que incloïen les versions acurtades dels precursors *AtMIR390a* i *AtTAS1c*, fent servir expressió transitòria en *N.benthamiana* i expressió estable en *A. thaliana*. Vam trobar que es poden produir amiRNAs i syn-tasiRNAs altament efectius i correctament processats a partir de precursors mínims de només 89 i 54 nt respectivament. A més, vam observar que art-sRNAs autèntics es produeixen a partir dels precursors mínims i no utilitzant els precursors complets quan s'expressen des d'un vector viral basat en ARN, com el virus X de la creïlla, resultant en un silenciament eficient de gens endògens de *N. benthamina*. A més, el

silenciament de gens mediat per art-sRNAs expressats a partir d'un vector viral es va a aconseguir amb èxit sense l'ús de transgènics i d'una manera escalable, utilitzant un esprai amb extractes crus infecciosos que contenen els vectors virals modificats. Aquests resultats manifesten que la longitud dels precursors d'art-sRNAs pot ser reduïda significantment sense comprometre l'eficàcia de silenciament, i que aquests precursors mínims ofereixen un avantatge biotecnològic sobre els precursors complets quan s'expressen a partir de vectors virals.

Abstract

Artificial small RNAs (art-sRNAs) are 21-nucleotide (nt) single-stranded RNA molecules computationally designed to silence genes with high efficacy and specificity. Art-sRNAs are classified into two main types: artificial microRNAs (amiRNAs) and synthetic trans-acting small interfering RNAs (syn-tasiRNAs). Although art-sRNAs are widely used to silence both endogenous and exogenous plant genes, there are still some unknown aspects limiting their applications. One of them is their movement capacity, since it has not been established whether they can move and silence endogenous genes in tissues other than where they are originally expressed. Consequently, achieving whole-plant gene silencing mediated by art-sRNAs, typically requires the generation of transgenic plants expressing full-length art-sRNA precursors, restricting their use as versatile biotechnological tools for functional genomics and crop improvement. In this thesis, we first investigated the systemic silencing capacity of art-sRNAs, and then engineered minimal art-sRNA precursors to facilitate transgene-free, virus-based expression of art-sRNAs at the whole-plant level.

Firstly, we studied the local and systemic silencing capacity of art-sRNAs targeting the magnesium chelatase subunit CHLI-encoding *SULPHUR* (*NbSu*) gene, using transient expression assays in *Nicotiana benthamiana.* Both amiRNAs and syn-tasiRNAs were found to induce systemic silencing of *NbSu*, which required high art-sRNA expression near the leaf petiole. This systemic activity was facilitated by the vascular movement of 21-nt art-sRNA duplexes throughout the plant, allowing the silencing of plant genes in tissues different from where art-sRNAs are produced. This result highlights the biotechnological potential of locally expressed art-sRNAs to move long distances and trigger highly specific gene silencing throughout the plant.

Secondly, we focused on engineering amiRNA and syn-tasiRNA precursors of minimal size and derived from the endogenous *Arabidopsis thaliana* (Arabidopsis) *MIR390a* (521 nt) and *TAS1c* (1011 nt) precursors, respectively. We evaluated the silencing efficacy of a collection of constructs containing shortened versions of the *AtMIR390a* and *AtTAS1c* precursors, through both transient and stable expression in *N. benthamiana* and Arabidopsis, respectively. We found that highly effective and accurately processed amiRNAs and syn-tasiRNAs can be produced from minimal precursors of only 89 and 54 nt, respectively. Moreover, we observed that authentic art-sRNAs are produced from minimal –but not from full-length precursors– when expressed from an RNA-based viral vector, such as potato virus X, resulting in efficient silencing of endogenous genes in *N. benthamiana*. Furthermore, virus-induced gene silencing mediated by art-sRNAs was successfully achieved in a transgene-free and scalable manner by spraying

plants with infectious crude extracts containing the modified viral vectors. These results reveal that the length of art-sRNA precursors can be significantly shortened without compromising silencing efficacy, and that minimal precursors offer a biotechnological advantage over full-length precursors when expressed from viral vectors.

TABLE OF CONTENTS

A mi madre y a mi abuela

INTRODUCTION

1. Gene silencing in plants mediated by small RNAs

Plants, like many other organisms, have a dynamic gene expression network controlling developmental processes and facilitating environmental adaptation. RNA interference (RNAi) is a process that regulates gene expression through the recognition and cleavage of double-stranded RNA (dsRNA) molecules, leading to the generation of small RNAs (sRNAs) that mediate sequence-specific transcript degradation (post-transcriptional gene silencing, PTGS) or repression (transcriptional gene silencing, TGS) (Vaucheret et al., 2001; Vaucheret & Fagard, 2001). RNAi is conserved in eukaryotes and is essential during plant development and reproduction, promoting adaptability in response to biotic and abiotic stresses (Martínez de Alba et al., 2013). Plant sRNAs are 20-24 nucleotide (nt) molecules generated after the processing of a dsRNA precursor by a DICER LIKE (DCL) enzyme into sRNA duplexes. The length of the sRNA duplex depends on the processing DCL: DCL1 and DCL4 generate 21-nt duplexes while DCL2 and DCL3 produce 22-nt and 24-nt duplexes, respectively (Z. Xie et al., 2004). Once generated, one strand of the sRNA duplex, the guide strand, is loaded into an ARGONAUTE (AGO) protein to target high sequence complementary RNAs, either slicing them or repressing their translation, inducing PTGS, or directing DNA methylation resulting in TGS (Baulcombe, 2004).

In plants, sRNAs can be divided into two groups based on their precursor characteristics and biogenesis: microRNAs (miRNAs) and small interfering RNAs (siRNAs) (Axtell, 2013). MiRNAs are generated from a single-stranded RNA (ssRNA) precursor that acquires a dsRNA-like hairpin structure after transcription of a *MIRNA* locus, while siRNAs are produced from dsRNA precursors. When the synthesis of the dsRNA precursor is triggered by an upstream sRNA-guided cleavage, secondary siRNAs are generated. Many of these secondary siRNAs are produced in phase from the sRNA cleavage site, resulting in the generation of phased siRNAs (phasiRNAs). When these phasiRNAs act in *trans* targeting distinct RNAs, they are referred to as trans-acting siRNAs (tasiRNAs) (Figure 1) (Axtell, 2013; Fei et al., 2013).

2. Classes, biogenesis and functions of plant small RNAs

2.1. MicroRNAs

Plant miRNAs predominantly regulate the expression of transcription factors together with various protein families and long noncoding RNAs, among others. In this way, miRNAs act as master regulators of plant growth, development, phenotypic plasticity, as well as responses to

nutrient deficiencies, heat and cold stress and immunity (D'Ario et al., 2017; X. Song et al., 2019).

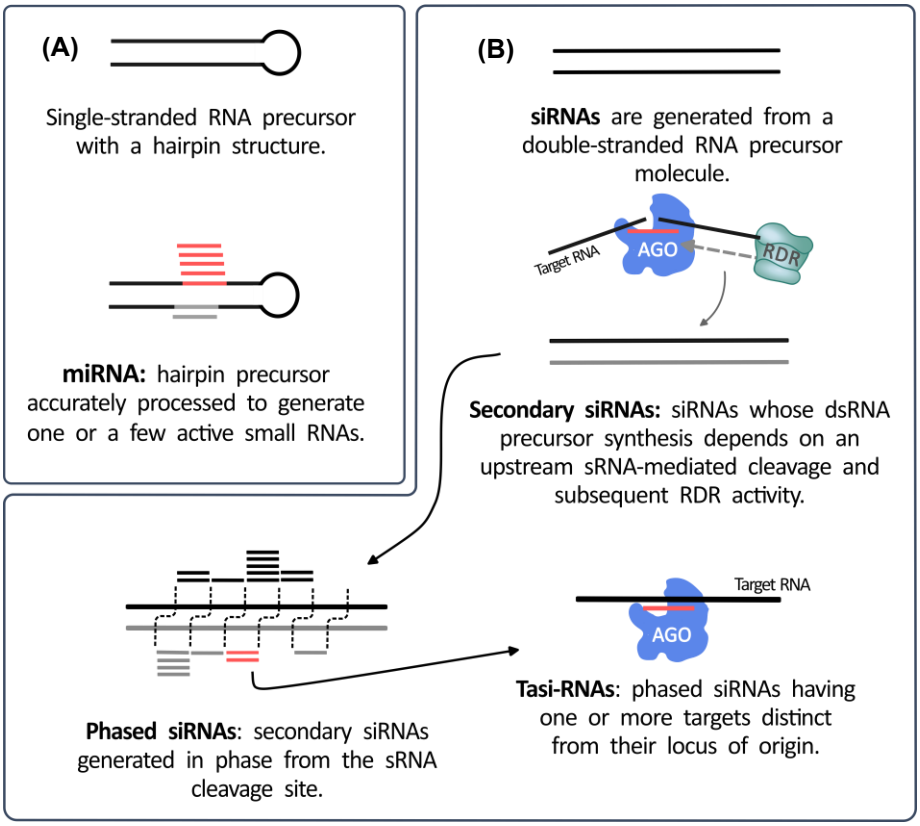

Figure 1. Hierarchical classification of small RNAs (sRNAs) based on their precursor molecules and biogenesis pathways. (**A**) sRNAs derived from a hairpin precursor. MicroRNA (miRNA) guide and star strand are depicted in red and grey respectively. (**B**) Double-stranded RNA (dsRNA) precursor molecule yielding small interfering RNAs (siRNAs). Following cleavage of the primary target RNA by the miRNA-ARGONAUTE (AGO) complex, a dsRNA molecule is synthesized by an RNA-DEPENDENT RNA POLYMERASE (RDR). Phased secondary siRNAs are generated from the dsRNA precursor, which will bind to secondary target RNAs. Black arrows indicate hierarchical relationships. Adapted from Axtell, 2013.

Plant miRNA biogenesis takes place entirely in the cell nucleus and is initiated by the transcription of *MIRNA* genes by the DNA dependent RNA polymerase II (Pol II) (Z. Xie, Allen, Fahlgren, et al., 2005). The primary miRNA (pri-miRNA) transcript, 5' capped and 3' polyadenylated, acquires an imperfect hairpin structure due to sequence self-complementarity and undergoes two sequential processing reactions, in highly specialized dicing bodies (D-bodies) (Fang & Spector, 2007). DCL1, which contains two ribonuclease III domains, cleaves the pri-miRNA to generate a precursor miRNA (pre-miRNA) and later a 21-nt miRNA guide

(miRNA) /miRNA star (miRNA*) duplex (Kurihara & Watanabe, 2004; Park et al., 2005). DCL1 associates with the dsRNA-binding protein HYPONASTIC LEAVES1 (HYL1) and the C2H2 zinc-finger protein SERRATE (SE) to form the microprocessor complex within the D-bodies, playing a central role in miRNA processing (Han et al., 2004; Lobbes et al., 2006). HYL1, along with SE, enhances the processing accuracy of pri-miRNAs by DCL1, while SE also promotes D-body formation (Dong et al., 2008; Kurihara et al., 2006; D. Xie et al., 2021). The resulting miRNA/miRNA* duplex typically has a 2-nt overhang and two hydroxyl groups at the 3' end, which are 2'-O-methylated by HUA ENHANCER 1 (HEN1) to increase duplex stability (B. Yu et al., 2005). The miRNA guide strand is loaded into AGO1 to form the RNA-induced silencing complex (RISC), while the miRNA* strand is usually degraded. The nuclear RISC complex is then exported to the cytoplasm, where it binds to highly complementary target sequences. Gene silencing mediated by miRNAs typically results in the cleavage and degradation of target transcripts, although it can also lead to translational repression or DNA methylation (Figure 2A) (Ding & Zhang, 2023; Zhan & Meyers, 2023).

The structure of plant pri-miRNAs varies significantly among different precursors, most likely due to the complexity of *MIRNA* gene transcription, which in some cases involves alternative splicing or multiple transcription start sites (Mencia et al., 2023; S. Zhang et al., 2015). Importantly, alterations affecting the structural features of miRNA precursors directly impact processing accuracy (Meyers et al., 2010). Generally, the pri-miRNA structure can be divided into distinct regions: an unstructured ssRNA region located upstream and downstream of the hairpin, a basal stem (BS), the miRNA/miRNA* duplex and a distal stem-loop (DSL) (Figure 3A). Depending on DCL1 recognition and initial cleavage, pri-miRNAs can be processed in either a base-to-loop or a loop-to-base format (Figure 3B). In the base-to-loop mechanism, DCL1 makes the first cut between 15 to 17 base pairs (bp) from a bulge or the ssRNA/dsRNA boundary (Bologna et al., 2013; Mateos et al., 2010; L. Song et al., 2010; Werner et al., 2010). The second cut is made 21 nt from the first, releasing the miRNA/miRNA* duplex. This type of processing is followed in most plant *MIRNA* families. However, some pri-miRNAs with a structured DSL region, are processed in a loop-to-base manner, where the first cut is made in the distal part of the precursor below the terminal loop (Bologna et al., 2009, 2013). Interestingly, some pri-miRNAs with multibranched terminal loops, such as pri-miR166, can be processed bidirectionally –either base-to-loop or loop-to-base (Figure 3B) (Zhu et al., 2013).

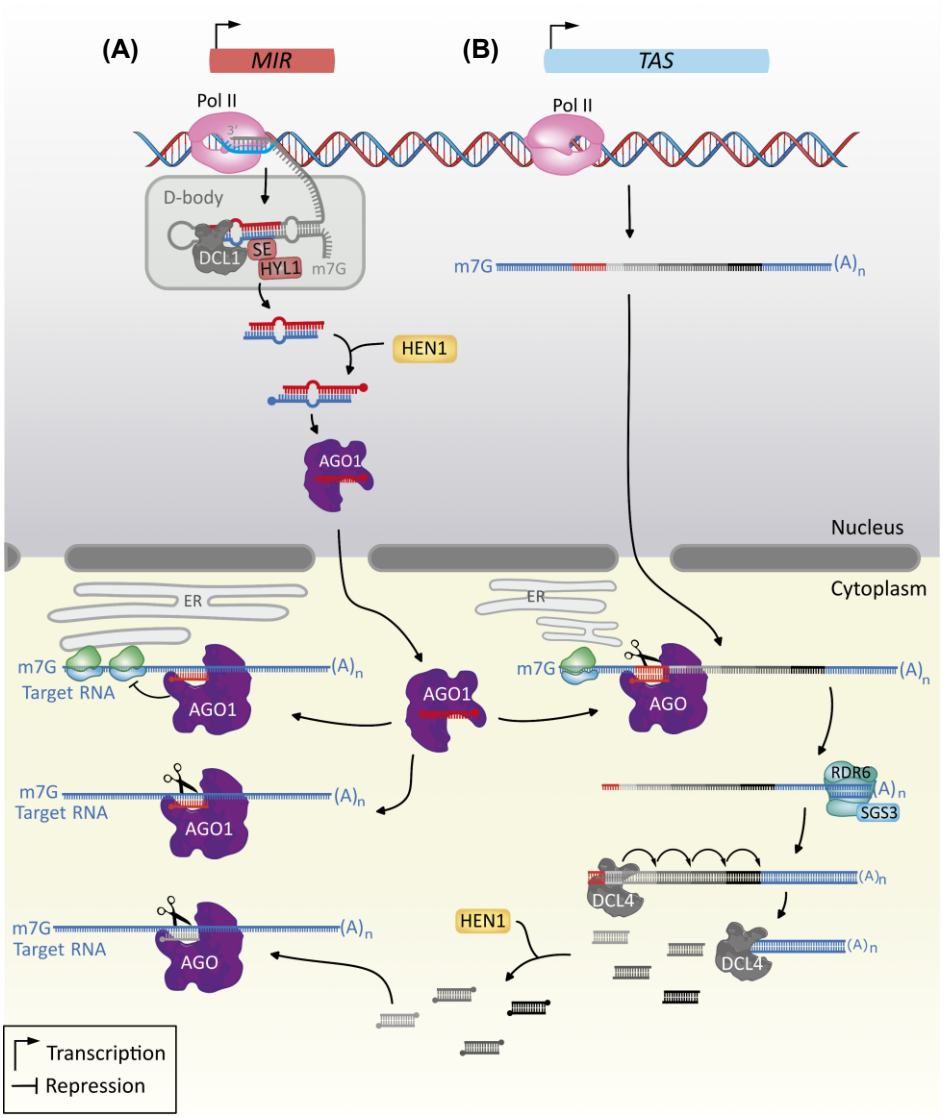

Figure 2. Key steps in the biogenesis pathways of microRNAs (miRNAs) and trans-acting small interfering RNAs (tasiRNAs). (**A**) The miRNA biogenesis pathway begins with the transcription of a *MIR* gene by the RNA POLYMERASE II (Pol II). The primary transcript is subsequently processed by DICER LIKE 1 (DCL1), HYPONASTIC LEAVES 1 (HYL1) and SERRATE (SE) to form a final miRNA duplex that is methylated by HUA ENHANCER 1 (HEN1). One of the strands of the duplex associates with ARGONAUTE 1 (AGO1), leading to cleavage or transcriptional inhibition of target RNAs. (**B**) The tasiRNA pathway begins with the transcription of a *TAS* gene by Pol II. Once in the cytoplasm, the *TAS* transcript is cleaved by a miRNA-AGO complex. The RNA-DEPENDENT RNA POLYMERASE 6 (RDR6) synthesizes a double-stranded RNA (dsRNA) from the cleaved product, with the help of SUPRESSOR OF GENE SILENCING 3 (SGS3). This dsRNA is cleaved every 21 nucleotides by DCL4 to form tasiRNA duplexes. After methylation by HEN1, one strand of the duplex is loaded into an AGO protein to silence target RNAs. ER: endoplasmic reticulum, D-body: dicing body. Adapted from Zhan & Meyers, 2023.

The vast majority of DCL1-generated miRNAs in plants are 21-nt long. However, in some cases, 22-nt miRNAs are formed due to the presence of an asymmetric bulge in the miRNA/miRNA* pairing in the precursor, resulting in DCL1 generating a 22/21 nt miRNA/miRNA* duplex (H. M. Chen et al., 2010; Cuperus, Carbonell, et al., 2010; Manavella et al., 2012) . Typically, when a 22-nt miRNA is loaded into AGO1 and mediates target RNA cleavage, a dsRNA is generated from the cleaved product by the RNA-DEPENDENT RNA POLYMERASE 6 (RDR6) and is subsequently processed by DCL4 generating a subset of secondary siRNAs. This process, known as transitivity, is considered an amplification of the silencing signal and plays important roles in gene silencing and sRNA movement (see below) (de Felippes & Waterhouse, 2020). When secondary siRNAs are produced following a phased pattern, they are named phasiRNAs. Additionally, when phasiRNAs are generated from a non-coding transcript and directed against genes unrelated to their precursor molecules, they are referred to as tasiRNAs, which represent the best-characterized class of phasiRNAs (de Felippes, 2019; Deng et al., 2018; Zhan & Meyers, 2023).

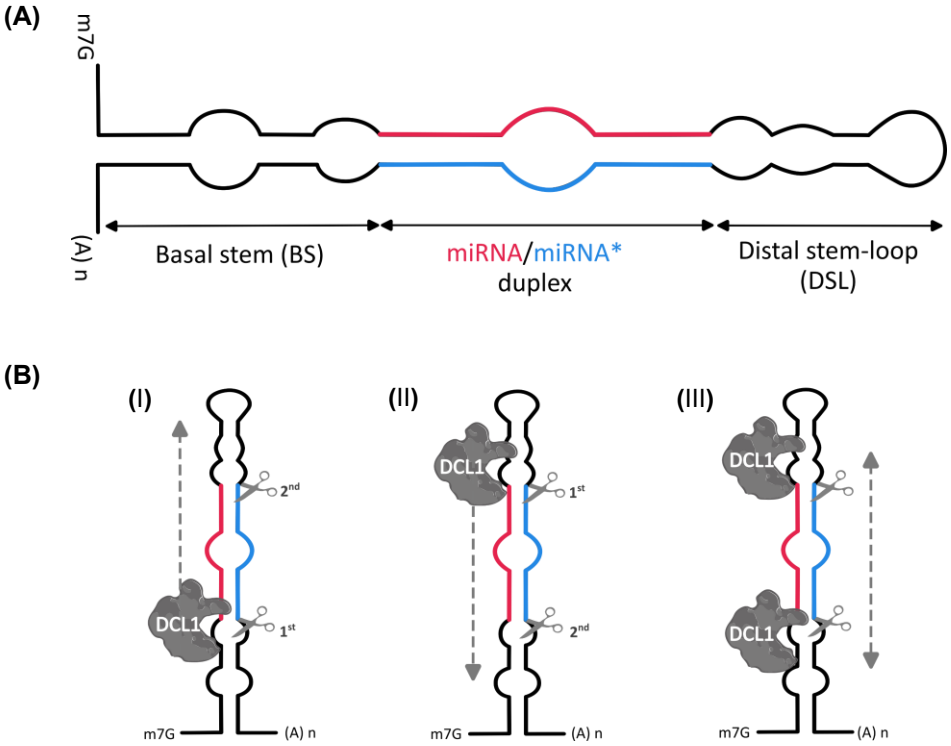

Figure 3. General structure of microRNA (miRNA) precursors and types of processing. (**A**) The primary miRNA (pri-miRNA) transcript folds into a hairpin-like structure which can be divided into three distinct regions: the basal stem (BS), the miRNA guide /miRNA star (miRNA/miRNA*) duplex, and a distal stem-loop (DSL, also known as terminal loop). The sequences upstream and downstream of these regions

are unstructured. (**B**) Types of pri-miRNA processing based on the initial recognition site and cleavage by DICER LIKE 1 (DCL1). (I) In base-to-loop processing, DCL1 initially recognizes and cleaves the pri-miRNA at the BS region. (II) In loop-to-base processing, DCL1 first cut is made at the DSL region. (III) In some exceptional cases, pri-miRNAs can undergo bidirectional processing, with cleavage occurring in both directions

2.2. Trans-acting small interfering RNAs

Like miRNAs, tasiRNAs mediate transcript cleavage of a diverse set of genes involved in developmental processes as well as stress responses. For instance, *TAS4*-derived tasiRNAs target the *MYB* transcription factor family, while *TAS3*-derived tasiRNAs regulate the expression of transcription factors from the auxin response factor (ARF) family (Fahlgren et al., 2006; Guan et al., 2014).

The biogenesis of plant tasiRNA begins with the transcription of a *TAS* gene by Pol II, producing a primary transcript that is 5'-capped and 3'-polyadenylated. After exiting the nucleus and entering the cytoplasm, the miRNA target site (TS) located within the transcript is recognized and cleaved by a 22-nt miRNA-containing RISC complex. Specifically, tasiRNA biogenesis occurs in cytoplasmic membrane-bound polysomes, where the *TAS* primary transcript is cleaved and a dsRNA molecule is generated by RDR6 (S. Li et al., 2016). SUPRESSOR OF GENE SILENCING 3 (SGS3) recruits enzymes like RDR6 to membrane-associated siRNA bodies and stabilizes the cleaved transcript, making it available for RDR6 (Jouannet et al., 2012; Yoshikawa et al., 2013, 2021). Similarly, SILENCING DEFICIENT 5 (SDE5) also participates in RDR6 recruitment (Hernandez-Pinzon et al., 2007). Once the dsRNA *TAS* precursor is generated, it is processed by DCL4, which, assisted by DOUBLE-STRANDED RNA BINDING PROTEIN 4 (DRB4), cleaves the dsRNA every 21-nt from the miRNA cleavage site, generating phased tasiRNA duplexes (Gasciolli et al., 2005; Nakazawa et al., 2007; Z. Xie, Allen, Wilken, et al., 2005). Thus, the initial miRNA guided cleavage site determines the tasiRNA sequences and their targets (Allen et al., 2005). Like miRNAs, tasiRNA duplexes are methylated by HEN1, and one strand of the duplex is loaded into AGO1 to guide the silencing of target RNAs (Figure 2B) (J. Li et al., 2005).

In *Arabidopsis thaliana* (Arabidopsis), four *TAS* families have been identified, each with different triggering miRNAs: miR173 triggers tasiRNA formation from *TAS1* and *TAS2*, miR390 from *TAS3*, and miR828 from *TAS4* (Rajagopalan et al., 2006). Additional *TAS* families exist outside of Arabidopsis (*TAS5* to *TAS10*) although they are currently poorly characterized (Deng et al., 2018; Y. Liu et al., 2020). Plant *TAS1/TAS2* and *TAS4* tasiRNAs follow the "one-hit model", where tasiRNA generation is triggered by a 22-nt miRNA. However, the *TAS3* transcripts follow a less common "two-hit" pathway, which differs from the latter in several aspects. Specifically,

TAS3 pathway is triggered by the 21-nt miR390, which associates almost exclusively with AGO7 and recognizes two distinct TS on the *TAS3* transcript (Endo et al., 2013; Montgomery, Howell, et al., 2008). The RISC complex formed by miR390 and AGO7 cleaves only the 3' TS of *TAS3* transcripts and, unlike in the "one-hit model", tasiRNAs are generated from the 5' cleavage fragment (Axtell et al., 2006). Interestingly, *TAS1* and *TAS2* have only been described in Arabidopsis, while *TAS3* is present in all land plants and *TAS4* is conserved in eudicots.

3. Small RNA movement in plants

The transmission of a silencing signal to distal parts of the plant was first reported more than 25 years ago (Palauqui, 1997; Voinnet & Baulcombe, 1997). It is now understood that plant sRNAs, including miRNAs and tasiRNAs, function in a non-cell-autonomous manner as the mobile signal (L. Liu & Chen, 2018). In terms of range, sRNA movement can be classified in local or short-range and systemic or long-range.

Short-range movement of sRNAs occurs through plasmodesmata (PD), extensions of the cell membrane which form a cytosolic continuity between adjacent cells and connect symplastically to the phloem, linking almost all cells (L. Liu & Chen, 2018; Otero et al., 2016). sRNAs short-range movement occurs between 10 and 15 cells from their site of origin (Dunoyer et al., 2007; Himber et al., 2003; Kalantidis et al., 2006; L. M. Smith et al., 2007). This movement range is partially controlled by the PD size exclusion limit, as seen in the embryonic hypocotyl, where sRNAs can move up to 35 cells due to PD aperture dilation (Kobayashi & Zambryski, 2007). Still the precise mechanisms controlling sRNA movement through PD remain unclear. The short-range mobility of miRNAs and tasiRNAs is crucial in developmental processes. For example, *TAS3*-derived tasiRNAs targeting ARFs move from their originating cells, creating a gradient that establishes the abaxial-adaxial polarity during leaf development (Chitwood et al., 2009). Importantly, the association of tasiRNA synthesis with membrane-bound polysomes may facilitate their movement to adjacent cells (Alvarez et al., 2006; Y. Liu et al., 2020; Parizotto et al., 2004). On the other hand, MiRNAs are generally considered less mobile than tasiRNAs, as their sites of origin and function often correlate. Nevertheless, miRNA movement to adjacent cells has also been reported, as in the case of miR390 in the apical meristem (Chitwood et al., 2009).

While PD enables sRNA transport between adjacent cells, the vascular tissue facilitates long-distance trafficking. It is widely accepted that sRNAs move long distances through the phloem, since miRNAs and siRNAs have been detected in phloem exudates and it is an RNA-friendly environment due to its lack of RNAses (Buhtz et al., 2008, 2010; Doering-Saad et al.,

2002; Yoo et al., 2004). Phloem sieve elements are connected to companion cells via highly modified PD, and it is believed that sRNAs move from their originating cells into companion cells for loading into the phloem, following a source-to-sink direction to reach target sink tissues (B.-K. Ham & Lucas, 2017). Grafting experiments have been extremely useful in identifying the roles of long-distance miRNAs in development, nutrient starvation and plant-pathogen interactions, among others. For example, the regulation of potato tuberization by long-distance mobile miR172 and miR156 was described through grafting experiments (Bhogale et al., 2014; Martin et al., 2009). Similarly, long-distance tasiRNAs play roles in biological processes such as plant resistance to viral infections (Shine et al., 2022).

Transitivity is a key factor affecting sRNA mobility, as it enhances the initial pool of sRNAs, thereby increasing their movement range through the vasculature (de Felippes & Waterhouse, 2020). This process is critical during viral infections, as it facilitates the systemic movement of viral-derived siRNAs (vd-siRNAs), resulting in plant-wide immunization (Lopez-Gomollon & Baulcombe, 2022). Still, several controversies and unanswered questions remain regarding sRNA mobility, such as the exact nature of the mobile signal. It is unclear whether sRNAs move intercellularly through PD and/or the phloem as ssRNA or as duplex RNA, and whether they move alone or in association with proteins. Additionally, the interaction of sRNAs with PD is poorly understood and requires further investigation.

4. Classic RNA interference strategies for targeted gene silencing

After the initial discovery of gene expression regulation mediated by sRNAs, the first step towards the development of methodologies for targeted gene silencing was taken in 1998 with the design of an RNAi strategy to control the expression of specific genes in the nematode *Caenorabtitis elegans* (Fire et al., 1998). Since then, several RNAi-based strategies have been developed in plants for functional genomics, pathogen resistance and crop improvement (Koeppe et al., 2023; Y.-W. Kuo & Falk, 2020).

4.1. Hairpin RNA interference

One of the “classic RNAi strategies” is the inverted repeat PTGS or hairpin RNAi (hpRNAi). The construct for hpRNAi includes a fragment of the target gene followed by an antisense sequence of the same fragment, separated by a spacer. After transcription, a hairpin-like RNA precursor is generated and recognized by plant DCLs (e.g. DCL2, DCL3 and/or DCL4) to produce a pool of sRNAs of different sizes (e.g. 21, 22 and 24 nt) targeting the gene(s) of interest (Figure 4A). This strategy requires the insertion of the T-DNA, from *Agrobacterium tumefaciens*, containing

the hpRNAi construct, which typically includes gene fragments between 300 and 800 bp, into the plant genome. The successful use of this strategy has been applied to silence endogenous genes and confer resistance to viruses in different plant species such as tobacco, tomato and orange trees (Tiwari et al., 2014; Watson et al., 2005).

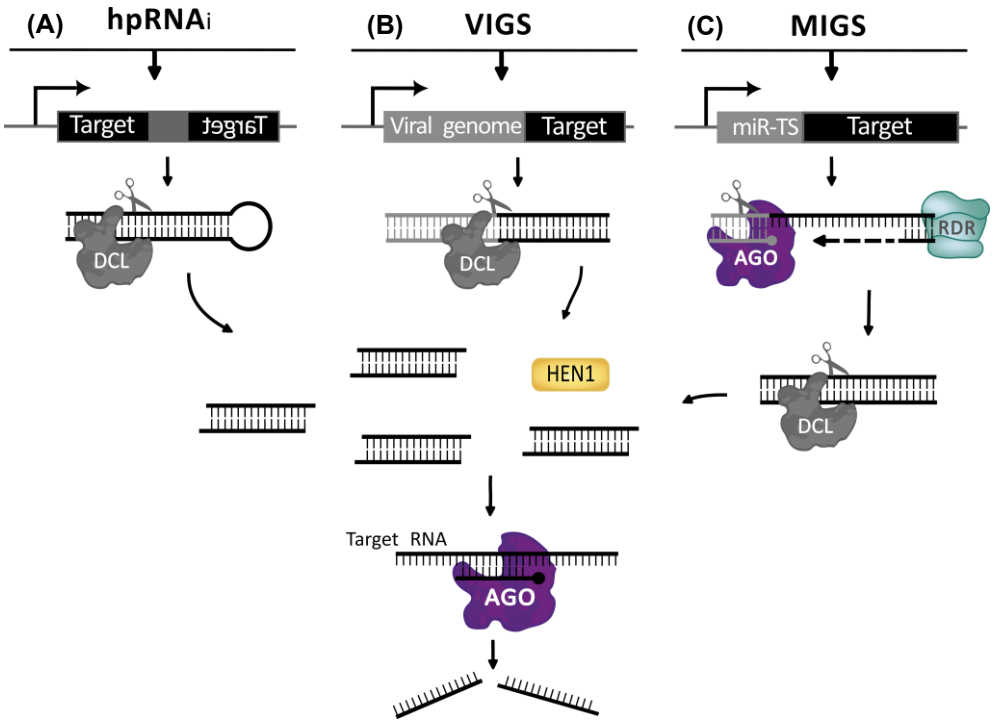

Figure 4. Classic RNA interference (RNAi) strategies for gene silencing in plants. (**A**) Hairpin RNAi (hpRNAi): the target gene sequence is cloned in both sense and antisense orientations, separated by a spacer, leading to the formation of a hairpin-like structure after transcription**.** (**B**) Virus-induced gene silencing (VIGS): the target sequence is incorporated into a vector containing the viral genome, which triggers gene silencing through the plant's RNAi machinery**.** (**C**) MicroRNA-induced gene silencing (MIGS): the target sequence is inserted downstream a 22-nt microRNA target site (miR-TS). Following cleavage by the microRNA-ARGONAUTE (miRNA-AGO) complex, an RNA-DEPENDENT RNA POLYMERASE (RDR) synthesizes a double-stranded RNA (dsRNA) precursor. In all strategies (**A**, **B** and **C**), the dsRNA precursor molecules are processed by different DICER LIKE proteins (DCL2, DCL3 or DCL4), generating pools of small RNA (sRNA) duplexes of different length and sequence. These sRNA duplexes are methylated by HUA ENHANCER1 (HEN1), after which one strand is loaded into AGO for subsequent sequence-specific binding and cleavage of the target RNA(s).

4.2. Virus-induced gene silencing

One of the drawbacks of hpRNAi is the requirement for plant genetic transformation. To overcome this limitation, alternative strategies were developed for research in non-model

species, including virus-induced gene silencing (VIGS). This technique exploits the plant's RNAi mechanisms in response to viral infections. When a virus enters the plant cell, viral transcription and/or replication generates dsRNA forms that are recognized by endogenous DCLs, leading to the production of vd-siRNAs that attenuate virus spread (Molnár et al., 2005). VIGS uses viral vectors that are modified to include target gene fragments, so the resulting vd-siRNAs effectively silence the target gene(s) of interest (Figure 4B). Initially, most VIGS vectors were RNA-based, since RNA viruses generally infect a wider variety of host plants than DNA viruses. Popular RNA-based VIGS vectors include cucumber mosaic virus, tobacco rattle virus and potato virus X for dicot species, and foxtail mosaic virus for monocots (Shi et al., 2021; Zulfiqar et al., 2023). Nowadays numerous DNA-based vectors, particularly from the *Geminiviridae* family, are also available for use in dicots like tomato mottle virus, and monocots like tungro bacilliform virus (Zulfiqar et al., 2023). Regardless of vector type, the insert size is limited due to physical constraints of the viral capsid and/or instability of the inserted fragment during viral replication. Typically, VIGS vectors accommodate gene fragments ranging from 200 to 400 bp (Rössner et al., 2022). VIGS has been used in functional genomics for more than two decades, allowing gene elucidation in non-model species where genetic transformation is time-consuming and laborious, including woody plants (H. Yan et al., 2018).

4.3. MicroRNA-induce gene silencing

More recently, another RNAi technique called miRNA-induced gene silencing (MIGS) was developed based on the transitivity mechanism initiated by 22-nt miRNAs. In MIGS design, a 22-nt miRNA TS is placed upstream of a gene fragment, leading to the generation of phasiRNAs following miRNA-mediated RISC target recognition (Figure 4C) (de Felippes et al., 2012). Typically, miR173, the 22-nt miRNA that triggers the formation of tasiRNAs from *TAS1* and *TAS2* transcripts, is used to trigger tasiRNA formation from MIGS constructs including miR173 TS. MIGS designs are relatively straightforward and allow for the simultaneous silencing of multiple genes by placing different gene fragments in tandem, downstream of the 22-nt miRNA TS. MIGS has been successfully applied to silence genes in various species including Arabidopsis, *Nicotiana benthamiana*, soybean and rice (de Felippes, 2019).

4.4. Limitations of classic RNA interference strategies

Despite their widespread use in plants, classic RNAi techniques have several limitations: (i) the requirement for plant genetic transformation restricts the applicability of hpRNAi and MIGS; (ii) the use of viral vectors for VIGS-mediated crop improvement may be commercially undesirable due to regulatory concerns; and (iii) in MIGS, gene silencing is conditioned by the expression

pattern of the triggering miRNA. Moreover, classic RNAi strategies share a common limitation, which is the inability to predict the exact sequence of the sRNAs generated from the dsRNA precursors, which can reduce the specificity of the approach. Moreover, genes other than the intended target sharing sequence similarity may also be silenced. This undesirable off-target effect is a significant drawback of classic RNAi strategies and is difficult to avoid (Senthil-Kumar & Mysore, 2011).

5. Artificial small RNA-based gene silencing tools

More recently, a "second-generation" gene silencing tools has been developed, offering enhanced efficiency and specificity. These tools, based on artificial sRNAs (art-sRNAs), include artificial microRNAs (amiRNAs) and synthetic tasiRNAs (syn-tasiRNAs). Art-sRNAs are derived from miRNA or tasiRNA precursors engineered to incorporate amiRNA/amiRNA* or syn-tasiRNA sequences, respectively. These art-sRNAs are computationally designed for highly efficacy and specificity, with several web-based tools available for their design: WMD3 (Web MicroRNA Designer 3) (Ossowski et al., 2008), amiRNA Designer (Mickiewicz et al., 2016), microRNA Designer (www.smallrna.mtu.edu/Tang_Website/submit.htm, 2016), and P-SAMS (Plant Small RNA Maker Suite) (Fahlgren et al., 2016). Although the precise base-pairing requirements for productive sRNA/target RNA interaction are not fully understood, it is widely accepted that a high degree of sequence complementarity between the sRNA and its target RNA is essential for efficient silencing (Q. Liu et al., 2014). Likewise, mismatches between the sRNA and its target in the seed region of the sRNA (positions 2-14), dramatically reduce sRNA activity, while mismatches in positions 14-21 are better tolerated (Fahlgren & Carrington, 2010; Schwab et al., 2006). Each design tool employs specific parameters to optimize art-sRNA's performance, although for example WMD3 and P-SAMS, the most used web tools, consider several common features for optimal design (Figure 5): (i) a 5' uracil (U) in the guide strand for preferential loading into AGO1, (ii) a cytosine (C) at position 19 in the guide strand to produce a star strand with an AGO1 non-preferred 5' guanine (G) and (iii) include mismatches at positions 18-21 to reduce the likelihood of triggering transitivity, thereby enhancing specificity. These tools evaluate the specificity of designed art-sRNAs by analyzing all possible base-pairing interactions between the art-sRNA and all annotated transcripts of the target species. Hence, off-target analysis is only feasible in species with well-annotated transcriptomes. Despite the thorough *in silico* design, predicting the *in vivo* efficacy of art-sRNAs remains challenging, as some target RNA regions may be less accessible than others due to secondary structure or RNA-protein interactions. As a result, design tools typically provide multiple optimal art-sRNA candidates, whose individual *in vivo* performance requires experimental validation.

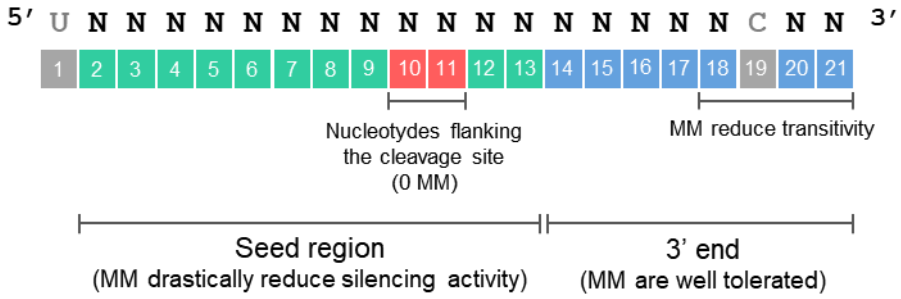

Figure 5. Artificial small RNA (art-sRNA) guide sequence positions and design rules*. The 21 nucleotide positions of the art-sRNA guide sequence are represented and numbered underneath. **N** represents any of the 4 RNA nucleotides (**A**, **C**, **U**, or **G**). The specific nucleotide sequence of the art-sRNA guide strand will vary depending on the selected target sequence, except for positions 1 and 19 (from 5' to 3'). Position 1 is always a **U** to favor ARGONAUTE 1 (AGO1) association, while position 19 is typically a **C** so that position 1 in the star sequence is a **G** to avoid AGO1 loading. The impact of mismatches (MM) between the art-sRNA guide sequence and the target RNA on silencing activity is emphasized. Positions 2 to 13 are colored green and represent the seed region where MM are critical, specifically in positions 10 and 11, which flank the cleavage site. The art-sRNA guide 3' end region is represented by blue boxes where MM are better tolerated. * Common design parameters applied by WMD3 and P-SAMS tools.

5.1. Artificial microRNAs

AmiRNAs are produced via the endogenous miRNA pathway, initiated by the transcription of the miRNA precursor. To generate amiRNAs, the native miRNA/miRNA* sequences within the precursor are replaced by 21-nt amiRNA and amiRNA* sequences. It is crucial that the secondary structure of the miRNA precursor is preserved when including these modifications to ensure proper recognition and cleavage by DCL1, enabling the effective release of the amiRNA/amiRNA* duplex. The amiRNA guide strand, typically containing a 5'U, preferentially associates with AGO1 to mediate the endonucleolytic cleavage or translational repression of the target gene(s) (Figure 6) (Tiwari et al., 2014).

AmiRNAs are typically designed to target a single transcript, although, in some cases, a single amiRNA can target multiple transcripts simultaneously if they share a sufficient degree of sequence similarity. For example, one amiRNA successfully silenced four MADS-box genes involved in flowering time and floral patterning, resulting in increased number of cauline leaves and altered floral morphology (Becker, 2003; Schwab et al., 2006). While most miRNA precursors are monocistronic, there are some examples of polycistronic precursors capable of generating multiple amiRNAs simultaneously. This strategy has been particularly advantageous for conferring antiviral protection. For example, rice *Osa-miR395* precursor containing five

stem-loop structures was used to confer resistance to a wheat virus by generating five distinct amiRNAs (Fahim et al., 2012). Alternatively, several amiRNAs can be produced simultaneously by expressing multiple amiRNA precursors in tandem (Cisneros & Carbonell, 2020; Liang et al., 2012; Lunardon et al., 2021).

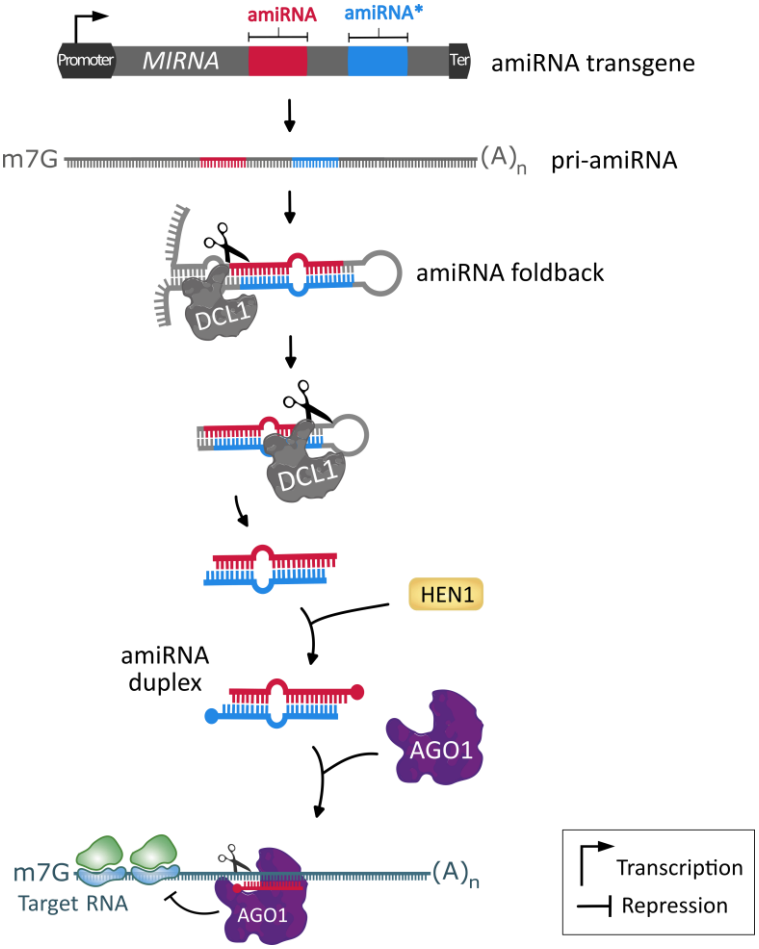

Figure 6. Artificial microRNA (amiRNA) biogenesis pathway. The original miRNA guide/miRNA star (miRNA/miRNA*) sequences in the miRNA precursor are replaced by computationally designed amiRNA/amiRNA* sequences. The amiRNA precursor maintains its hairpin structure to ensure proper recognition and cleavage by DICER LIKE 1 (DCL1) and undergoes the canonical miRNA pathway, ultimately silencing the target gene of interest. Ter: terminator, Pri-amiRNA: amiRNA primary transcript AGO1: ARGONAUTE 1, HEN1: HUA ENHANCER 1.

AmiRNAs have been extremely helpful in functional genomics, enabling the identification of genes that regulate growth, development including important processes such as floral transitioning. Moreover, they have been used to confer resistance against biotic stresses,

including viruses, as well as abiotic stresses such as drought and high temperatures. Importantly, different miRNA precursors have been used to produce amiRNAs in various plant species including eudicots, monocots, mosses and algae (reviewed in (Carbonell, 2017; Cisneros et al., 2021; Kamthan et al., 2015; Tiwari et al., 2014)). The success of amiRNA-based silencing strategies relies on the accumulation of high levels of accurately processed amiRNAs. The processing accuracy of amiRNA precursor is determined by the specific precursor used. Ideally, the precursor should be conserved across species to ensure a correct processing in multiple species and should be relatively short to facilitate construct generation. The *MIR390* precursor family meets these requirements and has been used to express amiRNAs in both eudicots and monocots (Carbonell, 2017; Cisneros et al., 2021; Cisneros & Carbonell, 2020). In particular, the *AtMIR390a* has a short DSL region, leading to a base-to-loop processing that favors the accurate generation of amiRNAs (Figure 7). This characteristic has also facilitated the development of *pri-AtMIR390a*-based gateway-compatible vectors for rapid and cost-effective amiRNA expression in plants (Carbonell et al., 2014). *AtMIR390a* has been extensively used to silence endogenous and viral RNAs in various species (Berbati et al., 2023; Carbonell, 2019; Cisneros et al., 2021; Lunardon et al., 2021; Vasav et al., 2023).

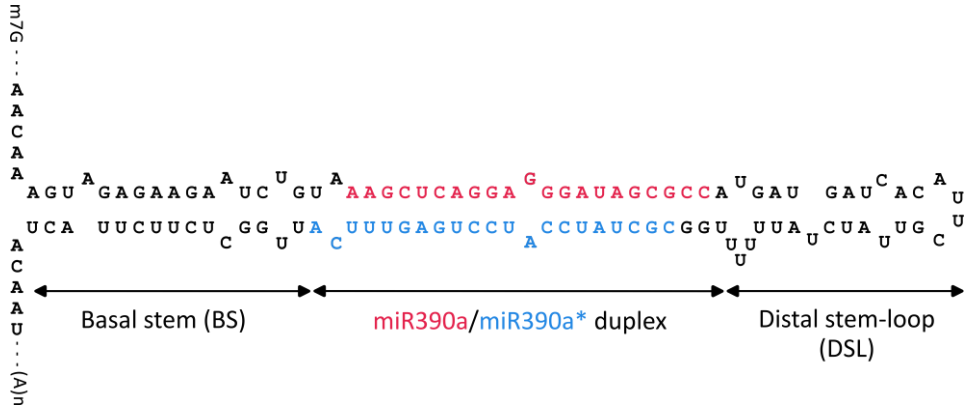

Figure 7. Sequence and secondary structure of the *AtMIR390a* primary transcript foldback. Letters in pink and blue indicate the AtmiR390a guide and star sequences, respectively. The secondary structure of minimal free energy was predicted with RNAfold web tool (Hofacker, 2003)

5.2. Synthetic trans-acting small interfering RNAs

Syn-tasiRNAs are generated via the endogenous tasiRNA biogenesis pathway. They are produced in plants from a transgene containing a *TAS* precursor, in which some of the native tasiRNAs are replaced by one or several syn-tasiRNAs positioned in tandem. After transcription

of the transgene, the primary transcript is recognized and cleaved by a 22-nt miRNA/AGO complex. Subsequently, RDR6 is recruited to produce a dsRNA from one of the *TAS* cleaved products, which is recognized by DCL4. Then DLC4 cleaves every 21 nt releasing the syn-tasiRNA duplexes in phase. Ultimately, the guide strand of the syn-tasiRNA duplex, which contains a 5' U, is loaded into AGO1 to silence the intended target(s) (Figure 8).

To date, only the Arabidopsis *AtTAS1a*, *AtTAS1c* and *AtTAS3a* precursors have been used to produce syn-tasiRNAs (Carbonell, 2019; Cisneros et al., 2021; Lunardon et al., 2021). Importantly, while *TAS3* is conserved across plants, *TAS1* is only present in Arabidopsis. Therefore, when expressing syn-tasiRNAs from *AtTAS1* in other species, the co-expression of AtmiR173 is required. *AtTAS1c* has been used to generate syn-tasiRNAs in Arabidopsis, *N. benthamiana* and tomato plants, resulting in high accumulation and accurate processing of syn-tasiRNAs in all cases (Carbonell et al., 2014, 2019; Carbonell & Daròs, 2017; Gutiérrez-Nava et al., 2008; Montgomery, Yoo, et al., 2008). Finally, the recent development of *AtTAS1c*-based Gateway-compatible vectors has simplified the generation of constructs for syn-tasiRNA expression in plants, expanding the use of this gene silencing tool (López-Dolz et al., 2020).

An important feature of the syn-tasiRNA approach is its capacity to generate multiple syn-tasiRNAs simultaneously from a single modified *TAS* precursor. This multiplexing ability can be used to produce multiple syn-tasiRNAs targeting different regions within the same gene or distinct sequence-unrelated genes. For instance, multigene silencing was achieved in Arabidopsis by expressing one syn-tasiRNA for the simultaneous silencing of three *MYB* transcripts (*TRIPTYCHON*, *CAPRICE* and *ENHANCER OF TRIPTYCHON AND CAPRICE2*) along with another syn-tasiRNA for silencing the *FLOWERING LOCUS T* (*FT*) gene (Carbonell et al., 2014). The intrinsic multiplexing ability of syn-tasiRNAs offers a significant advantage in antiviral strategies by enabling the simultaneous targeting of multiple regions of the viral genome, reducing the likelihood of viral escape through genome mutations. This was shown in a comparative study where tomato lines expressing a single amiRNA were analyzed in parallel with lines expressing four syn-tasiRNAs against tomato spotted wilt virus. The majority of lines expressing the four syn-tasiRNAs exhibited complete resistance, whereas most amiRNA-expressing lines remained susceptible to viral infection (Carbonell et al., 2019). Finally, another interesting feature of the syn-tasiRNA strategy is the positional effect of the syn-tasiRNA, where syn-tasiRNAs placed farther from the miRNA TS accumulate at lower levels, thus allowing for the fine-tuning of the degree of gene silencing (López-Dolz et al., 2020).

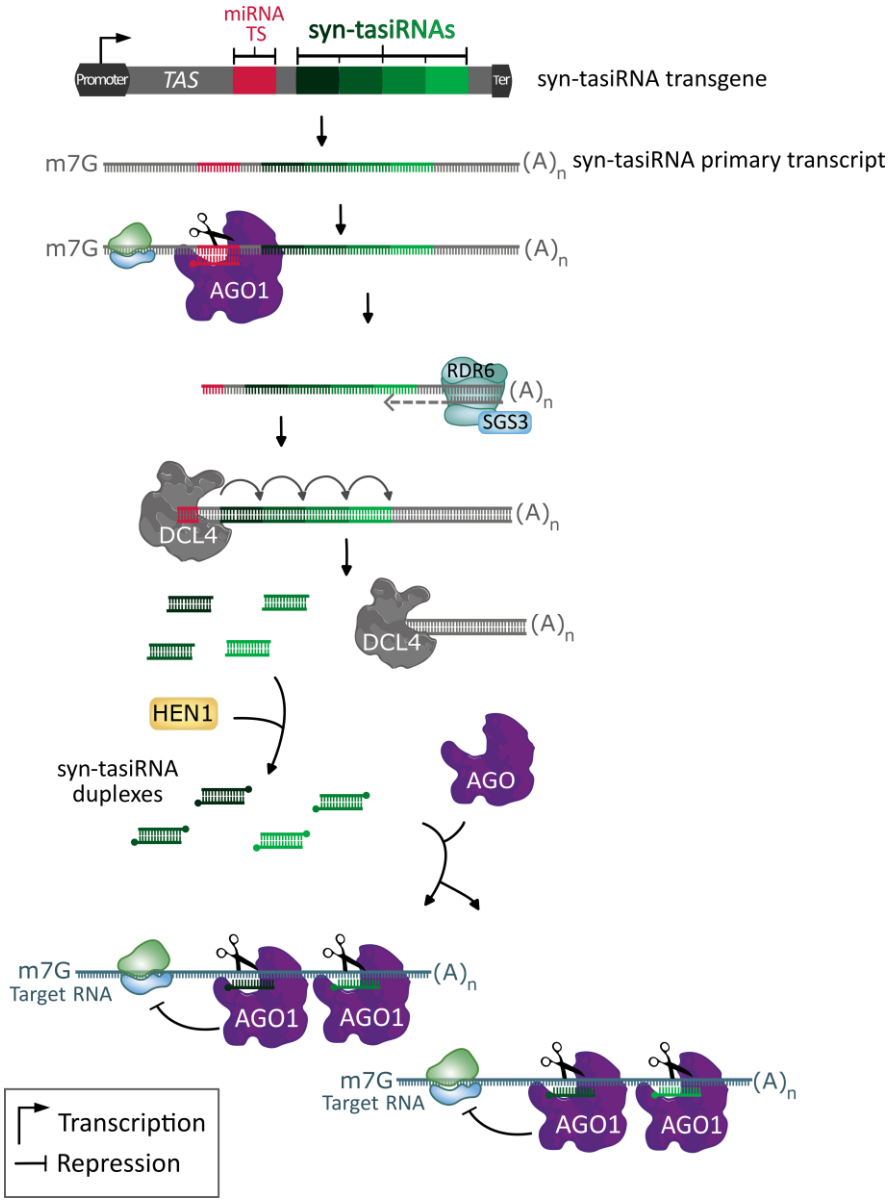

Figure 8. Synthetic trans-acting small interfering RNAS (syn-tasiRNAs) biosynthesis pathway. One or several syn-tasiRNAs are inserted in tandem replacing the original tasiRNA sequences in a *TAS* precursor. After transcription, the primary transcript undergoes the canonical tasiRNA pathway. The syn-tasiRNAs produced can target different regions of the same gene or multiple genes simultaneously. Ter: terminator, miRNA TS: microRNA target site, AGO1: ARGONAUTE1, RDR6: RNA-DEPENDENT RNA POLYMERASE 6, SGS3: SUPRESSOR OF GENE SILENCING 3, DCL4: DICER LIKE 4, HEN1: HUA ENHANCER 1.

6. Analysis of the silencing activity of artificial small RNAs

Following the design and generation of the art-sRNA construct, its silencing activity must be assessed *in vivo*, typically via *Agrobacterium*-mediated transient expression. The silencing efficiency of art-sRNA candidates should be evaluated using different molecular approaches, including: (i) detection of the art-sRNA precursor by PCR, (ii) measurement of art-sRNA accumulation by Northern blot, (ii) quantification of target gene silencing levels by RT-qPCR and (IV) sequencing the sRNA species present in the expressed tissue to confirm the production of authentic art-sRNAs and the absence of secondary sRNAs. It is also recommended to use reporter genes as art-sRNA targets, allowing for a rapid identification of the most effective art-sRNA candidates, later confirmed by molecular analyses. One of the most commonly used reporter systems is based on silencing the GREEN FLUORESCENT PROTEIN (GFP) in *N. benthamiana* 16C transgenic plants, which constitutively express GFP. Despite its popularity, the GFP-based reporter system has some limitations, such as the requirement for ultraviolet light to visualize gene silencing, and the need for specific equipment (e.g. microscopes) to measure silencing intensity. Additionally, endogenes are preferred as reporter agents over transgenes, which are more prone to be silenced and therefore may not accurately reflect the real silencing efficiency of the art-sRNA (Dadami et al., 2013, 2014). As an alternative to the GFP-based reporter system there are several examples of endogenes acting as reporters like *CHLORINA42* (*CH42*) or *FT* in Arabidopsis. Silencing these genes induces visible phenotypes –bleaching for CH42 and late flowering for *FT*– which can be easily visualized and quantified without specific equipment (de Felippes & Weigel, 2009; Schwab et al., 2006).

7. Strategies for the application of artificial small RNAs to plants

7.1 *Agrobacterium*-mediated expression of artificial small RNA constructs

After selecting an optimal art-sRNA, it is typically expressed in the plant species of interest via *Agrobacterium*-mediated stable transformation. This method involves the transfer of *Agrobacterium* T-DNA containing the art-sRNA construct into the plant genome, resulting in a genetically modified organism (GMO). *Agrobacterium*-mediated stable transformation is a well-stablished protocol for obtaining uniform expression of art-sRNAs at the whole-plant level. However, it is a time-consuming, species-specific procedure that is constantly being adapted to expand its applicability across a wider range of species (Lyu, 2022). Furthermore, GMOs are subject to strict legislation in several regions worldwide, and their use may even be limited by negative public perception (Naveen & Sontakke, 2024). These challenges motivate the

development of new art-sRNA expression and application techniques that avoid the generation of GMOs.

7.2. Exogenous application of artificial small RNAs

An alternative to *Agrobacterium*-mediated transformation is the exogenous application of art-sRNA precursors. The exogenous application of dsRNA precursors and siRNA duplexes has already been successfully used to silence endogenous genes and confer resistance to various pathogens, using delivery methods such as infiltration, spraying or biolistics (Koeppe et al., 2023). Similarly, endogenous miRNAs have been successfully delivered to Arabidopsis seedlings through liquid media (Betti et al., 2021). In some cases, the systemic movement of exogenously applied sRNAs has been observed, leading to non-transgenic target gene silencing in distal parts of the plant, a process reported to depend on transitivity (Dalakouras et al., 2020). However, this approach has two major limitations: first, the delivery of dsRNA molecules is inefficient due to RNA instability outside the cell, and second, cost-effective systems for large-scale production of dsRNAs are not available. The first limitation could be overcome by the conjugation of ssRNA and dsRNA molecules with nanoparticles (Yong et al., 2024), while there is still a need to develop cost-effective methods for RNA production (Basso et al., 2019). In any case, the exogenous application of art-sRNA precursors may increase specificity compared to dsRNA precursors, reducing off-target effects. Nevertheless, the capacity of topically delivered art-sRNAs to induce systemic silencing (SS) upon local application remains unknown, as their mobility from local to distal tissues has not been reported yet. Therefore, further investigation into the mobility of art-sRNAs could contribute to the development of non-transgenic approaches for widespread gene silencing.

7.3. Expression of artificial small RNAs through viral vectors

Another strategy involves using the previously described VIGS technique to drive the expression of art-sRNA precursors. Indeed, VIGS has already been successfully used to express amiRNA precursors for targeting endogenous genes (Gu et al., 2014; Jian et al., 2017; Ju et al., 2017; Kuo & Falk, 2022; Y. Tang et al., 2010). In the amiRNA-mediated VIGS (amiR-VIGS) strategy, whole-plant gene silencing is achieved following local *Agrobacterium*-mediated inoculation of the viral vector. Moreover, VIGS is a highly versatile system, enabling art-sRNA expression in non-model species, as reported for cotton and wheat (Gu et al., 2014; Jian et al., 2017). Most viruses used in amiR-VIGS belong to the *Geminiviridae* family, with ssDNA genomes that facilitate amiRNA precursor processing from the viral vector due to their nuclear replication (Ju et al., 2017; Kuo & Falk, 2022; Y. Tang et al., 2010). Numerous geminiviruses

are stable, accumulate to high levels in infected cells and therefore are suitable for use as viral vectors (Carrillo-Tripp et al., 2006; Lozano-Durán, 2016). However, DNA-based viral vectors encounter certain limitations, such as a restricted host range, limited cargo capacity and the risks of foreign DNA insertion into the plant genome (Khakhar & Voytas, 2021; Mahmood et al., 2023). In contrast, ssRNA-based viruses replicate in the cytoplasm, avoiding the risk of foreign DNA insertion, and typically exhibit a wider host range. Despite these advantages, there are only a few reported cases of successful amiR-VIGS using RNA-based viral vectors in plants (Jian et al., 2017; Kuo and Falk 2022). The relative lack of success with RNA-based vectors in amiR-VIGS may be due to their limited cargo capacity, which impairs mobility and delivery efficiency when large sequences are inserted (Pasin et al., 2019). Importantly there are no previous reports of the successful syn-tasiRNA expression using VIGS (syn-tasiR-VIGS). Therefore, further research is needed to develop methods for a consistent and non-transgenic application of art-sRNA precursors from RNA-based viral vectors.

OBJECTIVES

The main objective of this thesis is to deepen the understanding of the silencing activity of art-sRNAs by studying the systemic silencing they may induce and engineering minimal precursors for their transgene-free, virus-based expression in plants.

The specific objectives are:

1. To investigate the local and systemic silencing capacity of art-sRNAs and the factors that influence this process.
2. To engineer a minimal precursor for expressing amiRNAs from the *AtMIR390a* precursor.
3. To engineer a minimal precursor for expressing syn-tasiRNAs from the *AtTAS1c* precursor.
4. To explore whether engineered minimal precursors can produce *in vivo* authentic amiRNAs and syn-tasiRNAs when expressed from a viral vector.
5. To develop a transgene-free method for inducing whole-plant gene silencing using viral vector-derived art-sRNAs.

CHAPTER 1

Systemic Silencing of an Endogenous Plant Gene by Two Classes of Mobile 21-Nucleotide Artificial Small RNAs

Adriana E. Cisneros, Ainhoa de la Torre-Montaña and Alberto Carbonell

Adapted from the article published in 2022 at *The Plant Journal* 110(4):1166-1181. doi: 10.1111/tpj.15730

CHAPTER 1

Systemic Silencing of an Endogenous Plant Gene by Two Classes of Mobile 21-Nucleotide Artificial Small RNAs

Adriana E. Cisneros[a], Ainhoa de la Torre-Montaña[a] and Alberto Carbonell[a]

[a]*Instituto de Biología Molecular y Celular de Plantas (Consejo Superior de Investigaciones Científicas–Universitat Politècnica de València), 46022 Valencia, Spain*.

ABSTRACT

Artificial small RNAs (art-sRNAs) are 21-nucleotide (nt) small RNAs (sRNAs) computationally designed to silence plant genes or pathogenic RNAs with high efficacy and specificity. They are typically produced in transgenic plants to induce silencing at the whole-organism level but their expression in selected tissues for inactivating genes in distal tissues has not been reported. Here, art-sRNAs designed against the magnesium chelatase subunit CHLI-encoding *SULPHUR* gene (*NbSu*) were agroinfiltrated in *Nicotiana benthamiana* leaves, and the induction of local and systemic silencing was analyzed phenotypically by monitoring the appearance of the characteristic bleached phenotype, and molecularly by analyzing art-sRNA processing, accumulation and targeting activity and efficacy. We found that the two classes of art-sRNAs, artificial microRNAs (amiRNAs) and synthetic trans-acting small interfering RNAs (syn-tasiRNAs), are able to induce systemic silencing of *NbSu*, which requires high art-sRNA expression in the vicinity of the leaf petiole but is independent on the production of secondary sRNAs from *NbSu* mRNAs. Moreover, we revealed that 21-nt amiRNA and syn-tasiRNA duplexes, and not their precursors, are the molecules moving between cells and through the phloem to systemically silence *NbSu* in upper leaves. All in all, our results indicate that 21-nt art-sRNAs can move throughout the plant to silence plant genes in tissues different from where they are produced. This highlights the biotechnological potential of art-sRNAs, which might be applied locally for triggering whole-plant and highly specific silencing to regulate gene expression or induce resistance against pathogenic RNAs in next-generation crops.

Keywords: systemic silencing, small RNA movement, cell non-autonomous, artificial microRNA, synthetic trans-acting siRNA, transitivity**,** *Nicotiana benthamiana*

INTRODUCTION

Eukaryotic small RNAs (sRNAs) are responsible for the sequence-specific degradation of highly sequence complementary RNA molecules, a process known as RNA silencing. In plants, sRNAs arise from the processing of a double-stranded RNA (dsRNA) by DICER-LIKE (DCL) enzymes into 21-24 nucleotide (nt) duplexes. Typically, one of the strands of the duplex (the guide strand) is incorporated into an ARGONAUTE (AGO) protein that recognizes and inactivates complementary target RNA by diverse mechanisms (Axtell, 2013; Bologna and Voinnet, 2014; Borges and Martienssen, 2015). In some contexts, silencing can be amplified through the production of secondary sRNAs by RNA-DEPENDENT RNA POLYMERASES (RDRs), for instance upon the targeting of RNAs by 22-nt sRNAs (Cuperus *et al.*, 2010; Chen *et al.*, 2010), a process termed transitivity. RNA silencing can also function non-cell autonomously in plants as sRNAs can spread from cell to cell, over long-distances and even between different plants or interacting organisms (Weiberg *et al.*, 2015; Liu and Chen, 2018; Dunker *et al.*, 2020). For instance, sRNA short-range movement extends 10-15 cells away from the production site and occurs via plasmodesmata connecting the cytoplasm of adjacent cells, while long-distance traffic to distal tissues occurs through the phloem (Molnar *et al.*, 2011).

Artificial sRNAs (art-sRNAs), such as artificial microRNAs (amiRNAs) and synthetic trans-acting small interfering RNAs (syn-tasiRNAs) are 21-nt sRNAs computationally designed to selectively silence one or more target genes with high specificity and efficacy (Ossowski *et al.*, 2008; Zhang, 2014; Tiwari *et al.*, 2014; Carbonell, 2017; Carbonell, 2019). AmiRNAs are typically produced *in planta* by expressing an endogenous miRNA precursor in which the sequences of the endogenous miRNA/miRNA* are replaced by the amiRNA/amiRNA* sequences. AmiRNA primary transcript is sequentially processed by DCL1 to release the 21-nt amiRNA duplex. Syn-tasiRNAs are produced by expressing an endogenous *TAS* precursor including one or more syn-tasiRNA sequences replacing endogenous tasiRNA sequences. In this case, the syn-tasiRNA primary transcript is cleaved by a miRNA/AGO complex, RDR6-including complexes produce a dsRNA from one of the *TAS* cleaved fragments, and the resulting dsRNA is sequentially processed by DCL4 in 21-nt syn-tasiRNA duplexes in phase with the miRNA trigger target site. For both art-sRNA classes, the guide strand of the art-sRNA duplex (typically including a 5' U) associates with AGO1 to silence complementary RNA(s). Art-sRNAs are extensively used in plants to regulate gene expression in gene function studies and to induce antiviral resistance [reviewed recently in (Cisneros and Carbonell, 2020; Cisneros *et al.*, 2021)]. However, one major limitation of current art-sRNA approaches is that art-sRNA are usually expressed in transgenic organisms, which hinders the commercialization of art-sRNA-expressing crops in regions where genetically modified organisms (GMOs) are banned. In this

context, the possibility of expressing art-sRNAs in one tissue for triggering the systemic silencing (SS) of a target RNA in a different tissue should facilitate the control of gene expression and/or induce antiviral resistance at the whole-plant level and in line with international laws. Unfortunately, the molecular bases governing the induction and spread of SS are not always clear, particularly for endogenes, what has hampered the development of efficient methods for triggering SS in plants.

Here we report that the transient expression in *Nicotiana benthamiana* leaves of amiR-NbSu-2, a 21-nt amiRNA designed to silence the magnesium chelatase subunit CHLI-encoding *SULPHUR* gene (*NbSu*), induces obvious SS in upper non-agroinfiltrated leaves. SS was characterized by a strong near-vein chlorosis and reduced *NbSu* mRNA levels and was triggered only when amiR-NbSu-2 was highly expressed in tissues neighboring the petiole. Interestingly, the expression of a 22-nt form of amiR-NbSu-2 did not induce SS despite triggering the biogenesis of 21-nt phased secondary small interfering RNAs (siRNAs) from *NbSu* mRNAs. By combining sRNA high-throughput sequencing, 5' RLM-RACE and RT-PCR analyses we show that amiR-NbSu-2 is present and active in systemically silenced tissues, where it specifically cleaves *NbSu* mRNAs. Moreover, the transient expression of syn-tasiR-NbSu-2, a 21-nt syn-tasiRNA of identical sequence to amiR-NbSu-2, also triggers SS in a similar way. Our results indicate that both amiRNAs and syn-tasiRNAs can trigger the silencing of a plant endogenous gene in a distal tissue from where they are produced, in a process not requiring transitivity. They also suggest that both classes of art-sRNAs are able to move as 21-nt sRNA duplexes from cell to cell via plasmodesmata and long-distances to sink tissues through the phloem.

RESULTS

Local silencing of *N. benthamiana magnesium chelatase subunit CHLI* (*NbSu*) by specific amiRNAs causes strong bleaching phenotype in amiRNA-expressing tissues

Two amiRNA constructs (*35S:amiR-NbSu-1* and *35S:amiR-NbSu-2*), each expressing an amiRNA with no predicted off-targets in *N. benthamiana* and targeting a unique site in *NbSu* mRNA, were generated and independently agroinfiltrated in two areas of two leaves from three different *N. benthamiana* plants (Figure 1A). As a negative control, the *35S:amiR-GUS*$_{Nb}$ construct expressing a highly specific amiRNA against *Escherichia coli* b-glucuronidase *GUS* gene was also generated and agroinfiltrated. At 7 days post-agroinfiltration (dpa), areas agroinfiltrated with anti-*NbSu* amiRNA constructs displayed a visually obvious bleached

phenotype characteristic of *NbSu* knock-down (Tang *et al.*, 2010), while areas expressing *35S:amiR-GUS*$_{Nb}$ did not (Figure 1B). The chlorophyll analysis of agroinfiltrated areas showed a similar decrease in chlorophyll content in bleached areas expressing anti-*NbSu* amiRNA constructs compared to areas expressing the control construct (Figure 1C). To molecularly characterize amiRNA activity, two leaves of each of three different *N. benthamiana* plants were independently agroinfiltrated in the whole leaf surface with the amiRNA constructs described above, and amiRNA and target mRNA accumulation were analyzed at 2 dpa. RNA blot assays of RNA preparations from agroinfiltrated leaves showed that both anti-*NbSu* amiRNAs accumulated as single-size sRNA species, with amiR-NbSu-2 accumulating to significantly higher levels than amiR-NbSu-1 (Figure 1D). Finally, RT-qPCR analysis revealed that samples expressing anti-*NbSu* amiRNAs accumulated significantly lower levels of *NbSu* mRNA than control samples (Figure 1E). Taken together, these results indicate that both anti-*NbSu* amiRNAs are highly active and induce a strong bleaching phenotype in the tissue where they are expressed.

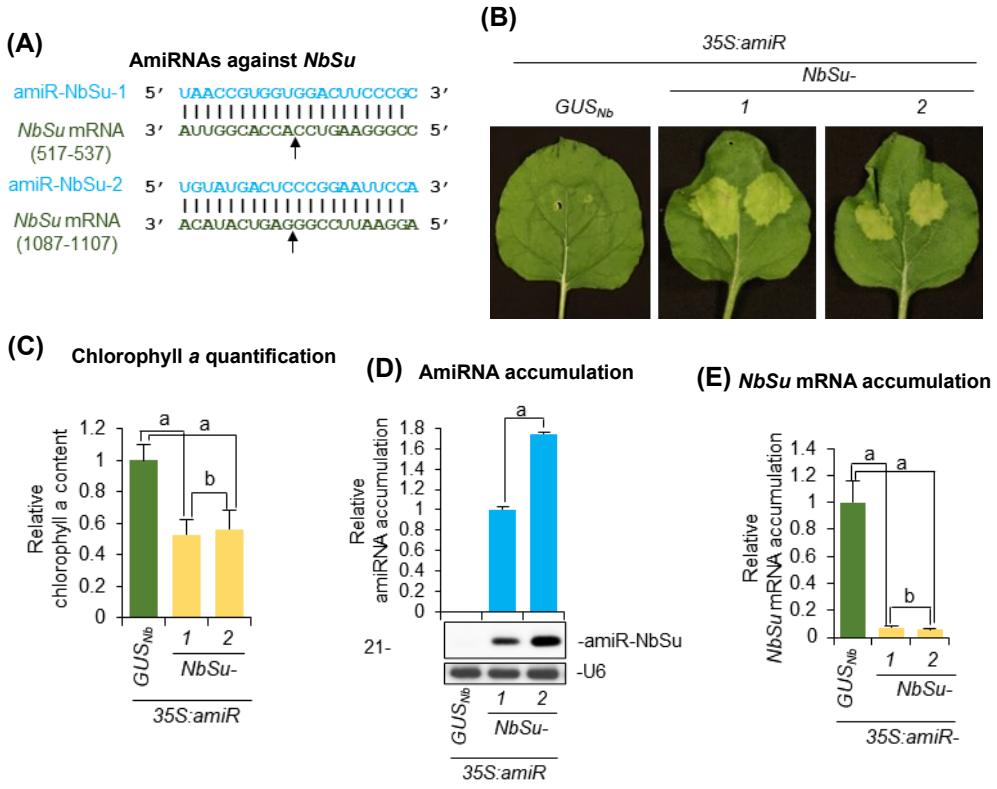

Figure 1. Functional analysis of artificial microRNAs (amiRNAs) against *Nicotiana benthamiana SULPHUR* (amiR-NbSu) in agroinfiltrated leaves. (**A**) Base-pairing of amiRNAs and *NbSu* target mRNAs. Coordinates of the complete target site in *NbSu* mRNAs are given. The arrows indicate the

amiRNA-predicted cleavage site. (**B**) Photos at 7 days post-agroinfiltration (dpa) of leaves agroinfiltrated with the different amiRNA constructs. (**C**) Bar graph showing the relative content of chlorophyll *a* in agroinfiltrated areas (*35S:amiR-GUS*$_{Nb}$ = 1.0). Bars with the letter 'a' are significantly different from that of sample *35S:amiR-GUS*$_{Nb}$ ($P < 0.01$ in pairwise Student's *t*-test comparisons). (**D**) Northern blot detection of amiR-NbSu amiRNAs in RNA preparations from agroinfiltrated leaves at 2 dpa. The graph at top shows the mean ($n = 3$) + standard deviation amiR-NbSu relative accumulation (*35S:amiR-NbSu-1* = 1.0). Bar with the letter 'a' is significantly different from that of sample *35S:amiR-NbSu-1*. Other details are as in Figure 1C. (**E**) Accumulation of *NbSu* mRNA. Mean relative level (n = 3) + standard error of *NbSu* mRNAs after normalization to *PROTEIN PHOSPHATASE 2A* (*PP2A*), as determined by quantitative RT-PCR (qPCR) (*35S:amiR-GUS*$_{Nb}$ = 1.0 in all comparisons). Other details are as in Figure1B.

Systemic silencing of *NbSu* in distal tissues is induced by the agroinfiltration of one of the two anti-*NbSu* amiRNA

Remarkably, when amiRNA constructs were agroinfiltrated in the whole surface of *N. benthamiana* leaves, a bleaching phenotype was also observed in upper non-agroinfiltrated leaves as early as 3 dpa only in plants agroinfiltrated with *35S:amiR-NbSu-2*. The distal bleaching phenotype was characterized by a vein-proximal chlorosis and was more intense at 7 dpa and even more at 14 dpa (Figure 2A). A closer analysis of chlorophyll autofluorescence confirmed that the bleached areas extended beyond the veins (Figure 2B), most likely to 10-15 cells as reported for siRNAs (Himber *et al.*, 2003). Importantly, RT-qPCR analysis showed that *NbSu* mRNA accumulation in distal silenced tissues was significantly decreased in plants expressing *35S:amiR-NbSu-2* compared to plants expressing *35S:amiR-GUS*$_{Nb}$ (Figure 2C). Moreover, this decrease was correlated with the bleaching intensity, as *NbSu* mRNA levels were significantly lower at 14 dpa compared to 7 dpa (Figure 2C). All in all, these results suggest that a silencing signal moves from source agroinfiltrated tissues to upper parts of the plants.

Systemic silencing requires amiRNA expression near the petiole and positively correlates with the level of amiRNA accumulation

Our previous experiment revealed that amiR-NbSu-2 triggered SS only when expressed in the whole leaf surface, but not when the amiRNA was expressed in a distal region of the leaf. Thus, we hypothesized that the movement of the silencing signal might require the expression of amiR-NbSu-2 in tissues surrounding the petiole connecting the leaf and stem vasculatures. To confirm this, *35S:amiR-NbSu-2* was independently agroinfiltrated in the basal region of one leaf of three different plants. The same construct was independently agroinfiltrated in the whole leaf surface or in a distal region of a leaf of three different plants as positive and negative control, respectively. The presence of local and systemic silencing was monitored by the appearance of bleaching in the agroinfiltrated area or near the leaf veins, respectively. Interestingly, all plants agroinfiltrated in the basal region of the leaf displayed SS, although with a slight delay and to a

lower intensity compared to plants agroinfiltrated in the whole leaf surface (Figure 3A and 3B). In contrast, plants agroinfiltrated in the distal region of the leaf did not display SS (Figure 3A and 3B). These results indicate that amiR-NbSu-2 must be expressed in leaf areas proximal to the petiole for triggering SS.

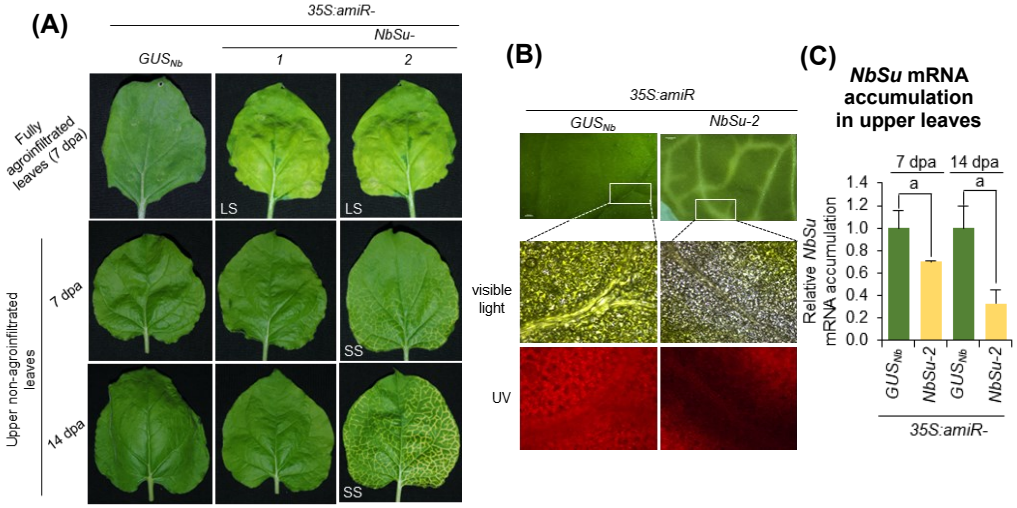

Figure 2. Analysis of upper non-agroinfiltrated tissues showing systemic silencing. (**A**) Photos of fully agroinfiltrated leaves at 7 d days post-agroinfiltration (dpa) (top), and of upper non-agroinfiltrated leaves at 7 dpa (middle) and 14 dpa (bottom). LS and SS refer to local and systemic silencing, respectively. A white arrow point to areas displaying near-vein chlorosis. (**B**) Photos of areas surrounding leaf nerves under visible or ultraviolet (UV) light from plants agroinfiltrated with *35S:amiR-GUS*$_{Nb}$ or *35S:amiR-NbSu-2*. (**C**) Accumulation of *NbSu* mRNA at 7 and 14 dpa in upper leaves of plants agroinfiltrated with *35S:amiR-GUS*$_{Nb}$ or *35S:amiR-NbSu-2*. Mean relative level (n = 3) + standard error of *NbSu* mRNAs after normalization to *PROTEIN PHOSPHATASE 2A* (*PP2A*), as determined by quantitative RT-PCR (qPCR) (*35S:amiR-GUS*$_{Nb}$ (7 dpa) = 1.0 in all comparisons). Other details are as in Fig 1B.

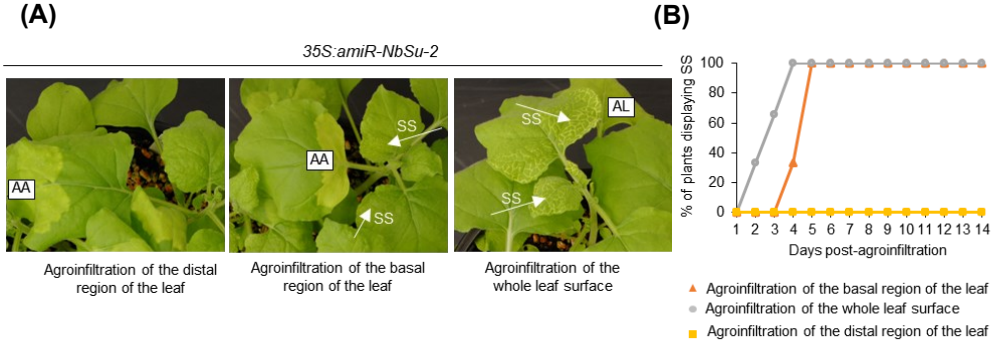

Figure 3. **Effects on systemic silencing of the place of expression of amiR-NbSu-2 in *N. benthamiana* leaves.** (**A**) Photos of plants at 7 days post-agroinfiltration (dpa). AA and AL refer to agroinfiltrated area and agroinfiltrated leaf, respectively. Near-vein chlorotic areas result of systemic silencing (SS) are pointed with

a white arrow. (**B**) Two-dimensional line graph showing, for each of the three-plant sets listed in the box, the percentage of plants displaying systemic silencing per day during 14 dpa.

Next, we studied if the appearance or intensity of systemic silencing induced by amiR-NbSu-1 and amiR-NbSu-2, respectively, could be correlated with the level of expression of the amiRNA in agroinfiltrated leaves. For that purpose, *35S:amiR-NbSu-1* and *35S:amiR-NbSu-2* were agroinfiltrated as before at two different final optical densities (ODs): 0.5 (the OD used in previous experiments) and 1.0. *35S:amiR-GUS$_{Nb}$* was also agroinfiltrated at 0.5 as negative control. In addition, constructs were also independently agroinfiltrated in two areas of two leaves of three plants to better visualize the degree of bleaching due to the high color contrast between yellow agroinfiltrated areas and dark green non-infiltrated areas. At 7 dpa, all agroinfiltrated areas were bleached except those agroinfiltrated with *35S:amiR-GUS$_{Nb}$* (Figure 4A, top panel). At 14 dpa, near-vein bleaching was more intense in upper leaves of plants with leaves fully agroinfiltrated with *35S:amiR-NbSu-2* at the highest OD (OD=1) (Figure 4A, lower panel). As before, no SS was observed in upper leaves of plants agroinfiltrated with *35S:amiR-NbSu-1* at OD=0.5. However, mild near-vein bleaching was detected in upper leaves of plants agroinfiltrated with *35S:amiR-NbSu-1* at OD=1 (Figure 4A, lower panel). RNA blot assays of RNA preparations from agroinfiltrated areas showed that, for both amiRNAs, amiRNA accumulation significantly increased with the OD at which the construct was agroinfiltrated (Figure 4B). Remarkably, near-vein bleaching intensity in upper leaves positively correlated with amiRNA accumulation in agroinfiltrated leaves. For instance, the strongest SS was observed in upper leaves of plants accumulating the highest amount of amiRNA in agroinfiltrated leaves, as observed in plants expressing *35S:amiR-NbSu-2* at OD=1. Interestingly, plants expressing *35S:amiR-NbSu-1* at OD=1 and *35S:amiR-NbSu-2* at OD=0.5 accumulated similar (intermediate) amounts of amiRNA in agroinfiltrated tissues (Figure 4B), although upper leaves of amiR-NbSu-2 expressing plants displayed more intense bleaching (Figure 4A, lower panel). Finally, RT-qPCR analysis confirmed the significant decrease of *NbSu* mRNA in leaves agroinfiltrated with any of the two anti-*NbSu* amiRNAs at any of the two ODs (Figure 4C). Still, for both amiRNAs, no significant differences in *NbSu* mRNA accumulation were observed when the amiRNA was expressed to a different OD (Figure 4C).

To further confirm that induction of SS was positively correlated with the level of amiRNA expression, *35S:amiR-NbSu-2* was agroinfiltrated at final ODs of 1, 0.5, 0.25, 0.125 and 0.0625. As before, *35S:amiR-GUS$_{Nb}$* was also agroinfiltrated at OD=0.5 as negative control. Visual analysis of agroinfiltrated areas revealed that all areas expressing *35S:amiR-NbSu-2* showed the bleaching phenotype, although the degree of bleaching was progressively reduced as the amiRNA was agroinfiltrated to a lower OD (Figure 4D). In contrast, systemic near-vein bleaching

was only observed in upper leaves of plants agroinfiltrated in the whole leaf surface with *35S:amiR-NbSu-2* to an OD≥0.25 (Figure 4D). Moreover, the intensity and spread of bleaching in upper leaves gradually decreased with the OD at which the construct was agroinfiltrated (Figure 4D). Taken together, these results indicate that the degree of SS positively correlates with the level of expression of the trigger amiRNA in the agroinfiltrated tissue.

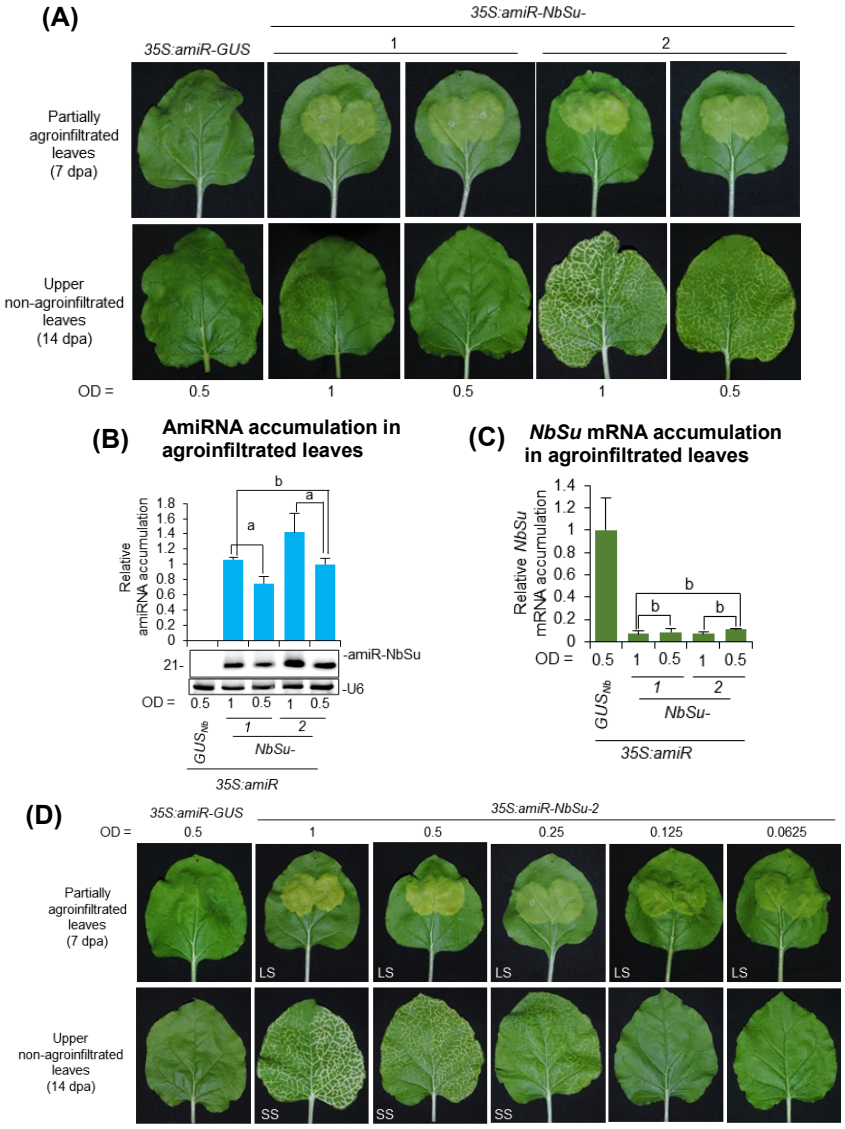

Figure 4. Effects of amiRNA expression level on systemic silencing induction. (**A**) Photos of partially agroinfiltrated leaves at 7 days post-agroinfiltration (dpa) (top), and of upper non-agroinfiltrated leaves at 14 dpa (bottom). AmiRNA constructs were agroinfiltrated to a final optical density (OD) of 1 or 0.5, as indicated. Other details are as in Figure 2A. (**B**) Northern blot detection of amiR-NbSu amiRNAs in RNA

preparations from agroinfiltrated leaves at 2 dpa. AmiRNA constructs were agroinfiltrated to a final OD of 1 or 0.5, as indicated. The graph at top shows the mean (*n* = 3) + standard deviation amiR-NbSu relative accumulation (*35S:amiR-NbSu-1* = 1.0). Bars with the letter 'a' are significantly different from that of sample *35S:amiR-NbSu-2* at OD = 0.5, while bar with the letter 'b' is not. Other details are as in Figure 1B. (**C**) Accumulation of *NbSu* mRNA in agroinfiltrated leaves. Mean relative level (n = 3) + standard error of *NbSu* mRNAs after normalization to *PROTEIN PHOSPHATASE 2A* (*PP2A*), as determined by quantitative RT-PCR (qPCR) [*35S:amiR-GUS*$_{Nb}$ (OD = 0.5) = 1.0 in all comparisons]. Other details are as in Figure 1B. (**D**) Photos of partially agroinfiltrated leaves at 7 dpa (top), and of upper non-agroinfiltrated leaves at 14 dpa (bottom). AmiRNA constructs were agroinfiltrated to a final OD of 1, 0.5, 0.25, 0.125 or 0.0625, as indicated. Other details are as in Figure 2A.

Secondary sRNAs are not the mobile signal

In some cases, sRNA-mediated cleavage of target RNAs can trigger the production of phased 21-nt secondary sRNAs from DCL4-processed dsRNAs synthesized by RDR6 complexes from one of the target cleaved products. This process of transitivity expands the set of sRNAs that can regulate a particular target and indeed enhances both cell autonomous and systemic silencing [reviewed recently in (de Felippes and Waterhouse, 2020)]. In this scenario, we hypothesized that both local and systemic silencing of *NbSu* might be explained, at least in part, by the activity of secondary sRNAs produced from *NbSu* mRNAs upon amiR-NbSu-2 targeting. Because transitivity is typically triggered by 22-nt sRNAs (Cuperus *et al.*, 2010; Chen *et al.*, 2010), we reasoned that 22-nt forms of amiR-NbSu-2 could enhance both local and systemic silencing. To this purpose, we engineered the *35S:amiR-NbSu-2-22* construct for expressing a 22-nt form of amiR-NbSu-2 (amiR-NbSu-2-22) from a modified *AtMIR390a* precursor as described before (Cuperus *et al.*, 2010) (Figure 5A). AmiR-NbSu-2-22 was engineered to fully base pair with *NbSu* mRNA to further enhance transitivity (Figure 5A).

35S:amiR-NbSu-2-22 was agroinfiltrated in two full leaves of each of three independent plants. For comparative purposes, *35S:amiR-NbSu-2* expressing a 21-nt form of amiR-NbSu-2 (Figure 1D) was also tested (Figure 5A), as well as the control construct expressing amiR-GUS$_{Nb}$. At 7 dpa, all leaves expressing 21- or 22-nt forms of amiR-NbSu-2 showed similar bleaching phenotype (Figure 5B) and chlorophyll content (Figure 5C). In contrast, only upper leaves of plants expressing 21-nt amiR-NbSu-2 showed near-vein bleaching (Figure 5B). RNA blot analysis of RNA preparations from agroinfiltrated leaves showed that amiR-NbSu-2-22 accumulated mainly as 22-nt sRNA species, and to apparently lower levels than 21-nt amiR-NbSu-2 (Figure 5D). To confirm the correct processing of amiRNA precursors and analyze the presence of *NbSu*-derived secondary sRNAs, sRNA libraries from leaves expressing *35S:amiR-GUS*$_{Nb}$, *35S:amiR-NbSu-2* and *35S:amiR-NbSu-2-22* were prepared and sequenced (Figure S3). In samples expressing *35S:amiR-NbSu-2*, the majority (82%) of 19-24-nt (+) reads corresponded to authentic 21-nt amiR-NbSu-2 (Figure 5E) while only 0.001% of the reads corresponded to misprocessed 22-nt forms. In contrast, only 23% of the reads from samples

expressing *35S:amiR-NbSu-2-22* corresponded to correct 22-nt forms, confirming our ability to produce authentic 22-nt forms of amiR-NbSu-2 *in vivo*. Unexpectedly, 57 % of reads in *35S:amiR-NbSu-2-22* samples corresponded to 21-nt forms of amiR-NbSu-2, which were not observed in the northern blot assay (Figure 5D). Still, it cannot be ruled out that sRNA library preparation and/or sequencing protocols contain biases that may preferentially increase the final number of 21-nt reads corresponding to amiR-NbSu-2. In any case, to be noted is that the lower proportion of correct 22-nt forms compared to 21-nt forms of amiR-NbSu-2 from *AtMIR390a*-based precursors was expected, as similar results were obtained before expressing 21-nt and 22-nt forms of *A. thaliana* miR173 (Cuperus *et al.*, 2010). Finally, in *35S:amiR-GUS$_{Nb}$*-expressing leaves, the majority (70%) of the reads corresponded to authentic 21-nt amiR-GUS$_{Nb}$ (Figure 5E) supporting the correct processing of *AtMIR390a-GUS$_{Nb}$* precursors.

Next, we analyzed the presence of predicted *NbSu*-derived secondary sRNAs in phase with amiR-NbSu-2 or amiR-NbSu-2-22 cleavage sites in agroinfiltrated leaves expressing *35S:amiR-NbSu-2* or *35S:amiR-NbSu-2-22*, respectively (Figure 5F, Data S1). No reads corresponding to 21-nt predicted phased sRNAs were observed among the sRNA reads sequenced from *35S:amiR-NbSu-2*-expressing leaves and mapping to *NbSu* (Data S1). In contrast, 39.4% of 21-nt sRNA reads from leaves expressing *35S:amiR-NbSu-2-22* were in register with amiR-NbSu-2-22 cleavage site (phasing register of 1) (Figure 5F, Data S1), confirming the presence of *NbSu*-derived secondary sRNAs only in *35S:amiR-NbSu-2-22* samples. Taken together, these results indicate that the accumulation of *NbSu*-derived secondary siRNAs triggered by amiR-NbSu-2-22 does not induce SS. Finally, *NbSu* target mRNA accumulation analyzed by RT-qPCR was drastically reduced in agroinfiltrated leaves expressing either 21- or 22-nt forms of amiR-NbSu-2 (Figure 5G).

To further confirm that the silencing effects induced by amiR-NbSu-2 were not caused by secondary sRNAs produced from targeted *NbSu* mRNAs, *35S:amiR-NbSu-2* and *35S:amiR-GUS$_{Nb}$* were agroinfiltrated in the whole surface of two leaves of three independent *N. benthamiana* DCL4i and RDR6i knock-down plants as well as in wild-type plants (Figure S1). DCL4i and RDR6i plants accumulate low levels of DCL4 and RDR6 respectively (Schwach *et al.*, 2005; Dadami *et al.*, 2013) (Figure S1A), which are key components of secondary sRNA biogenesis pathways. As before, constructs were also infiltrated in two areas of two leaves of three independent plants for each plant genotype for better visualization of the bleaching phenotype. Similar bleached phenotypes were observed both in agroinfiltrated areas and upper non-agroinfiltrated leaves of wild-type, DCL4i or RDR6i plants expressing *35S:amiR-NbSu-2*, while no bleached phenotypes were observed in control agroinfiltrations (Figure S1B).

Therefore, these results strongly suggest that neither the local nor the systemic silencing of *NbSu* is caused by *NbSu*-derived secondary sRNAs.

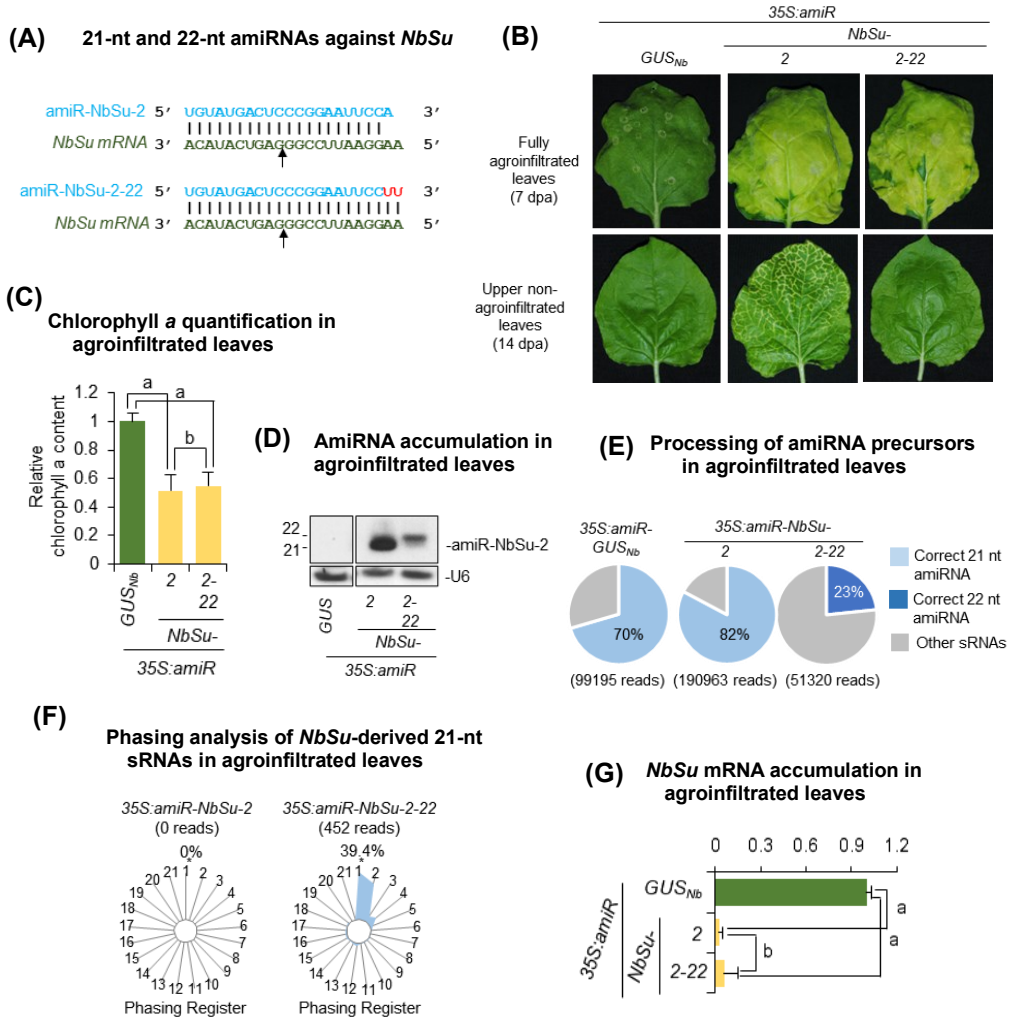

Figure 5. Comparative analysis of silencing effects triggered by 21-nucleotide (nt) or 22-nt forms of amiR-NbSu-2. (**A**) Base-pairing of -amiRNAs and *NbSu* target mRNAs. Nucleotides changed or added respect to amiR-NbSu-2 are in red. Other details are as in Figure 1A. (**B**) Top, photos at 7 days post-agroinfiltration (dpa) of leaves agroinfiltrated with the different amiRNA constructs. Bottom, photos at 14 dpa of upper non-agroinfiltrated leaves from plants agroinfiltrated with the different constructs. (**C**) Bar graph showing the relative content of chlorophyll *a* in agroinfiltrated areas (*35S:amiR-GUS*$_{Nb}$ = 1.0). Other details are as in Figure 1C and 2A. (**D**) Northern blot detection of amiR-NbSu-2 21 and 22-nt forms in RNA preparations from agroinfiltrated leaves at 2 dpa. (**E**) AmiRNA processing from *AtMIR390a*-based precursors. Pie charts show percentages of reads corresponding to expected, accurately processed 21-nt or 22-nt mature amiRNAs (light or dark grey sections, respectively) o to other 19-24 nt sRNAs (grey

sectors). (**F**) Phasing analysis of *NbSu*-derived 21-nt sRNAs. Radar plots show proportions of 21-nt reads corresponding to each of the 21 registers from *AtTAS1c* transcripts, with position 1 designated as immediately after the amiR-NbSu-2/amiR-NbSu-2-22 guided cleavage site. The percentage of 21-nt reads corresponding to phasing register 1 is indicated. (**G**) Accumulation of *NbSu* mRNA in agroinfiltrated leaves. Other details are as in Figure 1E.

AmiR-NbSu-2 moves from agroinfiltrated tissue to upper, distal silenced tissues

Next, we reasoned that the SS of *NbSu* in *35S:amiR-NbSu-2*-expressing plants could be the direct result of amiR-NbSu-2 cleavage activity in upper tissues. First, to check the presence of amiR-NbSu-2 in upper bleached tissues, sRNA libraries were prepared from leaf areas including the near-vein bleached phenotype, as well as control libraries from upper tissues of amiR-GUS_{Nb}-expressing plants. Reads corresponding to amiR-NbSu-2 were detected to a relatively high number (70 reads per million, RPM) in upper leaves, although this number was clearly lower than that of reads from agroinfiltrated leaves (5338 RPM) (Figure 6A). Importantly, amiR-NbSu-2 reads were essentially absent in both agroinfiltrated and upper leaves from plants expressing amiR-GUS_{Nb} (Figure S2), thus confirming the specificity of the sequencing results. The presence of amiR-GUS_{Nb} was also confirmed both in agroinfiltrated leaves and upper leaves from plants expressing amiR-GUS_{Nb} but not from plants expressing amiR-NbSu-2 (Figure S2). Interestingly, reads corresponding to amiRNA star strands (amiRNA*) of both amiRNAs were detected in agroinfiltrated and in upper leaves (Figure 6A). Thus, these results indicate that amiRNA duplexes are present in upper tissues. And second, to check amiR-NbSu-2 cleavage activity in distal tissues, RNA ligase-mediated rapid amplification of 5' cDNA ends (5'RLM-RACE) analysis was done in upper leaves of amiR-NbSu-2-expressing plants showing the near-vein bleaching phenotype (Figure 6B). For control purposes, the same analysis was done in similar leaves of plants agroinfiltrated with *35S:amiR-GUS_{Nb}*. 3' cleavage products of the expected size (213 bp) were detected in samples expressing amiR-NbSu-2- but not in samples from amiR-GUS_{Nb}-expressing plants (Figure 6B). Sequencing analysis confirmed that all (12/12) the sequences comprising these products contained a canonical 5' end position predicted for amiR-NbSu-2-guided cleavage (Figure 6B). These results indicate that amiR-NbSu-2 is cleaving *NbSu* mRNAs at the predicted position in upper non-agroinfiltrated tissues.

Finally, we reasoned that the presence of amiR-NbSu-2 in upper tissues could result from the movement of the amiRNA precursor or of the amiRNA duplex itself from the agroinfiltrated leaves. To clarify the identity of the mobile molecule(s) causing SS, the presence of 521-nt *AtMIR390a-NbSu-2* amiRNA precursors was analyzed by RT-PCR in both source and recipient tissues. *AtMIR390a-NbSu-2* precursors were detected in RNA preparations of infiltrated leaves but not from those from upper leaves (Figure 6C) thus suggesting that amiR-NbSu-2 duplexes and not their precursors may be the mobile entities causing SS.

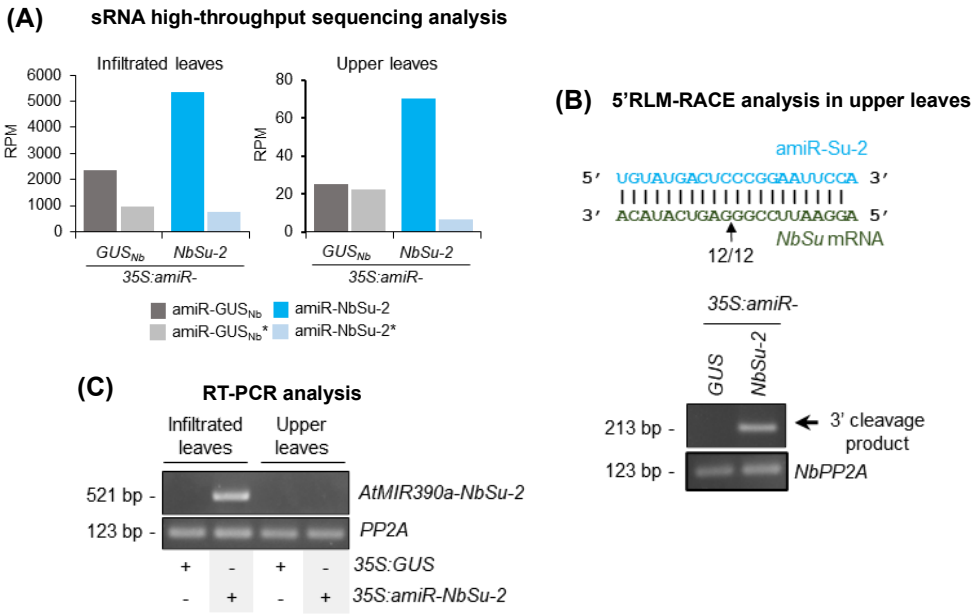

Figure 6. Analysis of amiRNA presence and activity in distal tissues. (**A**) Bar graph showing the accumulation (reads per million, RPM) of both amiRNA duplex strands revealed by high-throughput sequencing of small RNA libraries prepared from agroinfiltrated leaves (left) or from upper non-agroinfiltrated leaves (right). Bars representing amiR-GUS$_{Nb}$ guide and star strands RPMs are in dark and light grey, respectively. Bars representing amiR-NbSu-2 guide and star strands RPMs are in dark and light blue, respectively. (**B**) RT-PCR detection of *AtMIR390a-NbSu-2* precursors in agroinfiltrated or upper non-agroinfiltrated leaves (top). RT-PCR products corresponding to the control *NbPP2A* are also shown (bottom). (**C**) 5' RLM-RACE analysis of amiR-NbSu-2-guided cleavage of *NbSu* in upper leaves. At the top panel, the predicted base-pairing between amiR-NbSu-2 and *NbSu* mRNA is shown, and the expected amiR-NbSu-2-based cleavage site is indicated by an arrow. The proportion of cloned 5'-RLM-RACE products at the at the expected cleavage site is shown for amiR-NbSu-2-expressing leaves. At the bottom panel, ethidium bromide-stained gel shows 5'-RLM-RACE products corresponding to the 3' cleavage product from amiR-NbSu-2-guided cleavage (top gel), and RT-PCR products corresponding to the control *NbPP2A* gene (bottom gel). The position and size of the expected amiRNA-based 5'-RLM-RACE products are indicated, as well as the position and size of control RT-PCR products.

SS can also be triggered by a 21-nucleotide syn-tasiRNA

Mobility of plant miRNAs and tasiRNAs may differ according to previous reports (de Felippes *et al.*, 2011), and tasiRNAs have only been shown to move short-range as non-cell-autonomous signals (Chitwood *et al.*, 2009). Here, we explored if syn-tasiR-NbSu-2, a syn-tasiRNA of identical sequence to amiR-NbSu-2, was able to trigger SS. To that purpose, the *35S:syn-tasiR-NbSu-2* construct was generated, as well as the *35S:syn-tasiR-GUS$_{Nb}$* control construct aimed to express syn-tasiR-GUS$_{Nb}$, a syn-tasiRNA with identical sequence to that of amiR-GUS$_{Nb}$ (Figure 7A). Both constructs were independently agroinfiltrated in *N. benthamiana* plants as explained before, and in parallel with *35S:amiR-NbSu-2* for control purposes. At 7 dpa, areas

agroinfiltrated with *35S:amiR-NbSu-2* or *35S:syn-tasiR-NbSu-2* showed comparable bleaching degree (Figure 7B), which was confirmed by a similar decrease in chlorophyll levels in these areas (Figure 7C). Interestingly, amiR-NbSu-2 accumulated to significantly higher levels than syn-tasiR-NbSu-2 (Figure 7D) but induced comparable down-regulation of *NbSu* mRNA in agroinfiltrated leaves (Figure 7E). To confirm the correct processing of *AtTAS1c*-based syn-tasiRNA precursors, sRNA libraries from leaves expressing *35S:syn-tasiR-GUS$_{Nb}$* and *35S:syn-tasiR-NbSu-2* were prepared and sequenced. Both precursors were processed accurately, as 78 and 65 % of the reads corresponded to authentic 21-nt syn-tasiR-GUS$_{Nb}$ and syn-tasiR-NbSu-2, respectively (Figure 7F). Importantly, systemic near-vein bleaching was observed in upper leaves from plants expressing *35S:syn-tasiR-NbSu-2*, although with a lower intensity than in similar leaves from *35S:amiR-NbSu-2*-expressing plants (Figure 7B). Not surprisingly, *NbSu* mRNA accumulation was significantly lower in distal bleached tissues from plants expressing amiR-NbSu-2 compared to plants expressing syn-tasiR-NbSu-2 (Figure 7G). Also, as shown for amiR-NbSu-2, syn-tasiR-NbSu-2 must also be expressed in leaf areas proximal to the petiole for triggering SS (Figure S4). Finally, we tested the speed of syn-tasiR-NbSu-2 and amiR-NbSu-2 movement by removing the agroinfiltrated leaves 1, 2, 3, 4 or 5 dpa and scoring the say of near-vein leaf chlorosis appearance in apical leaves. For syn-tasiR-NbSu-2, 50% and 100% of plants exhibited SS when the agroinfiltrated leaves were removed 2 and 3 dpa, respectively, while all plants in which the *35S:amiR-NbSu-2*-expressing leaves were removed at 2 dpa showed SS (Figure S5). These results suggest that the production and translocation of the amiRNA and syn-tasiRNA duplexes occurs within 1-2 and 1-3 dpa, respectively.

To analyze the presence of syn-tasiRNAs in upper tissues, sRNA libraries were prepared from near-vein bleached samples of syn-tasiR-NbSu-2-expressing plants, together with control libraries from similar tissues of syn-tasiR-GUS$_{Nb}$-expressing plants. Reads corresponding to syn-tasiR-NbSu-2 were detected in upper leaves (9.4 RPM), although to a much lower number than in agroinfiltrated leaves (2280 RPM) (Figure 8A), and were essentially absent in *35S:syn-tasiR-GUS$_{Nb}$* samples (Figure S3). The presence syn-tasiR-GUS$_{Nb}$ was also confirmed in upper (6.9 RPM) and in agroinfiltrated tissues (3399 RPM), and was negligible in *35S:syn-tasiR-NbSu-2* samples (Figure S3). Reads corresponding to syn-tasiRNA star strands (syn-tasiRNA*) of both syn-tasiRNA species were also detected in both agroinfiltrated and upper tissue, thus indicating the syn-tasiRNA duplexes are present in upper tissues. 5'RLM-RACE analysis confirmed the presence of 3' products derived from syn-tasiR-NbSu-2 cleavage of *NbSu* mRNAs in near-vein bleached tissues (Figure 8B). Finally, *AtTAS1c-NbSu-2* precursors could only be detected in agroinfiltrated tissues but not in upper leaves (Figure 8C). All together, these

results suggest that 21-nt syn-tasiRNA duplexes can also move from transiently expressing tissues to upper distal parts of the plant to silence target mRNAs.

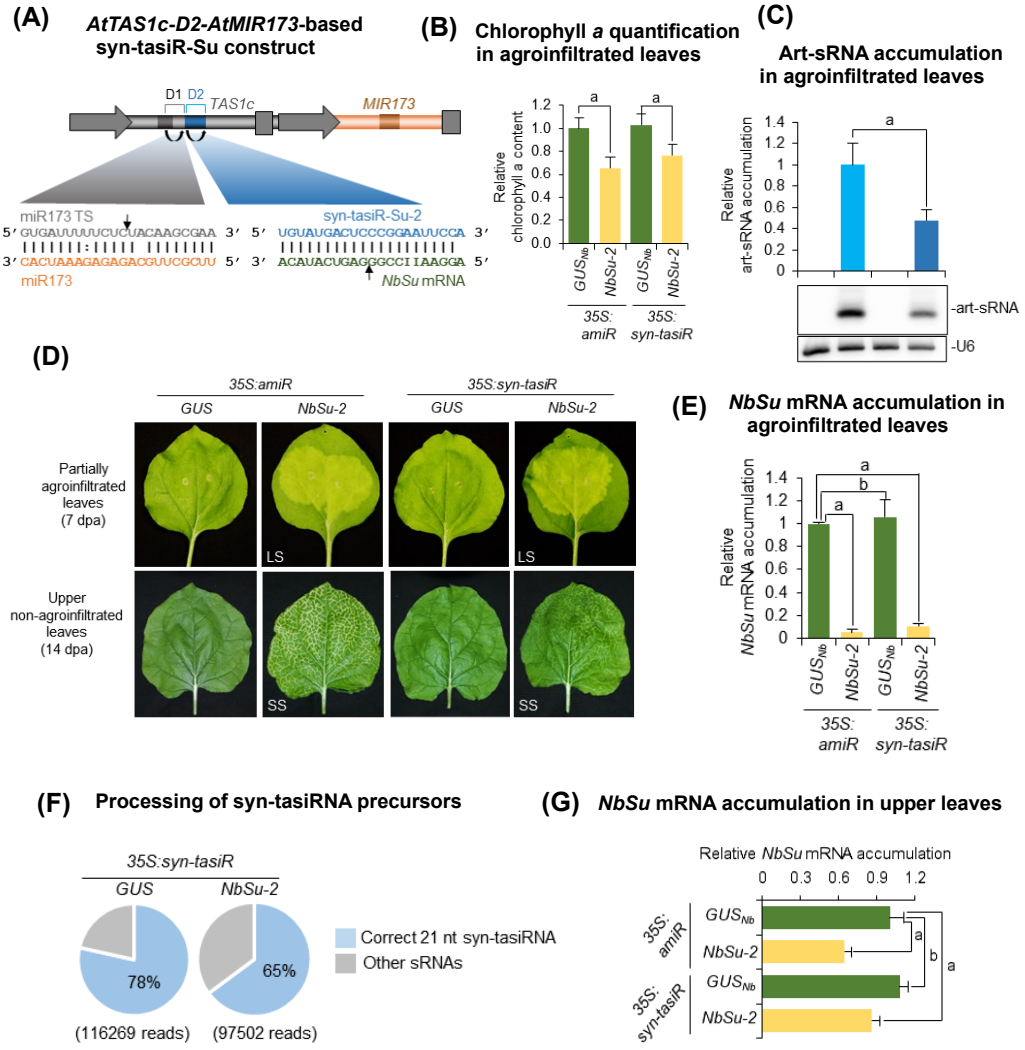

Figure 7. Functional analysis of synthetic trans-acting small interfering RNAs (syn-tasiRNAs) against *Nicotiana benthamiana SULPHUR* (amiR-NbSu) in agroinfiltrated and upper leaves. (**A**) Diagram of the *35S:syn-tasiR-Su-2* construct. *AtMIR173* and miR173 sequences are shown in light and dark brown, respectively, while syn-tasiR-NbSu-2 and NbSu mRNA sequences are in blue and green, respectively. tasiRNA positions 3'D1[+] and 3'D2[+] are indicated by brackets, with position 3'D2[+] highlighted in blue. Curved black arrows indicate DCL4 processing sites. Black linear arrow indicate sRNA-guided cleavage sites. ts refers to target site. (**B**) Photos of partially agroinfiltrated leaves at 7 days-post agroinfiltration (dpa) (top), and of upper non-agroinfiltrated leaves at 14 dpa (bottom). Other details are as in Figure 2A. (**C**) Bar graph showing the relative content of chlorophyll *a* in agroinfiltrated areas (*35S:amiR-GUS*$_{Nb}$ = 1.0). Other details are as in Figure 1C and 2A. (**D**) Northern blot detection of artificial small RNAs (art-sRNAs) against *NbSu* in RNA preparations from agroinfiltrated leaves at 2 dpa. The graph at top shows

the mean (*n* = 3) + standard deviation art-sRNA relative accumulation (*35S:amiR-NbSu-2* = 1.0). Bar with the letter 'a' is significantly different from that of sample *35S:amiR-NbSu-2*. Other details are as in Figure 1C. (**E**) Accumulation of *NbSu* mRNA in agroinfiltrated leaves. Other details are as in Figure 1E. (**F**) Syn-tasiRNA processing from *AtTAS1c*-based precursors. Pie charts show percentages of reads, with the percentage of 21-nt reads of accurately processed mature syn-tasiRNAs indicated in the blue sectors. Grey sectors represent the percentage of 19-24 nt reads of other small RNAs. (**G**) Accumulation of *NbSu* mRNA in upper non-agroinfiltrated leaves. Other details are as in Figure 1E.

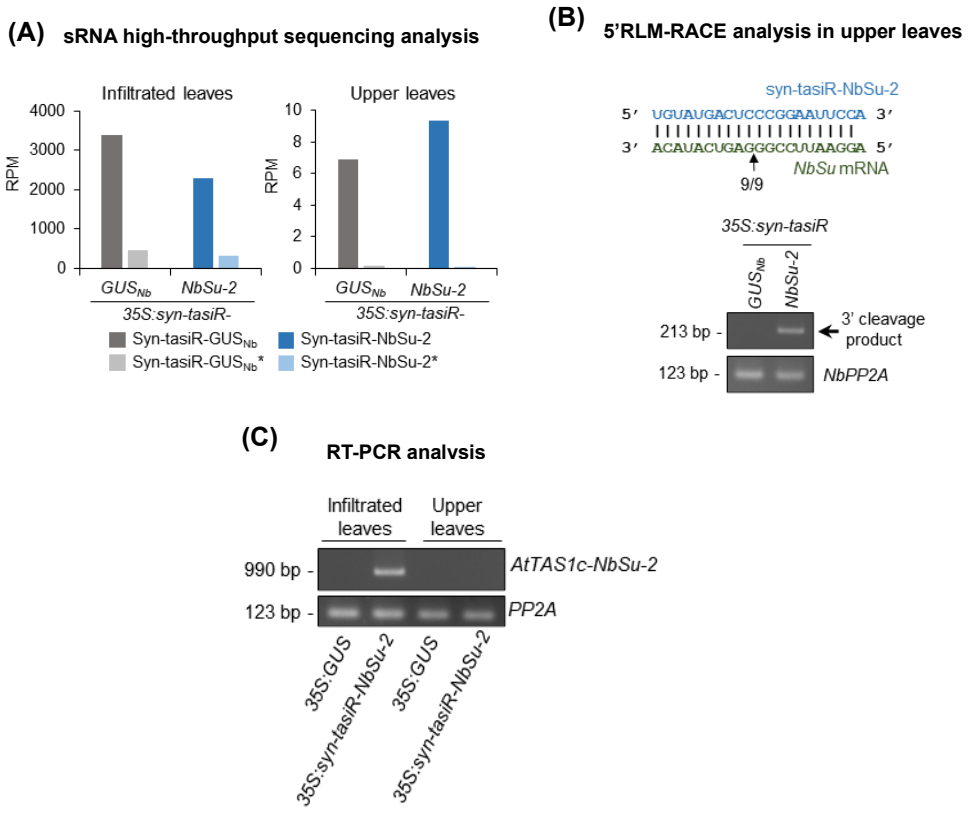

Figure 8. **Analysis of syn-tasiRNA presence and activity in distal tissues.** (**A**) Bar graph showing the accumulation (reads per million, RPM) of both syn-tasiRNA duplex strands revealed by high-throughput sequencing of small RNA libraries prepared from agroinfiltrated leaves (left) or from upper non-agroinfiltrated leaves (right). Bars representing syn-tasiR-GUS_{Nb} guide and star strands RPMs are in dark and light grey, respectively. Bars representing syn-tasiR-NbSu-2 guide and star strands RPMs are in dark and light blue, respectively. (**B**) 5' RLM-RACE analysis of syn-tasiR-NbSu-2-guided cleavage of *NbSu* in upper leaves. At the top panel, the predicted base-pairing between syn-tasiR-NbSu-2 and *NbSu* mRNA is shown, and the expected syn-tasiR-NbSu-2-based cleavage site is indicated by an arrow. Other details are as in Figure 5C. (**C**) RT-PCR detection of *AtTAS1c-NbSu-2* precursors in agroinfiltrated or upper non-agroinfiltrated leaves (top). Other details are as in Figure 5B.

DISCUSSION

Here we report the ability of two classes of 21-nt art-sRNAs, such as amiRNAs and syn-tasiRNAs, to move throughout the plant away from their production sites and systemically silence a plant endogenous gene. AmiR-NbSu-2 and syn-tasiR-NbSu-2 were agroinfiltrated in the whole surface of *N. benthamiana* leaves and induced the SS of *NbSu* which was easily detected as a strong chlorosis near the veins of upper distal leaves. Importantly, we were able to visualize the SS of *NbSu* because of the characteristic bleaching phenotype derived from *NbSu* down-regulation, which is clearly visible to the naked eye. In this sense, the *N. benthamiana*/amiR-NbSu-2 and *N. benthamiana*/syn-tasiR-NbSu-2 experimental systems may represent valuable tools with a clear and visible readout for the analysis of determinants controlling the induction and/or spread of the SS triggered by plant sRNAs.

Our initial experiments comparing the induction of local and systemic silencing by amiR-NbSu-1 and amiR-NbSu-2 showed that while local silencing efficiency was similar for both amiRNAs, SS was triggered only by amiR-NbSu-2. Because amiR-NSu-2 accumulated to significantly higher levels compared to amiR-NbSu-1 in agroinfiltrated tissues, we explored if the degree of SS was dependent on the local accumulation level of the amiRNA. Subsequent experiments testing SS induction upon agroinfiltration of amiRNA constructs to different ODs showed that the intensity of SS triggered by amiR-NbSu-2 indeed positively correlated with the expression level of amiR-NbSu-2 in agroinfiltrated leaves. Moreover, amiR-NbSu-1 was able to trigger SS only when expressed at the higher OD tested (OD=1), thus highlighting that amiRNA expression level is a critical factor for SS induction. Similarly, the systemic movement of siRNAs has also been positively correlated with their expression level, when a higher copy number of a triggering transgene led to more efficient acquired silencing (Palauqui and Balzergue, 1999).

Another critical factor controlling SS induction could be the place of expression of the art-sRNA. It has been previously suggested that the limited entry of endogenous miRNAs into the phloem suggests that the expression in phloem companion cells might be a requirement for long-distance transport of miRNAs (Skopelitis *et al.*, 2018; Subramanian, 2019). Indeed, long-distance signalling miRNAs such as miR395 and miR399, known to control shoot-to-root communication upon S and P starvation, respectively, are expressed in companion cells of the phloem (Kawashima *et al.*, 2009) and in several vascular tissues including the phloem (Aung *et al.*, 2006). In our experiments, amiR-NbSu-2 and syn-tasiR-NbSu-2 triggered SS only when agroinfiltrated in areas neighbouring the leaf petiole but not in distal regions of the leaf. Thus, it is likely that amiR-NbSu-2 and syn-tasiR-NbSu-2, when expressed near the petiole, can reach the companion cells and be loaded into the sieve elements of the phloem for long-distance

movement. To be noted is that although the movement of a SS signal can be bidirectional in plants (Voinnet *et al.*, 1998), in our experimental conditions we could only detect near-vein chlorosis in leaves above those agroinfiltrated with *35S:amiR-NbSu-2* or *35S:syn-tasiR-NbSu-2*, but not in lower leaves (Table S1). This probably reflects that the pattern of spread of art-sRNA duplexes follows the movement of photoassimilates or viruses in plants, from source (older) to sink (younger) leaves (Voinnet *et al.*, 1998; Leisner and Turgeon, 1993).

Although a few miRNAs can move systemically in plants (see below), siRNAs are considered to be more mobile at long distances. For instance, secondary siRNAs generated from transgenes or from invading viruses propagate the spread of silencing from a single leaf systemically throughout the plant, and siRNAs (especially those of 24 nts) travel systemically to direct DNA methylation of transposable elements in target tissues, including meristematic and meiotically active cells (Liu and Chen, 2018; Molnar *et al.*, 2010). However, tasiRNA mobility appears to be more limited, as exemplified by miR390a-*TAS3*-dependent tasiRNA-AUXIN RESPONSE FACTORs (tasi-ARFs) that are produced in the upper side of the leaf and diffuse to create a gradient that patterns the adaxial-abaxial axis of leaves (Chitwood *et al.*, 2009). Thus, our results showing syn-tasiRNA systemic movement indicate that tasiRNAs can actually move long-distances, and it is possible that the overexpression of syn-tasiR-NbSu-2 in our experiments has facilitated this.

An interesting result is that amiR-NbSu-2 and syn-tasiR-NbSu-2, despite having identical sequences, caused distinct degrees of SS. SS triggered by amiR-NbSu-2 was more intense and extended much further than that induced by syn-tasiR-NbSu-2. Which factor(s) could explain the differences in SS intensity caused by both classes of art-sRNAs? The simplest explanation may be that the accumulation level of the art-sRNA plays a critical role in this matter, as amiR-NbSu-2 accumulated in agroinfiltrated source tissues to significantly higher levels compared to syn-tasiR-NbSu-2, which may facilitate its earlier entry to the phloem stream (Figure S5). Still, we cannot rule out that other factors such as the specific genetic requirements for amiRNA and syn-tasiRNA biogenesis may contribute to these differences. Interestingly, Arabidopsis transgenic plants expressing a syn-tasiRNA against *SULPHUR* (tasiR-SUL) from the companion cell-expressing *SUC2* promoter have extended bleaching compared to plants expressing an amiRNA (amiR-SUL) of identical sequence from the same promoter, despite tasiR-SUL accumulates to significantly lower levels compared to amiR-SUL (de Felippes *et al.*, 2011). In this case, more secondary sRNAs were detected in tasiR-SUL plants than in amiR-SUL plants, which was proposed to contribute to the spreading of tasiR-SUL triggered silencing (de Felippes *et al.*, 2011). Because tasiRNA biogenesis occurs on membrane-bound polysomes (Hou *et al.*, 2016; Li *et al.*, 2016), it has also been suggested that this may have facilitated tasiR-

SUL delivery to adjacent cells through plasmodesmata, which are extensions of cellular membranes (Liu *et al.*, 2020). In our experiments, the lack of secondary sRNAs in leaves expressing amiR-NbSu-2 or syn-tasiR-NbSu-2 and the transient expression of both art-sRNA classes may explain the different effects obtained in our system.

It has been proposed that the ability to trigger transitivity (secondary siRNA biogenesis) to amplify and spread the silencing signal to nearby cells may be also a critical factor for effective long-distance movement of miRNAs (Skopelitis *et al.*, 2018). Indeed, both systemically mobile miR395 and miR399 can trigger transitive silencing (Manavella *et al.*, 2012), as well as the majority of the miRNAs shown to move from a parasitic plant to its host plants and silence host genes (Shahid *et al.*, 2018). Also, it was shown that transgenic Arabidopsis expressing a 22-nt but not a 21-nt amiRNA against *CHALCONE SYNTHASE* (*CHS*) induced widespread silencing of CHS, most likely due to the greater mobility of secondary sRNAs and/or the additive effect of both amiRNA and phasiRNA-directed target mRNA cleavage (McHale *et al.*, 2013). Here, essentially no reads corresponding to 21-nt predicted phased sRNAs were observed among the sRNA reads mapping to *NbSu* and sequenced from agroinfiltrated and systemically silenced tissues of plants expressing *35S:amiR-NbSu-2* or *35S:syn-tasiR-NbSu-2* (Data S1). This indicates that 21-nt forms of amiR-NbSu-2 and syn-tasiR-NbSu-2 do not trigger the production of phased 21-nt secondary sRNAs neither in agroinfiltrated nor in upper tissues. In contrast, 22-nt forms of amiR-NbSu-2 triggered transitivity in agroinfiltrated tissues but not SS in distal tissues. Thus, in our system the ability to trigger transitivity is not a critical factor promoting SS. Indeed, amiR-NbSu-2-22 forms and *NbSu*-derived phased secondary sRNAs accumulated to much lower levels compared to 21-nt amiR-NbSu-2 forms, which may have limited the capacity of inducing SS. In any case, it is possible that SS induced by 22-nt amiRNAs might allow target silencing in distal tissues beyond the 10-15 cells but has the drawback of a high risk of off-target effects, as the large population of generated secondary sRNAs may end up targeting other cellular mRNAs besides the intended target RNA (Senthil-Kumar and Mysore, 2011).

Another interesting result is that both amiRNA and syn-tasiRNA duplexes, and not their precursors, seem to be the molecules moving systemically. Our results seem to support the current prevailing view for both plant miRNAs (Buhtz *et al.*, 2010; Skopelitis *et al.*, 2018; Liu and Chen, 2018; Brioudes *et al.*, 2021) and siRNAs (Devers *et al.*, 2020) that processed sRNAs and not their precursors are the moving entities. Nonetheless, some miRNA precursors such as *MIR156* and *MIR2111* are expressed specifically within the phloem (Tsikou *et al.*, 2018; Yang *et al.*, 2013), and recent results show that i) miR390b precursors enable the phloem transport of foreign RNA systemically in *N. benthamiana* and ii) sequences of multiple miRNA precursors are identified in a *Cucurbita maxima* phloem transcriptome (Lezzhov *et al.*, 2019). These

observations suggest that, at least for some miRNAs, miRNA phloem signalling might involve the precursor molecules. Moreover, it could be argued that anti-*NbSu* art-sRNAs could also be moving systemically bound to AGOs. However, this seems unlikely because i) star strands of both art-sRNA classes are present in distal tissues, ii) AGO proteins are systematically absent from Arabidopsis phloem sap proteomes (Batailler *et al.*, 2012; Guelette *et al.*, 2012; Carella *et al.*, 2016), and iii) AGO proteins generally act cell autonomously and are retained in traversed cells (Devers *et al.*, 2020). In any case, the question of the molecular forms under which plant sRNAs move between cells and long distance is still a matter of study and debate. Here, we propose a model (Figure 9) in which art-sRNA duplexes are produced in source cells by DCL-mediated processing of their precursors, move cell to cell through plasmodesmata and long-distance through the phloem stream, exit the phloem and move 10-15 cells away to silence target RNAs.

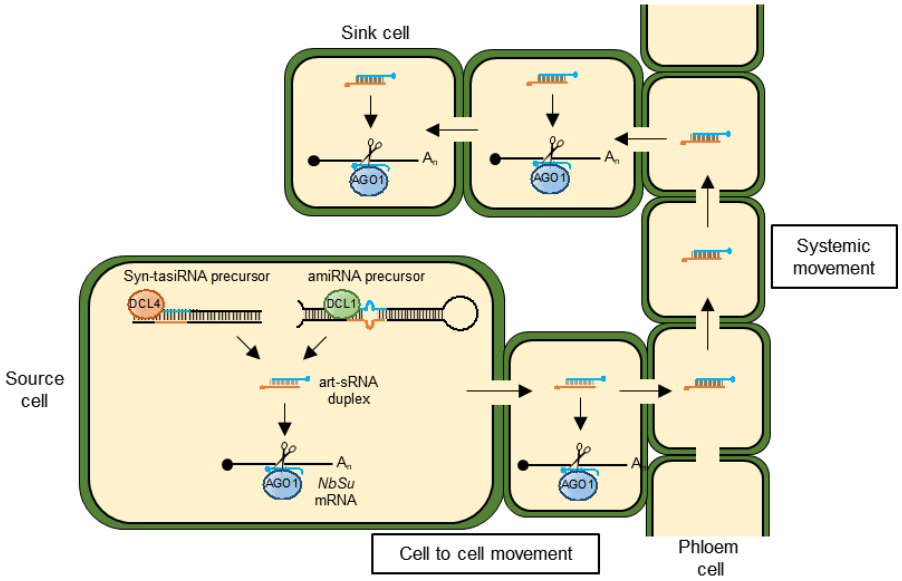

Figure 9. Model describing artificial small RNA (art-sRNA) biogenesis, silencing activity and movement from source to distal plant tissues. Art-sRNA duplexes are produced in source cells by DCL1- or DCL4-mediated processing of artificial microRNA (amiRNA) or synthetic trans-acting small interfering RNA (syn-tasiRNA) precursors, respectively. The guide strand (in blue) of the art-sRNA duplex is incorporated into ARGONAUTE1 (AGO1) to bind and cleave *NbSu* target mRNAs. Art-sRNA duplexes most likely move cell to cell through plasmodesmata and long-distance through the phloem stream using the sieves elements. Art-sRNA duplexes may exit the sieve elements and move 10-15 cells away.

Importantly, the ability of art-sRNA duplexes of moving from the production site to other distal tissues could be exploited to induce the intentional SS of plant genes and also of pathogenic target RNAs. For instance, we recently described a high-throughput methodology in *N. benthamiana* to identify art-sRNAs with high antiviral activity (Carbonell and Daròs, 2019), and reported that several amiRNAs and syn-tasiRNAs against *Tomato spotted wilt virus* (TSWV) expressed in the whole surface of *N. benthamiana* leaves which were further inoculated with TSWV two days later fully protected plants (Carbonell *et al.*, 2019). The complete absence of virus in upper leaves was somehow surprising, as art-sRNAs were transiently (and not constitutively) expressed. Considering our results presented here, now we suspect that anti-TSWV art-sRNAs were probably moving systemically to the upper leaves and accumulating in a 10-15 cell layer near the veins to block virus exit from the phloem and ultimately preventing its spread. Moreover, this may be the basis of a previously proposed antiviral mechanism in plants in which, upon viral infection, virus derived siRNAs would move from production sites into the phloem to finally reach the meristems and surrounding cells of the shoot apex ahead of the systemically mobile virus (Schwach *et al.*, 2005; Ratcliff *et al.*, 1997). As a consequence, the virus will be suppressed as it enters the meristematic cells so the infection is never established and the plant initiates its recovery (Melnyk *et al.*, 2011). Besides its antiviral function, other observations have highlighted the role of SS as a natural signaling mechanism involved in plant development and physiology. For instance, the control of phosphate, copper and sulphate homeostasis relies on the systemic movement of miR399, miR398 and miR395, respectively (Pant *et al.*, 2008; Matthewman *et al.*, 2012; Buhtz *et al.*, 2010; Fujii *et al.*, 2005), while the dynamic and systemic fine-tuning of infection and nodulation by nitrogen and symbiotic rhizobia is controlled by mobile miR2111 (Gautrat *et al.*, 2020; Tsikou *et al.*, 2018).

To conclude, the possibility of expressing art-sRNAs in a plant tissue and trigger the specific silencing of endogenous plant genes or even pathogenic RNAs in distal tissues in a transitivity-independent manner has undoubtedly high biotechnological potential, especially if art-sRNAs are applied exogenously in a GMO-free way. Indeed, antiviral systemic effects of sprayed dsRNAs in plant leaves have recently be reported (Koch *et al.*, 2016; Mitter *et al.*, 2017). In this context, the exogenous application of amiRNAs or syn-tasiRNAs would have the inherent advantage of their higher specificity, as they function in a transitivity-independent manner and lead to reduced off-target risks compared to dsRNA-based approaches. The optimization of methods for producing and topically applying art-sRNA precursors are also necessary for the biotechnological use of art-sRNAs for highly specific silencing at the whole-individual level in next-generation crops.

METHODS

Plant materials and growing conditions

Nicotiana benthamiana plants were grown in a growth chamber at 25ºC with a 12-light/12 h-dark photoperiod. DCL4i and RDR6i seeds were reported previously (Schwach *et al.*, 2005; Dadami *et al.*, 2013).

DNA constructs

AmiRNA constructs *35S:amiR-GUS$_{Nb}$*, *35S:amiR-NbSu-1*, *35S:amiR-NbSu-2*, *35S:amiR-NbSu-2-22* were obtained by ligating annealed oligo pairs D2057/D2058, D2065/D2066, D2067/D2068 and AC-310/AC-311, respectively, into *pMDC32B-AtMIR390a-B/c* (Addgene plasmid 51776) as described (Carbonell *et al.*, 2014). Syn-tasiRNA construct *35S:syn-tasiR-AtTAS1c-NbSu-2* was obtained by ligating annealed oligo pair AC-257/AC-258 into *pMDC32B-AtTAS1c-D2-B/c-AtMIR173* (Addgene plasmid 137885) as described (López-Dolz *et al.*, 2020). *35S:GUS* and *35S:syn-tasiR-GUS$_{Nb}$* were reported previously (Taiowa A. Montgomery *et al.*, 2008; López-Dolz *et al.*, 2020). All DNA oligonucleotides used for generating the constructs described above are listed in Table S2.

AmiRNA Designs

P-SAMS script (https://github.com/carringtonlab/p-sams) returning unlimited optimal results was used to obtain the complete list of optimal amiRNAs targeting *NbSu* or *E. coli GUS* with high specificity (Data S2). The off-targeting filtering in *N. benthamiana* transcriptome v5.1 (Nakasugi *et al.*, 2014) was enabled in all amiRNA designs to avoid undesired off-target effects and increase specificity.

Transient expression of constructs

Agroinfiltration of constructs in *N. benthamiana* leaves was done as described (Llave *et al.*, 2002; Cuperus *et al.*, 2010), using *A. tumefaciens* GV3101 strain.

RNA preparation

Total RNA from *N. benthamiana* leaves was isolated in extraction buffer (1 M guanidinium thiocyanate, 1 M ammonium thiocyanate, 0.1 M sodium acetate, 5 % glycerol, 38 % water saturated phenol), followed by chloroform extraction. RNA was precipitated in 0.5X isopropanol for 20 min. Triplicate samples from pools of two leaves were analyzed.

Real-time RT-qPCR

Real-time RT-qPCR was done essentially as described (López-Dolz *et al.*, 2020) in a QuantStudio 3 Real-Time PCR System (Thermo Fisher Scientific). *NbSu* target RNA expression levels were calculated relative to *N. benthamiana PROTEIN PHOSPHATASE 2A* (*NbPP2A*) reference gene using the delta delta cycle threshold comparative method of the QuantStudio Design and Analysis Software (version 1.5.1.; Thermo Fisher Scientific). Primers used for RT-qPCR are listed in Table S2.

Small RNA blot assays

Total RNA (20 µg) was separated in 17% polyacrylamide gels containing 0.5 x Tris/Borate EDTA (TBE) and 7 M urea and transferred to positively charged nylon membrane. Probe synthesis using [γ-^{32}P]ATP (PerkinElmer) and T4 polynucleotide kinase (Thermo Fisher Scientific) and Northern-blot hybridizations were done at 38ºC in PerfectHyb Plus Hybridization Buffer (Sigma-Aldrich) as described (T. A. Montgomery *et al.*, 2008; Carbonell *et al.*, 2014). A Typhoon IP Imager System (Cytiva) was used to produce digital images from radioactive membranes, and band quantification was done using the ImageQuantTL v10.0 software (Cytiva). Oligonucleotides used as probes for sRNA blots are listed in Table S2.

Microscopy

Whole leaves were placed in a Petri dish, illuminated by two lateral light sources. Images were obtained under bright field with a Magnifier Leica MZ16F, software LAS V4.12. Sections of 1 cm^2 were cut from whole leaves, placed between a glass slide and a coverslip and observed under a Leica 500 microscope using the LAS V4.9 software and 40x objective Lens (Leica, 40x/0.75 HCX PL Fluotar). Images were obtained under bright field and under an UV-A filter (340-380 nm excitation; 425 nm emission).

5'-RLM-RACE

RNA ligase-mediated rapid amplification of 5' cDNA ends was done using the GeneRacer kit (Life Technologies) as described (Carbonell *et al.*, 2015), except that the 5' end of cDNA specific to *NbSu* was directly amplified in a single PCR using the GeneRacer 5' and gene-specific AC-532 oligonucleotides. 5' RLM-RACE products were gel purified and cloned using the Zero Blunt TOPO PCR Cloning Kit (Life Technologies), introduced in *Escherichia coli* DH5a, screened for inserts, and sequenced. Control PCR reactions to amplify *NbPP2A* were done using oligonucleotides AC-365 and AC-366. The sequences of the oligonucleotides used are listed in Table S2.

Small RNA sequencing and data analysis

Total RNA was analyzed for quantity, purity and integrity with a 2100 Bioanalyzer (RNA 6000 Nano kit; Agilent), and submitted to BGI (Hong Kong, China) for sRNA library preparation and sRNA sequencing in DNBSEQ Platform. After reception of quality-trimmed, adaptor-removed clean reads from BGI, fastx_collapser (Hannon, 2010) was used to collapse identical reads into a single sequence, while maintaining read counts. A custom Python script was then used to map each clean, unique read against the forward and reverse strands of both the Nbv5.1tr6204879 transcript (Data S1), and the precursor of the art-sRNA overexpressed in each sample (Data S3), not allowing mismatches or gaps. The Python script was also used to calculate the counts and RPMs (reads per million mapped reads) for each mapping position.

Processing accuracy of amiRNA foldbacks and syntasiRNA transcripts was assessed by quantifying the proportion of 19-24 nt sRNA (+) reads that mapped within ± 4 nt of the 5' end of the amiRNA guide or DCL4 processing position 3'D2[+], respectively, as reported before (Cuperus *et al.*, 2010; Carbonell *et al.*, 2015). Phasing register tables were built by calculating the proportion of 21-nt sRNA (+) reads in each register relative to the amiR-NbSu-2 cleavage site for all 21-nt positions downstream of the cleavage site, as described before (Carbonell *et al.*, 2014).

Accession numbers

N. benthamiana and *E. coli* genes and corresponding locus identifiers are *NbSu* (Nbv5.1tr6204879), *NbPP2A* (Nbv5.1tr6224808) and *EcGUS* (AJ571699).

Acknowledgements

We would like to thank Javier Forment (IBMCP) for helping in the sRNA sequencing data analysis and the greenhouse staff of IBMCP for the maintenance of plants. DCL4i and RDR6i seeds were kind gifts from Drs. Kriton Kalantidis and David Baulcombe. This work was supported by grants from Ministerio de Ciencia, Innovación y Universidades (MCIU, Spain), Agencia Estatal de Investigación (AEI, Spain) and Fondo Europeo de Desarrollo Regional (FEDER, European Union) [RTI2018-095118-A-100 and RYC-2017-21648 to A.C., and PRE2019-088439 to A.E.C.].

Author contributions

AC planned and designed the research. AEC, ADM and AC performed experiments. AEC and AC analysed data and AC wrote the manuscript.

Data availability

High-throughput sequencing data can be found in the Sequence Read Archive (SRA) database under accession number PRJNA811353.

Supplemental information

Supplemental figures and tables can be found at the end of this chapter. Supplementary Table 2 and additional supporting information may be found in the online version of this article as well as in Mendeley Data Resource.

REFERENCES

Aung, K., Lin, S.-I., Wu, C.-C., Huang, Y.-T., Su, C. and Chiou, T.-J. (2006) pho2, a Phosphate Overaccumulator, Is Caused by a Nonsense Mutation in a MicroRNA399 Target Gene. *Plant Physiology*, **141**, 1000–1011.

Axtell, M.J. (2013) Classification and comparison of small RNAs from plants. *Annual review of plant biology*, **64**, 137–59.

Batailler, B., Lemaître, T., Vilaine, F., Sanchez, C., Renard, D., Cayla, T., Beneteau, J. and Dinant, S. (2012) Soluble and filamentous proteins in Arabidopsis sieve elements. *Plant, Cell & Environment*, **35**, 1258–1273.

Bologna, N.G. and Voinnet, O. (2014) The diversity, biogenesis, and activities of endogenous silencing small RNAs in Arabidopsis. *Annual review of plant biology*, **65**, 473–503.

Borges, F. and Martienssen, R.A. (2015) The expanding world of small RNAs in plants. *Nat Rev Mol Cell Biol*, **16**, 727–41.

Brioudes, F., Jay, F., Sarazin, A., Grentzinger, T., Devers, E.A. and Voinnet, O. (2021) HASTY, the Arabidopsis EXPORTIN5 ortholog, regulates cell-to-cell and vascular microRNA movement. *The EMBO Journal*, **n/a**, e107455.

Buhtz, A., Pieritz, J., Springer, F. and Kehr, J. (2010) Phloem small RNAs, nutrient stress responses, and systemic mobility. *BMC Plant Biology*, **10**, 64.

Carbonell, A. (2017) Artificial small RNA-based strategies for effective and specific gene silencing in plants. In T. Dalmay, ed. *Plant Gene Silencing: Mechanisms and Applications*. CABI Publishing, pp. 110–127.

Carbonell, A. (2019) Secondary Small Interfering RNA-Based Silencing Tools in Plants: An Update. *Front Plant Sci*, **10**, 687.

Carbonell, A. and Daròs, J.-A. (2019) Design, Synthesis, and Functional Analysis of Highly Specific Artificial Small RNAs with Antiviral Activity in Plants. *Methods Mol Biol*, **2028**, 231–246.

Carbonell, A., Fahlgren, N., Mitchell, S., Cox, K.L., Jr., Reilly, K.C., Mockler, T.C. and Carrington, J.C. (2015) Highly specific gene silencing in a monocot species by artificial microRNAs derived from chimeric miRNA precursors. *Plant J*, **82**, 1061–75.

Carbonell, A., Lopez, C. and Daròs, J.-A. (2019) Fast-Forward Identification of Highly Effective Artificial Small RNAs Against Different Tomato spotted wilt virus Isolates. *Mol Plant Microbe Interact*, **32**, 142–156.

Carbonell, A., Takeda, A., Fahlgren, N., Johnson, S.C., Cuperus, J.T. and Carrington, J.C. (2014) New generation of artificial MicroRNA and synthetic trans-acting small interfering RNA vectors for efficient gene silencing in Arabidopsis. *Plant Physiol*, **165**, 15–29.

Carella, P., Merl-Pham, J., Wilson, D.C., Dey, S., Hauck, S.M., Vlot, A.C. and Cameron, R.K. (2016) Comparative Proteomics Analysis of Phloem Exudates Collected during the Induction of Systemic Acquired Resistance. *Plant Physiology*, **171**, 1495–1510.

Chen, H.-M., Chen, L.-T., Patel, K., Li, Y.-H., Baulcombe, D.C. and Wu, S.-H. (2010) 22-nucleotide RNAs trigger secondary siRNA biogenesis in plants. *PNAS*, **107**, 15269–15274.

Chitwood, D.H., Nogueira, F.T., Howell, M.D., Montgomery, T.A., Carrington, J.C. and Timmermans, M.C. (2009) Pattern formation via small RNA mobility. *Genes Dev*, **23**, 549–54.

Cisneros, A.E. and Carbonell, A. (2020) Artificial Small RNA-Based Silencing Tools for Antiviral Resistance in Plants. *Plants*, **9**, 669.

Cisneros, A.E., Torre-Montaña, A. de la, Martín-García, T. and Carbonell, A. (2021) Artificial Small RNAs for Functional Genomics in Plants. In G. Tang, S. Teotia, X. Tang, and D. Singh, eds. *RNA-Based Technologies for Functional Genomics in Plants*. Concepts and Strategies in Plant Sciences. Cham: Springer International Publishing, pp. 1–29. Available at: https://doi.org/10.1007/978-3-030-64994-4_1 [Accessed April 14, 2021].

Cuperus, J.T., Carbonell, A., Fahlgren, N., et al. (2010) Unique functionality of 22-nt miRNAs in triggering RDR6-dependent siRNA biogenesis from target transcripts in Arabidopsis. *Nat Struct Mol Biol*, **17**, 997–1003.

Dadami, E., Boutla, A., Vrettos, N., Tzortzakaki, S., Karakasilioti, I. and Kalantidis, K. (2013) DICER-LIKE 4 but not DICER-LIKE 2 may have a positive effect on potato spindle tuber viroid accumulation in Nicotiana benthamiana. *Mol Plant*, **6**, 232–4.

Devers, E.A., Brosnan, C.A., Sarazin, A., et al. (2020) Movement and differential consumption of short interfering RNA duplexes underlie mobile RNA interference. *Nature Plants*, 1–11.

Dunker, F., Trutzenberg, A., Rothenpieler, J.S., et al. (2020) Oomycete small RNAs bind to the plant RNA-induced silencing complex for virulence A. A. Brakhage, C. S. Hardtke, and M. J. Axtell, eds. *eLife*, **9**, e56096.

Felippes, F.F. de, Ott, F. and Weigel, D. (2011) Comparative analysis of non-autonomous effects of tasiRNAs and miRNAs in Arabidopsis thaliana. *Nucleic Acids Res*, **39**, 2880–9.

Felippes, F.F. de and Waterhouse, P.M. (2020) The Whys and Wherefores of Transitivity in Plants. *Front. Plant Sci.*, **11**. Available at: https://www.frontiersin.org/articles/10.3389/fpls.2020.579376/full [Accessed September 1, 2020].

Fujii, H., Chiou, T.J., Lin, S.I., Aung, K. and Zhu, J.K. (2005) A miRNA involved in phosphate-starvation response in Arabidopsis. *Curr Biol*, **15**, 2038–43.

Gautrat, P., Laffont, C. and Frugier, F. (2020) Compact Root Architecture 2 Promotes Root Competence for Nodulation through the miR2111 Systemic Effector. *Current Biology*, **30**, 1339-1345.e3.

Guelette, B.S., Benning, U.F. and Hoffmann-Benning, S. (2012) Identification of lipids and lipid-binding proteins in phloem exudates from Arabidopsis thaliana. *Journal of Experimental Botany*, **63**, 3603–3616.

Hannon, G.J. (2010) FASTX-Toolkit (RRID:SCR_005534). http://hannonlab.cshl.edu/fastx_toolkit. Available at: http://hannonlab.cshl.edu/fastx_toolkit.

Himber, C., Dunoyer, P., Moissiard, G., Ritzenthaler, C. and Voinnet, O. (2003) Transitivity-dependent and -independent cell-to-cell movement of RNA silencing. *EMBO J*, **22**, 4523–33.

Hou, C.Y., Lee, W.C., Chou, H.C., Chen, A.P., Chou, S.J. and Chen, H.M. (2016) Global analysis of truncated RNA ends reveals new insights into ribosome stalling in plants. *Plant Cell*, **28**, 2398–2416.

Kawashima, C.G., Yoshimoto, N., Maruyama-Nakashita, A., Tsuchiya, Y.N., Saito, K., Takahashi, H. and Dalmay, T. (2009) Sulphur starvation induces the expression of microRNA-395 and one of its target genes but in different cell types. *Plant Journal*, **57**, 313–321.

Koch, A., Biedenkopf, D., Furch, A., et al. (2016) An RNAi-Based Control of Fusarium graminearum Infections Through Spraying of Long dsRNAs Involves a Plant Passage and Is

Controlled by the Fungal Silencing Machinery. *PLOS Pathogens*, **12**, e1005901.

Leisner, S.M. and Turgeon, R. (1993) Movement of virus and photoassimilate in the phloem: A comparative analysis. *BioEssays*, **15**, 741–748.

Lezzhov, A.A., Atabekova, A.K., Tolstyko, E.A., Lazareva, E.A. and Solovyev, A.G. (2019) RNA phloem transport mediated by pre-miRNA and viral tRNA-like structures. *Plant Sci*, **284**, 99–107.

Li, S., Le, B., Ma, X., et al. (2016) Biogenesis of phased siRNAs on membrane-bound polysomes in Arabidopsis. *Elife*, **5**, e22750.

Liu, L. and Chen, X. (2018) Intercellular and systemic trafficking of RNAs in plants. *Nature Plants*, **4**, 869–878.

Liu, Y., Teng, C., Xia, R. and Meyers, B.C. (2020) PhasiRNAs in Plants: Their Biogenesis, Genic Sources, and Roles in Stress Responses, Development, and Reproduction. *The Plant Cell*, **32**, 3059–3080.

Llave, C., Xie, Z., Kasschau, K.D. and Carrington, J.C. (2002) Cleavage of Scarecrow-like mRNA targets directed by a class of Arabidopsis miRNA. *Science (New York, N.Y*, **297**, 2053–6.

López-Dolz, L., Spada, M., Daròs, J.-A. and Carbonell, A. (2020) Fine-tune control of targeted RNAi efficacy by plant artificial small RNAs. *Nucleic Acids Res*, **48**, 6234–6250.

Manavella, P.A., Koenig, D. and Weigel, D. (2012) Plant secondary siRNA production determined by microRNA-duplex structure. *Proc Natl Acad Sci U S A*, **109**, 2461–6.

Matthewman, C.A., Kawashima, C.G., Huska, D., Csorba, T., Dalmay, T. and Kopriva, S. (2012) miR395 is a general component of the sulfate assimilation regulatory network in Arabidopsis. *FEBS Lett*, **586**, 3242–8.

McHale, M., Eamens, A.L., Finnegan, E.J. and Waterhouse, P.M. (2013) A 22-nt artificial microRNA mediates widespread RNA silencing in Arabidopsis. *Plant J*, **76**, 519–29.

Melnyk, C.W., Molnar, A. and Baulcombe, D.C. (2011) Intercellular and systemic movement of RNA silencing signals. *The EMBO Journal*, **30**, 3553–3563.

Mitter, N., Worrall, E.A., Robinson, K.E., et al. (2017) Clay nanosheets for topical delivery of RNAi for sustained protection against plant viruses. *Nat Plants*, **3**, 16207.

Molnar, A., Melnyk, C. and Baulcombe, D.C. (2011) Silencing signals in plants: a long journey for small RNAs. *Genome Biol*, **12**, 215.

Montgomery, T. A., Howell, M.D., Cuperus, J.T., et al. (2008) Specificity of ARGONAUTE7-miR390 interaction and dual functionality in TAS3 trans-acting siRNA formation. *Cell*, **133**, 128–41.

Montgomery, Taiowa A., Yoo, S.J., Fahlgren, N., et al. (2008) AGO1-miR173 complex initiates phased siRNA formation in plants. *PNAS*, **105**, 20055–20062.

Nakasugi, K., Crowhurst, R., Bally, J. and Waterhouse, P. (2014) Combining transcriptome assemblies from multiple de novo assemblers in the allo-tetraploid plant Nicotiana benthamiana. *PLoS One*, **9**, e91776.

Ossowski, S., Schwab, R. and Weigel, D. (2008) Gene silencing in plants using artificial microRNAs and other small RNAs. *The Plant journal : for cell and molecular biology*, **53**, 674–90.

Palauqui, J.-C. and Balzergue, S. (1999) Activation of systemic acquired silencing by localised introduction of DNA. *Current Biology*, **9**, 59–66.

Pant, B.D., Buhtz, A., Kehr, J. and Scheible, W.-R. (2008) MicroRNA399 is a long-distance signal for the regulation of plant phosphate homeostasis. *The Plant Journal*, **53**, 731–738.

Ratcliff, F., Harrison, B.D. and Baulcombe, D.C. (1997) A Similarity Between Viral Defense and Gene Silencing in Plants. *Science*, **276**, 1558–1560.

Schwach, F., Vaistij, F.E., Jones, L. and Baulcombe, D.C. (2005) An RNA-dependent RNA polymerase prevents meristem invasion by potato virus X and is required for the activity but not the production of a systemic silencing signal. *Plant physiology*, **138**, 1842–52.

Senthil-Kumar, M. and Mysore, K.S. (2011) Caveat of RNAi in Plants: The Off-Target Effect. In H. Kodama and A. Komamine, eds. *RNAi and Plant Gene Function Analysis: Methods and Protocols*. Methods in Molecular Biology. Totowa, NJ: Humana Press, pp. 13–25. Available at: https://doi.org/10.1007/978-1-61779-123-9_2 [Accessed December 18, 2019].

Shahid, S., Kim, G., Johnson, N.R., et al. (2018) MicroRNAs from the parasitic plant Cuscuta campestris target host messenger RNAs. *Nature*, **553**, 82–85.

Skopelitis, D.S., Hill, K., Klesen, S., Marco, C.F., Born, P. von, Chitwood, D.H. and Timmermans, M.C.P. (2018) Gating of miRNA movement at defined cell-cell interfaces governs their impact as positional signals. *Nat Commun*, **9**, 3107.

Subramanian, S. (2019) Little RNAs Go a Long Way: Long-Distance Signaling by MicroRNAs. *Molecular Plant*, **12**, 18–20.

Tang, Y., Wang, F., Zhao, J., Xie, K., Hong, Y. and Liu, Y. (2010) Virus-based microRNA expression for gene functional analysis in plants. *Plant physiology*, **153**, 632–41.

Tiwari, M., Sharma, D. and Trivedi, P.K. (2014) Artificial microRNA mediated gene silencing in plants: progress and perspectives. *Plant molecular biology*, **86**, 1–18.

Tsikou, D., Yan, Z., Holt, D.B., et al. (2018) Systemic control of legume susceptibility to rhizobial infection by a mobile microRNA. *Science*. Available at: https://www.science.org/doi/abs/10.1126/science.aat6907 [Accessed January 17, 2022].

Voinnet, O., Vain, P., Angell, S. and Baulcombe, D.C. (1998) Systemic Spread of Sequence-Specific Transgene RNA Degradation in Plants Is Initiated by Localized Introduction of Ectopic Promoterless DNA. *Cell*, **95**, 177–187.

Weiberg, A., Bellinger, M. and Jin, H. (2015) Conversations between kingdoms: small RNAs. *Current opinion in biotechnology*, **32**, 207–15.

Yang, L., Xu, M., Koo, Y., He, J. and Poethig, R.S. (2013) Sugar promotes vegetative phase change in Arabidopsis thaliana by repressing the expression of MIR156A and MIR156C R. Amasino, ed. *eLife*, **2**, e00260.

Zhang, Z.J. (2014) Artificial trans-acting small interfering RNA: a tool for plant biology study and crop improvements. *Planta*, **239**, 1139–46.

SUPPLEMENTARY INFORMATION

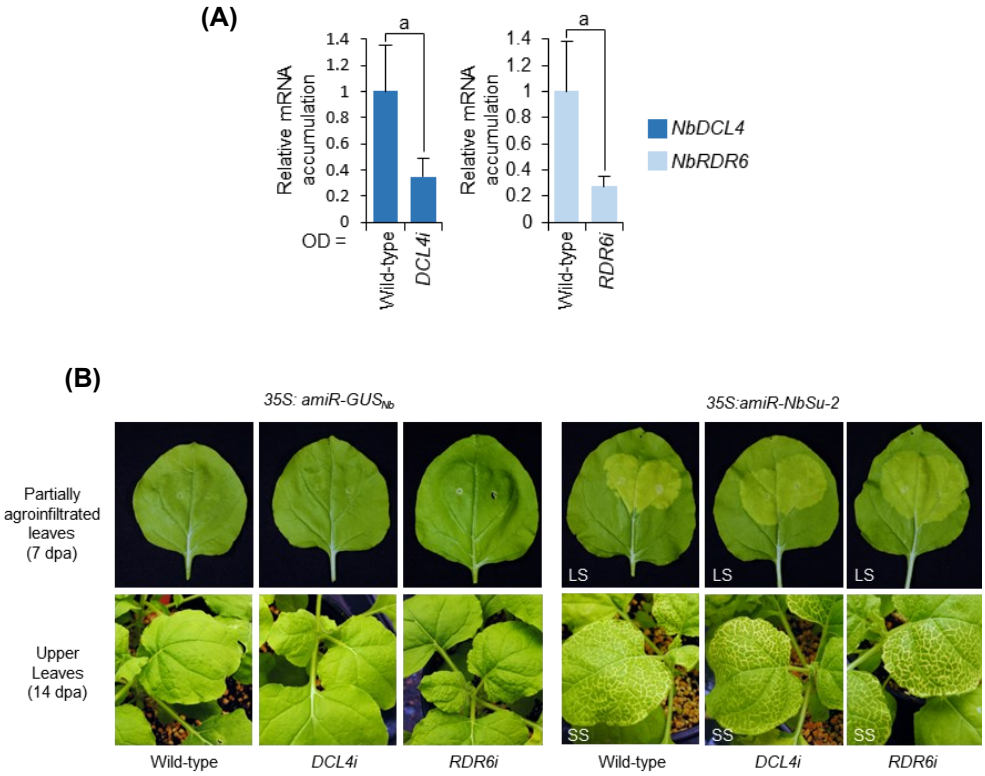

Figure S1. Genetic analysis of local and systemic silencing triggered by amiR-NbSu-2 in wild-type and in DCL4 (DCL4i) or RDR6 (RDR6i) knockdown plants. (**A**) Accumulation of *NbDCL4* and *NbRDR6* mRNAs in leaves of wilt-type, *DCL4i* and *RDR6i N. benthamiana* plants. Mean relative level (n=3) + standard error of mRNAs after normalization to *PROTEIN PHOSPHATASE 2A* (*PP2A*), as determined by quantitative RT-PCR (qPCR) (Wild-type = 1.0 in all comparisons). Other details are as in Fig 1B. (**B**) Photos of partially agroinfiltrated leaves at 7 days-post agroinfiltration (dpa) (top), and of upper non-agroinfiltrated leaves at 14 dpa (bottom). Other details are as in Fig. 2A.

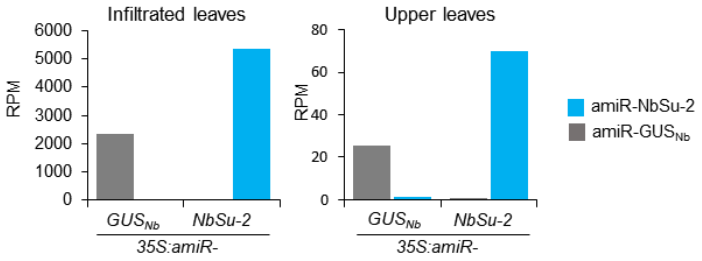

Figure S2. Bar graphs showing the number of amiR-GUS_{Nb} and amiR-NbSu-2 reads in *35S:amiR-GUS_{Nb}* and *35S:amiR-NbSu-2* expressing tissues and in upper leaves.

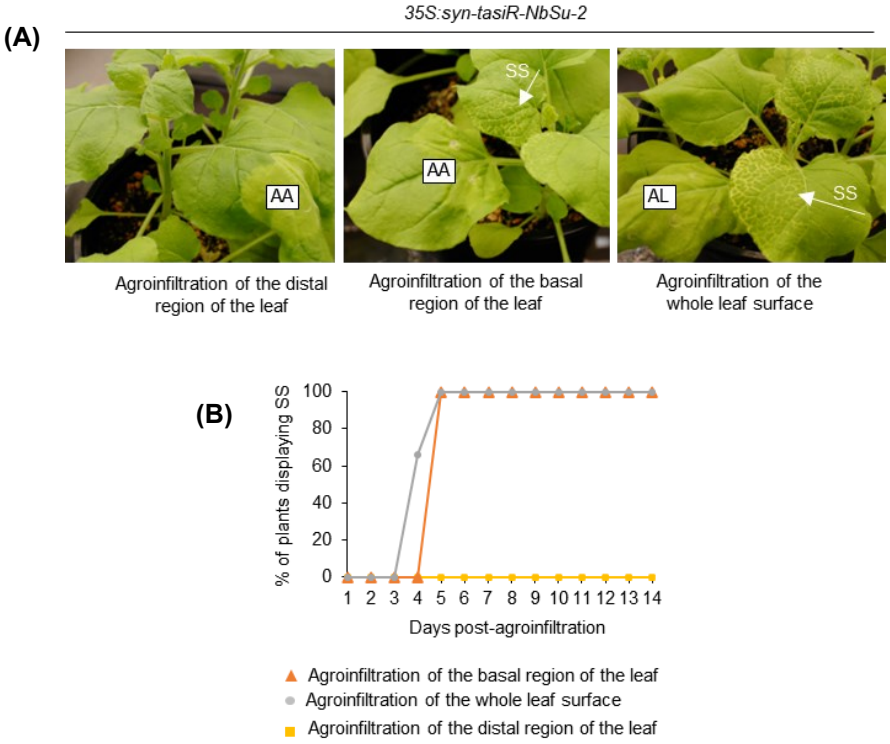

Figure S3. **Effects on systemic silencing of the place of expression of syn-tasiR-NbSu-2 in *N. benthamiana* leaves.** (**A**) Photos of plants at 7 days post-agroinfiltration (dpa). AA and AL refer to agroinfiltrated area and agroinfiltrated leaf, respectively. Near-vein chlorotic areas result of systemic silencing (SS) are pointed with a white arrow. (**B**) Two-dimensional line graph showing, for each of the three-plant sets listed in the box, the percentage of plants displaying systemic silencing per day during 14 dpa.

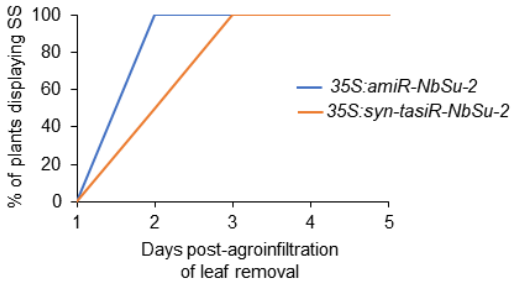

Figure S4. Speed of translocation of the systemic silencing (SS) signal. Bar graph shows the percentage of plants displaying SS after removal of the agroinfiltrated leaves at 1, 2, 3, 4 or 5 days post-agroinfiltration (dpa).

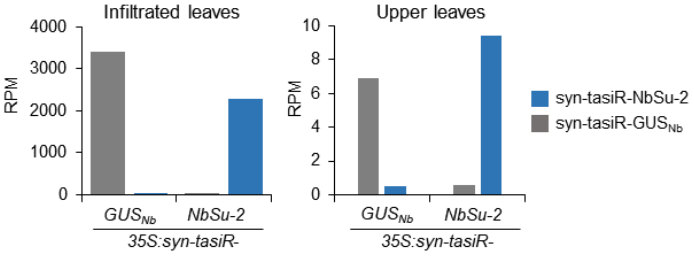

Figure S5. Bar graphs showing the number of syn-tasiR-GUS$_{Nb}$ and syn-tasiR-NbSu-2 reads in *35S:syn-tasiR-GUS$_{Nb}$* and *35S:syn-tasiR-NbSu-2* expressing tissues and in upper leaves.

Table S1. Artificial small RNA-induced systemic silencing (SS) appearance as leaf near-vein chlorosis in upper or lower non-agroinfiltrated leaves during 14 days post-agroinfiltration.

Art-sRNA construct	Agroinfiltrated leaves*	SS in lower leaves	SS in upper leaves
35S:amiR-NbSu-2	3-4	0/3	3/3
	5-6	0/3	3/3
	7-8	0/3	3/3
35S:syn-tasiR-NbSu-2	3-4	0/3	3/3
	5-6	0/3	3/3
	7-8	0/3	3/3

*leaf numbers refer to the age of the leaf, with leaf number 1 being the oldest leaf

CHAPTER 2

Transgene-Free, Virus-Based Gene Silencing in Plants by Artificial MicroRNAs Derived from Minimal Precursors

Adriana E. Cisneros, Tamara Martín-García, Anamarija Primc, Wojtek Kuziuta, Javier Sánchez-Vicente, Verónica Aragonés, José-Antonio Daròs and Alberto Carbonell

Adapted from the article published in 2023 at *Nucleic Acids Research* 51(19):10719-10736. doi: 10.1093/nar/gkad747

CHAPTER 2

Transgene-Free, Virus-Based Gene Silencing in Plants by Artificial MicroRNAs Derived from Minimal Precursors

Adriana E. Cisneros[a], Tamara Martín-García[a], Anamarija Primc[a,b], Wojtek Kuziuta[a,c], Javier Sánchez-Vicente[a,d], Verónica Aragonés[a], José-Antonio Daròs[a] and Alberto Carbonell[a]

[a] *Instituto de Biología Molecular y Celular de Plantas (IBMCP), CSIC-Universitat Politècnica de València, Av. de los Naranjos s/n 46022 Valencia, Spain.*

[b] *Current address: Center for Organismal Studies (COS), University of Heidelberg, Heidelberg, Germany.*

[c] *Current address: Syngenta, Bracknell, United Kingdom.*

[d] *Current address: Madeinplant S.L., Valencia, Spain.*

ABSTRACT

Artificial microRNAs (amiRNAs) are highly specific, 21-nucleotide (nt) small RNAs designed to silence target transcripts. In plants, their application as biotechnological tools for functional genomics or crop improvement is limited by the need of transgenically expressing long primary miRNA (pri-miRNA) precursors to produce the amiRNAs *in vivo*. Here we analyzed the minimal structural and sequence requirements for producing effective amiRNAs from the widely used, 521-nt long *AtMIR390a* pri-miRNA from *Arabidopsis thaliana.* We functionally screened in *Nicotiana benthamiana* a large collection of constructs transiently expressing amiRNAs against endogenous genes and from artificially shortened *MIR390*-based precursors and concluded that highly effective and accurately processed amiRNAs can be produced from a chimeric precursor of only 89 nt. This minimal precursor was further validated in *A. thaliana* transgenic plants expressing amiRNAs against endogenous genes. Remarkably, minimal but not full-length precursors produce authentic amiRNAs and induce widespread gene silencing in *N. benthamiana* when expressed from an RNA virus, which can be applied into leaves by spraying infectious crude extracts. Our results reveal that the length of amiRNA precursors can be shortened without affecting silencing efficacy, and that viral vectors including minimal amiRNA precursors can be applied in a transgene-free manner to induce whole-plant gene silencing.

Keywords: RNA interference, microRNA, potato virus X, *AtMIR390a*, amiR-VIGS

INTRODUCTION

MicroRNAs (miRNAs) are a class of 20-24-nucleotide (nt) endogenous small RNAs (sRNAs) that repress gene expression post-transcriptionally in plants and animals. Most plant miRNAs are 21-nt long and regulate the expression of genes encoding transcription factors and proteins that impact key biological processes such as growth, development, stress adaptation or hormone regulation (Bologna & Voinnet, 2014; Rogers & Chen, 2013). MiRNA biogenesis in plants [reviewed recently in(Achkar et al., 2016; Bajczyk et al., 2023; Jodder, 2021; Li & Yu, 2021; L. Zhang et al., 2022)] occurs entirely in the cell nucleus, and initiates with the transcription of *MIR* genes by RNA polymerase II, resulting in the synthesis of large primary miRNA precursors (or pri-miRNAs) that are highly variable in length (from hundreds to thousands of nucleotides) and in secondary structure. Pri-miRNAs are capped, spliced and polyadenylated, and harbor a characteristic foldback (or hairpin) structure that also varies in length (from 50 to 900 nt). MiRNA foldbacks have a common structure consisting of a ~15-17 base-pair (bp) basal stem (BS), a miRNA/miRNA* duplex, and a distal stem-loop (DSL) region variable in size and shape and flanked by single-stranded RNA (ssRNA) segments (Bologna et al., 2009; Cuperus et al., 2011). Processing of most pri-miRNAs occurs through a “base-to-loop” mechanism in which the nuclear RNase III DICER-LIKE1 (DCL1) associated with its accessory proteins SERRATE (SE) and HYPONASTIC LEAVES1 (HYL1) first cleaves at the BS of the foldback to release a shorter precursor miRNA (pre-miRNA). Next, a second cleavage at a 21-nt distance from the first cut releases the miRNA/miRNA* duplex including two-nucleotide 3’ overhangs that are 2’-*O*-methylated by the methyltransferase HUA ENHANCER1 (HEN1) (Achkar et al., 2016; Yu et al., 2017). Alternatively, for loop-to-base processed precursors, DCL1 produces a first cut that releases the terminal loop and then continues towards the base of the precursor to release the miRNA/miRNA* duplex (Addo-Quaye et al., 2009; Bologna et al., 2009). Typically, one of the strands of the duplex (the guide strand) is sorted out into an ARGONAUTE (AGO) protein (AGO1 for the majority of plant miRNAs) resulting in an RNA-induced silencing complex (RISC) that recognizes and silences complementary target RNAs mostly through their endonucleolytic cleavage, and less frequently through their translational repression (Axtell, 2013).

Artificial miRNAs (amiRNAs) are 21-nt miRNAs computationally designed for redirecting the endogenous miRNA biogenesis and silencing machineries to selectively suppress specific target RNAs with high efficacy and specificity (with no predicted off-targets) (Carbonell, 2017; Ossowski et al., 2008; Tiwari et al., 2014). AmiRNAs are produced *in planta* by expressing a modified *MIR* gene producing a pri-miRNA precursor in which the sequence of the native miRNA/miRNA* duplex is substituted by the sequence of the amiRNA/amiRNA* duplex. The

selection of an appropriate pri-miRNA backbone is critical for ensuring an efficient and accurate precursor processing and produce high amounts of amiRNAs necessary for effective target silencing. The 521-nt long pri-miRNA precursor derived from *Arabidopsis thaliana* (Arabidopsis) *MIR390a* (*pri-AtMIR390a*) is a highly efficient and accurately processed pri-miRNA compared to other plant pri-miRNAs used for producing amiRNAs(Carbonell et al., 2014; Lunardon et al., 2021). Moreover, *pri-AtMIR390a* has been used for expressing amiRNAs in multiple plant species including model and crop plants, to effectively silence both endogenous genes and viral RNAs (Carbonell, Lisón, et al., 2019; Cisneros et al., 2021; Lunardon et al., 2021; Vasav et al., 2023). Interestingly, *pri-AtMIR390a* has a relatively short DSL region of only 31 nt, allowing the synthesis of the complete foldback with just two oligonucleotides spanning this structure. This feature has facilitated the development of a cost-effective, high-throughput methodology to directly introduce amiRNA inserts into a series of “B/c” vectors including the *pri-AtMIR390a* sequence (Carbonell et al., 2014).

AmiRNAs are used as biotechnological tools for both functional genomics and crop improvement (Basso et al., 2019; Cisneros et al., 2021). However, a current limitation of the amiRNA technology is the use of relatively long precursors, mostly based on full-length pri-miRNA sequences, to produce the amiRNAs *in vivo*. Reducing the size of amiRNA precursors should have several biotechnological advantages such as a more cost-effective production of amiRNA constructs or a more efficient *in vitro* or in bacteria synthesis of amiRNA precursors for topical application to plants. Another limitation is the need to genetically modify plant genomes with amiRNA transgenes. The use of plant DNA viruses to successfully express authentic amiRNAs in *Nicotiana benthamiana* (Ju et al., 2017; Kuo & Falk, 2022; Y. Tang et al., 2010) is promising, although infections are typically triggered by the agroinfiltration of plant tissues with plasmids including the amiRNA-expressing viral vector and limited to a narrow list of host species. Therefore, this so-called amiRNA-based virus-induced gene silencing (amiR-VIGS) technology requires further optimization for its broader application in multiple plant species and to avoid the generation of genetically modified plant tissues.

Here, we further expanded our recently developed silencing sensor system in *N. benthamiana* (Cisneros et al., 2022) and used it to systematically analyze the minimal structural and sequence requirements for producing effective amiRNAs from the broadly used, 521-nt long *pri-AtMIR390a* precursor. We functionally screened a large collection of constructs expressing amiRNAs against the *N. benthamiana* magnesium chelatase subunit CHLI-encoding *SULPHUR* (*NbSu*) or the *1-DEOXY-D-XYLULOSE-5-PHOSPHATE SYNTHASE* (*NbDXS*) genes from *AtMIR390a*-based precursors with artificially shortened BS or DSL regions. By combining phenotypic, biochemical and molecular assays with high-throughput

sequencing-based analysis of precursor processing we show that highly effective, accurately processed amiRNAs can be produced in *N. benthamiana* from a shortened chimeric *MIR390*-based amiRNA precursor of only 89 nt. This "minimal" precursor includes the complete BS region of *pri-AtMIR390a* (with no additional ssRNA segments) and the DSL region derived from *Oryza sativa MIR390* (*OsMIR390*) with a 2-nt deletion. The precursor was further validated in Arabidopsis transgenic plants expressing amiRNAs for silencing *CHLORINA42* (*AtCH42*) or *FLOWERING LOCUS T* (*AtFT*) which resulted in bleaching and late flowering phenotypes, respectively. Finally, we show that the minimal precursor has the unique ability to produce authentic amiRNAs and trigger widespread gene silencing in *N. benthamiana* when expressed from an RNA virus vector sprayed to leaves in a non-transgenic, DNA-free manner.

RESULTS

A silencing sensor system in *N. benthamiana* for easily visualizing and quantifying amiRNA-induced silencing of endogenous genes

We recently described a silencing sensor system for easily visualizing and quantifying silencing of the magnesium chelatase subunit CHLI [hereafter *SULPHUR* gene (*NbSu*)] in *N. benthamiana* by the amiRNA amiR-NbSu-1 (Cisneros et al., 2022). To further expand the use of the sensor system, we tested if we could trigger a similar visible bleaching with amiRNAs directed against the *1-DEOXY-D-XYLULOSE-5-PHOSPHATE SYNTHASE* (*NbDXS*) gene. Briefly, three different constructs expressing amiRNAs targeting *NbDXS* at unique sites and with no predicted off-targets (Figure S2A, Data S1) were independently agroinfiltrated in two areas of two leaves from three different *N. benthamiana* plants, together with a negative control construct expressing an amiRNA against *Escherichia coli* b-glucuronidase GUS. At 7 dpa, areas agroinfiltrated with anti-*NbDXS* amiRNA constructs displayed a visually obvious bleaching predicted from *NbDXS* knockdown while areas expressing the control construct did not (Figure S2B). The chlorophyll analysis of agroinfiltrated areas showed a similar decrease in chlorophyll content in bleached areas expressing anti-*NbDXS* amiRNAs compared to areas expressing the control construct (Figure S2C). Next, two leaves of three different plants were independently agroinfiltrated in the whole leaf surface with each of the amiRNA constructs described above. sRNA blot assays of RNA preparations from agroinfiltrated leaves showed that all anti-*NbDXS* amiRNAs accumulated as single-size sRNA species, with amiR-NbDXS-1 accumulating to significantly higher levels than the other two amiRNAs (Figure S2D). RT-qPCR analysis revealed that all samples expressing anti-*NbDXS* amiRNAs accumulated significantly lower levels of *NbDXS* mRNA than control samples (Figure S2E). These results indicate that anti-

NbDXS amiRNAs are highly active and induce a strong bleaching phenotype in the tissue where they are expressed. Thus, the methodology described in (Cisneros et al., 2022) and outlined in Figure 1 was used in this work to test the effect on *NbSu* and *NbDXS* silencing efficacy of amiR-NbSu-1 (hereafter amiR-NbSu) and amiR-NbDXS-1 (hereafter amiR-NbDXS), respectively (Figure 2A), produced from *pri-AtMIR390a* precursors with reduced BS or DSL regions (see next four sections).

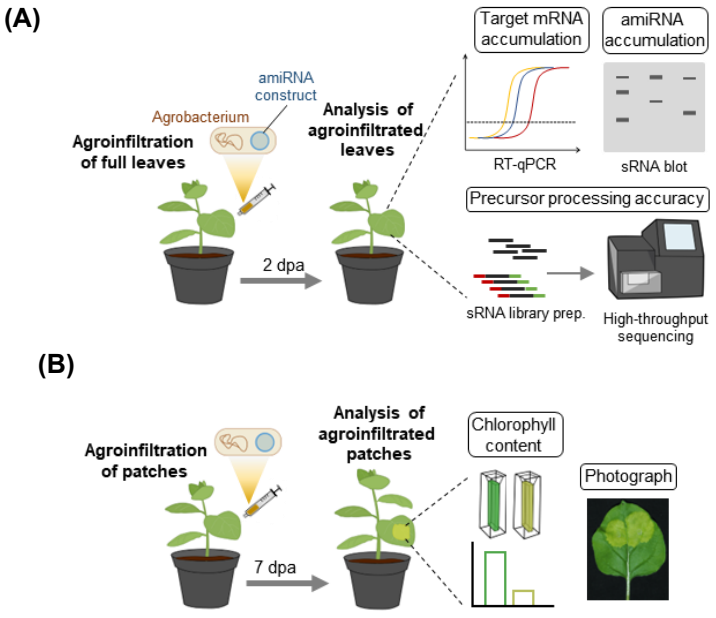

Figure 1. **Methodology for easily visualizing and quantifying the silencing activity of amiRNAs derived from *AtMIR390a*-based precursors**. (**A**) and (**B**), Steps for the analysis of fully agroinfiltrated leaves or patches, respectively.

Functional analysis of *pri-AtMIR390a*-based amiRNA precursors with shortened DSL regions

First, we analyzed the silencing activity of amiR-NbSu- and amiR-NbDXS-expressing constructs including *pri-AtMIR390a*-based precursors with progressively shorter DSL regions ranging from 31 nt of the full-length *pri-AtMIR390a* (or simply "*pri*") precursor to only 6 nt (Figure 2B). As expected, at 7 dpa areas expressing amiR-NbSu or amiR-NbDXS from the *pri* precursor displayed the reduced pigmentation characteristic of *NbSu* or *NbDXS* knock-down, while areas expressing amiR-GUS$_{Nb}$ did not (Figure 2C). Interestingly, a similar bleaching was also observed in areas expressing amiR-NbSu or amiR-NbDXS from *AtDSL-D6* and *AtDSL-D13* precursors, while a less intense bleaching was noticed in areas expressing amiR-NbSu (but not

amiR-NbDXS) from the *AtDSL-D21* precursor (Figure 2C). No bleaching was observed in areas expressing amiRNAs from the *AtDSL-D25* precursor (Figure 2C). Visual silencing phenotypes were confirmed by the chlorophyll analysis of agroinfiltrated areas, with bleached areas displaying lower chlorophyll *a* content than darker green areas (Figure 2D).

RNA blot assays of RNA preparations from agroinfiltrated leaves showed that amiR-NbSu and amiR-NbDXS accumulated to high levels when expressed from *pri* or from shorter *AtDSL-D6* and *AtDSL-D13* precursors (Figure 2E). In overexposed blots both amiRNAs were also detected although to low levels when expressed from *AtDSL-D21* and also from *AtDSL-D25* in the case of amiR-NbDXS (Figure 2E). Small RNA species of different sizes were also detected in some cases, most likely reflecting that the position of DCL1 cleavage is not always uniform, as proposed before (López-Dolz et al., 2020). Twenty-four-nt sRNAs present in the overexposed blots presumably arise from transgene-derived dsRNAs, which typically occurs in *N. benthamiana* when agroinfiltrating ectopic transgene constructs, as observed before (Hamilton et al., 2002). Finally, RT-qPCR analysis revealed that target mRNA expression was considerably reduced in samples expressing amiRNAs from *pri* or from shortened precursors compared to control samples, except for samples expressing amiR-NbSu or amiR-NbDXS from *AtDSL-D25* (Figure 2F). Notably, samples expressing amiRNAs from *pri* or from *AtDSL-D6* accumulated similar low target mRNA levels, while the expression of shorter *AtDSL-D13* and *AtDSL-D21* precursors generally induced a more moderate reduction in target mRNA levels (Figure 2F). In contrast, no significant reduction in target mRNA levels was observed when amiRNAs were expressed from *AtDSL-D25* (Figure 2F). These results indicate that the DSL region of *pri-AtMIR390a* can be shortened to some extent without significantly affecting amiRNA accumulation and target mRNA silencing.

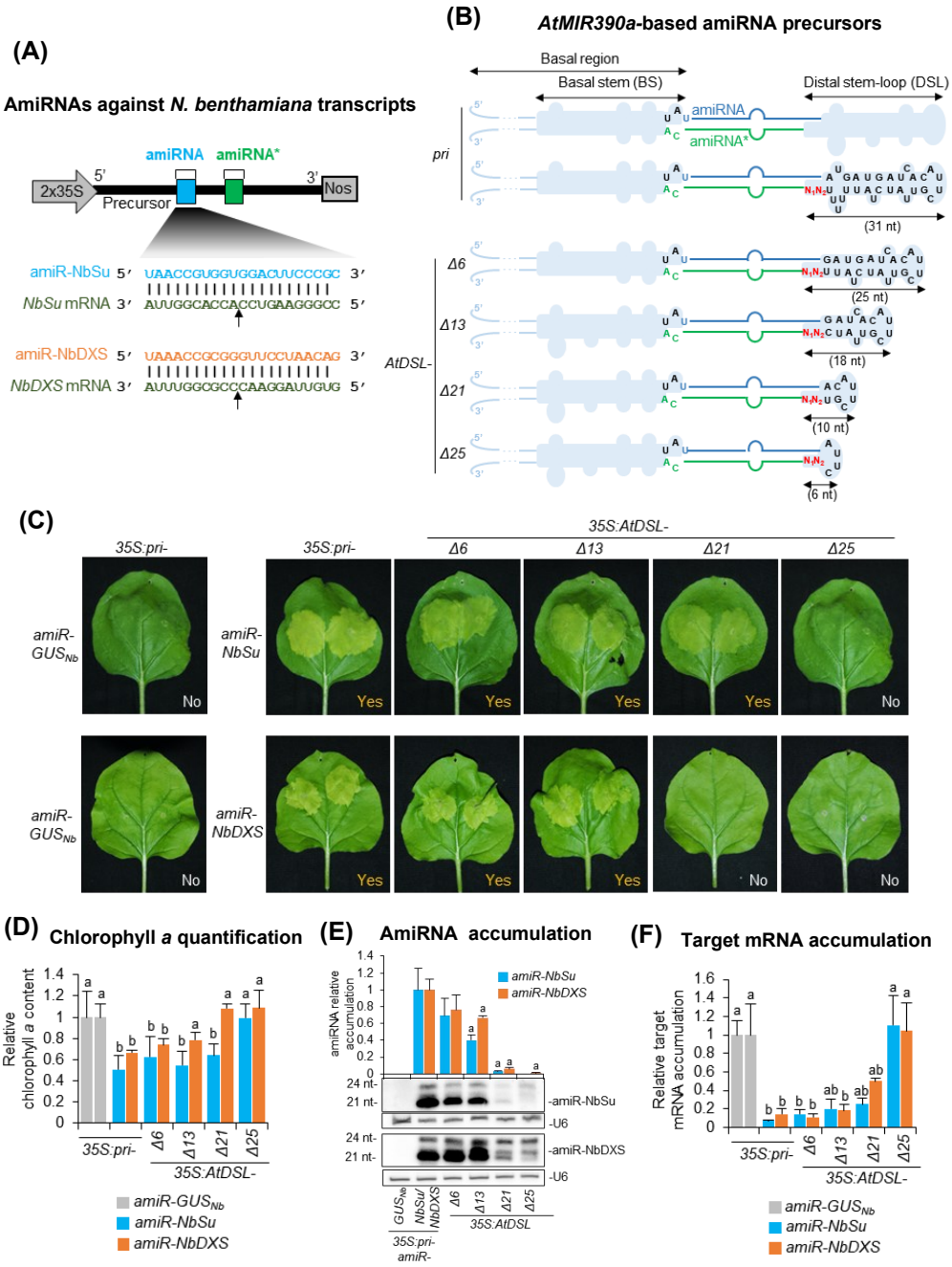

Figure 2. Functional analysis of constructs expressing amiR-NbSu or amiR-NbDXS against *N. benthamiana SULPHUR* (*NbSu*) or *DXS* (*NbDXS*), respectively, from *AtMIR390a*-based precursors with shortened distal stem-loop (DSL) region. (**A**), Diagram of *AtMIR390a*-based amiRNA constructs including the base-pairing of amiRNAs and target mRNAs. Nucleotides corresponding to the guide strand of the amiRNA against *NbSu* and *NbDXS* are in blue and orange, respectively, while nucleotides of target

mRNAs are in dark green. The arrows indicate the amiRNA-predicted cleavage site. (**B**) Diagrams of the amiRNA precursors with nucleotides corresponding to the amiRNA guide and amiRNA* strands are in blue and green, respectively, while those from *AtMIR390a* are in black. The two nucleotides specific to each amiRNA construct that are modified for preserving authentic *pri* foldback secondary structure are in red. The shapes corresponding to *pri* basal stem (BS) or DSL regions are in light blue. The size in nucleotides of the DSL region of each precursor is given. (**C**) Photos at 7 days post-agroinfiltration (dpa) of leaves agroinfiltrated with different constructs. "Yes" and "No" labels indicate the presence or absence of bleached patches, respectively. (**D**) Bar graph showing the relative content of chlorophyll *a* in patches agroinfiltrated with different constructs (*pri-amiR-GUS*$_{Nb}$ = 1.0). Bars with the letter "b" or "a" are significantly different from that of the corresponding control samples *pri-amiR-GUS*$_{Nb}$ or *pri-amiR-NbSu*/*pri-amiR-NbDXS*, respectively ($P < 0.05$ in pairwise Student's t-test comparisons). (**E**) Northern blot detection of amiR-NbSu and amiR-NbDXS in RNA preparations from agroinfiltrated leaves at 2 dpa. The graph at top shows the mean (n = 3) + standard deviation amiRNA relative accumulation (*pri-amiR-NbSu* = 1.0; *pri-amiR-NbDXS* = 1.0). Bars with a letter "a" are significantly different from that of sample *pri-amiR-NbSu* or *pri-amiR-NbDXS*. One blot from three biological replicates is shown. (**F**) Target mRNA accumulation in agroinfiltrated leaves. Mean relative level (n = 3) + standard error of *NbSu* or *NbDXS* mRNAs after normalization to *PROTEIN PHOSPHATASE 2A* (*PP2A*), as determined by quantitative RT-PCR (qPCR) (*pri-amiR-GUS*$_{Nb}$ = 1.0 in all comparisons). Other details are as in D.

AmiRNAs produced from *pri-AtMIR390a*-based precursors including shortened *OsMIR390*-derived DSL regions trigger gene silencing with high efficacy

The *OsMIR390* precursor has a DSL region (OsDSL) consisting of only 16 nt, which represents one of the shortest DSL regions from all conserved plant *MIRNA* precursors (Carbonell et al., 2015). Here, we reasoned that the *OsDSL* region might also tolerate nucleotide deletions while preserving efficient amiRNA production and target mRNA silencing. To test this, several constructs were generated for expressing amiR-NbSu and amiR-NbDXS from chimeric constructs including the complete (16-nt long) *OsDSL* region or progressively shortened versions of it (Figure 3A). In addition, a construct in which the 8-nt terminal loop of *OsMIR390* was replaced by the shorter 4-nt long terminal loop of *AtMIR390a* was also included in the analysis (Figure 3A). Areas agroinfiltrated with constructs expressing amiRNAs from *pri* or from chimeric *OsDSL* and *OsDSL-D2* precursors showed intense bleaching and similar reduction in the accumulation of chlorophyll *a* compared to controls (Figure 3B and 2C). In contrast, other agroinfiltrated areas displayed weaker bleaching and lower chlorophyll *a* content except those from controls and from areas expressing amiR-NbSu from *OsDSL-D6* which did not display any sign of silencing (Figure 3B and 3C). RNA blot analysis of RNA preparations from agroinfiltrated leaves revealed that amiRNAs accumulated to high levels in samples expressing the *pri* or chimeric *OsDSL* and *OsDSL-D2* precursors, while amiRNA levels dropped significantly in the rest of samples except for those expressing the *35S:OsDSL-D6-amiR-NbSu* construct in which amiR-NbSu was not detected (Figure 3D). RT-qPCR analysis revealed that target mRNA accumulation significantly decreased in all samples expressing amiRNAs from *pri* or from chimeric precursors compared to controls, except in samples expressing amiR-NbSu from

OsDSL-D4 and *OsDSL-D6* (Figure 3E). Importantly, target mRNA levels were similar in samples expressing amiRNAs from *pri* or from chimeric *OsDSL* and *OsDSL-D2* precursors (Figure 3E). Taken together, these results indicate that the *OsDSL* region can also be shortened –in this case down to 14 nt– in *AtMIR390a*-based precursors without compromising silencing efficacy.

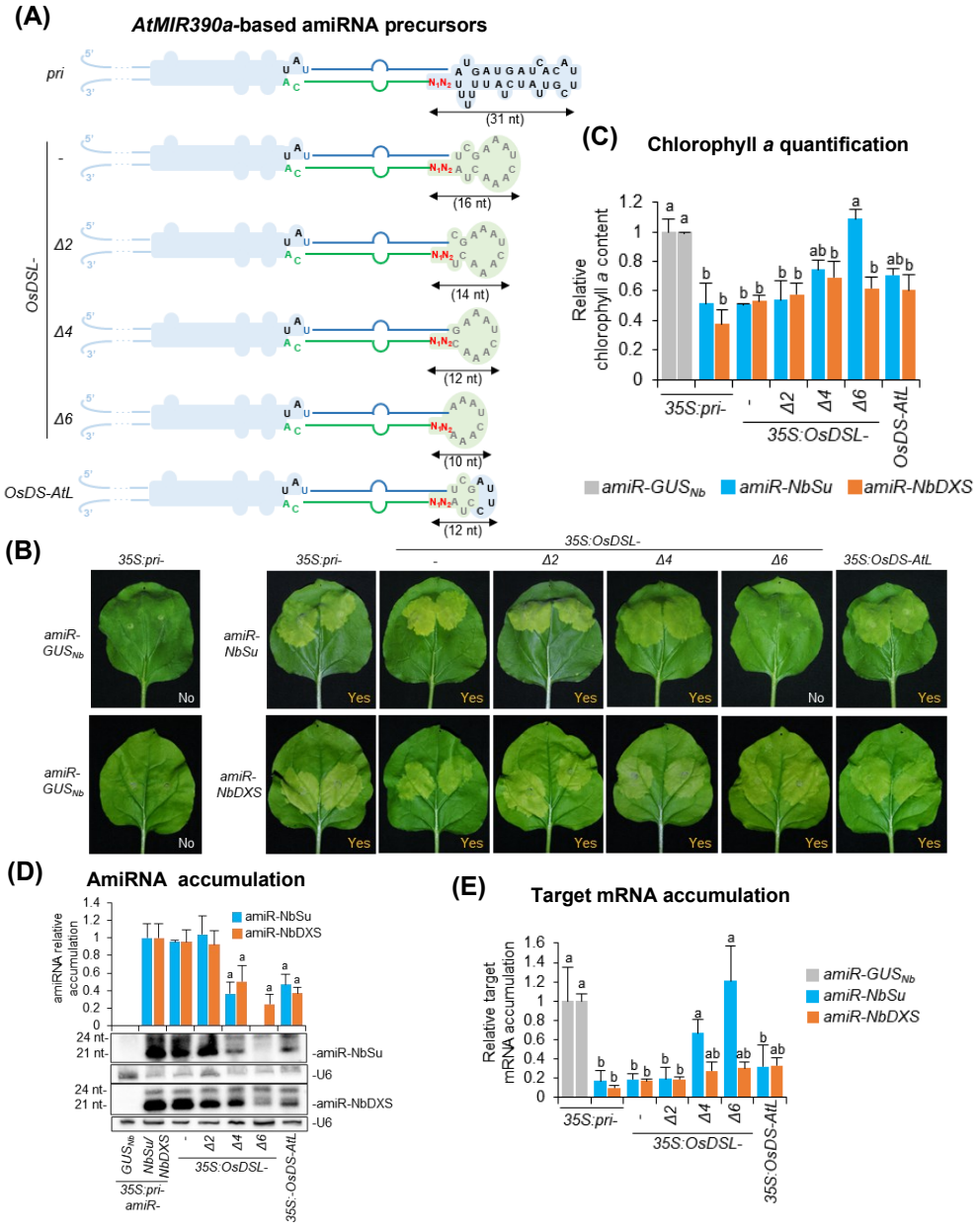

Figure 3. Functional analysis of constructs expressing amiR-NbSu or amiR-NbDXS against *N. benthamiana SULPHUR* (*NbSu*) or *DXS* (*NbDXS*) from chimeric precursors including intact

***AtMIR390a* basal region and shortened *OsMIR390* distal stem-loop (DSL) region**. (**A**) Diagrams of the amiRNA precursors. Nucleotides from *OsMIR390* are in grey. The shapes corresponding to *OsMIR390a* distal stem-loop regions are in light green. Other details are as in Figure 2B. (**B**) Photos at 7 days post-agroinfiltration (dpa) of leaves agroinfiltrated with different constructs. (**C**) Bar graph showing the relative content of chlorophyll *a* in patches agroinfiltrated with different constructs (*pri-amiR-GUS*$_{Nb}$ = 1.0). Other details are as in Figure 2D. (**D**) Northern blot detection of amiR-NbSu and amiR-NbDXS amiRNAs in RNA preparations from agroinfiltrated leaves at 2 dpa. Other details are as in Figures 2D and 2E. (**E**) Target mRNA accumulation in agroinfiltrated leaves. Other details are as in Figures 2D and 2F.

Functional analysis of *AtMIR390a*-based amiRNA precursors with shortened BS

Next, we analyzed if shortening the BS region of *pri-AtMIR390a* could affect amiRNA production and silencing efficacy. Several constructs for expressing amiR-NbSu and amiR-NbDXS were generated, in which the 448-nt BS region of *pri-AtMIR390a* was progressively shortened down to 2 nt (Figure 4A). Similar intense bleaching and reduced chlorophyll *a* level was observed in areas expressing amiR-NbSu or amiR-NbDXS from the *pri* or *BS* precursors (Figure 4B and 3C). In contrast, weaker bleaching was observed in areas expressing any of the two amiRNAs from *BS-D7*, or amiR-NbSu from *BS-D17*, *BS-D23* or *BS-31* (Figure 4B), corresponding with slight decreases in chlorophyll *a* content compared to controls (Figure 4C). No bleaching or changes in chlorophyll *a* content were observed in leaves expressing amiR-NbDXS from *BS-D17*, *BS-D23* or *BS-31* (Figure 4B and 4C). Both amiR-NbSu and amiR-NbDXS amiRNAs expressed from the *pri* or *BS* precursors accumulated to similarly high levels and induced comparable target mRNA silencing (Figure 4D and 4E). In contrast, their levels dropped significantly or were undetectable when expressed from *BS-D7*/*BS-D17* or *BS-D23/BS-D31*, respectively (Figure 4D) and induced significantly lower target mRNA downregulation (Figure 4E). All together these results indicate that a complete BS region is necessary for accurate precursor processing to produce high levels of amiRNAs, while further shortening this BS region drastically reduces amiRNA accumulation.

New high-throughput vectors for expressing amiRNAs from *AtMIR390a*-based precursors only including the BS

Previous high-throughput *AtMIR390a*-based amiRNA "B/c" vectors included the complete 521 bp sequence of the *pri-AtMIR390a* precursor (Carbonell et al., 2014). Here, we developed two additional "B/c" vectors for the efficient cloning and expression of amiRNAs from shortened precursors only including *AtMIR390a* BS (Figure S3). *pENTR-BS-AtMIR390a-B/c* Gateway-compatible entry vector was generated for direct cloning of amiRNA inserts and subsequent recombination into the preferred Gateway expression vector including the regulatory features of choice. *pMDC32B-BS-AtMIR390a-B/c* vector was generated for the direct cloning of amiRNA inserts into a binary expression vector. Both vectors contain a truncated *AtMIR390a* BS

sequence including a 1461-bp DNA cassette with the control of cell death (*ccd*B) gene flanked by two inverted *Bsa*I sites downstream the BS region. The generation of an amiRNA construct with these two new B/c vectors is similar to that described for previous *AtMIR390a-B/c*-based vectors (Carbonell et al., 2014) (Figure S4 and Appendix S1).

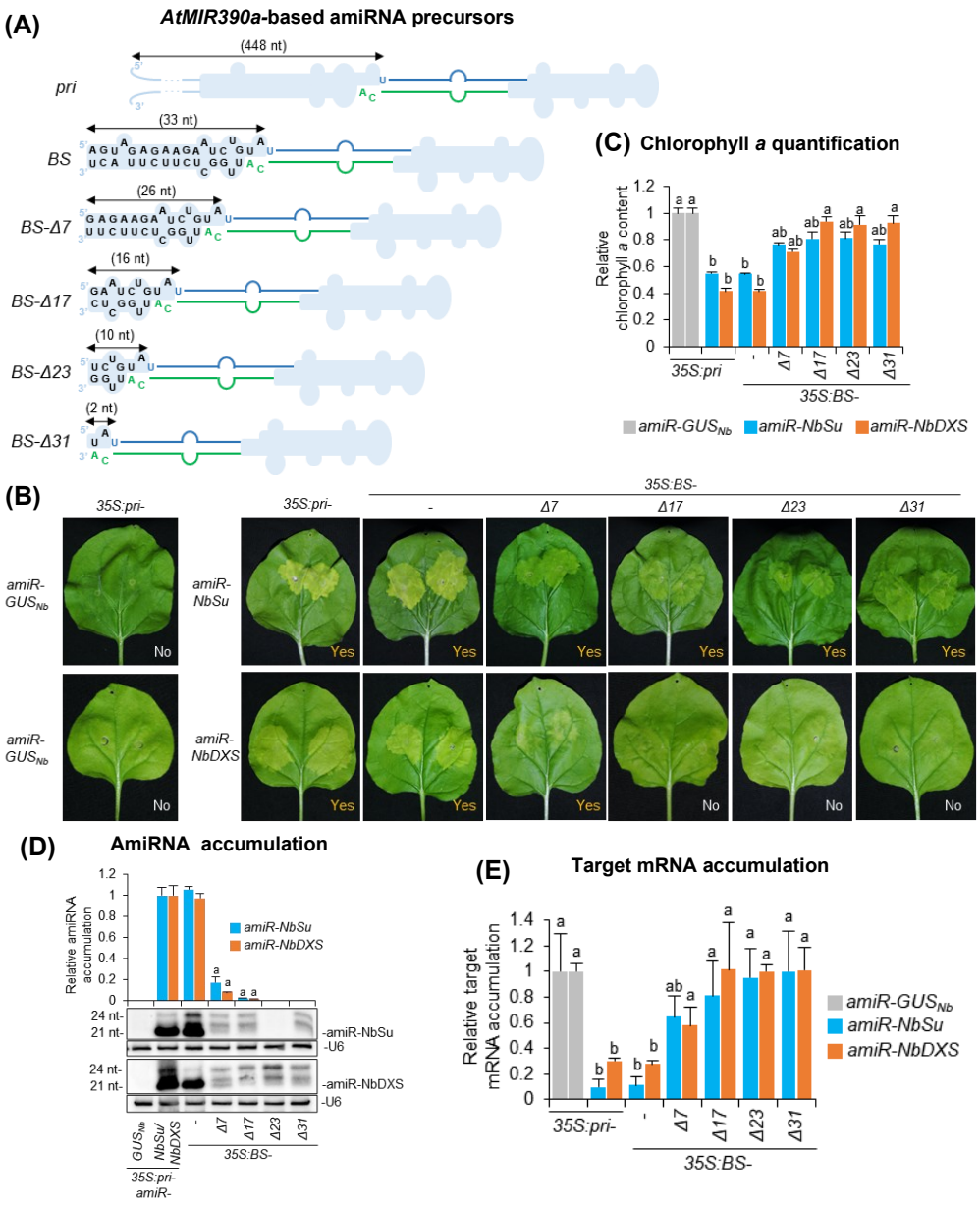

Figure 4. Functional analysis of constructs expressing the amiR-NbSu amiRNA against *N. benthamiana SULPHUR* (*NbSu*) or *DXS* (*NbDXS*) from *AtMIR390a* precursors with shortened basal

stem (BS) region. (**A**) Diagrams of the amiRNA precursors. The size in nucleotides of the BS region of each precursor is given. Other details are as in Figure 2B. (**B**) Photos at 7 days post-agroinfiltration (dpa) of leaves agroinfiltrated with different constructs. (**C**) Bar graph showing the relative content of chlorophyll *a* in patches agroinfiltrated with different constructs (*pri-amiR-GUS*$_{Nb}$ = 1.0). Other details are as in Figure 2D. (**D**) Northern blot detection of amiR-NbSu and amiR-NbDXS amiRNAs in RNA preparations from agroinfiltrated leaves at 2 dpa. Other details are as in Figures 2D and 2E. (**E**) Target mRNA accumulation in agroinfiltrated leaves. Other details are as in Figures 2D and 2F.

Transient expression of amiRNAs from shortened, *MIR390*-based chimeric precursors triggers effective silencing of *N. benthamiana* endogenous genes and of pathogenic viral RNAs

Because our previous results showed that the efficiency of amiRNA production and induced silencing of *N. benthamiana* endogenous genes were maintained in shortened precursors including the *BS* or *OsMIR390-D2* regions, the new "B/c" vectors were used to systemically test the effect of combining both regions in a single precursor. The resulting shortened chimeric *MIR390*-based precursor of only 89 nt was named *shc-MIR390* precursor (or simply "*shc*") (Figure 5A). First, we introduced into *pMDC32B-BS-AtMIR390a-B/c* the sequence corresponding to amiR-NbSu or amiR-NbDXS including the *OsMIR390-D2* region to generate the *35S:shc-amiR-NbSu* or *35S:shc-amiR-NbDXS* constructs, respectively. Both constructs were independently agroinfiltrated into *N. benthamiana* leaves together with control constructs, and induced similar strong bleaching, amiRNA accumulation and target mRNA downregulation in agroinfiltrated areas than their respective controls expressing these same amiRNAs from the full-length *pri* precursor (Figure 5B-D). To confirm the correct processing of *shc* precursors and compare it to that of the *pri*, sRNA libraries from leaves expressing *35S:pri-amiR-NbSu*, *35S:pri-amiR-NbDXS*, *35S:shc-amiR-NbSu* and *35S:shc-amiR-NbDXS* were prepared and sequenced. Interestingly, in samples expressing *35S:shc-amiR-NbSu* or *35S:shc-amiR-NbDXS,* the majority (95% and 90% respectively) of 19-24-nt (+) reads mapping within ± 4 nt of the 5' end of the amiRNA guide corresponded to authentic 21-nt amiR-NbSu or amiR-NbDXS (Figure 5E). These results indicate a high accuracy in the processing of *shc* precursors which was similar to that observed for the *pri* precursors (Figure 5E, Figure S5).

Next, we aimed to test if amiRNAs produced from the *shc* precursor could also be applied to silence exogenous transcripts, such as viral RNAs. Here, the sequence corresponding to the most efficient anti-tomato spotted wilt virus (TSWV) amiRNA (amiR-TSWV) identified in previous amiRNA screenings (Carbonell, López, et al., 2019) was expressed from the *shc* precursor in a *N. benthamiana* leaf inoculated two days later with TSWV (Figure S6A). At 7 days post-inoculation (dpi), all leaves inoculated with TSWV and expressing amiR-TSWV either from the *pri* or *shc* precursors did not display virus-induced symptoms, while leaves inoculated

with TSWV and expressing the control amiR-GUS$_{Nb}$ displayed multiple local lesions typical of TSWV infection (Figure S6B). AmiRNA accumulation analyzed by sRNA northern blot showed that amiR-TSWV accumulated to similar levels in tissues expressing *35S:shc-amiR-TSWV* or *35S:pri-amiR-TSWV* (Figure S6C). At 20 dpi, TSWV RNA was not detected in upper non-inoculated leaves from plants inoculated with TSWV and expressing *35S:shc-amiR-TSWV* or *35S:pri-amiR-TSWV*, while plants expressing *35S:pri-amiR-GUS$_{Nb}$* and inoculated with TSWV accumulated high levels of TSWV RNA (Figure S6C). Thus, these results indicate that the *shc* precursor can be used to express high levels of amiRNAs to induce antiviral resistance in plants.

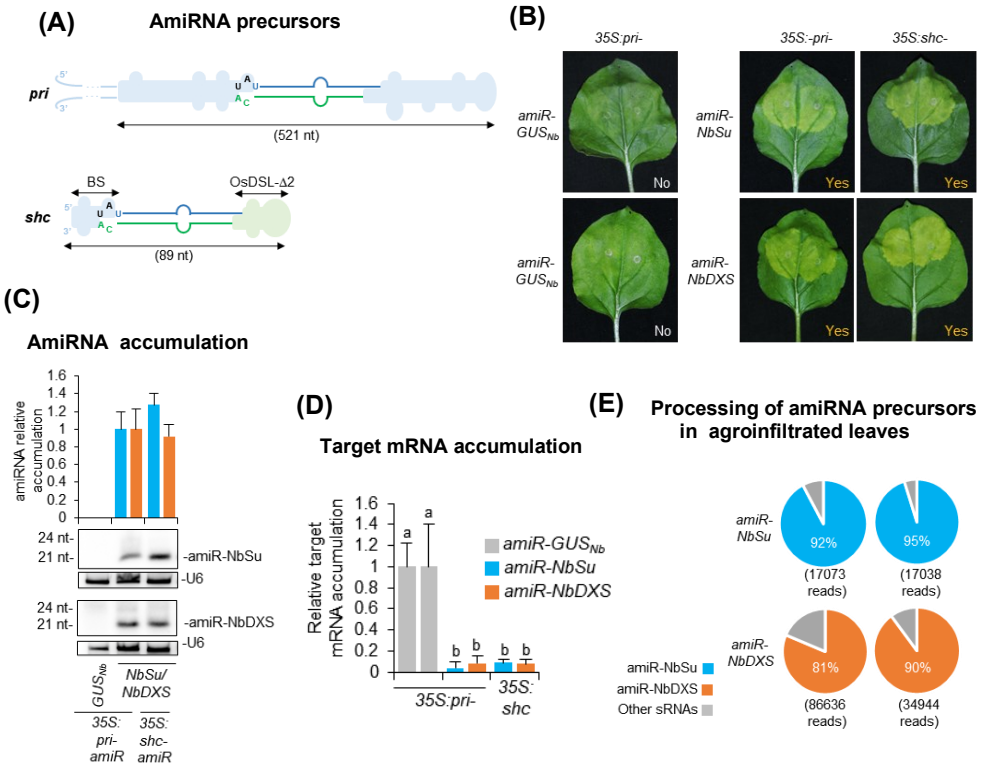

Figure 5. Functional analysis of constructs expressing the amiR-NbSu amiRNA against *N. benthamiana SULPHUR* (*NbSu*) or *DXS* (*NbDXS*) from *pri* and *shc* precursors. (**A**) Diagrams of the *pri* and *shc* amiRNA precursors. The total length of each precursor is indicated. Other details are as in Figure 2B. (**B**) Photos at 7 days post-agroinfiltration (dpa) of leaves agroinfiltrated with the two constructs. (**C**) Northern blot detection of amiR-NbSu and amiR-NbDXS amiRNAs in RNA preparations from agroinfiltrated leaves at 2 dpa. Other details are as in Figures 2D and 2E. (**D**) Target mRNA accumulation in agroinfiltrated leaves. Other details are as in Figures 2D and 2F. (**E**) amiRNA processing from *AtMIR390a*-based precursors. Pie charts show percentages of reads corresponding to expected, accurately processed 21-nucleotide mature amiR-NbSu and amiR-NbDXS (blue or orange sections, respectively) or to other 19–24-nucleotide sRNAs (gray sectors).

Stable expression of amiRNAs from *shc-MIR390* precursors leads to effective silencing of Arabidopsis endogenous genes

Next, we aimed to further confirm the functionality of *shc* precursors in a different plant species and when stably expressed in transgenic plants. For that purpose we used the amiR-AtFT/*AtFT* and amiR-AtCH42/*AtCH42* silencing sensor systems in Arabidopsis in which the transgenic expression of amiR-AtFT or amiR-AtCH42 from *pri-AtMIR390a* leads to a significant delay in flowering time or to an intense bleaching due to the targeting of endogenous *FLOWERING LOCUS T* (*AtFT*) or *CHLORINA 42* (*AtCH42*) endogenous genes, respectively (Carbonell et al., 2014). Here, we introduced amiR-AtFT and amiR-CH42 into *pMDC32B-BS-AtMIR390a-B/c* to generate the *35S:shc-amiR-AtFT* and *35S:shc-amiR-AtCH42* constructs, respectively (Figure 6A). These constructs were transformed independently into Arabidopsis Col-0 plants together with control constructs *35S:pri-amiR-GUS*$_{Ath}$, *35S:pri-amiR-AtFT* and *35S:pri-amiR-AtCH42* expressing an amiRNA against GUS (with no predicted off-targets in Arabidopsis), *AtFT* and *AtCH42*, respectively, from *pri-AtMIR390a*. To systemically compare the processing and induced silencing of amiR-AtFT or amiR-AtCH42 produced from *shc* and *pri* precursors, plant phenotypes, amiRNA and target mRNA accumulation and processing efficiency were measured in Arabidopsis T1 transgenic lines.

All *35S:pri-amiR-AtFT* (n=40) and *35S:shc-amiR-AtFT* (n=34) transformants flowered later than the average flowering time of the *35S:pri-amiR-GUS*$_{Ath}$ control lines (n=48) (Figure 6B, Table S2), and their average flowering time (54.7 $\pm$ 6 and 54.4 $\pm$ 3.2, respectively) was not significantly different between each other (Figure 6C). RNA-blot and RT-qPCR assays revealed that both amiR-AtFT and *AtFT* mRNA accumulation was similar in lines expressing amiR-AtFT from each of the two precursors (Figure 6D), and high-throughput sequencing of sRNAs showed that both precursors were efficiently processed, as in both cases 99% of the reads corresponded to authentic amiR-AtFT (Figure 6E, Figure S7). Similarly, all *35S:pri-amiR-AtCH42* (n=54) and *35S:shc-amiR-AtCH42* (n=38) transformants displayed bleaching of comparable degrees (Figure 6B and 6C; Table S2), accumulated similar levels of amiR-CH42 and AtCH42 mRNA (Figure 6D), and displayed effective precursor processing (Figure 6E, Figure S7). Taken together these results indicate that the *shc* precursor is functionally equivalent to the *pri* precursor in inducing highly effective silencing of endogenous genes when stably expressed in Arabidopsis.

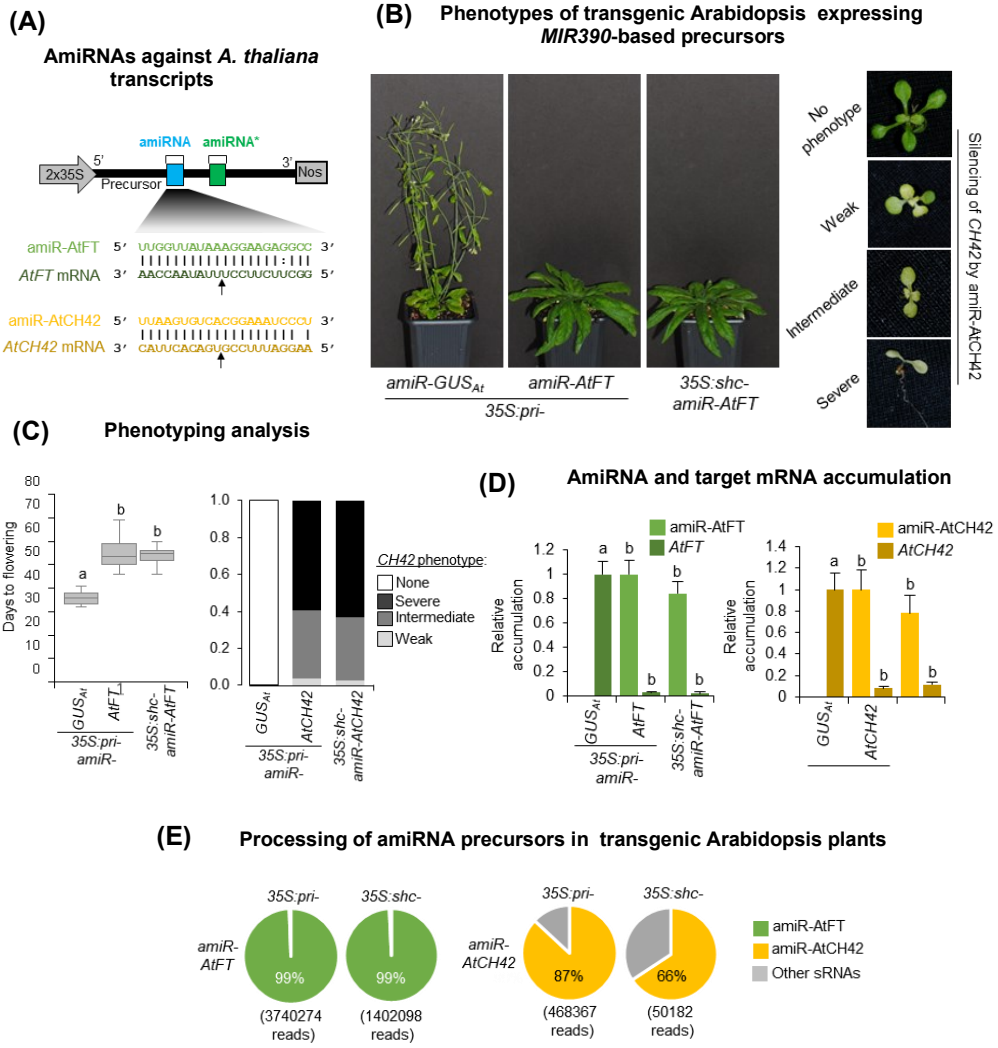

Figure 6. Functional analysis of constructs expressing the amiR-AtFT and amiR-AtCH42 amiRNAs against *A. thaliana FLOWERING LOCUS T* (*AtFT*) or *CHLORINE 42* (*AtCH42*) from *pri* and *shc* precursors. (**A**) Nucleotides corresponding to the guide strand of the amiRNA against *AtFT* and *AtCH42* are in light green and light yellow, respectively, while nucleotides of *AtFT* and *AtCH42* target mRNAs are in dark green and dark yellow, respectively. Other details are as in Figure 2A. (**B**) Representative images of Arabidopsis T1 transgenic plants expressing amiRNAs from different precursors. Left, 45-day-old adult plants expressing amiR-GUS$_{At}$ or amiR-AtFT. Right, 10-day-old T1 seedlings expressing amiR-AtCH42 and showing bleaching phenotypes of diverse degrees. (**C**) Phenotyping analysis. Left, box plot representing the mean flowering time of Arabidopsis T1 transgenic plants expressing amiR-GUS$_{At}$ or amiR-AtFT from different precursors. Pairwise Student's t-test comparisons are represented with the letter 'a' if significantly different ($P < 0.05$) and the letter 'b' if not ($P > 0.05$). Right, bar graph representing, for each line, the proportion of seedlings displaying a severe (black areas), intermediate (dark gray areas), or weak (light gray areas) bleaching phenotype, or with wild-type appearance (white areas). (**D**) amiRNA and target RNA

accumulation. Left, bar graph showing the relative accumulation of amiR-AtFT [mean relative level (n = 3) + standard deviation amiRNA relative accumulation, *pri-amiR-AtFT* = 1.0] and of *AtFT* mRNA [mean relative level (n = 3) + standard error of *AtFT* mRNAs after normalization to *ACTIN 2* (*AtACT2*), as determined by quantitative RT-qPCR, *pri-amiR-GUS*$_{At}$ = 1]. Right, bar graph showing the relative accumulation of amiR-AtCH42 [mean relative level (n = 3) + standard deviation amiRNA relative accumulation, *pri-amiR-AtCH42* = 1.0] and of *AtCH42* mRNA [mean relative level (n = 3) + standard error of *AtCH42* mRNAs after normalization to *ACTIN 2* (*AtACT2*), as determined by quantitative RT-qPCR, *pri-amiR-GUS*$_{At}$ = 1]. (**E**) amiRNA processing from *pri* or *shc* precursors. Pie charts show percentages of reads corresponding to expected, accurately processed 21-nucleotide mature amiR-AtFT and amiR-AtCH42 (green or yellow sections, respectively) or to other 19–24-nucleotide sRNAs (gray sectors).

Unique functionality of the *shc* precursor in triggering widespread gene silencing in *N. benthamiana* when expressed from a viral vector

Because cargo capacity of viral vectors is limited, and large inserts are typically eliminated during viral replication in VIGS vectors (Rössner et al., 2022), we hypothesized that the short (89-nt long) *shc* precursor fragment could be a more stable insert when included into a viral vector than the longer 521-nt *pri* precursor. To test this, *pri-amiR-NbSu* and *shc-amiR-NbSu* sequences were inserted into a PVX infectious clone to generate the *35S:PVX-pri-amiR-NbSu* and *35S:PVX-shc-amiR-NbSu* constructs, respectively (Figure 7A). These constructs were expected to express amiR-NbSu from *pri* and *shc* precursors, respectively, during PVX infection and induce the bleaching of PVX-infected tissues. In addition, the *35S:PVX-pri-amiR-GUS*$_{Nb}$ negative control construct was also generated. These three constructs together with the insert-free *35S:PVX* construct (Figure 7A) were independently agroinoculated in one leaf of three *N. benthamiana* plants. A “mock” set of plants was agroinfiltrated with the agroinfiltration solution. Mild leaf curling typical of PVX-induced symptoms was observed in upper non-agroinoculated leaves between 4 and 5 dpa in all plants agroinoculated with the *35S:PVX* and *35S:PVX-shc-amiR-NbSu* constructs (Figure 7B). However, curling in apical leaves from plants agroinoculated with the *35S:PVX-pri-amiR-GUS*$_{Nb}$ and *35S:PVX-pri-amiR-NbSu* constructs appeared 3-4 days later, between 7 and 9 dpa (Figure 7B). Interestingly, bleaching of apical leaves appeared at 8-9 dpa only in plants agroinoculated with the *35S:PVX-shc-amiR-NbSu* construct, and at 14 dpa extended to most of the apical tissues of infected plants (Figure 7C). Additional analyses confirmed the decrease in chlorophyll *a* level in bleached tissues (Figure 7D). Plants were monitored until 28 dpa, and only those expressing the *35S:PVX-shc-amiR-NbSu* construct displayed the characteristic yellowing derived from *NbSu* silencing. RNA-blot and RT-qPCR analyses showed that only tissues from plants expressing *35S:PVX-shc-amiR-NbSu* accumulated high levels of amiR-NbSu (Figure 7E) and low levels of *NbSu* mRNA (Figure 7F). Interestingly, sRNA sequencing from apical leaves of plants agroinoculated with *35S:PVX-shc-amiR-NbSu* revealed that the shc-amiR-NbSu precursor inserted into PVX was accurately

processed (Figure 7G, Figure S8). Additional analyses showed that the percentages of sRNAs of (+) or (-) polarity derived from the PVX sequence are similar (48% and 52%, respectively), suggesting that these sRNAs originate from double-stranded RNA (dsRNA) intermediates produced by RNA-dependent RNA polymerases during PVX replication (Figure S9). In contrast, the majority (89%) of sRNAs derived from the shc-amiR-NbSu sequence included in PVX are of (+) polarity, similarly to when the same precursor is expressed without PVX (Figure S9). These results most likely indicate that amiR-NbSu originates from the *shc* precursor rather than from dsRNA intermediates of replication.

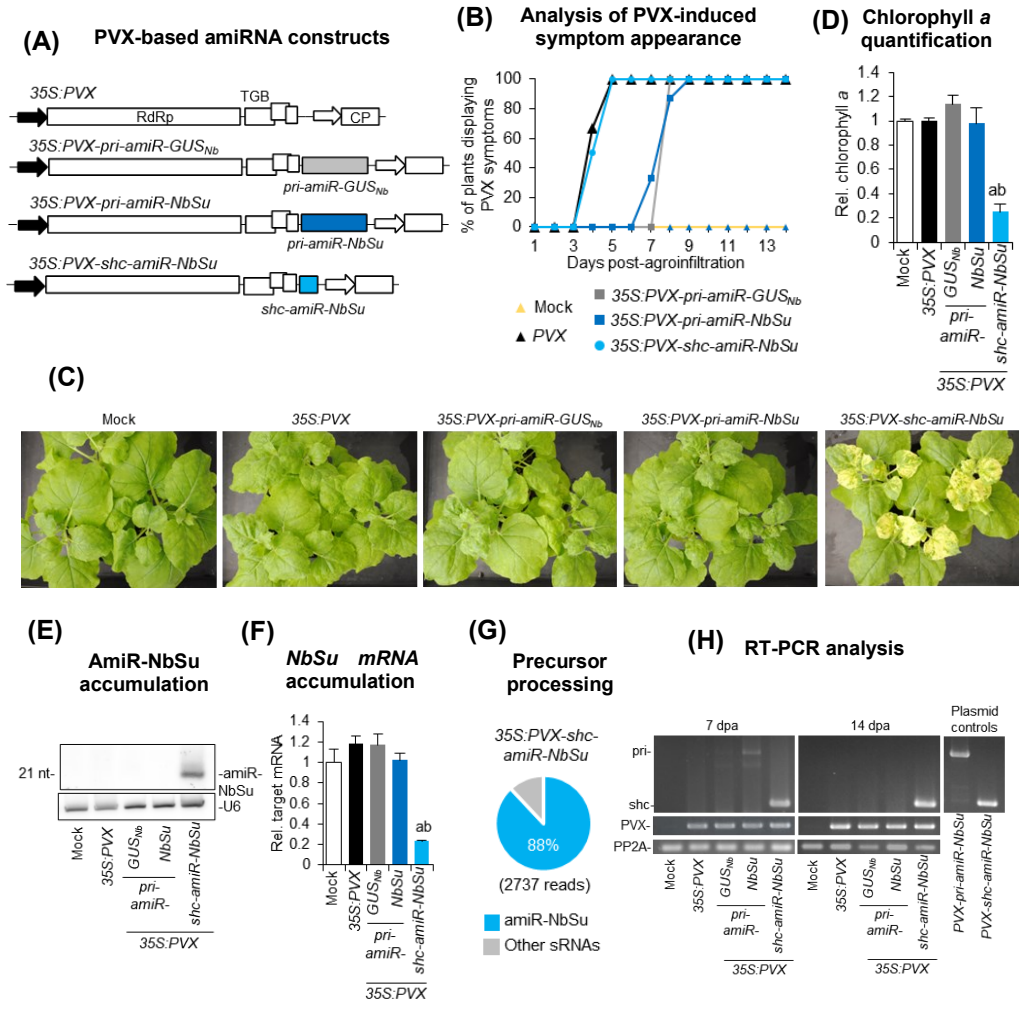

Figure 7. **Functional analysis of *Potato virus X* (PVX) constructs expressing amiRNAs from *pri* and *shc* precursors.** (**A**) Diagram of PVX-based constructs. *pri-amiR-GUS*$_{Nb}$, *pri-amiR-NbSu* and *shc-amiR-NbSu* cassettes are shown in grey, dark blue and light blue boxes, respectively. PVX genes RdRp, TGB

and CP are represented in white boxes, and CP promoter from *Bamboo mosaic virus* (BaMV) with a white arrow. (**B**) Two-dimensional line graph showing, for each of the three-plant sets listed, the percentage of symptomatic plants per day during 14 days. (**C**) Photos at 14 days post-agroinfiltration (dpa) of sets of three plants agroinfiltrated with the different constructs. (**D**) Bar graph showing the relative content of chlorophyll *a* in apical leaves from plants agroinfiltrated with different constructs (Mock = 1.0). Bar with the letter "a" are significantly different from that of the corresponding mock control samples ($P < 0.05$ in pairwise Student's t-test comparison). (**E**) Northern blot detection of amiR-NbSu in RNA preparations from apical leaves collected at 14 dpa and pooled from three independent plants. (**F**) Target *NbSu* mRNA accumulation in RNA preparations from apical leaves collected at 14 dpa and analyzed individually. Mean relative level (n = 3) + standard error of *NbSu* mRNAs after normalization to *PROTEIN PHOSPHATASE 2A* (*PP2A*), as determined by RT-qPCR (mock = 1.0 in all comparisons). Other details are as in D. (**G**) amiR-NbSu processing from the *shc* precursor included in PVX (*35S:PVX-shc-amiR-NbSu* construct). Pie chart show percentages of reads corresponding to expected, accurately processed 21-nucleotide mature amiR-NbSu (blue sections) or to other 19–24-nucleotide sRNAs (gray sectors). (**H**) RT-PCR detection of PVX, *pri* and *shc* precursors in apical leaves at 7 and 14 dpa. RT-PCR products corresponding to the control *NbPP2A* are also shown (bottom), as well as control amplifications of *pri* and *shc* fragments from plasmids.

Finally, the presence of both *pri* and *shc* precursors in apical leaves was analyzed by RT-PCR at 7 and 14 dpa with oligonucleotides flanking the precursor insertion site. At 7 dpa, the *shc* precursor was clearly amplified in plants expressing *35S:PVX-shc-amiR-NbSu*, while only the *pri* precursor of the *35S:PVX-pri-amiR-NbSu* samples was barely detected (Figure 7H). Indeed, at 14 dpa only the *shc* precursor was detected (Figure 7H). Importantly, PVX was detected in all plants expressing PVX-based constructs at the two timepoints analyzed (Figure 7H) thus excluding the possibility that the absence of *pri* precursors was due to a lack of infection in these samples. Sequencing analysis of RT-PCR products from each of the three *PVX-shc-amiR-NbSu* infected samples showed that no mutations accumulated in the *shc-amiR-NbSu* insert. These results indicate that the *pri* fragments are eliminated from the PVX vector during viral infection, while the shorter *shc* fragments are stable both structurally and at a sequence level.

A PVX-based, DNA-free system for inducing widespread silencing in plants with amiRNAs

Next, we explored the possibility of triggering widespread silencing in a DNA-free, non-transgenic manner, by using alternative methods to agroinfiltration for inoculating *shc*-containing PVX sequences. For this purpose, a crude extract from bleached apical leaves of each of the three individual plants agroinoculated with *35S:PVX-shc-amiR-NbSu* was prepared. Each crude extract was used as inoculum to mechanically inoculate one young *N. benthamiana* plant (Figure 8A). As controls, similar crude extracts were prepared from mock and empty PVX-agroinoculated plants and analyzed in parallel. Interestingly, all three plants mechanically inoculated with extracts derived from *35S:PVX-shc-amiR-NbSu* agroinfiltrated plants displayed prominent bleaching and accumulated authentic PVX-derived *shc-amiR-NbSu* precursors

(Figure 8B) with no sequence alterations as confirmed by sequencing of RT-PCR products. Plants inoculated with extracts from *35S:PVX*-agroinfiltrated plants displayed mild PVX characteristic symptoms and accumulate PVX RNAs, while plants inoculated with extracts derived from mock-inoculated plants remained symptomless and virus-free (Figure 8B).

Finally, we wondered if widespread silencing could also be triggered by applying PVX-shc-amiR-NbSu-containing raw extracts through spraying (Figure 8A). Remarkably, all three plants sprayed with crude extracts derived from *35S:PVX-shc-amiR-NbSu* agroinoculated plants displayed bleached apical leaves which accumulated authentic *shc-amiR-NbSu* precursors with no sequence alterations as confirmed by sequencing of the RT-PCR products (Figure 8C). Importantly, plants sprayed with crude extracts from *35S:PVX*-agroinoculated plants or mock-inoculated plants displayed only mild PVX-derived symptoms or no symptoms at all, respectively, and no bleaching (Figure 8C). These results indicate that crude extracts can be directly sprayed to leaves to trigger amiR-VIGS in *N. benthamiana* in a non-transgenic, DNA-free manner.

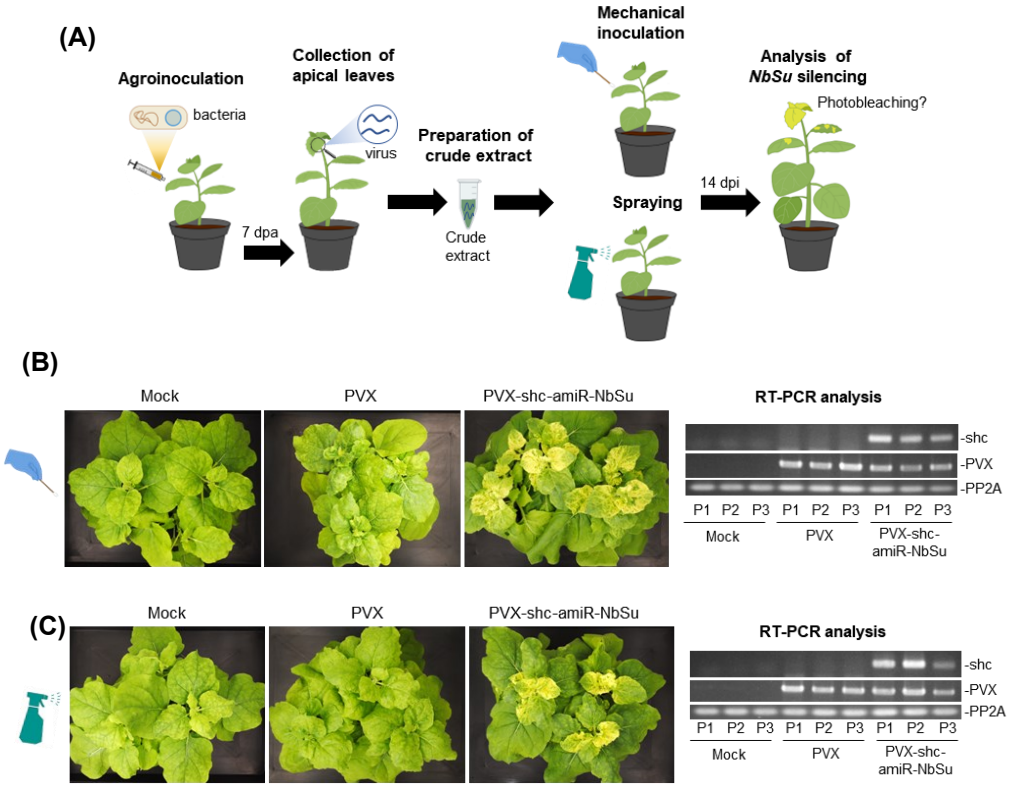

Figure 8. **Non-transgenic, DNA-free widespread gene silencing through amiR-VIGS**. (**A**) Experimental set up to test gene silencing triggered by *PVX-shc-amiR-NbSu*. (**B**) Widespread *NbSu* silencing induced by

mechanically inoculated crude extracts. Left, photos at 14 days post-agroinfiltration (dpa) of sets of three plants mechanically inoculated with different crude extracts obtained from agroinoculated plants. Right, RT-PCR detection of PVX and *shc* precursors in apical leaves at 14 dpa. RT-PCR products corresponding to the control *NbPP2A* are also shown (bottom). (**C**) Widespread *NbSu* silencing induced by sprayed crude extracts. Left, photos at 14 days post-agroinfiltration (dpa) of sets of three plants sprayed with different crude extracts obtained from agroinoculated plants. Right, RT-PCR detection of PVX and *shc* precursors in apical leaves at 14 dpa. Other details are as in B.

DISCUSSION

In this work, we have systematically analyzed the minimal structural and sequence requirements for producing effective amiRNAs from the 521-nt long *AtMIR390a* precursor. Our analyses show that highly effective amiRNAs can be produced from the considerably shorter *shc* precursor of only 89 nt, including the BS of *AtMIR390a* and the DSL of *OsMIR390* with a 2-nt deletion. The unique ability of *shc* precursors to stably and efficiently express authentic amiRNAs from an RNA viral vector, such as that derived from PVX, highlights the utility of engineering such class of minimal precursors for transgene-free widespread gene silencing in plants.

Effects on miRNA accumulation of sequence modifications at the BS of the precursor

Systematic mutational analyses done in several plant pri-miRNAs for analyzing miRNA production have shown that, for base-to-loop processed precursors, sequence modifications at the BS region have more deleterious effects in both foldback processing efficiency and accuracy than mutations in the DSL region, while deletions of nucleotides of the ssRNA segments seem largely neutral (Bajczyk et al., 2023; Li & Yu, 2021). In several plant *MIRNA* precursors, a single change in the BS ~15 nt below the miRNA is sufficient to completely abolish their processing (Mateos et al., 2010; Song et al., 2010; Werner et al., 2010), as observed for instance in *AtMIR390a*, in which a G-to-A point mutation in the base of the foldback resulted in misprocessing of the miR390/miR390* duplex and subsequent reduction in *TAS3*-derived tasiRNA levels (Cuperus, Montgomery, et al., 2010). All in all, these studies support the idea that base-to-loop precursors require a BS of ~15 nt for DCL1 recognition and accurate first cleavage(Cuperus et al., 2011).

Our results generally agree with this, as shortening *AtMIR390a* BS drastically affects both amiRNA accumulation and induced target mRNA silencing. Still, it is worth to note that some degree of amiRNA accumulation and target mRNA silencing was observed when expressing amiRNAs from the *BS-D7* precursor, suggesting that DCL1 activity may not be completely

abolished when processing *AtMIR390a*-based amiRNA precursors with a BS shorter than 15 nt. Pertinent to this context, it was reported that an artificially shortened form of *AtMIR166b* precursor with only six nucleotides at the BS was processed *in vivo*, releasing miR166b and causing developmental defects (Chorostecki et al., 2017). Importantly, it seems that an intact BS of *AtMIR390a* is necessary but sufficient for high amiRNA accumulation to levels comparable to those obtained with the *pri-AtMIR390a* precursor. Similarly, it was previously reported that miR171 was efficiently and accurately released from the *AtMIR171* foldback in *N. benthamiana* (Parizotto et al., 2004), thus reinforcing the idea that ssRNA segments seem dispensable for efficient and accurate miRNA precursor processing. In contrast, in the case of loop-to-base precursors, the BS region is probably dispensable for processing, as shown with the efficient processing of an *AtMIR157c*-based precursor lacking the BS region (Moro et al., 2018). In a more recent genome-wide study, a set of sequence features for the processing of plant pri-miRNA precursors were identified (Rojas et al., 2020). In particular, specific nucleotide pairs at the precursors' DCL1 cleavage sites were observed, with the identity of the nucleotides located at the mismatched positions of the BS having a big impact on the processing efficiency. Here, we did not analyze the effect of changing the identity of the nucleotides that are mismatched in *AtMIR390a* BS. Hence, we cannot rule out that some of these changes might, for instance, increase amiRNA accumulation, as observed for miR172 when expressed from *pri-AtMIR172a* with intentionally paired nucleotides at the first DCL1 cleavage site (Rojas et al., 2020).

Effects of sequence modifications at the DSL of the precursor on miRNA accumulation

For base-to-loop processed miRNA precursors, a few reports have shown that their native DSL region can be modified without compromising the processing of the precursor. For instance, eliminating bulges at the DSL does not interfere with miR167 biogenesis from *AtMIR167a* precursors (Song et al., 2010), while an *AtMIR166b* precursor with a truncated DSL region of only 22-nt accumulated miR166b to levels similar to those obtained with the wild-type precursor (Chorostecki et al., 2017). Here, deletions of 6-13 nt in the stem of *AtMIR390a* DSL were tolerated, while further shortening of the stem dramatically decreased or abolished amiRNA biogenesis. Interestingly, the chimeric *pri-AtMIR390a-OsDSL* precursor including *OsMIR390* DSL produced high amounts of amiR-NbSu and amiR-NbCla in *N. benthamiana* agroinfiltrated leaves, as reported before for other amiRNA sequences (Carbonell et al., 2015). In this work, we further deleted the distal stem of *OsMIR390* while maintaining the terminal loop and found that a 2-nt deletion was tolerated, while longer deletions had a negative effect of amiRNA

accumulation. This result suggests that a minimal distal stem length is required for efficient processing, as proposed before for explaining miR172 misprocessing from an *AtMIR172* precursor lacking the terminal loop (Mateos et al., 2010).

A DNA-free, RNA virus-based system to induce widespread gene silencing in plants

AmiRNAs expressed from viral vectors have been used before in plants for silencing endogenous genes. In particular, nuclear-replicating viruses of DNA genome such as cabbage leaf curl virus (CaLCuV), tomato yellow leaf curl China virus (TYLCCNV) or tomato mottle virus (ToMoV) successfully expressed authentic amiRNAs in *N. benthamiana* (Ju et al., 2017; Kuo & Falk, 2022; Y. Tang et al., 2010), while the cytoplasmic-replicating tobacco mosaic virus (TMV) of RNA genome failed to produce effective amiRNAs in this same host (Kuo & Falk, 2022). Interestingly, there is only one example in plants of the use of cytoplasmic-replicating RNA virus [barley stripe mosaic virus (BSMV)] to express amiRNAs (Jian et al., 2017), although the accumulation of authentic amiRNAs *in vivo* was not proven. Still, a major drawback of the mentioned nuclear-replicating DNA viruses for use in amiR-VIGS is their limited host-range and, in some cases, tissue tropism, with viral replication restricted to phloem cells.

Here we used PVX, a plus (+) single-stranded RNA virus infecting 62 plant species of 27 families including important crops in the family *Solanaceae* (e.g. potato, tomato, pepper or tobacco) (Adams et al., 2004; Loebenstein & Gaba, 2012), to efficiently produce authentic amiRNAs in *N. benthamiana* as shown by northern blot and high-throughput sRNA sequencing. Where the *shc* precursors are accurately processed from PVX RNAs to release authentic 21-nt amiRNAs and which DCL is involved in this process is unknown. What is known is that PVX replicates in the cytoplasm and that DCL4 is the primary plant DCL functioning in antiviral defense against RNA viruses and producing 21-nt sRNAs from diced viral RNAs (Bouché et al., 2006; Deleris et al., 2006). It is also known that DCL4, besides its ability for processing long dsRNA precursors, can access flexibly structured single-stranded RNA substrates such as pre-miRNA-like RNAs, as shown in the biogenesis of several sRNAs derived from the satellite RNA of cucumber mosaic virus (Du et al., 2007). Despite DCL4 could be the DCL generating amiR-NbSu from PVX RNAs, we cannot rule out that DCL1 might be transiently translocated to the cytoplasm to process the amiRNA precursor, similarly to what has been described with the redistribution of Drosha during a Sindbis virus infection in an animal system (Shapiro et al., 2010, 2012). Alternatively, DCL1 might also act in the cytoplasm right after its synthesis and before being shuttled to the nucleus. We cannot either rule out that PVX RNA fragments that act as amiRNA precursors or the whole PVX genomic RNA enter transiently into the nucleus

allowing DCL1 processing and release of the amiRNA, although this last scenario seems more unlikely. In any case, *35S:PVX-amiR-NbSu*-triggered *NbSu* silencing in *DCL4i* knockdown plants is significantly reduced compared to wild-type and DCL1i knockdown *N. benthamiana* plants (Figure S10). These results suggest that DCL4 could be the main DCL responsible for the generation of amiR-NbSu from PVX RNAs in the cytoplasm acting directly on the precursor. In any case, the precision in the processing of the *shc* precursor from viral RNAs is remarkable (Figure 7G and Figure S8), and essentially no 21-nt secondary, phased sRNAs derived from amiRNA targets were detected (Data S3, Figure S11) suggesting a lack of transitivity that reinforces the specificity of the PVX-based amiR-VIGS approach.

Interestingly, our data presented in Figure S8 suggests that amiR-NbSu is processed from PVX (+) strand RNAs and not from RdRP-derived dsRNA replication intermediates. Processing of PVX genomic RNA to produce amiR-NbSu seems unlikely, as this may have a deep impact on virus infectivity. Also, it may be difficult that amiR-NbSu precursor folds properly when embedded within the large genomic RNA. In contrast, based on the design of the PVX-based amiR-VIGS construct, the amiR-NbSu precursor is at the 5' terminus of the subgenomic RNA, which may allow its proper folding for accurate amiR-NbSu release. For all these reasons, amiR-NbSu may be derived from the subgenomic (+) RNA generated during the infection rather than from PVX genomic RNA.

The use of viral vectors in VIGS approaches typically depends on the agroinfiltration of plant tissues with DNA construct(s) for triggering the viral infection (Rössner et al., 2022). Therefore, although not stably transformed, transgenic plant tissues are produced, what certainly limits the biotechnological applications of this type of strategies. Our system uses crude extracts as inoculum, which are obtained from apical (non-agroinfiltrated) leaves infected with PVX variants carrying the amiRNA precursor. Hence, the use of crude extracts for triggering amiR-VIGS circumvents this limitation, while the delivery of raw extracts to plants through spraying should allow to scale up this methodology for large-surface applications in fields. A key aspect to highlight is the high stability of the *shc* precursor, which is retained in PVX genome even after one passage without sequence alterations, despite the well-known proneness of PVX to lose inserted foreign sequences through *in planta* recombination (Lacomme & Chapman, 2008). Noteworthy, in this work, we used a PVX vector that incorporates a deletion of the amino-terminal end of the CP and a heterologous promoter derived from another potexvirus, BaMV, that was previously shown to contribute to insert stability (Dickmeis et al., 2014). In any case, the small size and high sequence stability of the *shc* precursor in PVX, as well as the high specificity intrinsic of the amiRNA approach, make this PVX-based amiR-VIGS strategy an attractive alternative to classic dsRNA-based VIGS in plants. Indeed, the degree of target

silencing induced by PVX constructs expressing amiR-NbSu from the *shc* precursor or a *NbSu* transcript fragment of the same size (89 nt) is similar (Figure S12). These results support that PVX-based amiR-VIGS with *shc* precursors is highly effective and may be preferred to classic dsRNA-based VIGS because of its higher specificity, at least when similar size inserts are used. AmiRNAs are computationally designed to exclusively silence the intended target(s) while target gene fragments included in classic VIGS constructs typically generate large populations of sRNAs of unpredicted size and sequence that can accidentally target cellular RNAs and induce undesired off-target effects.

Biotechnological interest of minimal amiRNA precursors

Several plant monocistronic miRNA precursors have been used to express amiRNAs in plants [reviewed in (Cisneros et al., 2021)]. Such precursors vary in structure and length, with an average length significantly higher than that of their corresponding miRNA foldback (Figure S13A), as most of them correspond to full-length pri-miRNA precursors. To our knowledge, the *shc-MIR390* precursor is the shortest of all amiRNA precursors tested in plants so far, being considerably shorter than its parental *pri-AtMIR390a* precursor (Figure S13B). Minimal amiRNA precursors may have several advantages. First, they should be more stable and retained in the viral genome for longer periods, as discussed before for PVX. This advantage may be of particular interest in amiR-VIGS experiments involving viruses with limited cargo capacity. Second, using shorter amiRNA precursor sequences should decrease the cost of producing amiRNA constructs, which is particularly convenient in high-throughput applications where large amounts of amiRNA constructs are generated for plant transformation (Hauser et al., 2013; Jover-Gil et al., 2014; Y. Zhang et al., 2018). Here, *shc* precursors are inserted into *BS-AtMIR390a-B/*c-based vectors after annealing two oligos of 58 bases, while cloning of amiRNA inserts in previous *AtMIR390a-B/c*-based vectors required the annealing of 75 bases-long oligonucleotides (Carbonell et al., 2014). Importantly, the reduction of the oligonucleotide length from 75 to 58 bases should allow for a more cost-effective oligo synthesis and at the lowest production scale (25 nmole) offered by the main oligo-manufacturing companies. And third, minimal amiRNA precursors may be more efficiently synthesized *in vitro* or in bacteria for topical application to plants, among other possible advantages. In any case, the use of minimal amiRNA precursors in a non-transgenic, DNA-free manner should definitely accelerate the development of next-generation RNAi treatments of crops in line with international regulations.

METHODS

Plant materials and growth conditions

N. benthamiana and *Arabidopsis thaliana* (Arabidopsis) Col-0 plants were grown in a growth chamber at 25ºC with a 12 h-light/12 h-dark photoperiod or at 22ºC with a 16 h-light/8 h-dark photoperiod, respectively. *DCL1i* and *DCL4i N. benthamiana* knockdown plants were described previously (Dadami et al., 2013). Arabidopsis Col-0 plants were genetically transformed using the floral dip method (Clough & Bent, 1998) with the *Agrobacterium tumefaciens* GV3101 strain. T1 transgenic Arabidopsis were grown as previously (López-Dolz et al., 2020). Photographs were taken with a Nikon D3000 digital camera with AF-S DX NIKKOR 18–55 mm f/3.5–5.6G VR lens.

Plant phenotyping

Plant phenotyping analyses were conducted in blind as described (López-Dolz et al., 2020). Briefly, the flowering time of each independent line is the number of days elapsed from seed plating to first bud opening (or "days to flowering"). The "CH42" phenotype was scored in 10 days old seedlings and was reported as "weak", "intermediate" or "severe" if seedlings had more than two leaves, exactly two leaves or no leaves at all (only two cotyledons), respectively.

Artificial small RNA design

AmiR-GUS$_{Nb}$, amiR-GUS$_{At}$, amiR-NbSu, and amiR-AtCH42 amiRNA design was described before (Cisneros et al., 2022; López-Dolz et al., 2020; Schwab et al., 2006).

P-SAMS script (https://github.com/carringtonlab/p-sams) (Fahlgren et al., 2016) returning unlimited optimal results was used to obtain the complete list of optimal amiRNAs targeting *NbDXS* with high specificity (Data S1). The off-targeting filtering in *N. benthamiana* transcriptome v5.1 (Nakasugi et al., 2014) was enabled in the design to increase amiRNA specificity.

DNA constructs

Oligonucleotides AC-627 and AC-628 were annealed and ligated into *pENTR-D-TOPO* to generate *pENTR-BS-AtMIR390a-BB* including the *BS* sequence interrupted by two inverted *Bsa*I restriction sites. The *B/c* cassette was excised from *Bsa*I-digested *pENTR-AtMIR390a-B/c* (Addgene plasmid #51778), (Carbonell et al., 2014) and ligated into *Bsa*I-digested *pENTR-BS-AtMIR390a-BB* to generated *pENTR-BS-AtMIR390a-B/c*. The *BS-AtMIR390a-BB* cassette from

pENTR-AtMIR390a-BB was transferred by LR recombination into *pMDC32B* (Carbonell et al., 2014), a version of *pMDC32* (Curtis & Grossniklaus, 2003; Nakasugi et al., 2014) with mutated *Bsa*I site, to generate *pMDC32B-BS-AtMIR390a-BB*. Finally, the *B/c* cassette was excised from *Bsa*I-digested *pENTR-AtMIR390a-B/c* and ligated into *Bsa*I-digested *pMDC32B-BS-AtMIR390a-BB* to generate *pMDC32B-BS-AtMIR390a-B/c.* AmiRNA *pENTR-BS-AtMIR390a-B/c* (Addgene plasmid 199559) and *pMDC32B-BS-AtMIR390a-B/c* vectors (Addgene plasmid 199560) are available from Addgene at (http://www.addgene.org/).

Constructs *35S:AtDSL-D6-amiR-NbSu*, *35S:AtDSL-D13-amiR-NbSu*, *35S:AtDSL-D21-amiR-NbSu*, *35S:AtDSL-D25-amiR-NbSu*, *35S:pri-amiR-NbDXS*, *35S:AtDSL-D6-amiR-NbDXS*, *35S:AtDSL-D13-amiR-NbDXS*, *35S:AtDSL-D21-amiR-NbDXS*, *35S:AtDSL-D25-amiR-NbDXS*, *35S:OsDSL-amiR-NbSu*, *35S:OsDSL-D2-amiR-NbSu*, *35S:OsDSL-D4-amiR-NbSu*, *35S:OsDSL-D6-amiR-NbSu*, *35S:OsDS-AtL-amiR-NbSu*, *35S:OsDSL-amiR-NbDXS*, *35S:OsDSL-D2-amiR-NbDXS*, *35S:OsDSL-D4-amiR-NbDXS*, *35S:OsDSL-D6-amiR-NbDXS*, *35S:OsDS-AtL-amiR-NbDXS* were obtained by ligating annealed oligonucleotide pairs listed in Table S1 into *pMDC32B-AtMIR390a-B/c* (Addgene plasmid 51776) as described (Carbonell et al., 2014). BS cassettes from *35S:pri-amiR-NbSu* (Cisneros et al., 2022) and *35S:pri-amiR-NbDXS* were amplified with oligo pairs AC-335/AC336, inserted into *pENTR-D-TOPO* and transferred by LR recombination into *pMDC32B* to generate *35S:BS-amiR-NbSu* and *35S:BS-amiR-NbDXS*, respectively.

DsDNA oligonucleotides AC-558, AC-559, AC-560, AC-561, AC-611, AC-612, AC-613 and AC-14 were ligated into *pENTR-D-TOPO* to generate *pENTR-BS-D7-amiR-NbSu*, *pENTR-BS-D17-amiR-NbSu*, *pENTR-BS-D23-amiR-NbSu*, *pENTR-BS-D31-amiR-NbSu*, *pENTR-BS-D7-amiR-NbDXS*, *pENTR-BS-D17-amiR-NbDXS*, *pENTR-BS-D23-amiR-NbDXS*, and *pENTR-BS-D31-amiR-NbDXS*, respectively. *BS* cassettes were transferred by LR recombination to *pMDC32B* to generate *35S:BS-D7-amiR-NbSu*, *35S:BS-D17-amiR-NbSu*, *35S:BS-D23-amiR-NbSu*, *35S:BS-D31-amiR-NbSu*, *35S:BS-D7-amiR-NbDXS*, *35S:BS-D17-amiR-NbDXS*, *35S:BS-D23-amiR-NbDXS*, *35S:BS-D31-amiR-NbDXS*.

Constructs *35S:shc-amiR-NbSu*, *35S:shc-amiR-NbDXS*, *35S:shc-amiR-TSWV*, *35S:shc-amiR-AtCH42, 35S:shc-amiR-AtFT* were obtained by ligating annealed oligonucleotide pairs AC-486/AC-487, AC-603/AC-604, AC-672/AC-673, AC-623/AC-624 and AC-621/AC-622, respectively into *pMDC32B-BS-AtMIR390a-B/c* as described (Appendix S1) (Carbonell, 2019).

The potato virus X (PVX) vector consisted of a modified version of PVX-MT799816.1 (Uranga et al., 2021). The PVX vector was cloned into *pLX-B2* (Pasin et al., 2017) flanked by the 35S CaMV promoter and terminator and an hepatitis delta virus ribozyme (Schürer et al.,

2002), to produce *pLB-PVX-MluI*. For PVX-based amiRNA constructs, *pri-* and *shc*-based cassettes were amplified from *35S:pri-amiR-GUS*$_{Nb}$/*35S:pri-amiR-NbSu* or *35S:shc-amiR-NbSu* constructs with oligonucleotides AC-648/AC-662 and AC-650/AC-663, respectively, gel purified and assembled into *Mlu*I-digested and gel-purified *pLB-PVX-MluI* in the presence of GeneArt Gibson Assembly HiFi Master Mix (Invitrogen) to generate *35S:PVX-pri-amiR-GUS*$_{Nb}$, *35S:PVX-pri-amiR-NbSu* and *35S:PVX-shc-amiR-NbSu*. See Appendix S2 for a general protocol to generate PVX-based amiRNA constructs. All precursors were expressed from endogenous PVX coat protein (CP) promoter. An heterologous promoter derived from bamboo mosaic virus (BaMV) drives the expression of PVX CP, which contains the deletion of the 29 initial codons to enhance the stability of the recombinant clones (Dickmeis et al., 2014). *35S:PVX* was obtained by digesting *pLB-PVX-Z* with *Mlu*I, gel purifying and re-ligating the backbone band. For *35S:PVX-NbSu(89)*, *NbSu(89)* cassette including 89 nucleotides from *NbSu* (positions 1004 to 1092 in reverse orientation) was amplified from *pLX-TRV2-CHLI* (Aragonés et al., 2022) with oligos AC-919/AC-921, and inserted in *pLB-PVX-MluI* as described above for amiRNA precursors.

AmiRNA constructs *35S:pri-amiR-GUS*$_{Nb}$ and *35S:pri-amiR-NbSu* were reported previously (Cisneros et al., 2022). All DNA oligonucleotides used for generating the constructs described above are listed in Table S1. The sequences of all amiRNA precursors are listed in Appendix S3. The sequences of the *BS-AtMIR390a*-based B/c amiRNA vectors are listed in Appendix S4.

Transient expression of constructs and mechanical inoculation of viruses

DNA constructs were agroinfiltrated in *N. benthamiana* leaves as described (Cuperus, Carbonell, et al., 2010; Llave et al., 2002), using *A. tumefaciens* GV3101 strain. Infection assays with TSWV LL-N.05 isolate were done as described (Carbonell, López, et al., 2019; Carbonell & Daròs, 2019). Mechanical inoculation with crude extracts from PVX infected plants was done as described for TSWV.

Chlorophyll extraction and analysis

Pigments from *N. benthamiana* infiltrated leaf tissues were extracted as described (Carbonell et al., 2015). Absorbance measurements and content in chlorophyll *a* were calculated as described (López-Dolz et al., 2020).

RNA preparation

Total RNA from *N. benthamiana* leaves or from Arabidopsis seedlings was isolated as follows. Tissue was ground in liquid nitrogen to fine powder and homogenized in extraction buffer (1 M

guanidinium thiocyanate, 1 M ammonium thiocyanate, 0.1 M sodium acetate, 5% glycerol, 38% water-saturated phenol). Next, RNA was extracted by chloroform extraction and precipitated after adding 0.5 volumes of isopropanol for 20 min. Triplicate samples from pools of two *N. benthamiana* leaves or 9-12 Arabidopsis seedlings were analyzed.

Real-time RT-qPCR

cDNA was obtained from 500 ng of DNaseI-treated total RNA from apical leaves at 14 days-post agroinoculation (dpa), using the PrimeScript RT Reagent Kit (Perfect Real Time) (Takara) according to the manufacturer's instructions.

Real time RT-qPCR was done as described in a QuantStudio 3 Real-Time PCR system (Thermo Fisher Scientific). *NbSu*/*NbDXS/PVX* and *AtCH42* target RNA expression levels were calculated relative to *N. benthamiana PROTEIN PHOSPHATASE 2A* (*NbPP2A*) and Arabidopsis *ACTIN 2* (*AtACT2*) reference genes, respectively, using the delta delta cycle threshold comparative method of the QuantStudio Design and Analysis Software (version 1.5.1.; Thermo Fisher Scientific). Oligonucleotides used for RT-qPCR are listed in Table S1.

Small RNA blot assays

Small RNA blot assays and band quantification from radioactive membranes were done as described (Cisneros et al., 2022). Oligonucleotides used as probes for sRNA blots are listed in Table S1.

Small RNA sequencing and data analysis

Total RNA quantity, purity and integrity was analyzed with a 2100 Bioanalyzer (RNA 6000 Nano kit, Agilent) and submitted to BGI (Hong Kong, China) for sRNA library preparation and SE50 sequencing in a DNBSEQ-G-400 sequencer (BGI). After reception of quality-trimmed, adaptor removed clean reads from BGI, fastx_collapser (http://hannonlab.cshl.edu/fastx_toolkit) (Hannon, 2010) was used to collapse identical reads into a single sequence, while maintaining read counts. A custom Python script was then used to map each clean, unique read against the forward strand of the amiRNA precursor overexpressed in each sample (Data S2) not allowing mismatches or gaps, and also to calculate the counts and RPMs (reads per million mapped reads) for each mapping position. Processing accuracy of amiRNA foldbacks was assessed by quantifying the proportion of 19-24 nt sRNA (+) reads that mapped within ± 4 nt of the 5' end of the amiRNA guide as reported before (Carbonell et al., 2015; Cuperus, Carbonell, et al., 2010). Phasing register tables were built by calculating the proportion of 21-nucleotide sRNA (+) reads in each register relative to the corresponding amiRNA cleavage site for all 21-

nucleotide positions downstream of the cleavage site, as described previously (Carbonell et al., 2014). List of 21-nucleotide sRNA (+) reads of target RNAs and species-specific tasiRNA-generating controls (*AtTAS1c* in Arabidopsis and *AtTAS3* in *N. benthamiana*) are shown in Data S3.

Stability and sequence analyses of amiRNA precursors during viral infections

Total RNA from apical leaves of each of the three biological replicates was pooled before cDNA synthesis, which was performed as explained above. PCR to detect amiRNA precursors, PVX and *NPP2A* was performed using oligonucleotide pairs AC-654/AC-655, AC-657/AC-658 and AC-365/AC-366 (Table S1), respectively, and Phusion DNA polymerase (ThermoFisher Scientific). PCR products were analyzed by agarose gel electrophoresis, and products of the expected sized were excised from the gel and sequenced.

Preparation and spraying of crude extracts obtained from virus infected plants

For each plant, 1g from 1-2 apical leaves was ground to fine powder, homogenized in 5 ml of buffer (50 mM potassium phosphate pH 8.0, 1% polyvinylpyrrolidone 10 and 1% polyethylene glycol 6000), filtered with sterile Miracloth (Millipore) and transferred to a 30-ml high-density polyethylene vaporizer (Yizhao). All volume (~5 ml) was sprayed to two different leaves (third and fourth leaves counting from the bottom) of a 3-week old *N. benthamiana* plant, at a 5-10 cm distance (Figure S1).

Gene and virus identifiers

Arabidopsis and *N. benthamiana* gene identifiers are *AtACT2* (AT3G18780), *AtCH42* (AT4G18480), *AtFT* (AT1G65480), *NbSu* (Nbv5.1tr6204879), *NbDXS* (Nbv5.1tr6224823) and *NbPP2A* (Nbv5.1tr6224808). TSWV LL-N.05 segment L, M and S genome identifiers are KP008128, FM163373 and KP008129, respectively. PVX sequence variant MT799816.1 was cloned into a derivative of *pLX-B2* (KY825137.1).

Ackowledgements

We thank Javier Forment (IBMCP) for helping in the sRNA sequencing data analysis and the greenhouse staff of IBMCP for the maintenance of plants. *DCL1i* and *DCL4i* seeds were kind gifts from Dr. Kriton Kalantidis.

Funding

This work was supported by grants or fellowships from Ministerio de Ciencia y Universidades (MCU, Spain), Agencia Estatal de Investigación (AEI, Spain) and Fondo Europeo de Desarrollo Regional (FEDER, European Union) [PID2021-122186OB-100 and RYC-2017-21648 to A.C., PID2020-114691RB-I00 to J.-A.D, and PRE2019-088439 to A.E.C.], from Consejo Superior de Investigaciones Científicas (CSIC, Spain) [JAEINT_20_01312 to T.M.G] and from European Commission [Erasmus+ Grant Agreement 2020-1-DE01-KA103-005653 to A.P.].

Author contributions

AEC and TMG did most of the experimental work with the help of AP and WK. JSV, VA and JAD performed the first experiment noticing gene silencing with amiRNAs expressed with shortened precursors from PVX vectors. AEC, TMG and AC analyzed the data. AC conceived the research, supervised the project and wrote the manuscript with input from the rest of the authors.

Data availability

High-throughput sequencing data can be found in the Sequence Read Archive (SRA) database under accession number PRJNA957136. The code used for P-SAMS amiRNA designs is available at https://github.com/carringtonlab/p-sams. New *BS-AtMIR390a-B/c* vectors are available from Addgene at (http://www.addgene.org/).

Supplemental information

Supplemental figures and tables can be found at the end of this chapter. Supplementary Table 1, appendices and additional data may be found in the online version of this article as well as in Mendeley Data resource.

REFERENCES

Achkar, N. P., Cambiagno, D. A., & Manavella, P. A. (2016). miRNA Biogenesis: A Dynamic Pathway. *Trends Plant Sci*, **21**(12), 1034–1044.

Adams, M. J., Antoniw, J. F., Bar-Joseph, M., Brunt, A. A., Candresse, T., Foster, G. D., Martelli, G. P., Milne, R. G., Zavriev, S. K., & Fauquet, C. M. (2004). The new plant virus family *Flexiviridae* and assessment of molecular criteria for species demarcation. *Arch Virol*, **149**(5), 1045–1060.

Addo-Quaye, C., Snyder, J. A., Park, Y. B., Li, Y. F., Sunkar, R., & Axtell, M. J. (2009). Sliced microRNA targets and precise loop-first

processing of MIR319 hairpins revealed by analysis of the *Physcomitrella patens* degradome. *RNA*, **15**(12), 2112–2121.

Aragonés, V., Aliaga, F., Pasin, F., & Daròs, J. A. (2022). Simplifying plant gene silencing and genome editing logistics by a one-Agrobacterium system for simultaneous delivery of multipartite virus vectors. *Biotechnol J*, **17**(7).

Axtell, M. J. (2013). Classification and comparison of small RNAs from plants. *Annu Rev Plant Biol*, **64**, 137–159.

Bajczyk, M., Jarmolowski, A., Jozwiak, M., Pacak, A., Pietrykowska, H., Sierocka, I., Swida-Barteczka, A., Szewc, L., & Szweykowska-Kulinska, Z. (2023). Recent Insights into Plant miRNA Biogenesis: Multiple Layers of miRNA Level Regulation. *Plants*, **12**(2).

Basso, M. F., Ferreira, P. C. G., Kobayashi, A. K., Harmon, F. G., Nepomuceno, A. L., Molinari, H. B. C., & Grossi-de-Sa, M. F. (2019). MicroRNAs and new biotechnological tools for its modulation and improving stress tolerance in plants. *Plant Biotechnol J*, **17**(8), 1482–1500.

Bologna, N. G., Mateos, J. L., Bresso, E. G., & Palatnik, J. F. (2009). A loop-to-base processing mechanism underlies the biogenesis of plant microRNAs miR319 and miR159. *EMBO J*, **28**(23), 3646–3656.

Bologna, N. G., & Voinnet, O. (2014). The diversity, biogenesis, and activities of endogenous silencing small RNAs in Arabidopsis. *Annu Rev Plant Biol*, **65**, 473–503.

Bouché, N., Lauressergues, D., Gasciolli, V., & Vaucheret, H. (2006). An antagonistic function for Arabidopsis DCL2 in development and a new function for DCL4 in generating viral siRNAs. *EMBO Journal*, **25**(14), 3347–3356.

Carbonell, A. (2017). Artificial small RNA-based strategies for effective and specific gene silencing in plants. In D. Tamas (Ed.), *Plant Gene Silencing: Mechanisms and Applications* (pp. 110–127). CABI Biotechnology Series, CABI Publishing.

Carbonell, A. (2019). Design and high-throughput generation of artificial small RNA constructs for plants. In *Methods in Molecular Biology* (Vol. 1932, pp. 247–260).

Carbonell, A., & Daròs, J.-A. (2019). Design, Synthesis, and Functional Analysis of Highly Specific Artificial Small RNAs with Antiviral Activity in Plants. In *Antiviral Resistance in Plants: Methods and Protocols.* (Vol. 2028, pp. 167–183).

Carbonell, A., Fahlgren, N., Mitchell, S., Cox, K. L., Reilly, K. C., Mockler, T. C., & Carrington, J. C. (2015). Highly specific gene silencing in a monocot species by artificial microRNAs derived from chimeric miRNA precursors. *Plant Journal*, **82**(6), 1061–1075.

Carbonell, A., Lisón, P., & Daròs, J.-A. (2019). Multi-targeting of viral RNAs with synthetic trans-acting small interfering RNAs enhances plant antiviral resistance. *The Plant Journal*, **100**(4), 720–737.

Carbonell, A., López, C., & Daròs, J. A. (2019). Fast-forward identification of highly effective artificial small RNAs against different *Tomato Spotted Wilt Virus* isolates. *Molecular Plant-Microbe Interactions*, **32**(2), 142–156.

Carbonell, A., Takeda, A., Fahlgren, N., Johnson, S. C., Cuperus, J. T., & Carrington, J. C. (2014). New generation of artificial MicroRNA and synthetic trans-acting small interfering RNA vectors for efficient gene silencing in Arabidopsis. *Plant Physiol*, **165**(1), 15–29.

Chorostecki, U., Moro, B., Rojas, A. M. L., Debernardi, J. M., Schapire, A. L., Notredame, C., & Palatnik, J. F. (2017). Evolutionary footprints reveal insights into plant microRNA biogenesis. *Plant Cell*, **29**(6), 1248–1261.

Cisneros, A. E., de la Torre-Montaña, A., & Carbonell, A. (2022). Systemic silencing of an endogenous plant gene by two classes of mobile 21-nucleotide artificial small RNAs. *Plant Journal*, **110**(4), 1166–1181.

Cisneros, A. E., de la Torre-Montaña, A., Martín-García, T., & Carbonell, A. (2021). Artificial Small RNAs for Functional Genomics in Plants. In G. Tang, S. Teotia, X. Tang, & D. Singh

(Eds.), *RNA-based Technologies For Functional Genomics in Plants* (pp. 1–29). Springer International Publishing.

Clough, S. J., & Bent, A. F. (1998). Floral dip: a simplified method for *Agrobacterium* - mediated transformation of *Arabidopsis thaliana*. *The Plant Journal*, **16**(6), 735–743.

Cuperus, J. T., Carbonell, A., Fahlgren, N., Garcia-Ruiz, H., Burke, R. T., Takeda, A., Sullivan, C. M., Gilbert, S. D., Montgomery, T. A., & Carrington, J. C. (2010). Unique functionality of 22-nt miRNAs in triggering RDR6-dependent siRNA biogenesis from target transcripts in Arabidopsis. *Nat Struct Mol Biol*, **17**(8), 997–1003.

Cuperus, J. T., Fahlgren, N., & Carrington, J. C. (2011). Evolution and functional diversification of MIRNA genes. *Plant Cell*, **23**(2), 431–442.

Cuperus, J. T., Montgomery, T. A., Fahlgren, N., Burke, R. T., Townsend, T., Sullivan, C. M., & Carrington, J. C. (2010). Identification of MIR390a precursor processing-defective mutants in Arabidopsis by direct genome sequencing. *Proc Natl Acad Sci U S A*, **107**(1), 466–471.

Curtis, M. D., & Grossniklaus, U. (2003). A Gateway Cloning Vector Set for High-Throughput Functional Analysis of Genes in Planta. *Plant Physiol*, **133**(2), 462–469.

Dadami, E., Boutla, A., Vrettos, N., Tzortzakaki, S., Karakasilioti, I., & Kalantidis, K. (2013). DICER-LIKE 4 but not DICER-LIKE 2 may have a positive effect on potato spindle tuber viroid accumulation in *Nicotiana benthamiana*. *Mol Plant*, **6**, 232–234.

Deleris, A., Javier Gallego-Bartolome, Jinsong Bao, Kristin D. Kasschau, James C. Carrington, & Olivier Voinnet. (2006). Hierarchical Action and Inhibition of Plant Dicer-Like Proteins in Antiviral Defense. *Science (1979)*, **313**(5783), 68–71.

Dickmeis, C., Fischer, R., & Commandeur, U. (2014). Potato virus X-based expression vectors are stabilized for long-term production of proteins and larger inserts. *Biotechnol J*, **9**(11), 1369–1379.

Du, Q.-S., Duan, C.-G., Zhang, Z.-H., Fang, Y.-Y., Fang, R.-X., Xie, Q., & Guo, H.-S. (2007). DCL4 Targets *Cucumber Mosaic Virus* Satellite RNA at Novel Secondary Structures. *J Virol*, **81**(17), 9142–9151.

Fahlgren, N., Hill, S. T., Carrington, J. C., & Carbonell, A. (2016). P-SAMS: a web site for plant artificial microRNA and synthetic *trans*-acting small interfering RNA design. *Bioinformatics*, **32**(1), 157–158.

Hamilton, A., Voinnet, O., Chappell, L., & Baulcombe, D. (2002). Two classes of short interfering RNA in RNA silencing. *EMBO J*, **21**(17), 4671–4679.

Hannon, G. J. (2010). *FASTX-Toolkit (RRID:SCR_005534)*. Http://Hannonlab.Cshl.Edu/Fastx_toolkit .

Hauser, F., Chen, W., Deinlein, U., Chang, K., Ossowski, S., Fitz, J., Hannon, G. J., & Schroeder, J. I. (2013). A genomic-scale artificial MicroRNA library as a tool to investigate the functionally redundant gene space in arabidopsis. *Plant Cell*, **25**(8), 2848–2863.

Jian, C., Han, R., Chi, Q., Wang, S., Ma, M., Liu, X., & Zhao, H. (2017). Virus-based MicroRNA silencing and overexpressing in common wheat (*Triticum aestivum L.*). *Front Plant Sci*, **8**.

Jodder, J. (2021). Regulation of pri-MIRNA processing: mechanistic insights into the miRNA homeostasis in plant. *Plant Cell Rep*, **40**(5), 783–798.

Jover-Gil, S., Paz-Ares, J., Micol, J. L., & Ponce, M. R. (2014). Multi-gene silencing in Arabidopsis: A collection of artificial microRNAs targeting groups of paralogs encoding transcription factors. *Plant Journal*, **80**(1), 149–160.

Ju, Z., Cao, D., Gao, C., Zuo, J., Zhai, B., Li, S., Zhu, H., Fu, D., Luo, Y., & Zhu, B. (2017). A viral satellite DNA vector (TYLCCNV) for functional analysis of miRNAs and siRNAs in plants. *Plant Physiol*, **173**(4), 1940–1952.

Kuo, Y. W., & Falk, B. W. (2022). Artificial microRNA guide strand selection from duplexes with no mismatches shows a purine-rich preference for virus- and non-virus-based

expression vectors in plants. *Plant Biotechnol J*, **20**(6), 1069–1084.

Lacomme, C., & Chapman, S. (2008). Use of potato virus X (PVX)-based vectors for gene expression and virus-induced gene silencing (VIGS). In *Current Protocols in Microbiology* (Issue SUPPL. 8). John Wiley and Sons Inc.

Li, M., & Yu, B. (2021). Recent advances in the regulation of plant miRNA biogenesis. *RNA Biol*, **18**(12), 2087–2096.

Llave, C., Xie, Z., Kasschau, K. D., & Carrington, J. C. (2002). Cleavage of *Scarecrow-like* mRNA Targets Directed by a Class of *Arabidopsis* miRNA. *Science (1979)*, **297**(5589), 2053–2056.

Loebenstein, G., & Gaba, V. (2012). Viruses of Potato. In G. Loebenstein & H. Lecoq (Eds.), *Advances in Virus Research, Viruses and Virus Diseases of Vegetables in the Mediterranean Basin* (Vol. 84, pp. 209–246). Academic Press.

López-Dolz, L., Spada, M., Daròs, J.-A., & Carbonell, A. (2020). Fine-Tune Control of Targeted RNAi Efficacy by Plant Artificial Small. *Nucleic Acids Res*, **48**(11), 6234–6250.

Lunardon, A., Kariuki, S. M., & Axtell, M. J. (2021). aExpression and processing of polycistronic artificial microRNAs and trans-acting siRNAs from transiently introduced transgenes in miRNA *Solanum lycopersicum* and *Nicotiana benthamiana*. *Plant Journal*, **106**(4), 1087–1104.

Mateos, J. L., Bologna, N. G., Chorostecki, U., & Palatnik, J. F. (2010). Identification of MicroRNA Processing Determinants by Random Mutagenesis of Arabidopsis MIR172a Precursor. *Current Biology*, **20**(1), 49–54.

Moro, B., Chorostecki, U., Arikit, S., Suarez, I. P., Hobartner, C., Rasia, R. M., Meyers, B. C., & Palatnik, J. F. (2018). Efficiency and precision of microRNA biogenesis modes in plants. *Nucleic Acids Res*, **46**(20), 10709–10723.

Nakasugi, K., Crowhurst, R., Bally, J., & Waterhouse, P. (2014). Combining transcriptome assemblies from multiple de novoassemblers in the allo-tetraploid plant nicotiana benthamiana. *PLoS One*, **9**(3).

Ossowski, S., Schwab, R., & Weigel, D. (2008). Gene silencing in plants using artificial microRNAs and other small RNAs. *Plant Journal*, **53**(4), 674–690.

Parizotto, E. A., Dunoyer, P., Rahm, N., Himber, C., & Voinnet, O. (2004). In vivo investigation of the transcription, processing, endonucleolytic activity, and functional relevance of the spatial distribution of a plant miRNA. *Genes Dev*, **18**(18), 2237–2242.

Pasin, F., Bedoya, L. C., Bernabé-Orts, J. M., Gallo, A., Simón-Mateo, C., Orzaez, D., & García, J. A. (2017). Multiple T-DNA Delivery to Plants Using Novel Mini Binary Vectors with Compatible Replication Origins. *ACS Synth Biol*, **6**(10), 1962–1968.

Rogers, K., & Chen, X. (2013). Biogenesis, Turnover, and Mode of Action of Plant MicroRNAs. *Plant Cell*, **25**(7), 2383–2399.

Rojas, A. M. L., Drusin, S. I., Chorostecki, U., Mateos, J. L., Moro, B., Bologna, N. G., Bresso, E. G., Schapire, A., Rasia, R. M., Moreno, D. M., & Palatnik, J. F. (2020). Identification of key sequence features required for microRNA biogenesis in plants. *Nat Commun*, **11**(5320).

Rössner, C., Lotz, D., & Becker, A. (2022). VIGS Goes Viral: How VIGS Transforms Our Understanding of Plant Science. *Annu Rev Plant Biol*, **20**(73), 703–728.

Schürer, H., Lang, K., Schuster, J., & Mörl, M. (2002). A universal method to produce *in vitro* transcripts with homogeneous 3′ ends. *Nucleic Acids Res*, **30**(12), 56.

Schwab, R., Ossowski, S., Riester, M., Warthmann, N., & Weigel, D. (2006). Highly Specific Gene Silencing by Artificial MicroRNAs in Arabidopsis. *Plant Cell*, **18**(5), 1121–1133.

Shapiro, J. S., Langlois, R. A., Pham, A. M., & Tenoever, B. R. (2012). Evidence for a cytoplasmic microprocessor of pri-miRNAs. *RNA*, **18**(7), 1338–1346.

Shapiro, J. S., Varble, A., Pham, A. M., & Tenoever, B. R. (2010). Noncanonical

cytoplasmic processing of viral microRNAs. *RNA*, **16**(11), 2068–2074.

Song, L., Axtell, M. J., & Fedoroff, N. V. (2010). RNA Secondary Structural Determinants of miRNA Precursor Processing in Arabidopsis. *Current Biology*, **20**(1), 37–41.

Tang, Y., Wang, F., Zhao, J., Xie, K., Hong, Y., & Liu, Y. (2010). Virus-based microRNA expression for gene functional analysis in plants. *Plant Physiol*, **153**(2), 632–641.

Tiwari, M., Sharma, D., & Trivedi, P. K. (2014). Artificial microRNA mediated gene silencing in plants: Progress and perspectives. *Plant Mol Biol*, **86**, 1–18.

Uranga, M., Aragonés, V., Selma, S., Vázquez-Vilar, M., Orzáez, D., & Daròs, J. A. (2021). Efficient Cas9 multiplex editing using unspaced sgRNA arrays engineering in a Potato virus X vector. *Plant Journal*, **106**(2), 555–565.

Vasav, A. P., Meshram, B. G., Pable, A. A., & Barvkar, V. T. (2023). Artificial microRNA mediated silencing of cyclase and aldo–keto reductase genes reveal their involvement in the plumbagin biosynthetic pathway. *J Plant Res*, **136**(1), 47–62.

Werner, S., Wollmann, H., Schneeberger, K., & Weigel, D. (2010). Structure Determinants for Accurate Processing of miR172a in *Arabidopsis thaliana*. *Current Biology*, **20**(1), 42–48.

Yu, Y., Jia, T., & Chen, X. (2017). The 'how' and 'where' of plant micro RNAs. *New Phytologist*, **216**(4), 1002–1017.

Zhang, L., Xiang, Y., Chen, S., Shi, M., Jiang, X., He, Z., & Gao, S. (2022). Mechanisms of MicroRNA Biogenesis and Stability Control in Plants. *Front Plant Sci*, **13**(844149).

Zhang, Y., Nasser, V., Pisanty, O., Omary, M., Wulff, N., Di Donato, M., Tal, I., Hauser, F., Hao, P., Roth, O., Fromm, H., Schroeder, J. I., Geisler, M., Nour-Eldin, H. H., & Shani, E. (2018). A transportome-scale amiRNA-based screen identifies redundant roles of Arabidopsis ABCB6 and ABCB20 in auxin transport. *Nat Commun*, **9**(1).

SUPPLEMENTARY INFORMATION

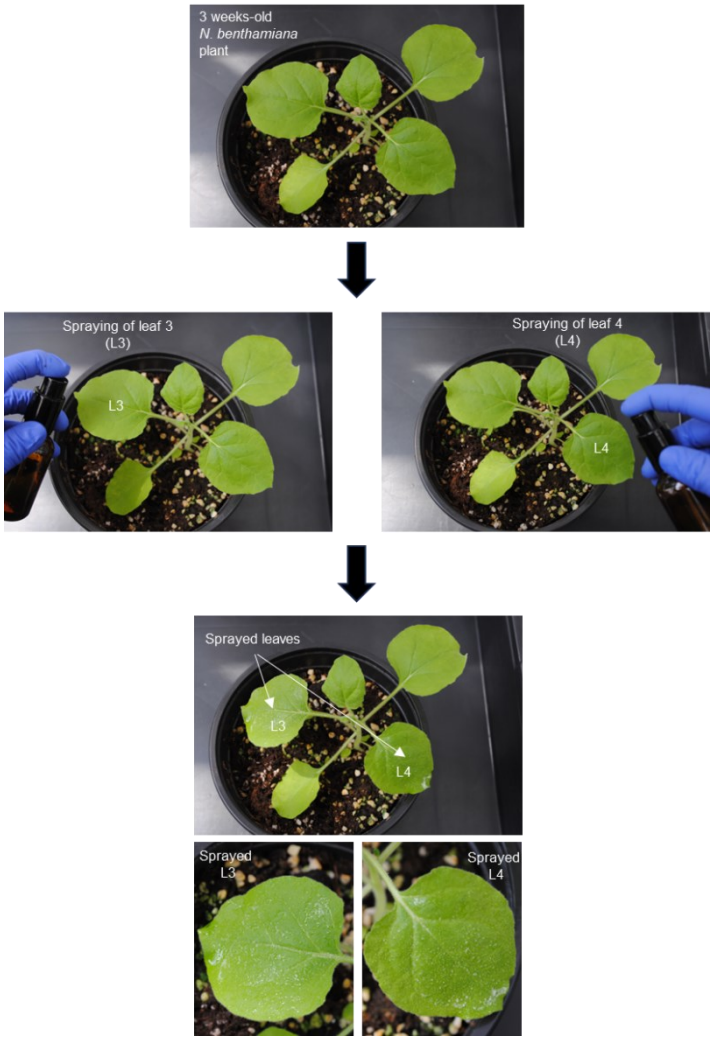

Figure S1. **Spraying of crude extracts obtained from virus infected plants**. Leaves 3 and 4 (counting form the bottom) of 3 weeks-old *Nicotiana benthamiana* plants (upper photograph) are consecutively sprayed at a 5-10 cm distance (middle photographs) using a high-density polyethylene vaporizer. Bottom photographs show leaves after the spraying.

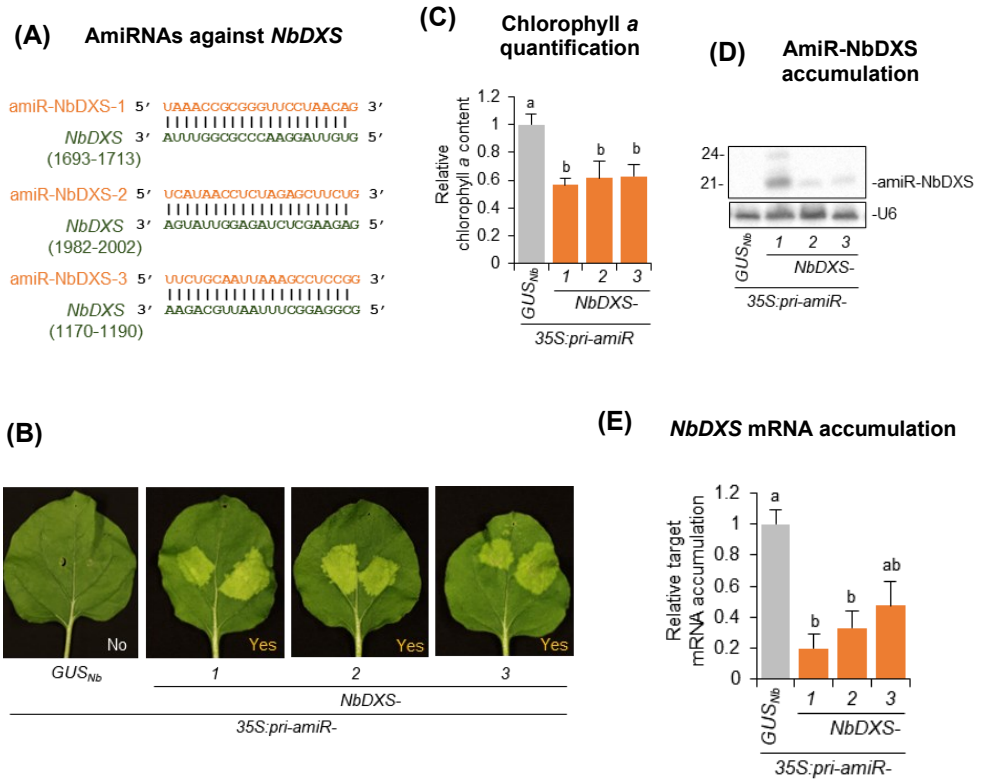

Figure S2. Functional analysis of artificial microRNAs (amiRNAs) against *N. benthamiana 1-DEOXY-D-XYLULOSE-5-PHOSPHATE SYNTHASE* (*NbDXS*) in agroinfiltrated leaves. (**A**) Base-pairing of amiRNAs and NbDXS target mRNAs. Coordinates of the complete target site in NbDXS mRNAs are given. The arrows indicate the amiRNA-predicted cleavage site. (**B**) Photographs at 7 days post-agroinfiltration (dpa) of leaves agroinfiltrated with the different amiRNA constructs. Photobleaching appearance or absence is labeled with a "Yes" or a "No". (**C**) Bar graph showing the relative content of chlorophyll *a* in agroinfiltrated areas (*35S:pri-amiR-GUS*$_{Nb}$ = 1.0). Bars with the letter 'a' are significantly different from that of sample *35S:pri-amiR-GUS*$_{Nb}$ ($P < 0.01$ in pairwise Student's t-test comparisons). (**D**) Northern blot detection of amiR-NbDXS amiRNAs in RNA preparations from agroinfiltrated leaves at 2 dpa. (**E**) Accumulation of *NbDXS* mRNA. Mean mean + SE relative level (n = 3) of *NbDXS* mRNAs after normalization to *PROTEIN PHOSPHATASE 2A* (*PP2A*), as determined by quantitative RT-PCR (qPCR) (*35S:pri-amiR-GUS*$_{Nb}$ = 1.0 in all comparisons). Other details are as shown in B.

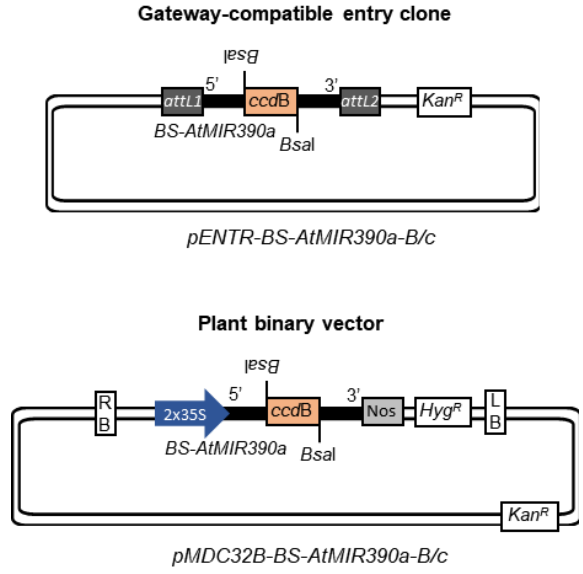

Figure S3. ***BS-AtMIR390a-B/c*-based vectors for direct cloning of amiRNAs**. Top, diagram of the Gateway-compatible *pENTR-BS-AtMIR390a-B/c* entry vector. Bottom, diagram of the *pMDC32B-BS-AtMIR390a-B/c* binary vector for in plant expression of amiRNAs. RB: right border; 35S: Cauliflower mosaic virus promoter; *Bsa*I: *Bsa*I recognition site, *ccd*B: gene encoding the gyrase toxin; LB: left border; attL1 and attL2: GATEWAY recombination sites. *Kan*^{R}: kanamycin resistance gene; *Hyg*^{R}: hygromycin resistance gene.

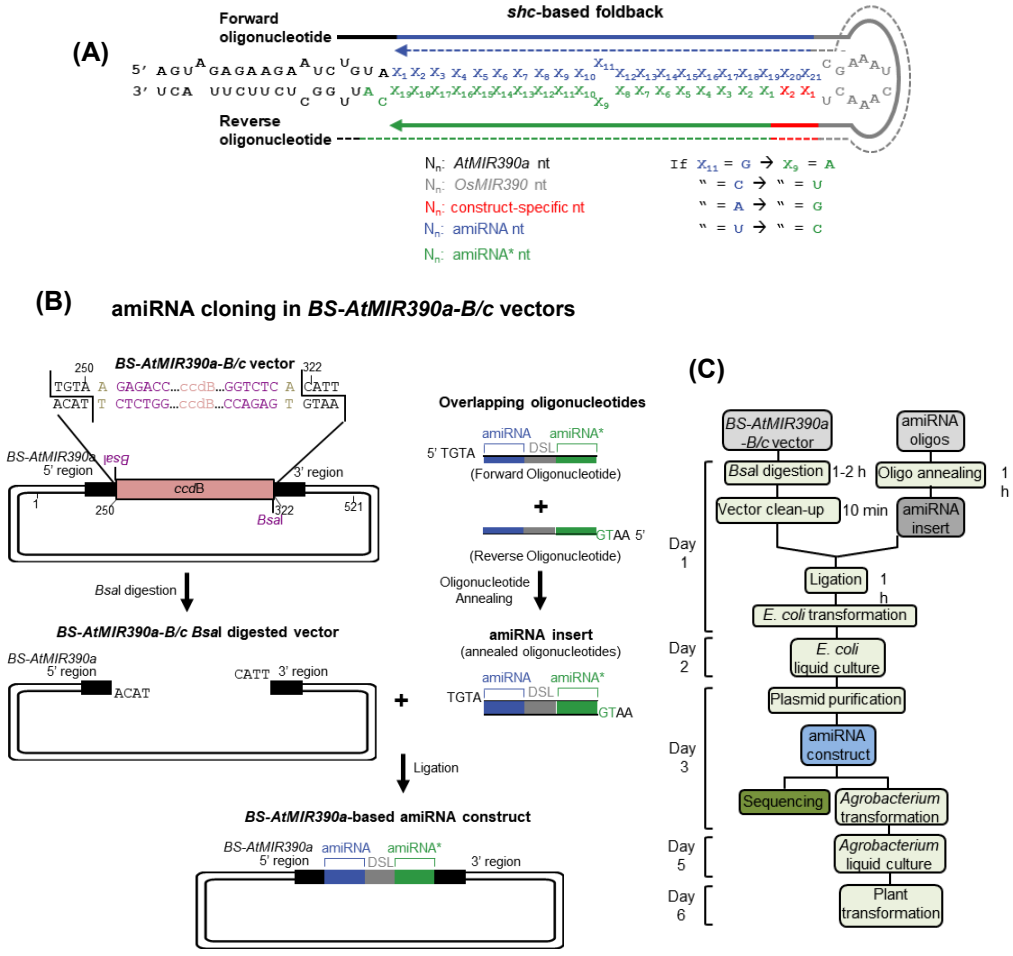

Figure S4. Direct cloning of amiRNAs in vectors containing a modified version of *BS-AtMIR390a* that includes a *ccd*B cassette flanked by two *Bsa*I sites (*Bsa*I/*ccd*B or 'B/c' vectors). (**A**) Design of two overlapping oligonucleotides for amiRNA cloning in *BS-AtMIR390a*-based "B/c" vectors including *OsMIR390* DSL sequences. Sequences covered by the forward and the reverse oligonucleotides are represented with continuous or dotted lines, respectively. Nucleotides of *BS-AtMIR390a* precursor, *OsMIR390*-derived distal stem loop (DSL), amiRNA guide strand and amiRNA* strand are in black, grey, blue and green, respectively. Other nucleotides that may be modified for preserving authentic *OsMIR390a* foldback secondary structure are in red. Rules for assigning identity to position 9 of the amiRNA* are indicated. (**B**) Diagram of the steps for amiRNA cloning in *pre-AtMIR390a-B/c* vectors. The amiRNA insert obtained after annealing the two overlapping oligonucleotides has 5'-TGTA and 5'-AATG overhangs and is directly inserted in a directional manner into a *BS-AtMIR390a-B/c* vector previously linearized with *Bsa*I. Nucleotides of the *Bsa*I sites and those arbitrarily chosen and used as spacers between the *Bsa*I recognition sites and the *BS-AtMIR390a* sequence are in purple and light brown, respectively. Other details are as described in panel A. (**C**) Flowchart of steps from amiRNA construct generation to plant transformation.

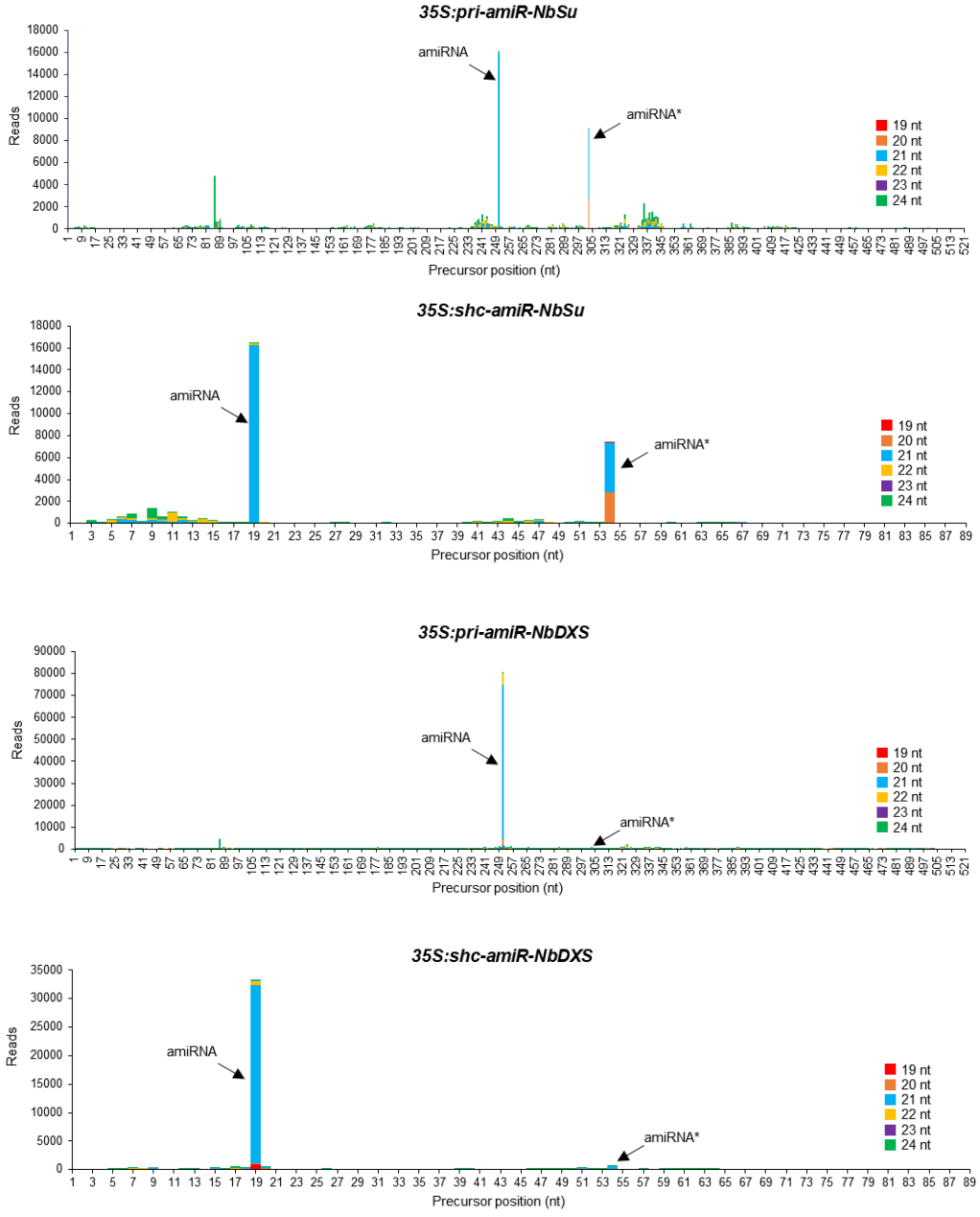

Figure S5. Mapping of 19-24 nucleotide small RNA reads to *pri* and *shc* precursors expressing amiR-NbSu or NbDXS amiRNAs. The *x*-axis indicates the position on the precursor in nucleotides of the 5' end of the sequence plotted. The *y*-axis is the small RNA coverage in total number of reads for each nucleotidic position.

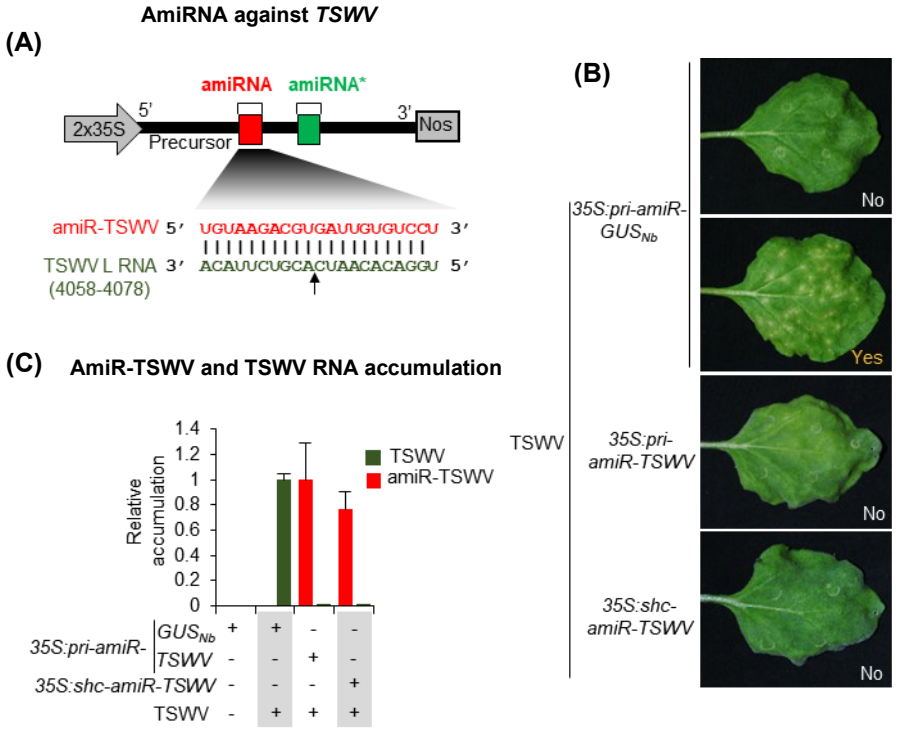

Figure S6. **Antiviral effects of constructs expressing amiR-TSWV, an amiRNA against *Tomato spotted wilt virus* (TSWV), from *pri* and *shc* precursors**. (**A**) Diagram of amiR-TSWV constructs expressing amiR-TSWV directed against TSWV segment L, with amiRNA and star strand positions in the precursor indicated with red and green color, respectively. Base-pairing between amiR-TSWV and its target site is shown, with the predicted cleavage position indicated by an arrow. (**B**) Photos at 7 days post-agroinfiltration (dpa) of leaves agroinfiltrated with the different constructs, some of which were further inoculated with TSWV. (**C**) Bar graph showing the relative accumulation of amiR-TSWV in agroinfiltrated leaves at 2 dpa [mean relative level (n = 3) + standard deviation amiRNA relative accumulation, *pri-amiR-TSWV* + TSWV= 1.0] and of TSWV RNA in apical leaves at 21 dpa [mean relative level (n = 3) + standard error of TSWV RNAs after normalization to *PROTEIN PHOSPHATASE 2A* (*PP2A*), as determined by quantitative RT-qPCR, *pri-amiR-GUS*$_{Nb}$ + TSWV= 1].

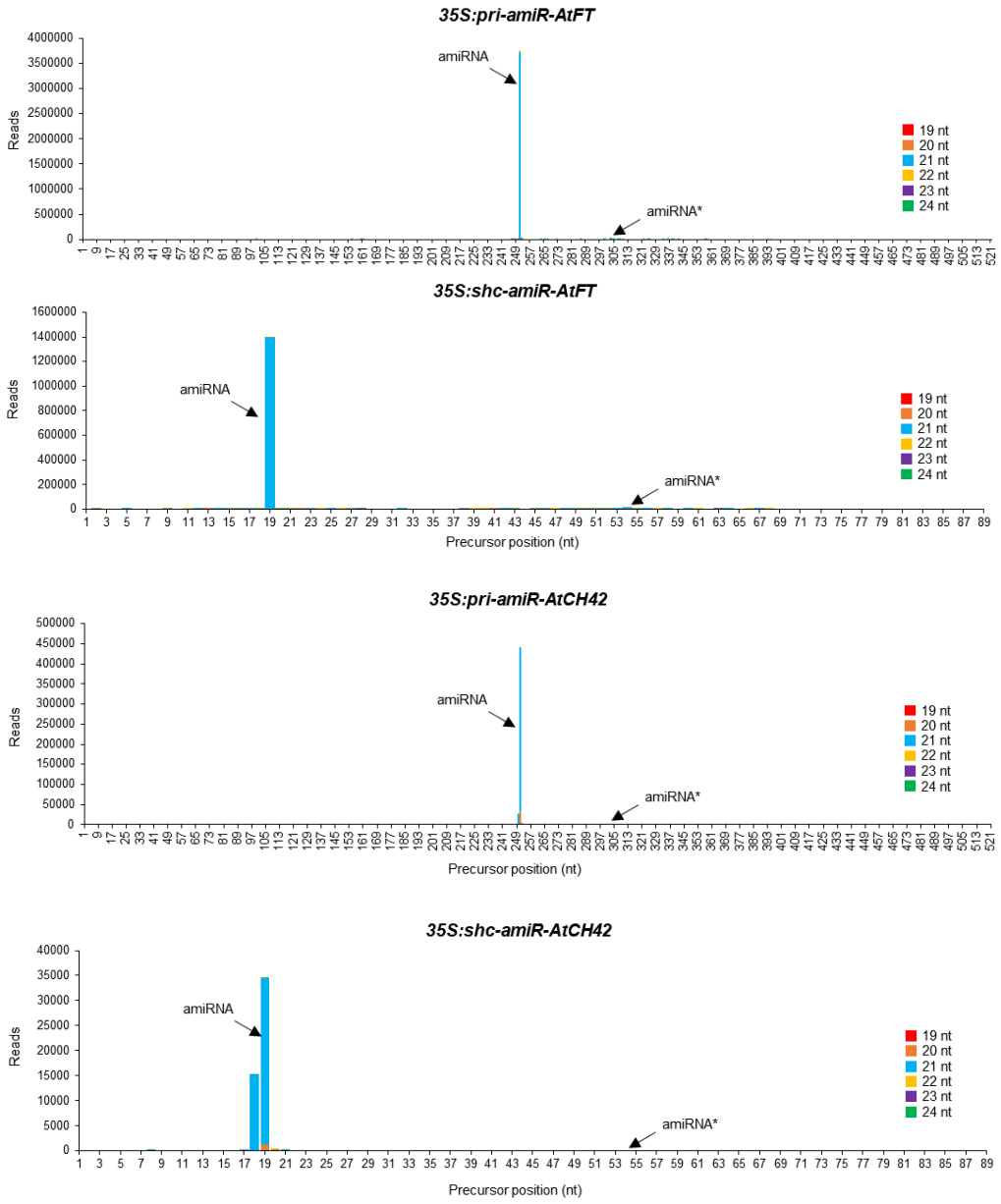

Figure S7. Mapping of 19-24 nucleotide small RNA reads to *pri* and *shc* precursors expressing amiR-AtFT or AtCH42 amiRNAs. The *x*-axis indicates the position on the precursor in nucleotides of the 5' end of the sequence plotted. The *y*-axis is the small RNA coverage in total number of reads for each nucleotidic position.

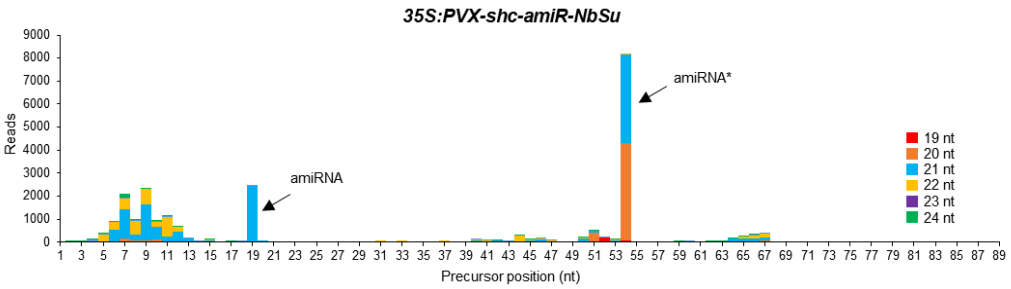

Figure S8. Mapping of 19-24 nucleotide small RNA reads to *shc* precursors expressing amiR-NbSu from PVX. The *x*-axis indicates the position on the precursor in nucleotides of the 5' end of the sequence plotted. The *y*-axis is the small RNA coverage in total number of reads for each nucleotidic position.

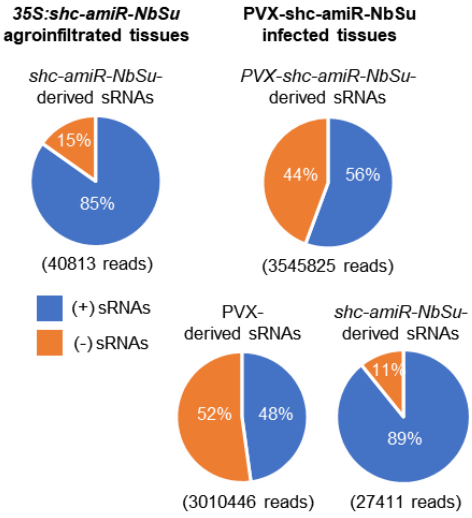

Figure S9. Sequencing analysis of sRNA reads from *35S:shc-amiR-NbSu* agroinfiltrated leaves and from PVX-sch-amiR-NbSu infected tissues. Pie charts showing percentages of reads corresponding to 19-24 nt sRNAs of (+) or (-) polarity (blue and orange sections, respectively).

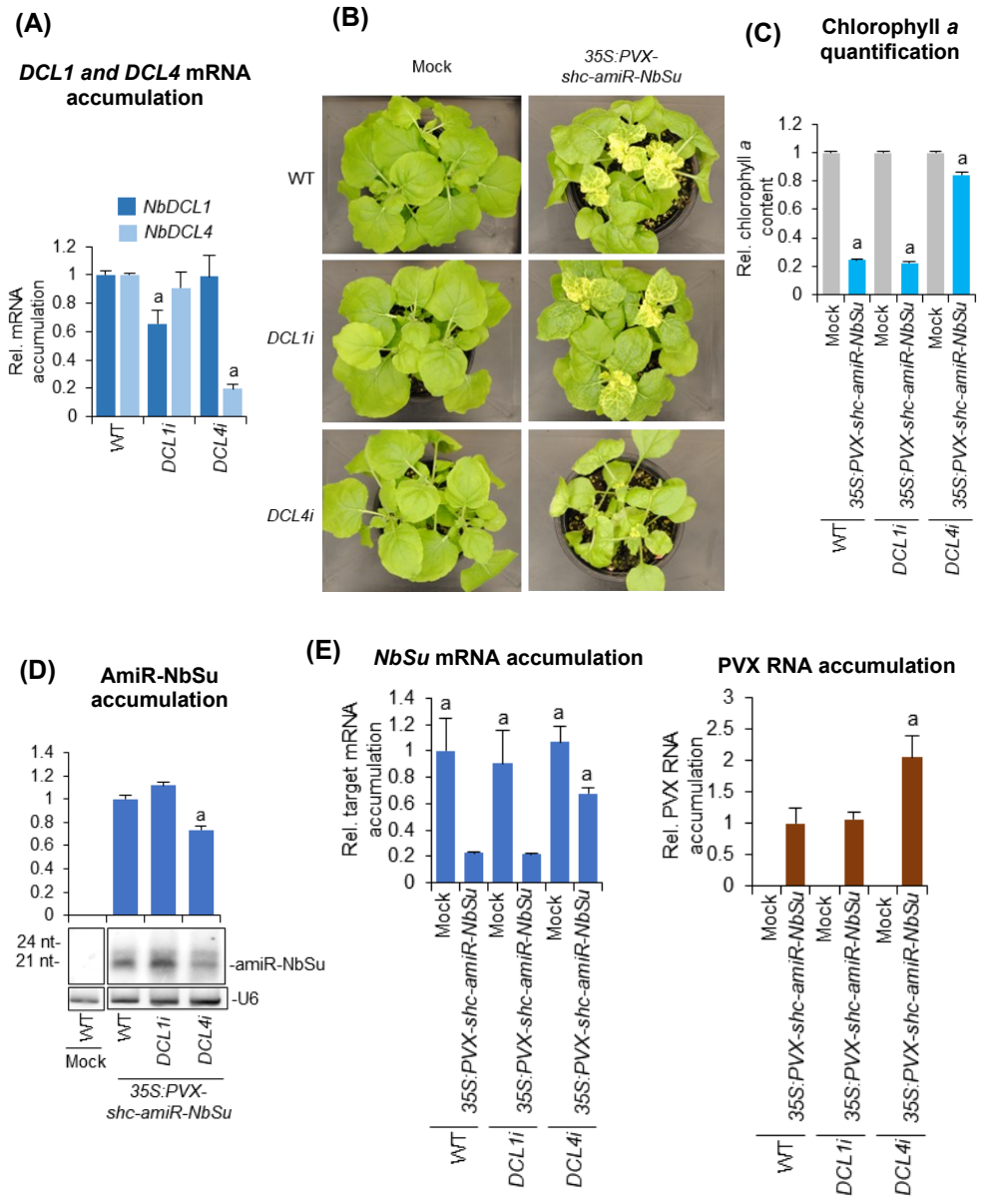

Figure S10. **Genetic analysis in wild-type (WT) and in *DCL1i* and *DCL4i* knockdown plants of *NbSu* silencing triggered by a *Potato virus X* (PVX) construct expressing amiR-NbSu from the *shc* precursor**. (**A**) *NbDCL1* and *NbDCL4* mRNA accumulation in RNA preparations from leaves of WT, *DCL1i* and *DCL4i N. benthamiana* plants. Mean relative level (n = 3) + standard error of mRNAs after normalization to *PROTEIN PHOSPHATASE 2A* (*PP2A*), as determined by RT-qPCR (WT = 1.0 in all comparisons). Bar with the letter "a" is significantly different from that of the corresponding WT samples ($P < 0.05$ in pairwise Student's t-test

comparison). (**B**) Photos at 14 days post-agroinfiltration (dpa) of sets of three plants mock inoculated or agroinfiltrated with the *35S:PVX-shc-amiR-NbSu* construct. (**C**) Bar graph showing the relative content of chlorophyll *a* in apical leaves from plants mock inoculated or agroinfiltrated with the *35S:PVX-shc-amiR-NbSu* construct (Mock = 1.0). Bar with the letter "a" is significantly different from that of the corresponding Mock control samples ($P < 0.05$ in pairwise Student's t-test comparison). (**D**) Northern blot detection of amiR-NbSu in RNA preparations from apical leaves collected at 14 dpa. The graph at top shows the mean (n = 3) + standard deviation amiRNA relative accumulation (WT = 1.0). Bar with a letter "a" is significantly different from that of the WT sample agroinfiltrated with the *35S:PVX-shc-amiR-NbSu* construct . One blot from three biological replicates is shown. (**E**) Target *NbSu* mRNA and PVX RNA accumulation in RNA preparations from apical leaves collected at 7 dpa and analyzed individually. Mean relative level (n = 3) + standard error of *NbSu* mRNAs and PVX RNAs after normalization to *PROTEIN PHOSPHATASE 2A* (*PP2A*), as determined by RT-qPCR (WT + mock = 1.0 in *NbSu* dataset, WT + *35S:PVX-shc-amiR-NbSu* = 1.0 in PVX dataset). Bar with the letter "a" is significantly different from that of the corresponding WT + *35S:PVX-shc-amiR-NbSu* samples ($P < 0.05$ in pairwise Student's t-test comparison).

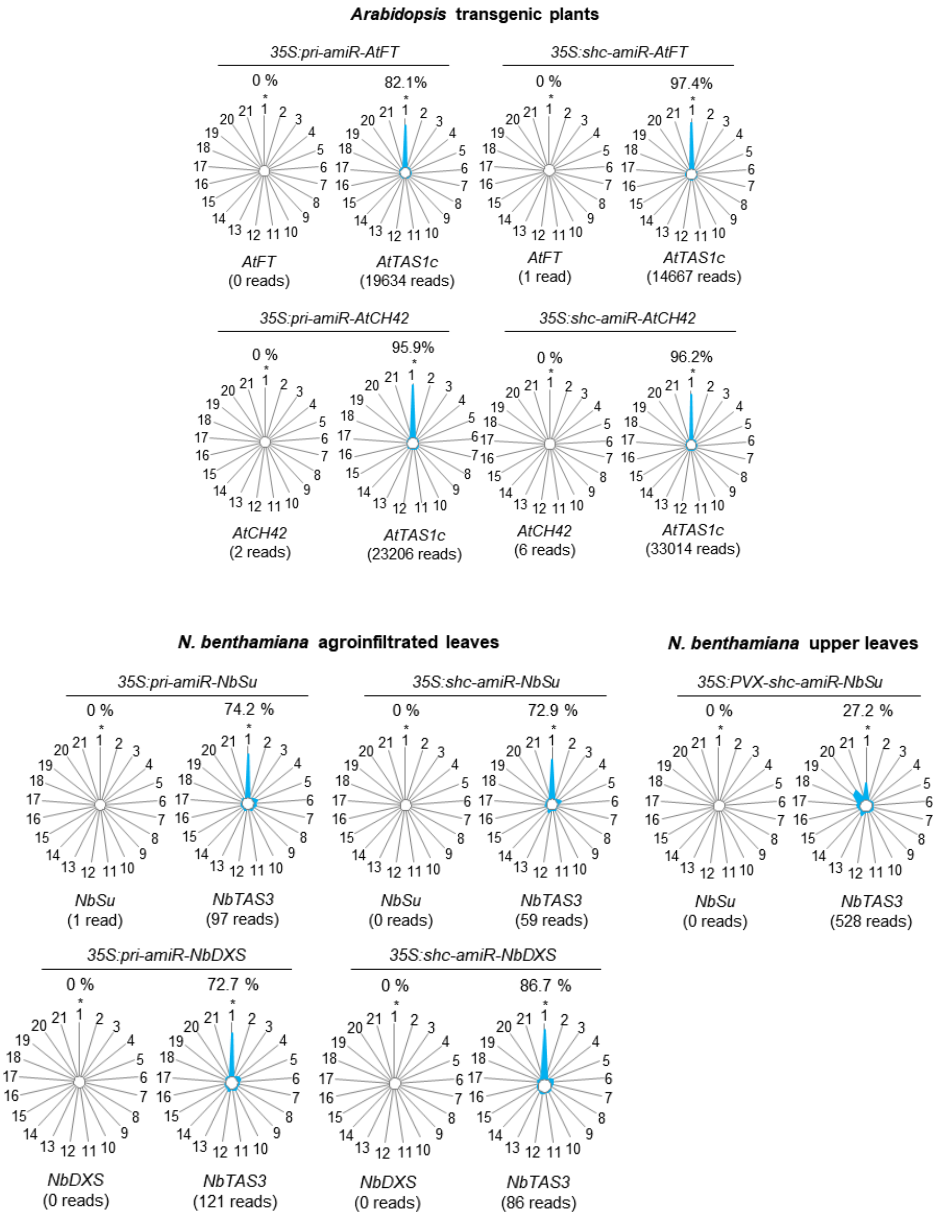

Figure S11. **Phasing analysis of amiRNA target RNA-derived 21 nucleotide small RNAs**. Radar plots show proportions of 21-nucleotide reads corresponding to each of the 21 registers from *AtFT*, *AtCH42*, *NbSu* and *NbDXS*, with position 1 designated as immediately after the amiRNA guided cleavage site. Control plots for *AtTAS1c* and *NbTAS3* are shown for *A. thaliana* and *N. benthamiana* datasets, respectively. The percentage of 21-nucleotide reads corresponding to phasing register 1 is indicated.

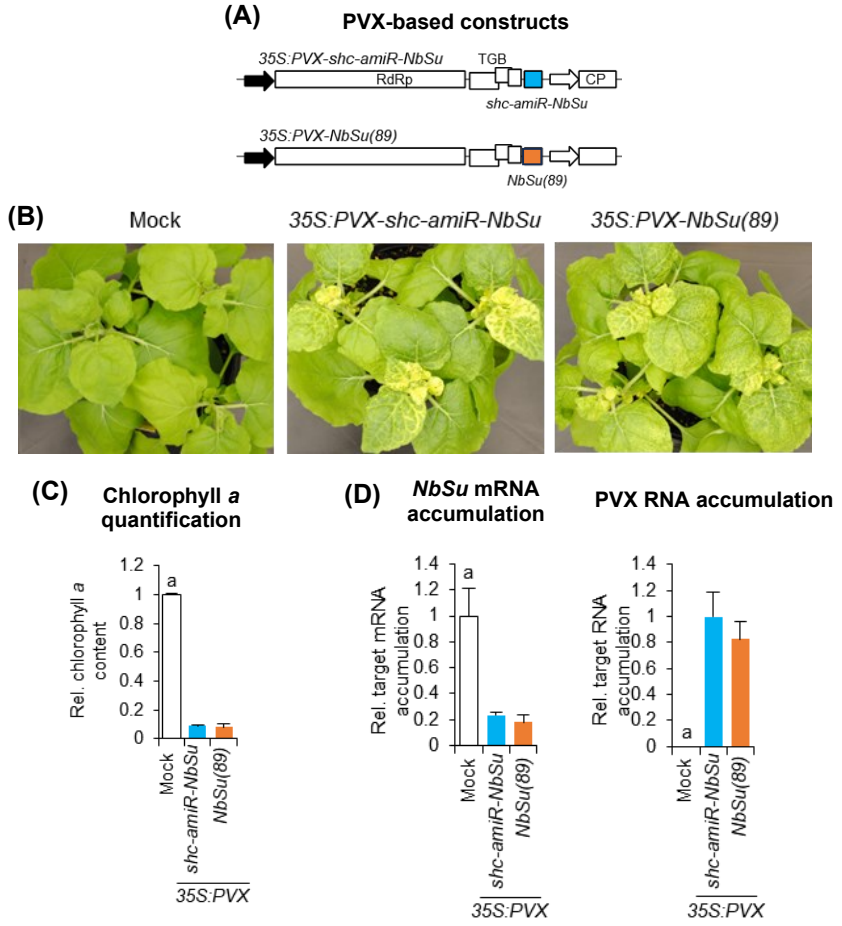

Figure S12. Comparative analysis of *Potato virus X* (PVX) constructs expressing amiR-NbSu from the *shc* precursor and a 89-nt long fragment of the *NbSu* gene. (**A**) Diagram of PVX-based constructs. *shc-amiR-NbSu* and *NbSu(89)* cassettes are shown in light blue and orange boxes, respectively. PVX genes RdRp, TGB and CP are represented in white boxes, and CP promoter from *Bamboo mosaic virus* (BaMV) with a white arrow. (**B**) Photos at 14 days post-agroinfiltration (dpa) of sets of three plants agroinfiltrated with the different constructs. (**C**) Bar graph showing the relative content of chlorophyll *a* in apical leaves from plants agroinfiltrated with different constructs (Mock = 1.0). Bar with the letter "a" is significantly different from that of the corresponding *35S:PVX-shc-amiR-NbSu* samples ($P < 0.05$ in pairwise Student's t-test comparison). (**D**) Target *NbSu* mRNA and PVX RNA accumulation in RNA preparations from apical leaves collected at 7 dpa and analyzed individually. Mean relative level (n = 3) + standard error of *NbSu* mRNAs and PVX RNAs after normalization to *PROTEIN PHOSPHATASE 2A* (*PP2A*), as determined by RT-qPCR (mock = 1.0 in *NbSu* dataset and *35S:PVX-shc-amiR-NbSu* = 1.0 in PVX dataset). Bar with the letter "a" is significantly different from that of the corresponding *35S:PVX-shc-amiR-NbSu* samples ($P < 0.05$ in pairwise Student's t-test comparison).

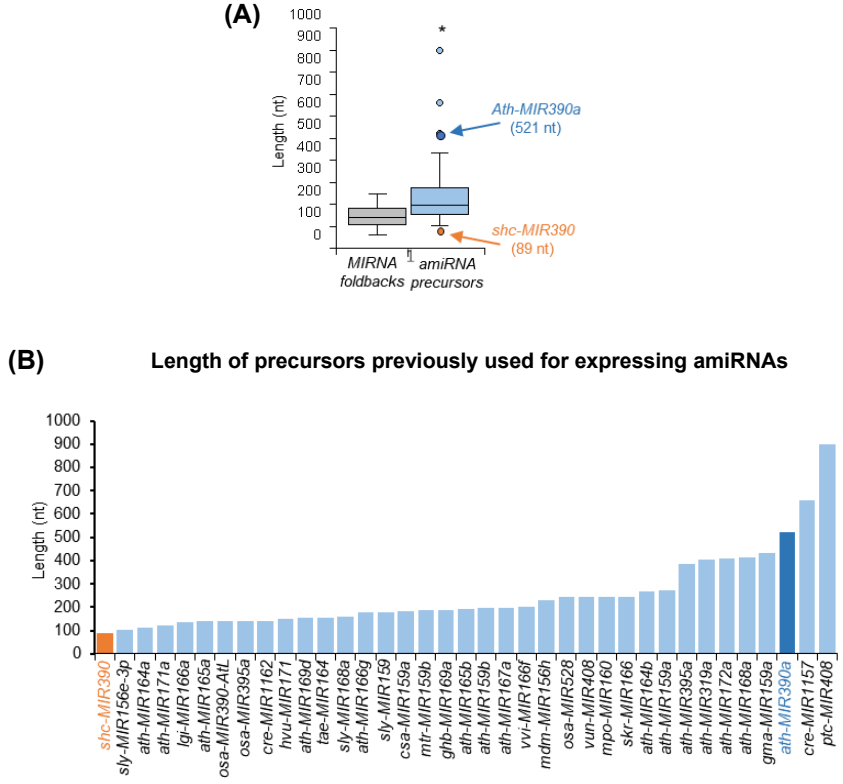

Figure S13. Analysis of the length of *MIRNA* foldbacks and amiRNA precursors used for gene silencing in plants.

Table S2: Phenotypic penetrance of amiRNAs expressed in *A. thaliana* Col-0 T1 transgenic plants

Construct	T1 analyzed	Phenotypic penetrance[a]
35S:pri-amiR-GUS$_{Ath}$	48	0%
35S:pri-amiR-AtFT	40	100%
35S:shc-amiR-AtFT	34	100%
35S:pri-amiR-GUS$_{Ath}$	73	0%
35S:pri-amiR-AtCH42	54	100% 3.7% weak 37% intermediate 59.3 % severe
35S:shc-amiR-AtCH42	38	100% 2.7% weak 34.2% intermediate 63.1 % severe

[a] The Ft phenotype was defined as a higher 'days to flowering' value when compared to the average 'days to flowering' value of the *35S:pri-amiR-GUS$_{Ath}$* control set. Ch42 phenotype is scored in 10 days-old seedling and is considered 'weak', 'intermediate' or 'severe' if seedlings have >2 leaves, exactly 2 leaves or no leaves (only 2 cotyledons), respectively.

CHAPTER 3

Syn-tasiR-VIGS: Virus-Based Gene Silencing in Plants by Synthetic Trans-acting Small Interfering RNAs Derived from Minimal Precursors

Adriana E. Cisneros, Juan José Llorens-Gámez, Anamarija Primc, Ana Alarcia-García, Ana Puertes and Alberto Carbonell

The results presented in this chapter will be included in an upcoming manuscript

CHAPTER 3

Syn-tasiR-VIGS: Virus-Based Gene Silencing in Plants by Synthetic Trans-acting Small Interfering RNAs Derived from Minimal Precursors

Adriana E. Cisneros[a], Juan José Llorens-Gámez[a], Anamarija Primc[a,b], Ana Alarcia-García[a], Ana Puertes[a] and Alberto Carbonell[a]

[a] *Instituto de Biología Molecular y Celular de Plantas (Consejo Superior de Investigaciones Científicas–Universitat Politècnica de València), 46022 Valencia, Spain.*

[b] *Current address: Center for Organismal Studies (COS), University of Heidelberg, Heidelberg, Germany.*

ABSTRACT

Synthetic trans-acting small interfering RNAs (syn-tasiRNAs) are a class of 21-nucleotide (nt)-long artificial small RNAs used for efficient and highly specific silencing of plant genes. Syn-tasiRNA biogenesis is triggered when a 22-nt microRNA (miRNA) cleaves a *TAS* RNA transcript containing one or more syn-tasiRNA sequences. Despite their popularity, their application in functional genomics and crop improvement is limited by the need for transgenic expression of long *TAS* precursors to produce syn-tasiRNAs. Here, we show that 54-nt "minimal" precursors, which consist of a 22-nt miRNA target site, an 11-nt spacer and a 21-nt syn-tasiRNA, are functionally active and produce high amounts of accurately processed syn-tasiRNAs for effective gene silencing in plants. These minimal precursors are as effective as syn-tasiRNAs produced from 1011-nt long *AtTAS1c* precursors when transgenically expressed in *Arabidopsis thaliana* or *Nicotiana benthamiana*. Moreover, we observed that authentic syn-tasiRNAs are generated from minimal but not from full-length *AtTAS1c*-based precursors when expressed from an RNA viral vector, such as potato virus X, to efficiently silence endogenous genes in *N. benthamiana*. Furthermore, syn-tasiRNA-based virus-induced gene silencing was applied to plants in a transgene-free and scalable manner by spraying infectious crude extracts containing the modified viral vectors. In summary, our results reveal that the size of syn-tasiRNA precursors can be significantly reduced without affecting their functionality, and that syn-tasiRNAs can be successfully expressed from viral vectors to induce widespread gene silencing in plants in a non-transgenic manner.

Keywords: RNA silencing, potato virus X, syn-tasiRNA precursor, *AtTAS1c*, syn-tasiR-VIGS.

INTRODUCTION

Gene expression manipulation in plants is a key tool for studying gene function, altering commercially relevant crop traits or conferring resistance to different stresses. Popular strategies to regulate gene expression in plants are based on the endogenous RNA interference (RNAi) machinery, initiated by the recognition and processing of double-stranded RNA (dsRNA) molecules into small RNA (sRNA) duplexes (Bernstein et al., 2001). One of the strands of the duplex, the guide strand, is loaded into an ARGONAUTE (AGO) protein, forming an RNA-induced silencing complex (RISC) that binds and silences target RNAs with high sequence homology to the guide strand, in a process known as gene silencing (Hammond et al., 2000, 2001).

sRNAs are short RNA molecules of 19-24 nucleotides (nt) divided into two main groups: microRNAs (miRNAs) and small interfering RNAs (siRNAs) [for a recent review see (Zhan & Meyers, 2023)]. Strategies to silence intended genes like hairpin RNAi or virus-induced gene silencing (VIGS), rely on siRNAs produced from long dsRNA precursors, while others like miRNA-induced gene silencing (MIGS) are based on the production of secondary siRNAs after miRNA target cleavage (de Felippes et al., 2012; Ossowski et al., 2008). Despite their popularity, these classical RNAi strategies present a major disadvantage: they generate a pool of unspecific sRNAs, which can lead to off-target effects when they unintentionally bind to cellular transcripts (Senthil-Kumar & Mysore, 2011).

A second generation of gene silencing tools was developed based on artificial sRNAs (art-sRNAs), which are 21-nt RNA molecules computationally designed to lack off-target effects while being highly effective (Carbonell, 2017). There are two main classes of art-sRNAs: artificial miRNAs (amiRNAs) and synthetic trans-acting siRNAs (syn-tasiRNAs), generated from the endogenous miRNA and trans-acting siRNA (tasiRNA) pathways, respectively. A specific feature of syn-tasiRNAs is their multiplexing capability, allowing for the production of several syn-tasiRNAs from a single RNA precursor (Carbonell, 2019). Syn-tasiRNAs are typically generated from *TAS* transgenes, where the endogenous tasiRNA sequences are replaced by one or several 21-nt syn-tasiRNA sequences in tandem, designed to target the gene(s) of interest (Carbonell, 2019; Z. J. Zhang, 2014). Such transgenes are transcribed by DNA-DEPENDENT RNA POLYMERASE II into a *TAS* primary transcript (or *TAS* precursor) that includes a 5' cap structure, a poly-A tail and a target site (TS) specific for a 22-nt miRNA (Chen et al., 2010; Cuperus et al., 2010). Once in the cytoplasm, the RISC complex, formed by the 22-nt miRNA and AGO1, mediates the endonucleolytic cleavage of the *TAS* precursor. SUPRESSOR OF GENE SILENCING 3 (SGS3) stabilizes the *TAS* precursor after cleavage,

which serves as a substrate for the RNA-DEPENDENT RNA POLYMERASE 6 (RDR6), synthesizing a dsRNA molecule. Once generated, the dsRNA is processed into 21-nt syn-tasiRNA duplexes by DICER LIKE 4 (DCL4) which cleaves every 21 nt from the miRNA cleavage site, generating a phasing register that will define syn-tasiRNAs sequences from each modified *TAS* precursor (Allen et al., 2005; Yoshikawa et al., 2005). HUA ENHANCER1 (HEN1) methylates the 3' end of both duplex strands, and then the guide strand is loaded into AGO1 to cleave or translationally repress complementary RNAs. Several aspects of syn-tasiRNAs design have boosted their application for functional genomics and crop improvement (Cisneros et al., 2021; Z. J. Zhang, 2014): (i) their unique multiplexing ability, (ii) their fine-tuning gene silencing capacity and (iii) the development of fast-forward methodologies for their design and generation (Baykal et al., 2016; Carbonell et al., 2014; Fahlgren et al., 2016; López-Dolz et al., 2020).

Arabidopsis thaliana (Arabidopsis) has eight *TAS* loci, belonging to four gene families (*TAS1a-c*, *TAS2*, *TAS3a-c* and *TAS4*), which can be modified to produce syn-tasiRNAs. *TAS* precursor selection is determinant to ensure high target transcript silencing levels, since both, syn-tasiRNA processing and accumulation, depend on the precursor used. So far, *AtTAS1a*, *AtTAS1c* and *AtTAS3a* have been used to successfully produce syn-tasiRNAs (Carbonell, 2019; Cisneros et al., 2022; Cisneros & Carbonell, 2020; Lunardon et al., 2021). Among them, the 990-nt long *AtTAS1c* is often the preferred precursor since syn-tasiRNAs are accurately processed and accumulate to high levels (Carbonell et al., 2014; Lunardon et al., 2021). The *AtTAS1c* precursor has been successfully used to produce highly efficient syn-tasiRNAs for silencing endogenous genes (Cisneros et al., 2021, 2022) and conferring resistance against plant viruses and viroids (Cisneros & Carbonell, 2020). *AtTAS1c*-based production of secondary siRNAs depends on Arabidopsis miR173a (AtmiR173a), which is only present in Arabidopsis and its close relatives. Therefore, the *AtMIR173* gene needs to be co-expressed with the *AtTAS1c* precursor to produce syn-tasiRNAs in non-Arabidopsis species. *Agrobacterium*-mediated plant transformation is the preferred system for expressing syn-tasiRNAs from *AtTAS1c*-based constructs in Arabidopsis or other species. However, transgenic plants or tissues are generated, limiting the biotechnological application of syn-tasiRNAs due to genotype-dependent and time-consuming plant transformation protocols, as well as transgene integration-related regulatory concerns (Su et al., 2023). The relatively large size of *AtTAS1c* precursor may become a limiting factor when using *Agrobacterium*-independent expression systems, specifically if *AtMIR173* co-expression is required. This is the case when producing syn-tasiRNA precursors through *in vitro* transcription for their exogenous application to plants, as RNA production efficiency and cost-effectiveness decrease with increasing insert size (A.-

M. Yu et al., 2020). Similarly, the use of viral vectors imposes size restrictions as they have limited cargo capacity and larger inserts accumulate more mutations and are frequently deleted during viral replication (Mahmood et al., 2023). Interestingly, there are no previous reports of the successful expression of syn-tasiRNAs in plants from viral vectors. Therefore, reducing the size of the *AtTAS1c* precursor might increase RNA production efficiency and insert stability when using *Agrobacterium* alternative expression systems.

Here, we obtained a minimal syn-tasiRNA precursor of only 54 nt, composed of three sequence elements: the 22 nt TS of AtmiR173a, a 11 nt original spacer from *AtTAS1c,* and the 21 nt syn-tasiRNA. We analyzed its silencing efficiency by stable expression in Arabidopsis targeting *CHLORINA42* (*AtCH42*) or *FLOWERING LOCUS T* (*AtFT*) (López-Dolz et al., 2020), which resulted in bleaching and late flowering phenotypes, respectively. The ability to produce phased syn-tasiRNAs from the minimal precursor was confirmed by the simultaneous production of two syn-tasiRNAs targeting *AtFT* and three *MYB* transcripts regulating trichome number, with plants displaying phenotypes of late flowering and increased trichome number (Carbonell et al., 2014). To simplify construct size and complexity when expressing syn-tasiRNAs from *AtTAS1c* precursor in non-Arabidopsis species, the AtmiR173a TS was substituted by the TS of endogenous 22-nt *Nicotiana benthamiana* miRNAs, and their syn-tasiRNA triggering ability was tested in our recently described silencing sensor system (Cisneros et al., 2022). Minimal precursors containing the NbmiR482a TS or the NbmiR6019a/b TS were accurately processed and synt-tasiRNAs accumulated to high levels in agroinfiltrated *N. benthamiana* leaves. Moreover, we report the successful syn-tasiRNA production from an RNA viral vector (syn-tasiR-VIGS), with increased stability, accumulation and silencing efficiency when expressed from the minimal precursor containing the NbmiR482a TS. Finally, we applied our previously described methodology based on spraying crude extracts generated from infected plants to induce transgene-free, syn-tasiR-VIGS-based gene silencing at the whole plant level (Cisneros et al., 2023).

RESULTS

Effective gene silencing in Arabidopsis by syn-tasiRNAs derived from minimal precursors

Previous work showed that phased secondary siRNAs can be generated from non-*TAS* transcripts including gene fragments fused to a 22-nt miRNA TS (Montgomery et al., 2008, de Felippes et al., 2012). Thus, we hypothesized that syn-tasiRNAs could similarly be produced from minimal precursors consisting exclusively of the endogenous 22-nt miRNA TS and the 11-

nt spacer from *AtTAS1c* fused to the syn-tasiRNA sequence, with a total length of 54 nt. To test this hypothesis, we used the syn-tasiR-AtFT/*AtFT* and syn-tasiR-AtCH42/*AtCH42* silencing sensor systems in Arabidopsis where transgenic expression of syn-tasiR-AtFT or syn-tasiR-AtCH42 from full-length *AtTAS1c* precursors at DCL4-processing position 3'D2[+] from the miRNA cleavage site induces a significant delay in flowering time or an intense bleaching due to the targeting of *AtFT* or *AtCH42* endogenous genes, respectively (López-Dolz et al., 2020). Here, we generated the *35S:AtmiR173TS-AtFT* and *35S:AtmiR173TS-AtCH42* constructs for expressing syn-tasiR-AtFT and syn-tasiR-AtCH42 (Figure 1A), respectively, from minimal precursors including exclusively the 22-nt TS sequence (GTGATTTTTCTCTACAAGCGAA) of AtmiR173a followed by the 11-nt spacer sequence (TAGACCATTTA) from *AtTAS1c* (Figure 1A).

These constructs were independently transformed into Arabidopsis Col-0 plants together with control constructs *35S:AtTAS1c-GUS*$_{At}$, *35S:AtTAS1c-AtFT* and *35S:AtTAS1c-AtCH42* expressing a syn-tasiRNA against *Escherichia coli uidA* β-glucuronidase gene (or *GUS*), *AtFT* and *AtCH42* (Figure 1A), respectively, from position 3'D2[+] in *AtTAS1c* (López-Dolz et al., 2020). To compare the activity of syn-tasiR-AtFT or syn-tasiR-AtCH42 produced from minimal and *AtTAS1c* precursors, plant phenotypes, syn-tasiRNA and target mRNA accumulation as well as precursor processing efficiency were measured in Arabidopsis T1 transgenic lines. All *35S:AtTAS1c-AtFT* (n = 65) and *35S:AtmiR173TS-AtFT* (n = 58) transformants flowered later than the average flowering time of the *35S:AtTAS1c-GUS*$_{At}$ and *35S:AtmiR173-GUS*$_{At}$ control lines (n = 58 and n = 64, respectively) (Figure 1B and 1C; Table S1). The average flowering time (39.3 ± 6.6 and 38.9 ± 6.6, respectively) was not significantly different between the two (Figure 1C). RT-qPCR assays revealed that *AtFT* mRNA accumulation was similar in lines expressing syn-tasiR-AtFT from each of the two precursors (Figure 1D), while RNA-blots showed that syn-tasiR-AtFT accumulated to significantly higher levels when expressed from full-length *AtTAS1c* precursor (Figure 1E). Finally, high-throughput sequencing of sRNAs revealed that both *AtTAS1c* and minimal precursors were efficiently processed, with 93% and 98% of the reads corresponded to authentic syn-tasiR-AtFT, respectively (Figure 1F). Similarly, all *35S:AtTAS1c-AtCH42* (n = 402) and *35S:AtmiR173TS-AtCH42* (n = 389) transformants displayed bleaching to comparable degrees (Figure 1B; Table S2), accumulated similar levels *AtCH42* mRNA (Figure 1D) and displayed effective precursor processing (Figure 1E and 1F), though reduced amounts of syn-tasiR-AtCH42 were observed in *35S:AtmiR173TS-AtCH42* transformants (Figure 1E).

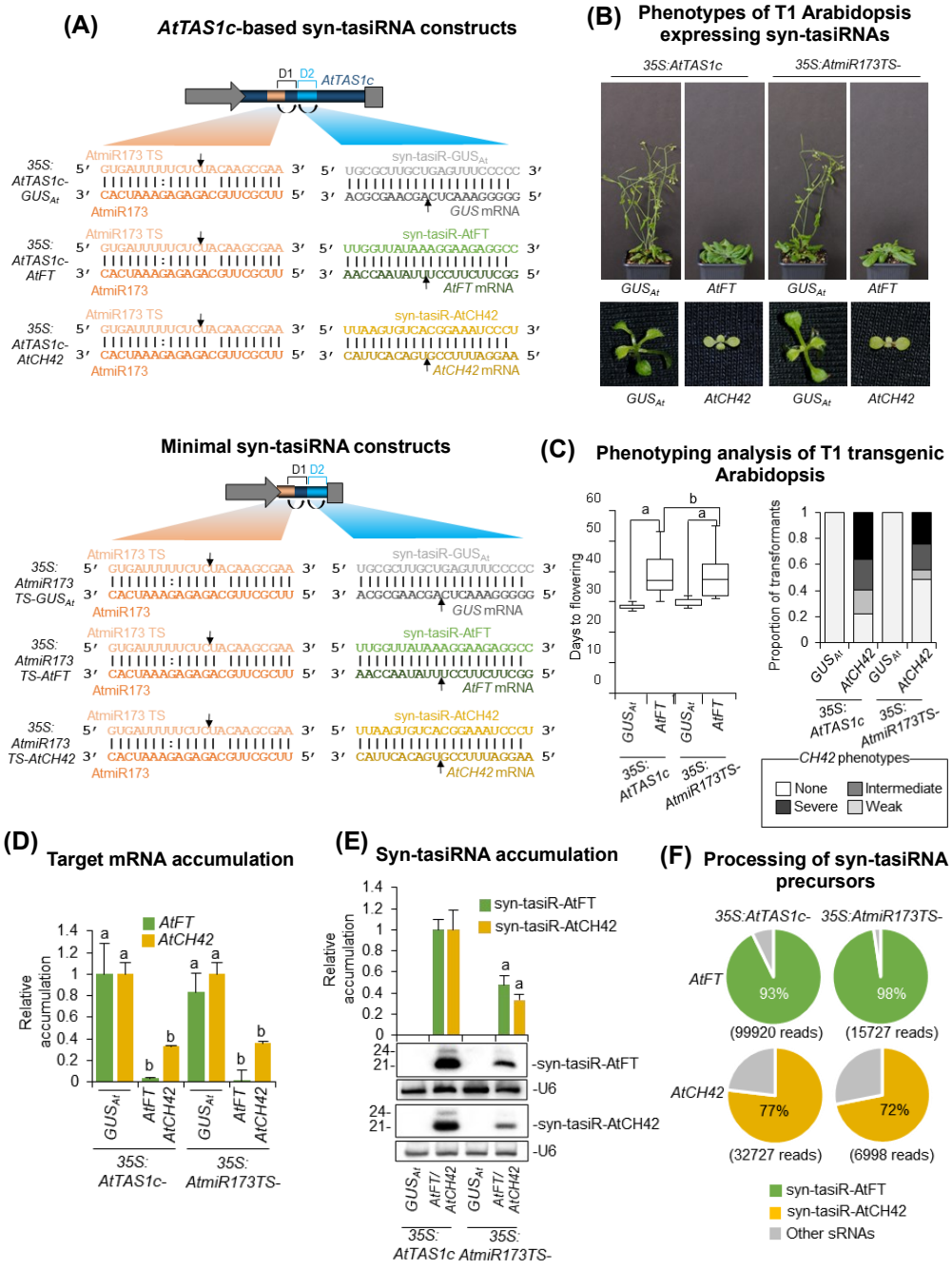

Figure 1. Functional analysis of constructs expressing syn-tasiR-AtFT or syn-tasiR-AtCH42 from *AtTAS1c*-based or from minimal precursors in transgenic Arabidopsis. (**A**) Diagram of the *AtTAS1c* full-length (up) and minimal (down) precursor molecule including the AtmiR173a/AtmiR173a target site (TS) and syn-tasiRNAs/target mRNA base-paring. Nucleotides corresponding to AtmiR173a and AtmiR173a TS

are in dark and light orange respectively. Nucleotides corresponding to syn-tasiR-GUS$_{At}$, syn-tasiR-AtFT and syn-tasiR-AtCH42 are in light grey, green and yellow respectively, while nucleotides of their target mRNAs are in dark grey, green and yellow respectively. Arrows indicate the AtmiR173a and syn-tasiRNAs predicted cleavage site. (**B**) Representative Arabidopsis plant pictures of T1 transgenic plants expressing syn-tasiRNAs from *AtTAS1c* full-length or minimal precursors. Up, 45-day-old adult plants expressing syn-tasiR-GUS$_{At}$ or syn-tasiR-AtFT. Down, 10-day-old T1 seedlings expressing syn-tasiR-GUS$_{At}$ or syn-tasiR-AtCH42. (**C**) Phenotypic comparison analysis of Arabidopsis T1 plants expressing syn-tasiRNA from *AtTAS1c* full-length or minimal precursors. Left, mean flowering time of plants expressing syn-tasiR-GUS$_{At}$ or syn-tasiR-AtFT. Pairwise Student's t-test comparisons are represented with the letter 'a' if significantly different ($P < 0.05$) and the letter 'b' if not ($P > 0.05$). Right, proportion of seedlings in each line displaying a severe (black areas), intermediate (dark grey areas), or weak (light grey areas) bleaching phenotype, or wild-type appearance (white areas). (**D**) Target mRNA accumulation. Relative accumulation of *AtFT* and *AtCH42* mRNA [mean relative level (n = 3) + standard error after normalization to *ACTIN* 2 (*AtACT2*), as determined by quantitative RT-qPCR, *35S:AtTAS1c-GUS$_{At}$* = 1]. Bars with the letter 'b' or 'a' are significantly different or not respectively from that of the corresponding control samples *35S:AtTAS1c-GUS$_{At}$* ($P < 0.05$ in pairwise Student's t-test comparisons) (**E**) Syn-tasiRNA accumulation. Northern blot detection of syn-tasiR-AtFT and syn-tasiR-AtCH42 in RNA preparations from T1 Arabidopsis transgenic plants. The graph at top shows the mean + SD (n = 3) syn-tasiRNA relative accumulation (control samples: *35S:AtTAS1c-AtFT* and *35S:AtTAS1c-AtCH42* = 1.0). Bars with the letter 'a' are significantly different from that of control samples. (**F**) Syn-tasiRNA processing from *35S:AtTAS1c*- or *35S:AtmiR173TS*- based precursors. Pie charts show percentages of reads corresponding to expected, accurately processed 21-nucleotide mature syn-tasiR-AtFT and syn-tasiR-AtCH42 (green or yellow sections, respectively) or to other 19–24 nt sRNAs (grey sectors).

Next, we aimed to analyze whether minimal precursors could be used to express multiple, accurately processed and phased syn-tasiRNAs for the simultaneous silencing of different endogenous genes. For this purpose we used the syn-tasiR-AtFT/syn-tasiR-AtTRY silencing sensor system in Arabidopsis, in which plants co-expressing both syn-tasiRNAs exhibit non-overlapping silencing phenotypes of delay in flowering time and an increase in trichome number, due to the silencing of *AtFT* and of three *MYB* transcripts [*TRIPTYCHON (AtTRY)*, *CAPRICE* (*AtCPC*) and *ENHANCER OF TRIPTYCHON AND CAPRICE2 (AtETC2)*] (Carbonell et al., 2014) (Figure 2A). Here, we compared the silencing efficacy of syn-tasiR-AtFT and syn-tasiR-AtTRY when co-expressed in unique dual configurations from positions 3'D2[+] and 3'D3[+] in full-length *AtTAS1c* (constructs *35S:AtTAS1c-AtFT-AtTRY* and *35S:AtTAS1c-AtTRY-AtFT*) or minimal precursors (constructs *35S:AtmiR173aTS-AtFT-AtTRY* and *35S:AtmiR173aTS-AtTRY-AtFT*) (Figure 2B). We also included in the analysis control constructs *35S:AtTAS1c-GUS$_{At}$* and *35S:AtmiR173aTS-GUS$_{At}$* for expressing syn-tasiR-GUS$_{At}$ in single configuration from position 3'D2[+] in full-length *AtTAS1c* or minimal precursors, respectively. All these constructs were transformed into Arabidopsis Col-0 plants, and T1 transformants were analyzed phenotypically by scoring the day of flowering and the trichome number in rosette leaves for each transformant, and molecularly by quantifying target mRNA and syn-tasiRNA accumulation in the different lines by RT-qPCR and RNA blot assays, respectively.

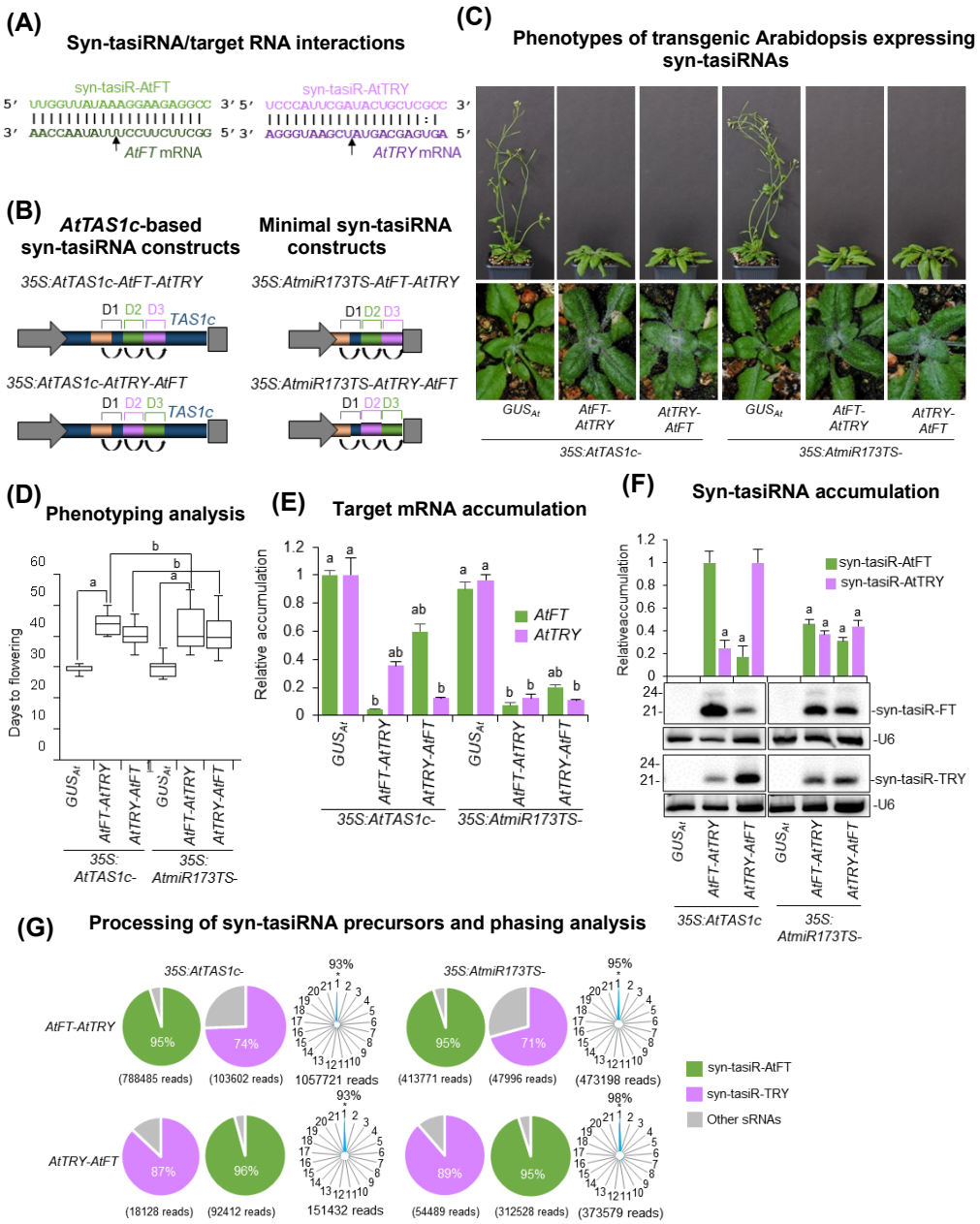

Figure 2. **Functional analysis of constructs expressing syn-tasiR-AtFT and syn-tasiR-AtTRY from *AtTAS1c*-based or from minimal precursors in transgenic *Arabidopsis***. (**A**) Diagram of the base-paring between syn-tasiR-AtFT and syn-tasiR-AtTRY with their target mRNAs. Nucleotides corresponding to syn-tasiR-AtFT and syn-tasiR-AtTRY are in light green and purple respectively, while nucleotides of their target mRNAs are in dark green and purple respectively. Arrows indicate the syn-tasiRNAs cleavage site in their target mRNAs. (**B**) Diagram of the *AtTAS1c* full-length (left) and minimal (right) precursor constructs. AtmiR173a target site (TS), syn-tasiR-AtFT and syn-tasiR-AtTRY are represented in orange, green and

purple respectively. Other details as in Figure 1A. (**C**) Representative pictures of Arabidopsis T1 transgenic lines expressing syn-tasiRNAs in tandem from *AtTAS1c* full-length or minimal precursors. The same plant was photographed at 20 days post-plating (dpp) to check for higher number of trichomes (down) and at 45 dpp to check for a delay in flowering (up). (**D**) Phenotypic analysis of Arabidopsis T1 plants expressing syn-tasiRNAs from *AtTAS1c* full-length or minimal precursors. Mean flowering time of plants expressing syn-tasiR-AtFT and syn-tasiR-AtTRY is represented. Other details as in Figure 1C. (**E**) Target mRNA accumulation. Relative accumulation of *AtFT* and *AtTRY* mRNA. Bars with the letter 'b' or 'a' are significantly different or not respectively from that of the corresponding control samples (control sample: *35S:AtTAS1c-GUS*$_{At}$ = 1, P < 0.05 in pairwise Student's t-test comparisons). Other details as in Figure 1D. (**F**) Northern blot of syn-tasiR-AtFT and syn-tasiR-AtCH42 in RNA preparations from T1 Arabidopsis transgenic plants (control samples *35S:AtTAS1c-AtFT-AtTRY* and *35S:AtTAS1c-AtTRY-AtFT* = 1.0). Other details as in Figure 1E. (**G**) Syn-tasiRNA processing and phasing analysis from *35S:AtTAS1c-* and *35S:AtmiR173TS*-based precursors. Pie charts show percentages of reads corresponding to expected, accurately processed 21-nt mature syn-tasiR-AtFT or syn-tasiR-AtTRY (green or purple sections, respectively) or to other 19-24 nt sRNAs (grey sectors). Phasing analysis represented by radar plots showing the proportion of 21-nt reads corresponding to each of the 21 registers from *AtTAS1c* transcripts, with position 1 designated as immediately after the AtmiR173a guided cleavage site. The percentage of 21-nt reads corresponding to phasing register 1 is indicated.

Regarding flowering time analysis, all transformants expressing the dual-configuration syn-tasiRNA constructs showed a delay in flowering compared to *35S:AtTAS1c-GUS*$_{At}$ or *35S:AtmiR173aTS-GUS*$_{At}$ control transformants (Figure 2C; Table S3). In particular, transformants expressing syn-tasiR-AtFT from minimal precursors at positions 3'D2[+] or 3'D3[+] had a mean flowering time of 43 ± 7.3 or 40.5 ± 5.4 days, respectively, which was similar to that of transformants expressing the same syn-tasiRNA from these same positions (43 ± 5.4 and 40.2 ± 3.9 days, respectively) from full-length precursors (Figure 2D). Regarding the trichome number analysis (Figure 2C), 80% and 72% of transformants expressing syn-tasiR-AtTRY from minimal precursors at positions 3'D2[+] or 3'D3[+], respectively, had a higher number of trichomes compared to the *35S:AtmiR173aTS-GUS*$_{At}$ control group, similarly to the transformants expressing the same syn-tasiRNA from these same positions (88% and 82%, respectively) in full-length precursors (Table S3). Interestingly, target mRNA accumulation analysis by RT-qPCR showed a similar and drastic decrease of *AtFT* and *AtTRY* mRNA levels in dual-configuration transformants compared to *35S:AtTAS1c-GUS*$_{At}$ and *35S:AtmiR173aTS-GUS*$_{At}$ controls, regardless of the size of precursor used (Figure 2E). RNA blot assays confirmed that both minimal and full-length precursors produced detectable levels of syn-tasiRNAs that accumulated as single 21-nt bands (Figure 2F), indicating accurate processing from both types of precursors. To further confirm the accuracy of precursor processing, sRNAs from the four dual-configuration transformants were sequenced and analyzed. Both classes of precursors were efficiently processed, with 95-96% and 71-89% of the reads corresponding to authentic syn-tasiR-AtFT or syn-tasiR-AtTRY, respectively (Figure 2G). Moreover, the tasiRNA pools

triggered by AtmiR173a were highly phased, with 93-98% of 21-nt reads corresponding to the first register (Figure 2G).

Overall, these results indicate that minimal syn-tasiRNA precursors, including the AtmiR173a TS and an 11-nt spacer, when stably expressed in Arabidopsis produce authentic 21-nt phased syn-tasiRNA species that induce highly effective silencing of endogenous genes, similarly to syn-tasiRNAs expressed from full-length *AtTAS1c* precursors.

Effective gene silencing in *N. benthamiana* by syn-tasiRNAs derived from minimal precursors

Next, we aimed to confirm in another plant species such as *Nicotiana benthamiana* that accurately processed and phased syn-tasiRNAs could be produced from minimal precursors. Since AtmiR173a is exclusively present in Arabidopsis and its close relatives, we hypothesized that syn-tasiRNAs could be generated in *N. benthamiana* from minimal precursors including a heterologous TS of an endogenous 22-nt miRNA such as NbmiR482a or NbmiR6019a/b, instead of the original AtmiR173a TS.

First, we explored whether syn-tasiRNA biogenesis could be triggered from the *35S:AtTAS1c-(NbmiR482aTS)-NbSu* or *35S:AtTAS1c-(NbmiR6019a/b/bTS)-NbSu* constructs engineered to produce syn-tasiR-NbSu, a syn-tasiRNA silencing the *N. benthamiana* magnesium chelatase subunit CHLI-encoding *SULPHUR* (*NbSu*) (Cisneros et al., 2022), from modified *AtTAS1c* precursors including NbmiR482a or NbmiR6019a/b TSs, respectively (Figure 3A). Both constructs were independently agroinfiltrated into two areas of two leaves from three different plants, together with control constructs *35S:AtTAS1c-GUS$_{Nb}$/AtMIR173a* and *35S:AtTAS1c-NbSu/AtMIR173a* (López-Dolz et al., 2020) for producing syn-tasiR-GUS$_{Nb}$ and syn-tasiR-NbSu, respectively, due to the co-expression of *AtMIR173a* (Figure 3A). Seven days post-agroinfiltration (dpa), all areas agroinfiltrated with anti-*NbSu* syn-tasiRNA constructs displayed a strong bleaching, as expected from *NbSu* knockdown, while areas expressing the control construct did not (Figure 3A). These bleached areas accumulated significantly reduced amounts of chlorophyll *a* compared to areas expressing the control syn-tasiRNA (Figure 3B). Next, two leaves from three different plants were independently agroinfiltrated over the entire leaf surface with each of the syn-tasiRNA constructs described above. RT-qPCR and RNA blot assays of RNA preparations obtained at 2 dpa from agroinfiltrated leaves showed that, in all samples expressing canonical or modified *AtTAS1c* precursors, *NbSu* mRNA accumulation was drastically reduced and syn-tasiR-NbSu accumulated as a single 21-nt band, although samples expressing *AtTAS1c(NbmiR6019a/bTS)* accumulated lower levels of syn-tasiR-NbSu than the the others (Figure 3C and 3D).

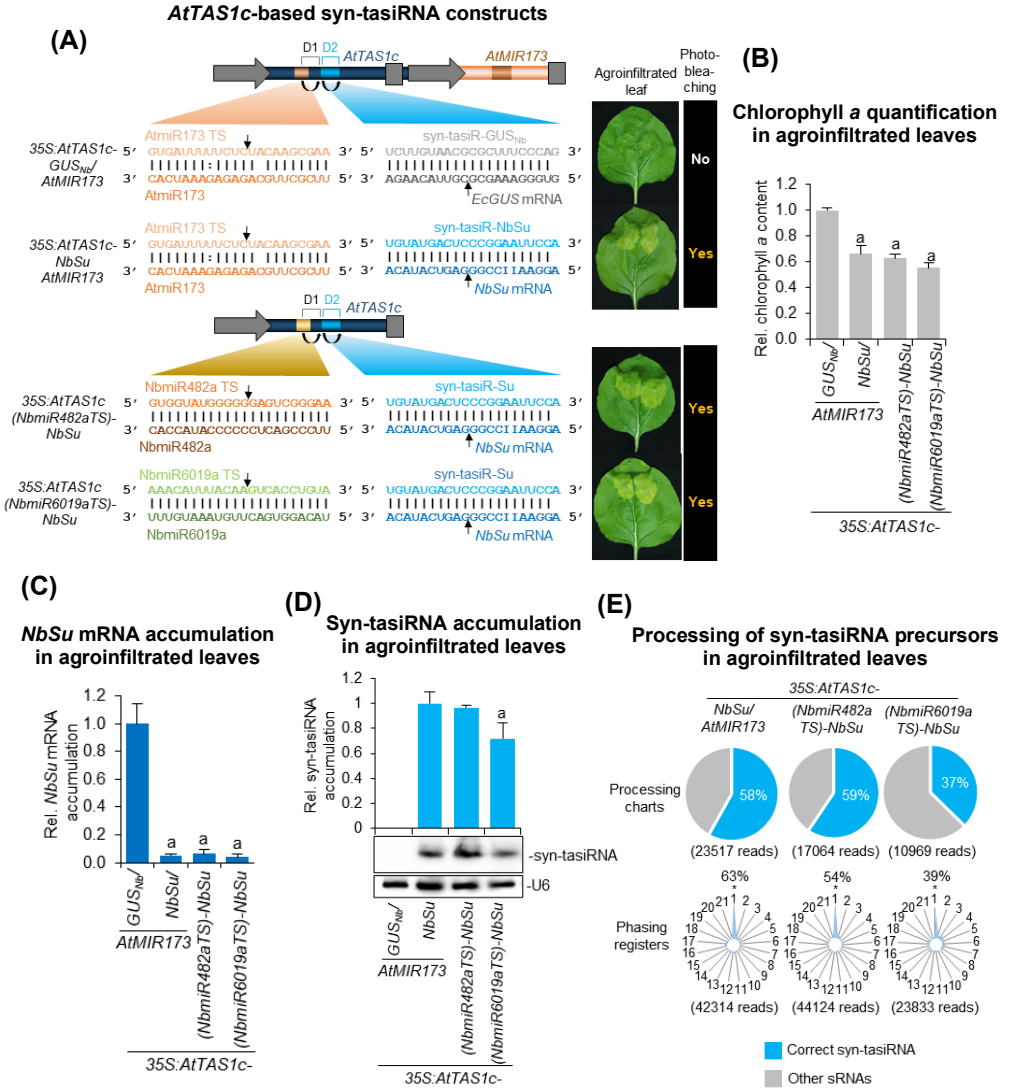

Figure 3. **Functional analysis in *N. benthamiana* leaves of constructs expressing syn-tasiR-NbSu from full-length *AtTAS1c* precursor sequences modified to include the NbmiR482a or NbmiR6019a/b target site (TS).** (**A**) Diagram of the *AtTAS1c* full-length (up) and modified (down) expression cassette including the triggering miRNAs TS and syn-tasiRNAs/target mRNA base-paring. Nucleotides corresponding to AtmiR173a and AtmiR173aTS are in dark and light orange respectively. Nucleotides corresponding to syn-tasiR-NbSu are in light blue, while nucleotides of its target mRNAs are in dark blue. Nucleotides corresponding to NbmiR482a and NbmiR6019a/b are in light brown and green respectively while those corresponding to their TS are in dark brown and green respectively. Other details as in Figure 1A. Pictures at 7 days post agroinfiltration (dpa) of leaves agroinfiltrated with each of the constructs are on the right, the appearance of a bleaching phenotype on the agroinfiltrated area is specified with a "Yes" and its absence with a "No". (**B**) Relative content of chlorophyll *a* in agroinfiltrated patches (control sample:

35S:AtTAS1c-AtMIR173-GUS$_{Nb}$ = 1.0). Bars with letter "a" are significantly different from that of control samples ($P < 0.05$ in pairwise Student's t -test comparisons). (**C**) Target mRNA accumulation. Relative *NbSu* mRNA accumulation in agroinfiltrated leaves at 2 dpa [mean relative level (n = 3) + standard error after normalization to *PROTEIN PHOSPHATASE 2A* (*NbPP2A*), as determined by quantitative RT-qPCR, control sample: *35S:AtTAS1c-AtMIR173-GUS*$_{Nb}$ = 1]. Other details as in B. (**D**) Syn-tasiRNA accumulation. Northern blot detection of syn-tasiR-NbSu in RNA preparations from agroinfiltrated leaves at 2 dpa (Control sample: *35S:AtTAS1c-AtMIR173-NbSu* = 1.0). Other details as in Figure 1E. (**E**) Syn-tasiRNA processing and phasing analysis from *35S:AtTAS1c*-derived precursors. Pie charts show percentages of reads corresponding to expected, accurately processed 21-nt mature syn-tasiR-NbSu in blue or to other 19-24 nt sRNAs in grey. Phasing analysis as in Figure 2G, with position 1 designated as immediately after AtmiR173a, NbmiR482a or NbmiR6019a/b guided cleavage site (from left to right).

Importantly, high-throughput sequencing analysis of sRNAs showed that *AtTAS1c(NbmiR482aTS)* and canonical *AtTAS1c* precursors were processed with similar accuracy, with 59% and 58% of reads within ± 4 nt of 3'D2 [+] corresponded to authentic syn-tasiR-NbSu, respectively, while this percentage was lower (37%) in samples expressing *AtTAS1c(NbmiR6019a/bTS)* precursors (Figure 3E). Moreover, highly phased syn-tasiRNAs were generated from canonical *AtTAS1c* or modified *AtTAS1c(NbmiR482aTS)* precursors, with 63% and 54% of 21-nt [+] reads, respectively, corresponding to the first register (Figure 3E). In the case of *AtTAS1c(NbmiR6019a/bTS)* precursors, only 39% of 21-nt [+] reads corresponded to the first register (Figure 3E).

Next, we decided to test whether syn-tasiRNA biogenesis could be triggered in *N. benthamiana* from the *35S:NbmiR482aTS-NbSu* and *35S:NbmiR6019a/bTS-NbSu* constructs engineered for syn-tasiR-NbSu expression from minimal precursors including NbmiR482a or NbmiR6019a/b TS, respectively (Figure 4A). Both constructs were agroinfiltrated in *N. benthamiana* and analyzed as explained before together with *35S:AtTAS1c-GUS*$_{Nb}$*/AtMIR173a*, *35S:AtTAS1c(NbmiR482aTS)-NbSu* and *35S:AtTAS1c(NbmiR6019a/bTS)-NbSu*, for comparison purposes (Figure 4A). All constructs engineered for expressing syn-tasiR-NbSu induced bleaching in the agroinfiltrated areas (Figure 4A), which correlated with drastic *NbSu* mRNA downregulation of *NbSu* mRNA compared to the negative control samples (Figure 4B). RNA blot assays confirmed the accumulation of syn-tasiR-NbSu as a single 21-nt sRNA species in all samples displaying bleaching, with samples expressing *NbmiR482aTS-NbSu* accumulating syn-tasiRNAs to levels similar to those of samples expressing *AtTAS1c(NbmiR482aTS)* precursors (Figure 4C). Moreover, the minimal *NbmiR482aTS* precursor was efficiently processed, as 63% of ±4 nt of 3'D2[+] reads corresponded to authentic syn-tasiR-NbSu (Figure 4D). This percentage was similar to that of full-length *AtTAS1c* precursor (58%, Figure 3E) and slightly higher than that of the minimal *NbmiR6019a/b*-based precursor (47%, Figure 4D).

Finally, to confirm that syn-tasiRNA biogenesis from minimal precursors in *N. benthamiana* is exclusively triggered by an endogenous 22-nt miRNA, leaves agroinfiltrated with the *35S:NbmiR156aTS-NbSu* and *35S:AtmiR173aTS-NbSu* constructs engineered for expressing syn-tasiR-NbSu from minimal precursors including either a *N. benthamiana* 21-nt miRNA TS or a heterologous 22-nt miRNA TS, respectively (Figure S1A), were analyzed. Results show that leaves agroinfiltrated with either of these two constructs displayed neither bleaching (Figure S1A) nor reduced chlorophyll *a* content (Figure S1B), nor accumulation of syn-tasiR-NbSu (Figure S1C). These results also suggest that bleaching observed in leaves agroinfiltrated with 35S:NbmiR482aTS-NbSu is due to the activity of syn-tasiR-NbSu rather than of potential siRNAs generated from transgene silencing. Taken together, all these results demonstrate that highly phased, accurately processed syn-tasiRNAs can be produced in *N. benthamiana* from minimal precursors including a heterologous TS from an endogenous 22-nt miRNA.

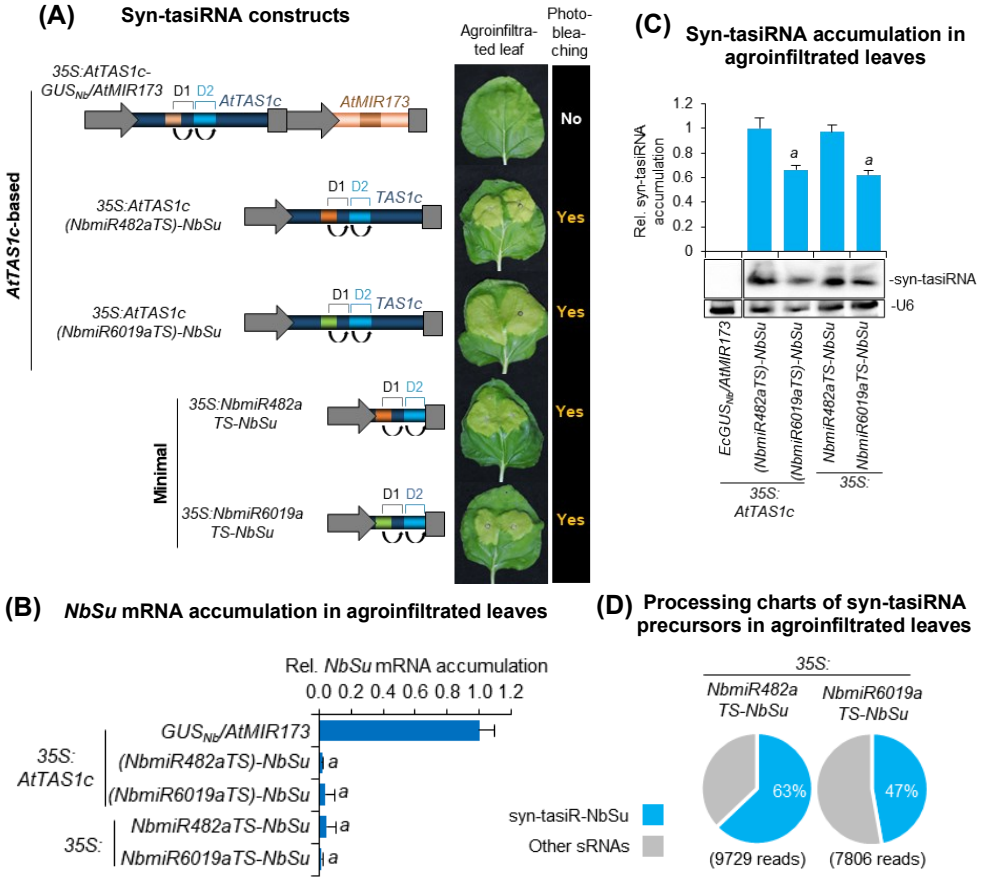

Figure 4. Functional analysis in *N. benthamiana* leaves of syn-tasiR-NbSu expressed from minimal precursors modified to include NbmiR482a or NbmiR6019a/b target site (TS). (**A**) Diagram of the

different engineered versions of the *AtTAS1c* precursors from the full-length canonical expression cassette, to the minimal modified to include NbmiR482aTS (brown square) or NbmiR6019a/bTS (green square) (from top to bottom). Other details as in Figure 3A. (**B**) Target mRNA accumulation. Details as in Figure 3C. (**C**) Syn-tasiRNA accumulation (control sample *35S:AtTAS1c(NbmiR482aTS)-NbSu* = 1.0). Other details as in Figure 1E. (**D**) Syn-tasiRNA processing from *35S:NbmiR482a-* or *35S:NbmiR6019a/b*-based precursors. Pie chart details as in Figure 3E.

Widespread gene silencing in *N. benthamiana* triggered by syn-tasiRNAs derived from minimal precursors and expressed from a viral vector

So far, the use of viral vectors to express syn-tasiRNAs for plant gene silencing has not been reported. Here, we tested this possibility and hypothesized that the 54-nt long *NbmiR482aTS*-based minimal precursor could be more stable when inserted in a viral vector than the classic, 1011-nt long *AtTAS1c(NbmiR482aTS)*-based precursor. As shown in previous experiments, minimal precursors including NbmiR482a TS, showed higher processing accuracy and syn-tasiRNA accumulation compared to those including NbmiR6019a/b TS (Figure 4C and 4D), therefore they were used preferentially in further experiments.

To analyze syn-tasiRNA production from a viral vector, *AtTAS1c(NbmiR482aTS)-NbSu* and *NbmiR482aTS-NbSu* sequences were inserted into a potato virus X (PVX) infectious clone to generate the *35S:PVX-AtTAS1c(NbmiR482aTS)-NbSu* and *35S:PVX-NbmiR482aTS-NbSu* constructs, respectively (Figure 5A). Both constructs were expected to express syn-tasiR-NbSu from full-length *AtTAS1c(NbmiR482aTS)* and minimal *NbmiR482aTS* precursors, respectively, during PVX infection, and induce bleaching of PVX-infected tissues. These two constructs, along with the insert-free *35S:PVX* construct (Figure 5A), were independently agroinoculated into one leaf of three *N. benthamiana* plants. A negative control set of plants ("mock") was infiltrated with the agroinfiltration solution. The appearance of mild PVX-induced symptoms and bleaching phenotypes were monitored over 28 dpa.

All plants agroinoculated with *35S:PVX* or *35S:PVX-NbmiR482aTS-NbSu* showed mild leaf curling typical of PVX-induced symptoms between 4 and 5 dpa (Figure 5B). In contrast, plants agroinoculated with *35S:PVX-AtTAS1c(NbmiR482aTS)-NbSu* displayed the curling phenotype 2-3 days later, between 7 and 8 dpa (Figure 5B). Interestingly, bleaching was observed in areas of certain apical leaves as soon as 7 dpa in plants agroinoculated with *35S:PVX-NbmiR482aTS-NbSu*, and by 14-21 dpa it extended to most of the apical tissues (Figure 5C). At these same timepoints, limited and mild bleaching was observed in plants agroinoculated with *35S:PVX-AtTAS1c(NbmiR482aTS)-NbSu*, while no bleaching was observed in plants expressing *35S:PVX* (Figure 5C). RT-qPCR and RNA blot analyses showed that only tissues expressing *35S:PVX-NbmiR482aTS-NbSu* accumulated low levels of *NbSu* mRNA (Figure 5D)

and high levels of syn-tasiR-NbSu (Figure 5E), respectively. In contrast, plants agroinoculated with *35S:PVX-AtTAS1c(NbmiR482aTS)-NbSu* displayed a slight decrease in *NbSu* mRNA levels and low levels of syn-tasiR-NbSu barely detectable by RNA blot assay (Figure 5E). Importantly, sRNA sequencing of RNA preparations from apical leaves of plants agroinoculated with *35S:PVX-NbmiR482aTS-NbSu* revealed that the *NbmiR482aTS-NbSu* precursor was accurately processed, with 55% of the ±4 nt of 3'D2[+] reads corresponding to authentic syn-tasiR-NbSu (Figure 5F). Plotting all 19-24-nt sRNA [+] reads that mapped to the entire *NbmiR482aTS-NbSu* precursor revealed a relatively low number of sRNAs overlapping with the 3'D2[+] position or, more generally, produced from the rest of the precursor (Figure 5F). Actually, the sRNA profile of 19-24-nt [+] reads mapping to the *NbmiR482aTS-NbSu* precursor was similar in *35S:PVX-NbmiR482aTS-NbSu* and *35S:NbmiR482aTS-NbSu* samples, indicating that the processing of the minimal precursor is not particularly altered during PVX replication (Figure S2).

Finally, the presence of *AtTAS1c(NbmiR482aTS)-NbSu* and *NbmiR482aTS-NbSu* precursors was analyzed by RT-PCR at 7 dpa with oligonucleotides flanking the precursor insertion site (Figure 5G). The 278-bp fragment corresponding to the *NbmiR482aTS-NbSu* precursors was clearly amplified, while the 1235-bp fragment of the *AtTAS1c(NbmiR482aTS)-NbSu* could not be detected. Importantly, PVX coat protein (CP) was detected in all samples expressing PVX-based constructs and *PROTEIN PHOSPHATASE 2A* (*NbPP2A*) amplification in all samples confirmed the quality of cDNA synthesis. Sanger sequencing of RT-PCR fragments amplified from the three *PVX-NbmiR482aTS-NbSu*-infected samples revealed no mutations in the entire insert (data not shown). Overall, these results show that accurately processed syn-tasiRNAs can be produced from minimal precursors inserted into a PVX vector for widespread silencing of endogenous genes such as *NbSu*.

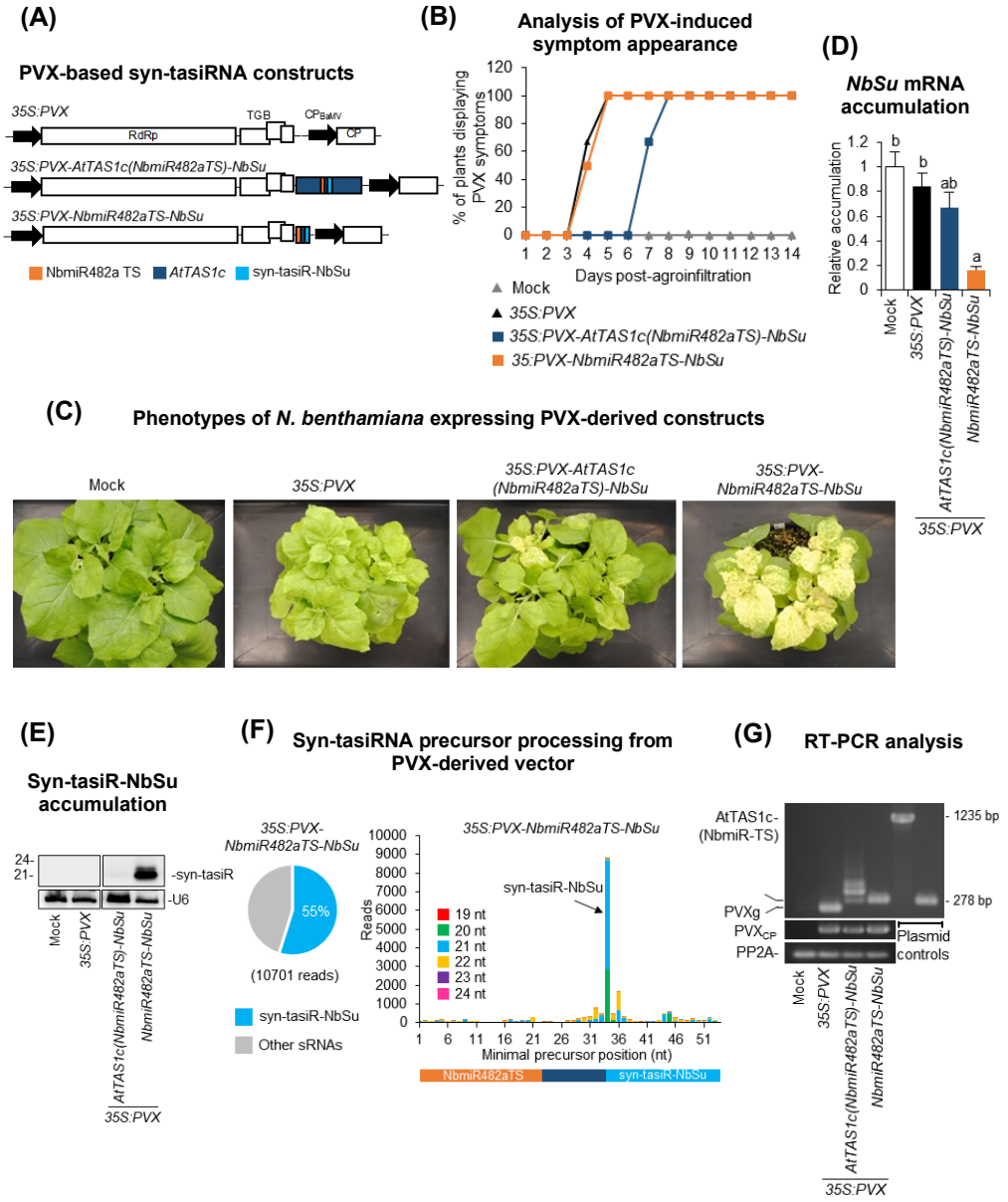

Figure 5. Functional analysis of potato virus X (PVX)-based constructs expressing full-length or minimal syn-tasiRNA precursors in *N. benthamiana*. (**A**) Diagram of PVX-derived constructs. PVX ORFs and promoters are represented as white boxes and black arrows respectively. Regions corresponding to *AtTAS1c*, NbmiR482aTS and syn-tasiR-NbSu are represented by dark blue, orange and light blue boxes, respectively. RdRP: RNA-dependent RNA-polymerase, TGB: triple gene block, CP: coat protein, CP_{BaMV}: Bamboo mosaic virus CP promoter. (**B**) PVX-induced symptom appearance. Percentage

of symptomatic plants per day, for each of the three-plant sets analysed, during the first 14 days post-agroinoculation. (**C**) Photos at 14 dpa of sets of three plants agroinoculated with the different constructs. (**D**) Target *NbSu* mRNA accumulation from apical leaves collected at 14 days post agroinoculation and analysed individually (mock = 1.0 in all comparisons). Bars with the letter 'a' or 'b' are significantly different or not respectively to mock control samples ($P < 0.05$ in pairwise Student's t-test comparison). (**E**) Syn-tasiRNA accumulation. Northern blot detection of syn-tasiR-NbSu in RNA preparations from apical leaves collected at 14 dpa and pooled from three independent plants. (**F)** syn-tasiRNA processing from *35S:PVX-NbmiR482a-NbSu*. Left, syn-tasiR-NbSu processing analysis, details as in Figure 3E. Right, mapping of 19-24 nt small RNA (sRNA) reads to the minimal precursor expressing syn-tasiR-NbSu from PVX. X-axis indicates the position on the precursor in nucleotides from the 5' end terminus of the precursor plotted. Orange, dark blue and light blue squares represent the first 22-nt positions corresponding to the NbmiR482aTS, the 11-nt of the spacer and the syn-tasiR-NbSu, respectively. Y-axis represents the sRNA coverage in total number of reads for each position. (**G**) RT-PCR detection of PVX, full-length and minimal precursors in apical leaves at 7 dpa. RT-PCR products corresponding to the *NbPP2A* and PVX vector controls are also shown (bottom), as well as control amplifications of full-length and minimal precursor fragments from plasmids (right). PVXg: band amplified on the *35S:PVX* vector by the precursor-specific PCR oligos.

Transgene-free, PVX-based syn-tasiR-VIGS

Finally, we explored the possibility of applying syn-tasiR-VIGS to plants in a DNA-free, non-transgenic manner. A diagram of the methodology is presented in Figure 6A. Briefly, six *N. benthamiana* plants were agroinoculated with *35S:PVX-NbmiR482a-NbSu*. At 6 dpa, apical leaves displaying mild PVX-induced symptoms were collected and combined to prepare a crude extract. This crude extract was then sprayed onto three *N. benthamiana* plants. Importantly, control crude extracts were obtained from mock and *35S:PVX*-agroinoculated plants and analyzed in parallel. Remarkably, all three *N. benthamiana* plants sprayed with the crude extract derived from *35S:PVX-NbmiR482a-NbSu* displayed bleaching characteristic of *NbSu* silencing (Figure 6B) and accumulated minimal syn-tasiRNA precursors (Figure 6C) with no sequence alterations as confirmed by Sanger sequencing of amplified RT-PCR products (data not shown). In all cases, control plants sprayed with *35S:PVX*-derived extracts displayed mild PVX symptoms but no bleaching, and accumulated PVX CP, while plants sprayed with mock crude extracts were virus-free and did not displayed any bleaching (Figure 6B and C). Collectively, these results indicate that crude extracts can be directly sprayed onto *N. benthamiana* leaves to trigger syn-tasiR-VIGS in a DNA-free, non-transgenic manner.

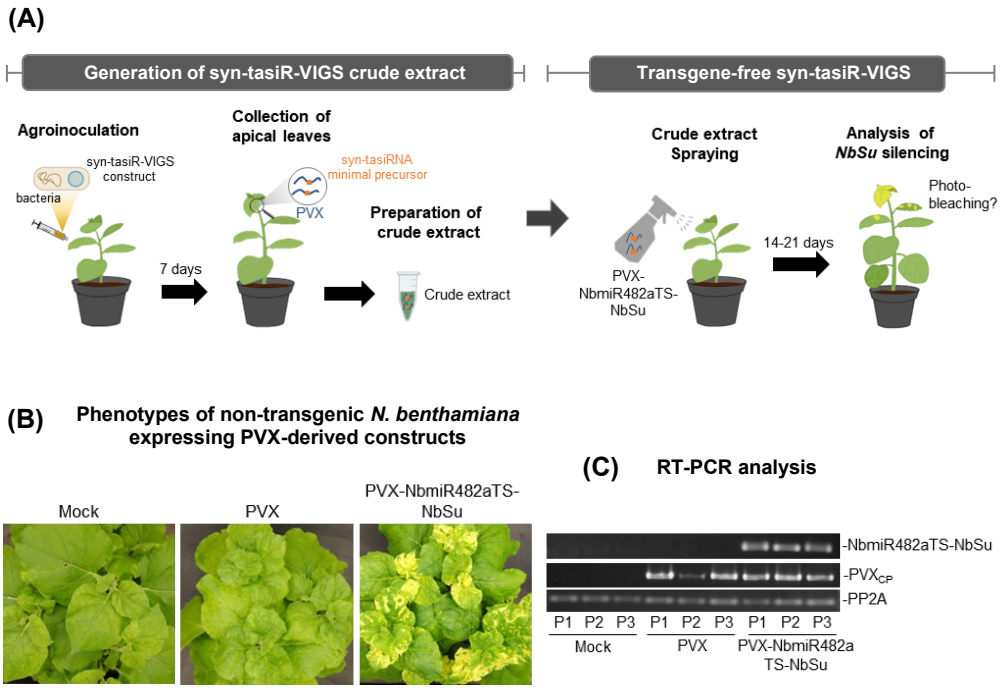

Figure 6. **Transgene-free widespread gene silencing through PVX-based Syn-tasiR-VIGS.** (**A**) Experimental procedure to induce transgene-free gene silencing triggered by PVX-NbmiR482aTS-NbSu in *N. benthamiana* plants. (**B**) Widespread *NbSu* silencing induced by sprayed crude extracts. Photos at 14 days post-agroinfiltration (dpa) of sets of three plants sprayed with different crude extracts obtained from agroinoculated plants. (**C**) RT-PCR detection of PVX coat protein fragment (PVX_{CP}) and *NbmiR482aTS-NbSu* precursors in apical leaves of each of the three plants inoculated (P1-P3) at 14 dpa. RT-PCR products corresponding to the control *NbPP2A* are also shown.

New high-throughput vectors for expressing syn-tasiRNAs from minimal precursors in Arabidopsis or *N. benthamiana* and for direct expression from PVX

We have designed two sets of vectors containing the endogenous miRNA TS, AtmiR173a TS for expression in Arabidopsis or NbmiR482a TS for expression in *N. benthamiana*, along with the 11-nt *AtTAS1c* spacer followed by the *ccd*B cassette flanked by two inverted *Bsa*I sites (Figure S3A and B). Specifically, *pENTR-AtmiR173aTS-B/c* and *pENTR-NbmiR482aTS-B/c* were developed as Gateway compatible vectors for direct cloning of syn-tasiRNAs and subsequent recombination into the Gateway expression vector of choice. The vectors *pMDC32B-AtmiR173aTS-B/c* and *pMDC32B-NbmiR482aTS-B/c* were generated for direct cloning of syn-tasiRNAs into a binary expression vector. Additionally, “universal” *pENTR-B/c* and *pMDC32B-B/c* vectors were developed to allow cloning of different miRNA TSs and

facilitate their use in different plant species. Minimal syn-tasiRNA precursor inserts can be cloned into the *pLB-PVX-MluI* vector containing a PVX genome with a *MluI* restriction site upstream the *CP* gene (Cisneros et al., 2023) (Figure S3C).

DISCUSSION

We have determined that precursor molecules consisting of a 22-nt endogenous miRNA TS and an 11-nt spacer are sufficient for the correct processing and accumulation of syn-tasiRNAs in plants. We provide evidence of the versatility of the syn-tasiRNA minimal precursor and its potential application across a wide range of species by substituting the original AtmiR173a TS for an *N. benthamiana* endogenous 22-nt miRNA TS, without compromising its silencing efficiency. We report for the first time the production of authentic syn-tasiRNAs from a viral vector, inducing widespread silencing of the target gene in inoculated plants. Remarkably, the minimal precursor outperforms the full-length *AtTAS1c* precursor in target gene silencing when expressed from a PVX-derived viral vector, highlighting the importance of using engineered minimal precursors to enhance the biotechnological applications of syn-tasiRNAs expression.

Effect of drastically shortening the length of the precursor on syn-tasiRNA accumulation

Phased tasiRNAs are generated from gene fragments placed downstream a 22-nt miRNA TS without the need for any regulatory sequences (Felippes & Weigel, 2009; Montgomery et al., 2008). In previous studies, the regulatory function of *cis* elements in the *AtTAS* genes was analyzed by deleting internal, 5' or 3' regions of some *AtTAS* precursor sequences. Specifically, the 930-nt full-length *AtTAS1a* was shortened to 252-nt by removing the 5’ region from the AtmiR173a TS and the downstream sequence from the 3’D9[+] position. It was concluded that none of the deleted sequences were determinant for syn-tasiRNA triggering, although syn-tasiRNA accumulation was negatively affected (de Felippes & Weigel, 2009). The 5’ region upstream of the AtmiR173a TS was also deleted in the *AtTAS1c* precursor without a clear effect on syn-tasiRNA production or accumulation. However, other precursor elements such as the poly(A) tail or the total transcript length were found to be determinant for proper syn-tasiRNA accumulation (Montgomery et al., 2008). Here, syn-tasiRNAs accumulated to lower levels in Arabidopsis plants expressing the minimal precursor compared to those expressing the full-length *AtTAS1c*, indicating that there might be some *cis* elements in the *AtTAS1* precursors that positively regulate syn-tasiRNA accumulation.

Despite being considered non-coding RNAs, ORFs have been found in the four Arabidopsis *TAS* families (de Felippes, 2019), and a link has been stablished between these ORFs and the tasiRNA production, since mutations affecting either the stop codon position or the overall ORF length (in those ORFs that are closer or comprise the miRNA TS) have been shown to impact tasiRNA accumulation (Bazin et al., 2017; Yoshikawa et al., 2016; Zhang et al., 2012). Different ORFs in the *AtTAS* transcripts from the four Arabidopsis *TAS* families were found not only to associate with ribosomes but also to be actively translated (Wu et al., 2024). A model was proposed in which ribosomes start translating the ORFs and stall near the miRNA TS through the interaction with the SGS3-AGO1-miRNA complex. This interaction is thought to stabilize the complex, thus increasing the amount of tasiRNA produced (Iwakawa et al., 2021). In particular, two ORFs are located in the 5' region upstream of the AtmiR173a TS (ORF1 and ORF2) in the *AtTAS1c* precursor, and a third ORF overlaps with ORF2 and includes the miRNA TS (Wu et al., 2024). Our minimal syn-tasiRNA precursor contains only the 11-nt spacer sequence from the original *AtTAS1c*, therefore the lack of any ORF-containing sequence, according to the previous findings, may explain the reduced syn-tasiRNA accumulation observed in Arabidopsis plants expressing syn-tasiR-AtFT and syn-tasiR-AtCH42 from minimal precursors compared to those expressing these same syn-tasiRNAs from full-length *AtTAS1c* precursors (Figure 1E). However, these differences in syn-tasiRNA accumulation seem to be less drastic than those reported in previous studies analyzing shortened versions of *AtTAS1* precursors (de Felippes & Weigel, 2009; Montgomery et al., 2008). This may be explained by the position from which the syn-tasiRNA is expressed since in our case, unlike in the previous studies, syn-tasiRNAs are expressed from the 3'D2[+] position, which has been shown to maximize both syn-tasiRNA accumulation and gene silencing efficiency (López-Dolz et al., 2020).

Finally, to ensure the correct processing of the different syn-tasiRNAs and to prevent off-target effects, the syn-tasiRNAs need to be released from the *TAS* precursor in phase from the miRNA cleavage site. Here, phasing is maintained during the processing of the minimal precursors (Figure 2G) which is in consistent with previous studies indicating that phasing depends on miRNA-AGO cleavage of the *TAS* transcript rather than on any *cis* regulatory element (Arribas-Hernández et al., 2016).

Effect of miRNA target site swap on syn-tasiRNA generation and silencing activity in *N. benthamiana*

Since AtmiR173a is only present in Arabidopsis and close relatives, the *AtMIR173* gene needs to be co-expressed to produce syn-tasiRNAs in other plant species. This strategy has been successfully used to produce syn-tasiRNAs through *Agrobacterium*-mediated expression of the

AtTAS1c gene in non-Arabidopsis species such as *N. benthamiana* and *Solanum lycopersicum* (Carbonell, 2019; Cisneros et al., 2021, 2022; Lunardon et al., 2021). However, these constructs exceed 1.5 kb in length, limiting the use of alternative expression systems such as viral vectors. Swapping the original AtmiR173a TS for an endogenous 22-nt miRNA TS to trigger syn-tasiRNA formation from *AtTAS1c* not only simplifies the generation of constructs but makes them more compact and could also reduce the risk of potential off-target effects caused by the ectopic expression of a foreign miRNA. A similar strategy has been followed to successfully silence several genes in soybean by the identification of five different 22-nt endogenous miRNAs capable of triggering the formation of secondary siRNA from MIGS constructs introduced into transgenic plants (Jacobs et al., 2016).

Seven *N. benthamiana* miRNA families include 22-nt miRNA members. Among them, miR482a and miR6019a/b stand out for their ability to trigger phased siRNA formation (Baksa et al., 2015). These two miRNA species are present in members of the *Solanaceae* family and play roles in the immune response to pathogen infections (Deng et al., 2018; Li, Pignatta, et al., 2012; Shivaprasad et al., 2012). In particular, miR482 is highly expressed in *N. benthamiana* seedlings, leaves and stems (Baksa et al., 2015) and its ability to trigger tasiRNA formation has been reported in tomato (Li, Orban, et al., 2012). On the other hand, despite the more moderate accumulation of miR6019a/b in *N. benthamiana* (Baksa et al., 2015), it can still efficiently trigger secondary siRNA formation from MIGS constructs transformed into *N. benthamiana* (Li, Pignatta, et al., 2012). We chose to test NbmiR482a and NbmiR6019a/b as endogenous *N. benthamiana* trigger miRNAs for the formation of syn-tasiRNAs by substituting the original AtmiR173a TS on the *AtTAS1c* sequence for NbmiR482a or NbmiR6019a/b TS in both full-length and minimal precursors. We then analyzed the level of expression of both miRNAs in *N. benthamiana* leaves expressing *AtTAS1c* full-length or minimal precursors. As reported for these miRNA families (Baksa et al., 2015), NbmiR482a is highly expressed in this tissue, whilst NbmiR6019a/b expression is more modest (Figure S4). Interestingly, syn-tasiRNA accumulation from *AtTAS1c* full-length precursors and target gene silencing efficiency are similar in plants overexpressing AtmiR173a and in plants having NbmiR482a as the endogenous trigger (Figure 3), indicating that NbmiR482a levels are not limiting.

It is worth mentioning that miRNA expression profiles are dynamic and vary between tissues, developmental stages and during infectious processes (D'Ario et al., 2017; Ma et al., 2022; Y. Yu et al., 2019). Therefore, selecting the appropriate miRNA to use as endogenous trigger may require a previous study of its expression pattern in different tissues or conditions. On the other hand, the particular expression profiles of certain miRNAs may allow us to make

syn-tasiRNA biogenesis tissue- or condition-specific, which could be an attractive strategy under certain circumstances.

Inducing widespread syn-tasiRNA-mediated gene silencing in plants using an RNA-based viral vector in a transgene-free and scalable manner

One of the major disadvantages of classic VIGS is its lack of high specificity. As an alternative, amiRNA expression from viral vectors (amiR-VIGS) is an example of efficient and highly specific method for target gene silencing. PVX is one of the preferred vectors for gene expression and VIGS (Lacomme & Chapman, 2008); however, insert sizes above 800 nt are not well tolerated (Avesani et al., 2007). Here, we have developed a minimal precursor of only 54-nt long and aimed to express syn-tasiRNAs using PVX through syn-tasiR-VIGS. Indeed, we report for the first time the production of authentic and highly active syn-tasiRNAs using VIGS technology.

PVX is a plus (+) single-stranded RNA virus that can infect 62 different species from 27 families, including several economically relevant crops from the *Solanaceae* family such as tomato or potato (Adams et al., 2004; Edwardson & Christie, 1997). Syn-tasiRNAs targeting *NbSu* were accurately generated and accumulated to high levels, as shown by high-throughput sRNA sequencing and northern blot, respectively, when expressed from a minimal precursor inserted in a PVX-derived vector. Since PVX replication and secondary siRNA generation take place in the cytoplasm, it is expected that the minimal precursors were processed by a cytoplasmic DCL. Among the different plant DCLs, DLC4 is known to generate tasiRNAs duplexes from *TAS* precursors in the cytoplasm (Gasciolli et al., 2005; Xie et al., 2005). Moreover, it is considered to be the primary antiviral DCL (Bouché et al., 2006; Deleris et al., 2006), particularly during PVX infections in *N. benthamiana* (Andika et al., 2015). For these reasons, DCL4 appears to be the main DCL responsible for the processing of syn-tasiRNA minimal precursors from PVX-based viral vectors.

sRNA sequencing data confirm the *in vivo* production of high levels of authentic 21-nt syn-tasiRNAs in phase with the NbmiR482a cleavage site. These data also reflect a relatively low proportion of sRNAs produced from the rest of the precursor, supporting the accuracy and specificity of the silencing machinery. Results in Figure S2 discard that syn-tasiRNAs are being generated from the RNA-dependent RNA polymerase-derived dsRNA viral intermediate. It is also unlikely that syn-tasiRNAs are generated from the (+) RNA viral genome, since it could negatively affect its replication and infectivity. In contrast, minimal syn-tasiRNA precursors may be processed from the PVX subgenomic RNA (sg-RNA) since the NbmiR482a TS is likely to be more accessible for miRNA recognition when located at the 5’ terminus of the sg-RNA rather than in an internal region of the viral genome.

Biotechnological tools like VIGS typically rely on *Agrobacterium*-mediated expression of the viral genome (Rössner et al., 2022). Despite being an efficient method to trigger viral infection, transgenic tissues are generated which may limit its applications due to commercial and/or legislative restrictions. We previously showed that amiR-VIGS can be triggered in a transgene-free manner by spraying plant leaves with an infectious crude extract obtained from plants expressing a modified viral vector containing an amiRNA minimal precursor (Cisneros et al., 2023). Here, we tested this approach for applying syn-tasiR-VIGS to plants. To do so, apical leaves of plants agroinoculated with PVX-based constructs containing the minimal syn-tasiRNA precursor were collected to prepare crude extracts. This approach avoids the limitations associated with transgenic tissue generation. Moreover, spraying crude extracts could potentially be scaled up to simultaneously infect a large number of plants, as previously proposed (Cisneros et al., 2023).

Since PVX-based vectors commonly introduce mutations or revert to their wild-type configuration through *in planta* recombination (Lacomme & Chapman, 2008), we used a PVX cDNA sequence incorporating a deletion of the amino-terminal end of the CP and a heterologous promoter derived from another potexvirus (Bamboo mosaic virus, BaMV) (Dickmeis et al., 2014) which should increase insert stability in PVX-based constructs. Noteworthy, the insert recombination rate and instability are often directly related to insert size (Avesani et al., 2007). In this work, we have reduced *AtTAS1c* precursor size by 96%, resulting in a clear impact on insert stability. The full-length precursor was eliminated from PVX genomic RNA only 7 days post-agroinoculation, whereas the minimal precursor remained stable and did not accumulate mutations even after one passage. In summary, the PVX-based syn-tasiR-VIGS strategy emerges as a powerful alternative to classic dsRNA-based VIGS to specifically silence endogenous genes at the whole plant level and in a non-transgenic manner.

Minimal syn-tasiRNA precursors as a biotechnological tool for gene silencing in plants

AtTAS1c has been extensively used in functional genomics as well as for crop improvement (Carbonell, 2019; Cisneros et al., 2021; Cisneros & Carbonell, 2020). In all those cases, either *AtMIR173a* was co-expressed with the modified *AtTAS1c* precursor, or the analyses were performed in Arabidopsis, where AtmiR173a is constitutively expressed. Thus, there was a need to expand the range of syn-tasiRNA applications, which was previously limited by size-related and species-specific restrictions. In this work, we developed a minimal syn-tasiRNA precursor that is only 54-nt long, which, to our knowledge, is the shortest syn-tasiRNA precursor tested in plants so far. The minimal syn-tasiRNA precursor has some advantages over the full-

length version. First, the cost of producing the precursor RNAs *in vitro* and *in bacteria* for possible exogenous applications should be reduced, as both systems are more efficient when producing shorter RNAs (A.-M. Yu et al., 2020). Second, the reduction in precursor size should also help lower construct-generation costs since. For instance, generating full-length *NbmiR482aTS*-based constructs involves PCR amplification from *pENTR:AtTAS1c-GUS*$_{Nb}$ (Cisneros et al., 2022) followed by LR recombination into *pMDC32* (Curtis & Grossniklaus, 2003), while minimal *NbmiR482aTS*-based precursors are produced by annealing two 54-nt oligos and directly inserting them into the *pMDC32B-B/c* vector through an efficient, zero-background Golden Gate cloning method (Carbonell et al., 2014). Importantly, 54-nt oligos are at the lowest production scale offered by the major oligo-manufacturing companies, making the cloning process more cost-effective. And third, as previously discussed, minimal syn-tasiRNA precursors are more stable than full-length when expressed from an RNA-based viral vector like PVX. In conclusion, the use of syn-tasiR-VIGS in a GMO-free and scalable manner for silencing plant genes across a wide range of species should facilitate functional genomics studies and the generation of crops with improved agronomic traits.

METHODS

Plant species and growth conditions

N. benthamiana plants were grown in a growth chamber at 25ºC with a 12 h-light/12 h-dark photoperiod. Arabidopsis Col-0 plants were grown in a growth chamber at 22ºC with a 16 h-light/8 h-dark photoperiod. Genetic transformation of Arabidopsis was done following the floral dip method (Clough & Bent, 1998) using the *Agrobacterium tumefaciens* GV3101 strain. T1 transgenic Arabidopsis were obtained as described (López-Dolz et al., 2020). A Nikon D3000 digital camera with AF-S DX NIKKOR 18-55 mm f/3.5–5.6G VR lens was used for photographing plants.

Arabidopsis phenotyping

Phenotyping analyses in Arabidopsis were performed in a blinded manner. Flowering time for each independent line was determined by counting the number of days from seed plating to first bud opening (or ‘days to flowering’). The ‘Ft’ phenotype was defined as a higher ‘days to flowering’ value when compared to the average ‘days to flowering’ value of the *35S:AtTAS1c-GUS*$_{At}$ control set. The ‘CH42’ phenotype was scored in 10-day-old seedlings and was considered ‘weak’, ‘intermediate’ or ‘severe’ if seedlings had more than two leaves, exactly two leaves or no leaves at all (only two cotyledons), respectively. A line was considered to have a

'Trich' phenotype when presenting a visually obvious increase in trichome number in rosette leaves of 14-day-old seedlings compared to transformants of the *35S:AtTAS1c-GUS$_{At}$* control set.

Artificial small RNA design

The guide sequences for syn-tasiR-GUS$_{At}$, syn-tasiR-AtFT, syn-tasiR-AtCH42, syn-tasiR-AtTRY, syn-tasiR-GUS$_{Nb}$ and syn-tasiR-NbSu were described previously (Carbonell & Daròs, 2017; Cisneros et al., 2022; López-Dolz et al., 2020; Schwab et al., 2006).

DNA constructs

Oligonucleotides AC-674 and AC-675 were annealed and ligated into *pENTR-D-TOPO* (Invitrogen) following manufacturer's instructions to generate *pENTR-BB* including two inverted *Bsa*I restriction sites. The *B/c* cassette was excised from *Bsa*I-digested *pENTR-AtMIR390a-B/c* (Addgene plasmid #51778) (Carbonell et al., 2014) and ligated into *Bsa*I-digested *pENTR-BB* to generate *pENTR-B/c*. The *BB* cassette from *pENTR-BB* was transferred by LR recombination into *pMDC32B* (Carbonell et al., 2014) to generate *pMDC32B-BB*. Finally, the *B/c* cassette was excised from *Bsa*I-digested *pENTR-B/c* and ligated into *Bsa*I-digested *pMDC32B-BB* to generate *pMDC32B-B/c*. Oligonucleotides AC-1093/AC-1094 and AC-900/AC-901 including minimal *AtmiR173aTS*, *NbmiR482aTS*- based precursors respectively, were annealed and ligated into *Bsa*I-digested *pENTR-B/c* and *pMDC32B-B/c* to generate *pENTR-AtmiR173aTS-BB*, *pENTR-NbmiR482aTS-BB*, *pMDC32B-AtmiR173aTS-BB* and *pMDC32B-NbmiR482aTS-BB* respectively. The *B/c* cassette was excised from *Bsa*I-digested *pENTR-AtTAS1c-D2-B/c* (Addgene plasmid #137883) (López-Dolz et al., 2020) and ligated into *Bsa*I-digested *pENTR-AtmiR173aTS-BB, pENTR-NbmiR482aTS-BB*, *pMDC32B-AtmiR173aTS-BB, pMDC32B-NbmiR482aTS-BB* to generate *pENTR-AtmiR173aTS-B/c pENTR-NbmiR482aTS-B/c*, *pMDC32B-AtmiR173aTS-B/c* and *pMDC32B-NbmiR482aTS-B/c* (Figure S3).

The following oligonucleotide pairs were annealed and ligated into *pENTR-D-TOPO* (Invitrogen) following manufacturer's instructions to generate the following constructs: AC-676/AC-677 for *pENTR-AtmiR173aTS-GUS$_{At}$,* AC-678/AC-679 for *pENTR-AtmiR173aTS-AtCH42,* AC-680/AC-681 for *pENTR-AtmiR173aTS-AtFT,* AC-682/AC-683 for *pENTR-AtmiR173aTS-AtFT-AtTrich*, AC-684/AC-685 for *pENTR-AtmiR173aTS-AtTrich-AtFT*, AC-639/AC-640 for *pENTR-NbmiR482aTS-GUS$_{Nb}$.* AC-643/AC-644 for *pENTR-NbmiR6019a/bTS-GUS$_{Nb}$*, AC-641/AC-642 for *pENTR-NbmiR482aTS-NbSu* and AC-645/AC-646 for *pENTR-NbmiR6019a/bTS-NbSu.*

Minimal precursor cassettes were transferred by LR recombination into *pMDC32* (Curtis & Grossniklaus, 2003) to generate *35S:AtmiR173aTS-GUS$_{At}$*, *35S:AtmiR173aTS-AtCH42*, *35S:AtmiR173aTS-AtFT*, *35S:AtmiR173aTS-AtFT-AtTrich*, *35S:AtmiR173aTS-AtTrich-AtFT*, *35S:NbmiR482aTS-GUS$_{Nb}$*, *35S:NbmiR6019a/bTS-GUS$_{Nb}$*, *35S:NbmiR482aTS-NbSu* and *35S:NbmiR6019a/bTS-NbSu*. Target site swaps were performed by mutagenic PCR using *pENTR:AtTAS1c-GUS$_{Nb}$* (Cisneros et al., 2022) as template and oligo pairs AC-631/AC-505 and AC-632/AC-507 to generate *pENTR-AtTAS1c(NbmiR482aTS)-NbSu* and *pENTR-AtTAS1c(NbmiR6019a/bTS)-NbSu*. *AtTAS1c*-based cassettes were transferred by LR recombination into *pMDC32* to generate *35S:AtTAS1c(NbmiR482aTS)-NbSu* and *35S:AtTAS1c(NbmiR6019a/bTS)-NbSu*. Constructs *35S:AtmiR482aTS-NbSu*, *35S:AtmiR156aTS-NbSu*, *35S:AtmiR173aTS-NbSu* were obtained by ligating annealed oligonucleotide pairs AC-716/AC-717, AC-719/AC-720, AC-721/AC-722, respectively, into *pMDC32B-B/c* as described (Carbonell et al., 2014).

For PVX-based syn-tasiRNA constructs, syn-tasiRNA cassette *AtTAS1c(NbmiR482aTS)-NbSu* was amplified from *35S:AtTAS1c(NbmiR482aTS)-NbSu* with oligo pair AC-712/AC-713 and gel purified. Syn-tasiRNA cassette *NbmiR482aTS-NbSu* was ordered as dsDNA oligonucleotide AC-666. The syn-tasiRNA cassette was assembled into *Mlu*I-digested and gel-purified previously described *pLB-PVX-MluI* (Cisneros et al., 2023) (Figure S3) in the presence of GeneArt Gibson Assembly HiFi Master Mix (Invitrogen) to generate *35S:PVX-NbmiR482aTS-NbSu*.

Syn-tasiRNA constructs *35S:AtTAS1c-GUS$_{At}$*, 35S*:AtTAS1c-AtFT, 35S:AtTAS1c-AtCH42, 35S:AtTAS1c-AtFT-AtTrich, 35S:AtTAS1c-AtTrich-AtFT, 35S:AtTAS1c-GUS$_{Nb}$/AtMIR173*, *35S:AtTAS1c-NbSu/AtMIR173* and *35S:PVX* constructs were described before (Carbonell et al., 2014; Cisneros et al., 2023; López-Dolz et al., 2020). All DNA oligonucleotides used in this study are listed in Table S4. The sequences of all syn-tasiRNA precursors are listed in Text S1. The sequences of newly developed 'B/c' vectors are listed in Text S2.

Transient expression of constructs and spray-based inoculation of viruses

Agrobacterium-mediated infiltration of DNA constructs in *N. benthamiana* leaves was performed as previously described (Cuperus et al., 2010; Llave et al., 2002). Preparation and spraying of crude extracts obtained from virus-infected *N. benthamiana* plants were performed as previously (Cisneros et al., 2023), including 5% silicon carbide (carborundum) in the inoculation buffer.

Chlorophyll extraction and analysis

Chlorophyll and other pigments from *N. bentamiana* leaves were extracted and analyzed as described (Carbonell et al., 2015; López-Dolz et al., 2020).

RNA preparation

Total RNA form *N. benthamiana* leaves or from Arabidopsis seedlings or inflorescences was isolated as described before (Cisneros et al., 2023). Triplicate samples from pools of two *N. benthamiana* leaves or 9-12 Arabidopsis seedlings or inflorescences were analyzed.

Real-time RT-qPCR

cDNA was obtained from 500 ng of DNAseI-treated total RNA from 10-day-old Arabidopsis seedlings, 60-day-old Arabidopsis plants, *N. benthamiana* leaves at 2 or 7 dpa, using the PrimeScript RT Reagent Kit (Perfect Real Time, Takara) according to manufacturer's instructions. Real time RT-qPCR was done using the same RNA samples that were used for sRNA-blot analysis. RT-qPCR was done on optical 96-well plates in a QuantStudio 3 Real-Time PCR system (Thermo Fisher Scientific, Waltham, MA, USA) using the following program: 20 s at 95ºC, followed by 40 cycles of 95ºC for 3 s and 60ºC for 30 s, with an additional melt curve stage consisting of 15 s at 95ºC, 1 min at 60ºC and 15 s at 95ºC. The 20-ml reaction mixture contained 10 ml of 2× TB Green Premix Ex Taq (Takara), 2 ml of diluted complementary DNA (1:5), 0.4 ml of ROX II Reference Dye (50X) and 300 nM of each gene-specific primer. Oligonucleotides used for RT-qPCR are listed in Table S4. Target mRNA expression levels were calculated relative to reference genes *AtACT2* and *NbPP2A* in Arabidopsis and *N. benthamiana*, respectively, using the delta delta cycle threshold comparative method of QuantStudio Design and Analysis software, version 1.5.1 (Thermo Fisher Scientific). Three independent biological replicates and two technical replicates for each biological replicate were analyzed.

Stability and sequence analyses of syn-tasiRNA precursors during viral infections

Total RNA from apical leaves of each of the three biological replicates was pooled before cDNA synthesis. PCR to detect syn-tasiRNA precursors, PVX and *NPP2A* was performed using oligonucleotide pairs AC-654/AC-655, AC-657/AC-658 and AC365/AC-366 (Table S4), respectively, and Phusion DNA polymerase (ThermoFisher Scientific). PCR products were

analyzed by agarose gel electrophoresis, and products of the expected sizes were excised from the gel and sequenced.

Small RNA blot assays

Small RNA blot assays and band quantification from radioactive membranes were done as described (Cisneros et al., 2022). Oligonucleotides used as probes for sRNA blots are listed in Table S4.

Small RNA sequencing and data analysis

The quantity, purity and integrity of total RNA was analyzed with a 2100 Bioanalyzer (RNA 6000 Nano kit, Agilent) and submitted to BGI (Hong Kong, China) for sRNA library construction and SE50 high-throughput sequencing in a DNBSEQ-G-400 sequencer. Quality-trimmed, adaptor-removed clean reads received from BGI were used with the fastx_collapser toolkit (http://hannonlab.cshl.edu/fastx toolkit) (Hannon, 2010) to collapse identical reads into a single sequence, while maintaining read counts. Clean, unique reads were mapped against the forward strand of the syn-tasiRNA precursor expressed in each sample using a custom Python script not allowing mismatches or gaps, and also to calculate the counts and RPMs (reads per million mapped reads) for each mapping position. Processing accuracy of syn-tasiRNA precursors was assessed by quantifying the proportion of 19–24 nt sRNA (+) reads that mapped within ± 4 nt of the 5′ end of the syn-tasiRNA guide as previously reported (Carbonell et al., 2015; Cuperus et al., 2010). Phasing register tables were built by calculating the proportion of 21-nt sRNA (+) reads in each register relative to the corresponding amiRNA cleavage site for all 21-nt positions downstream of the cleavage site, as described previously (Carbonell et al., 2014).

Statistical analysis

Statistical tests are described in the figure legends. Significant differences were determined with two-tailed Student's t-test.

Gene and virus identifiers

Arabidopsis and *N. benthamiana* gene identifiers are *AtACT2* (AT3G18780), *AtCH42* (AT4G18480), *AtFT* (AT1G65480), *AtTRY* (AT5G53200), *NbSu* (Nbv5.1tr6204879) and *NbPP2A* (Nbv5.1tr6224808). PVX-based constructs include PVX sequence variant

MT799816.1. *Escherichia coli* b-glucuronidase *uidA* gene sequence corresponds to GenBank accession number S69414.1.

Acknowledgements

We thank Javier Forment (IBMCP) for assistance with the sRNA sequencing data analysis and the greenhouse staff at IBMCP for plant maintenance.

Funding

This work was supported by grants or fellowships from Ministerio de Ciencia y Universidades (MCU, Spain), Agencia Estatal de Investigación (AEI, Spain) and Fondo Europeo de Desarrollo Regional (FEDER, European Union) [PID2021-122186OB-100 and RYC-2017-21648 to A.C., and PRE2019-088439 and PRE2022-102565 to A.E.C. and J.L.-G., respectively], NextGenerationEU/PRTR (European Union) [CNS2022-135107 to A.C.], from Consejo Superior de Investigaciones Científicas (CSIC, Spain) [JAEINT_21_00860 to A.P.-E.] and from European Commission [Erasmus+ Grant Agreement 2020-1-DE01-KA103-005653 to A.P.].

Author contributions

A.E.C., J.L.-G., and A.P. did most of the experimental work with the help of A.A. and A.P. A.E.C. and A.C. analyzed the data. A.C. conceived the research and supervised the project. A.E.C. and A.C. wrote the manuscript with input from the rest of the authors.

Supplemental information

Supplemental figures and tables can be found at the end of this chapter. Supplementary table 4 and data texts are accessible through Mendeley Data Resource.

REFERENCES

Adams, M. J., Antoniw, J. F., Bar-Joseph, M., Brunt, A. A., Candresse, T., Foster, G. D., Martelli, G. P., Milne, R. G., Zavriev, S. K., & Fauquet, C. M. (2004). The new plant virus family *Flexiviridae* and assessment of molecular criteria for species demarcation. *Arch Virol*, **149**(5), 1045–1060.

Allen, E., Xie, Z., Gustafson, A. M., & Carrington, J. C. (2005). microRNA-Directed Phasing during Trans-Acting siRNA Biogenesis in Plants. *Cell*, **121**(2), 207–221.

Andika, I. B., Maruyama, K., Sun, L., Kondo, H., Tamada, T., & Suzuki, N. (2015). Differential contributions of plant Dicer-like proteins to antiviral defences against potato virus X in leaves and roots. *Plant Journal*, **81**(5), 781–793.

Arribas-Hernández, L., Marchais, A., Poulsen, C., Haase, B., Hauptmann, J., Benes, V., Meister, G., & Brodersen, P. (2016). The slicer activity of ARGONAUTE1 is required specifically for the phasing, not production, of trans-acting short interfering RNAs in Arabidopsis. *Plant Cell*, **28**(7), 1563–1580.

Avesani, L., Marconi, G., Morandini, F., Albertini, E., Bruschetta, M., Bortesi, L., Pezzotti, M., & Porceddu, A. (2007). Stability of Potato virus X expression vectors is related to insert size: Implications for replication models and risk assessment. *Transgenic Res*, **16**(5), 587–597.

Baksa, I., Nagy, T., Barta, E., Havelda, Z., Várallyay, É., Silhavy, D., Burgyán, J., & Szittya, G. (2015). Identification of *Nicotiana benthamiana* microRNAs and their targets using high throughput sequencing and degradome analysis. *BMC Genomics*, **16**(1).

Baykal, U., Liu, H., Chen, X., Nguyen, H. T., & Zhang, Z. J. (2016). Novel constructs for efficient cloning of sRNA-encoding DNA and uniform silencing of plant genes employing artificial trans-acting small interfering RNA. *Plant Cell Rep*, **35**(10), 2137–2150.

Bazin, J., Baerenfaller, K., Gosai, S. J., Gregory, B. D., Crespi, M., & Bailey-Serres, J. (2017). Global analysis of ribosome-associated noncoding RNAs unveils new modes of translational regulation. *Proc Natl Acad Sci U S A*, **114**(46), E10018–E10027.

Bernstein, E., Caudy, A. A., Hammond, S. M., & Hannon, G. J. (2001). Role for a bidentate ribonuclease in the initiation step of RNA interference. *Nature*, **409**(6818), 363–366.

Bouché, N., Lauressergues, D., Gasciolli, V., & Vaucheret, H. (2006). An antagonistic function for Arabidopsis DCL2 in development and a new function for DCL4 in generating viral siRNAs. *EMBO Journal*, **25**(14), 3347–3356.

Carbonell, A. (2017). Artificial small RNA-based strategies for effective and specific gene silencing in plants. In D. Tamas (Ed.), *Plant Gene Silencing: Mechanisms and Applications* (pp. 110–127). CABI Biotechnology Series, CABI Publishing.

Carbonell, A. (2019). Secondary small interfering RNA-based silencing tools in plants: An update. *Front Plant Sci*, **10**, 1–5.

Carbonell, A., & Daròs, J.-A. A. (2017). Artificial microRNAs and synthetic trans-acting small interfering RNAs interfere with viroid infection. *Mol Plant Pathol*, **18**(5), 746–753.

Carbonell, A., Fahlgren, N., Mitchell, S., Cox, K. L., Reilly, K. C., Mockler, T. C., & Carrington, J. C. (2015). Highly specific gene silencing in a monocot species by artificial microRNAs derived from chimeric miRNA precursors. *Plant Journal*, **82**(6), 1061–1075.

Carbonell, A., Takeda, A., Fahlgren, N., Johnson, S. C., Cuperus, J. T., & Carrington, J. C. (2014). New generation of artificial MicroRNA and synthetic trans-acting small interfering RNA vectors for efficient gene silencing in Arabidopsis. *Plant Physiol*, **165**(1), 15–29.

Chen, H. M., Chen, L. T., Patel, K., Li, Y. H., Baulcombe, D. C., & Wu, S. H. (2010). 22-Nucleotide RNAs trigger secondary siRNA biogenesis in plants. *Proc Natl Acad Sci U S A*, **107**(34), 15269–15274.

Cisneros, A. E., & Carbonell, A. (2020). Artificial small RNA-based silencing tools for antiviral resistance in plants. *Plants*, **9**(6).

Cisneros, A. E., de la Torre-Montaña, A., & Carbonell, A. (2022). Systemic silencing of an endogenous plant gene by two classes of mobile 21-nucleotide artificial small RNAs. *Plant Journal*, **110**(4), 1166–1181.

Cisneros, A. E., de la Torre-Montaña, A., Martín-García, T., & Carbonell, A. (2021). Artificial Small RNAs for Functional Genomics in Plants. In G. Tang, S. Teotia, X. Tang, & D. Singh (Eds.), *RNA-based Technologies For Functional Genomics in Plants* (pp. 1–29). Springer International Publishing.

Cisneros, A. E., Martín-García, T., Primc, A., Kuziuta, W., Sánchez-Vicente, J., Aragonés, V., Daròs, J. A., & Carbonell, A. (2023). Transgene-free, virus-based gene silencing in plants by artificial microRNAs derived from minimal precursors. *Nucleic Acids Res*, **51**(19), 10719–10736.

Clough, S. J., & Bent, A. F. (1998). Floral dip: a simplified method for *Agrobacterium* - mediated transformation of *Arabidopsis thaliana*. *The Plant Journal*, **16**(6), 735–743.

Cuperus, J. T., Carbonell, A., Fahlgren, N., Garcia-Ruiz, H., Burke, R. T., Takeda, A., Sullivan, C. M., Gilbert, S. D., Montgomery, T. A., & Carrington, J. C. (2010). Unique functionality of 22-nt miRNAs in triggering RDR6-dependent siRNA biogenesis from target transcripts in Arabidopsis. *Nat Struct Mol Biol*, **17**(8), 997–1003.

Curtis, M. D., & Grossniklaus, U. (2003). A Gateway Cloning Vector Set for High-Throughput Functional Analysis of Genes in Planta. *Plant Physiol*, **133**(2), 462–469.

D'Ario, M., Griffiths-Jones, S., & Kim, M. (2017). Small RNAs: Big Impact on Plant Development. *Trends Plant Sci*, **22**(12), 1056–1068.

de Felippes, F. F. (2019). Gene Regulation Mediated by microRNA-Triggered Secondary Small RNAs in Plants. *Plants*, **8**(112).

de Felippes, F. F., Wang, J. W., & Weigel, D. (2012). MIGS: MiRNA-induced gene silencing. *Plant Journal*, **70**(3), 541–547.

de Felippes, F. F., & Weigel, D. (2009). Triggering the formation of tasiRNAs in *Arabidopsis thaliana*: The role of microRNA miR173. *EMBO Rep*, **10**(3), 264–270.

Deleris, A., Javier Gallego-Bartolome, Jinsong Bao, Kristin D. Kasschau, James C. Carrington, & Olivier Voinnet. (2006). Hierarchical Action and Inhibition of Plant Dicer-Like Proteins in Antiviral Defense. *Science (1979)*, **313**(5783), 68–71.

Deng, P., Muhammad, S., Cao, M., & Wu, L. (2018). Biogenesis and regulatory hierarchy of phased small interfering RNAs in plants. *Plant Biotechnol J*, **16**(5), 965–975.

Dickmeis, C., Fischer, R., & Commandeur, U. (2014). Potato virus X-based expression vectors are stabilized for long-term production of proteins and larger inserts. *Biotechnol J*, **9**(11), 1369–1379.

Edwardson, J. R., & Christie, R. G. (1997). *Viruses infecting peppers and other solanaceous crops.: Vol. Volume 1*.

Fahlgren, N., Hill, S. T., Carrington, J. C., & Carbonell, A. (2016). P-SAMS: a web site for plant artificial microRNA and synthetic *trans*-acting small interfering RNA design. *Bioinformatics*, **32**(1), 157–158.

Gasciolli, V., Mallory, A. C., Bartel, D. P., & Vaucheret, H. (2005). Partially redundant functions of arabidopsis DICER-like enzymes and a role for DCL4 in producing trans-acting siRNAs. *Current Biology*, **15**(16), 1494–1500.

Hammond, S. M., Bernstein, E., Beach, D., & Hannon, G. J. (2000). An RNA-directed nuclease mediates post-transcriptional gene silencing in Drosophila cells. *Nature*, **404**(6775), 293–296.

Hammond, S. M., Boettcher, S., Caudy, A. A., Kobayashi, R., & Hannon, G. J. (2001). Argonaute2, a link between genetic and biochemical analyses of RNAi. *Science (1979)*, **293**(5532), 1146–1150.

Hannon, G. J. (2010). *FASTX-Toolkit (RRID:SCR_005534)*.Http://Hannonlab.Cshl.Edu/Fastx_toolkit.

Iwakawa, H. oki, Lam, A. Y. W., Mine, A., Fujita, T., Kiyokawa, K., Yoshikawa, M., Takeda, A., Iwasaki, S., & Tomari, Y. (2021). Ribosome stalling caused by the Argonaute-microRNA-SGS3 complex regulates the production of secondary siRNAs in plants. *Cell Rep*, **35**(13).

Jacobs, T. B., Lawler, N. J., Lafayette, P. R., Vodkin, L. O., & Parrott, W. A. (2016). Simple gene silencing using the trans-acting siRNA pathway. *Plant Biotechnol J*, **14**(1), 117–127.

Lacomme, C., & Chapman, S. (2008). Use of potato virus X (PVX)-based vectors for gene expression and virus-induced gene silencing (VIGS). In *Current Protocols in Microbiology* (Issue SUPPL. 8). John Wiley and Sons Inc.

Li, F., Orban, R., & Baker, B. (2012). SoMART: A web server for plant miRNA,

tasiRNA and target gene analysis. *Plant Journal*, **70**(5), 891–901.

Li, F., Pignatta, D., Bendix, C., Brunkard, J. O., Cohn, M. M., Tung, J., Sun, H., Kumar, P., & Baker, B. (2012). MicroRNA regulation of plant innate immune receptors. *Proc Natl Acad Sci U S A*, **109**(5), 1790–1795.

Llave, C., Xie, Z., Kasschau, K. D., & Carrington, J. C. (2002). Cleavage of *Scarecrow-like* mRNA Targets Directed by a Class of *Arabidopsis* miRNA. *Science (1979)*, **297**(5589), 2053–2056.

López-Dolz, L., Spada, M., Daròs, J.-A., & Carbonell, A. (2020). Fine-Tune Control of Targeted RNAi Efficacy by Plant Artificial Small. *Nucleic Acids Res*.

Lunardon, A., Kariuki, S. M., & Axtell, M. J. (2021). aExpression and processing of polycistronic artificial microRNAs and trans-acting siRNAs from transiently introduced transgenes in miRNA *Solanum lycopersicum* and *Nicotiana benthamiana*. *Plant Journal*, **106**(4), 1087–1104.

Ma, X., Zhao, F., & Zhou, B. (2022). The Characters of Non-Coding RNAs and Their Biological Roles in Plant Development and Abiotic Stress Response. In *International Journal of Molecular Sciences* (Vol. 23, Issue 8). MDPI.

Mahmood, M. A., Naqvi, R. Z., Rahman, S. U., Amin, I., & Mansoor, S. (2023). Plant Virus-Derived Vectors for Plant Genome Engineering. *Viruses*, **15**(2).

Montgomery, T. A., Yoo, J., Fahlgren, N., Gilbert, S. D., Howell, M. D., Sullivan, C. M., Alexander, A., Nguyen, G., Allen, E., Hoon Ahn, J., & Carrington, J. C. (2008). AGO1-miR173 complex initiates phased siRNA formation in plants. *Proceedings of the National Academy of Sciences*, **105**(51). www.pnas.org/cgi/content/full/

Ossowski, S., Schwab, R., & Weigel, D. (2008). Gene silencing in plants using artificial microRNAs and other small RNAs. In *Plant Journal* (Vol. 53, Issue 4, pp. 674–690).

Rössner, C., Lotz, D., & Becker, A. (2022). VIGS Goes Viral: How VIGS Transforms Our Understanding of Plant Science. *Annual Review of Plant Biology* , **73**, 703–728.

Schwab, R., Ossowski, S., Riester, M., Warthmann, N., & Weigel, D. (2006). Highly Specific Gene Silencing by Artificial MicroRNAs in Arabidopsis. *Plant Cell*, **18**(5), 1121–1133.

Senthil-Kumar, M., & Mysore, K. S. (2011). *Caveat of RNAi in Plants: The Off-Target Effect*. 13–25.

Shivaprasad, P. V., Chen, H. M., Patel, K., Bond, D. M., Santos, B. A. C. M., & Baulcombe, D. C. (2012). A microRNA superfamily regulates nucleotide binding site-leucine-rich repeats and other mRNAs. *Plant Cell*, **24**(3), 859–874.

Su, W., Xu, M., Radani, Y., & Yang, L. (2023). Technological Development and Application of Plant Genetic Transformation. In *International Journal of Molecular Sciences* (Vol. 24, Issue 13). Multidisciplinary Digital Publishing Institute (MDPI).

Wu, H. Y. L., Ai, Q., Teixeira, R. T., Nguyen, P. H. T., Song, G., Montes, C., Elmore, J. M., Walley, J. W., & Hsu, P. Y. (2024). Improved super-resolution ribosome profiling reveals prevalent translation of upstream ORFs and small ORFs in Arabidopsis. *Plant Cell*, **36**(3), 510–539.

Xie, Z., Allen, E., Wilken, A., & Carrington, J. C. (2005). DICER-LIKE 4 functions in trans-acting small interfering RNA biogenesis and vegetative phase change in *Arabidopsis thaliana*. *PNAS*, **102**(36), 12984–12989.
www.pnas.orgcgidoi10.1073pnas.0506426102

Yoshikawa, M., Iki, T., Numa, H., Miyashita, K., Meshi, T., & Ishikawa, M. (2016). A short open reading frame encompassing the microRNA173 target site plays a role in trans-acting small interfering RNA biogenesis. *Plant Physiol*, **171**(1), 359–368.

Yoshikawa, M., Peragine, A., Mee, Y. P., & Poethig, R. S. (2005). A pathway for the biogenesis of trans-acting siRNAs in Arabidopsis. *Genes Dev*, **19**(18), 2164–2175.

Yu, A.-M., Batra, N., Tu, M.-J., & Sweeney, C. (2020). Novel approaches for

efficient *in vivo* fermentation production of noncoding RNAs. *Appl Microbiol Biotechnol*, **104**(5), 1927–1937.

Yu, Y., Zhang, Y., Chen, X., & Chen, Y. (2019). Plant noncoding RNAs: Hidden players in development and stress responses. In *Annual Review of Cell and Developmental Biology* (Vol. 35, pp. 407–431). Annual Reviews Inc.

Zhan, J., & Meyers, B. C. (2023). Plant Small RNAs: Their Biogenesis, Regulatory Roles, and Functions. *Annu Rev Plant Biol*, **74**, 21–51.

Zhang, C., Ng, D. W. K., Lu, J., & Chen, Z. J. (2012). Roles of target site location and sequence complementarity in trans-acting siRNA formation in Arabidopsis. *Plant Journal*, **69**(2), 217–226.

Zhang, Z. J. (2014). Artificial trans-acting small interfering RNA: a tool for plant biology study and crop improvements. *Planta*, **239**(6), 1139–1146.

SUPPLEMENTARY INFORMATION

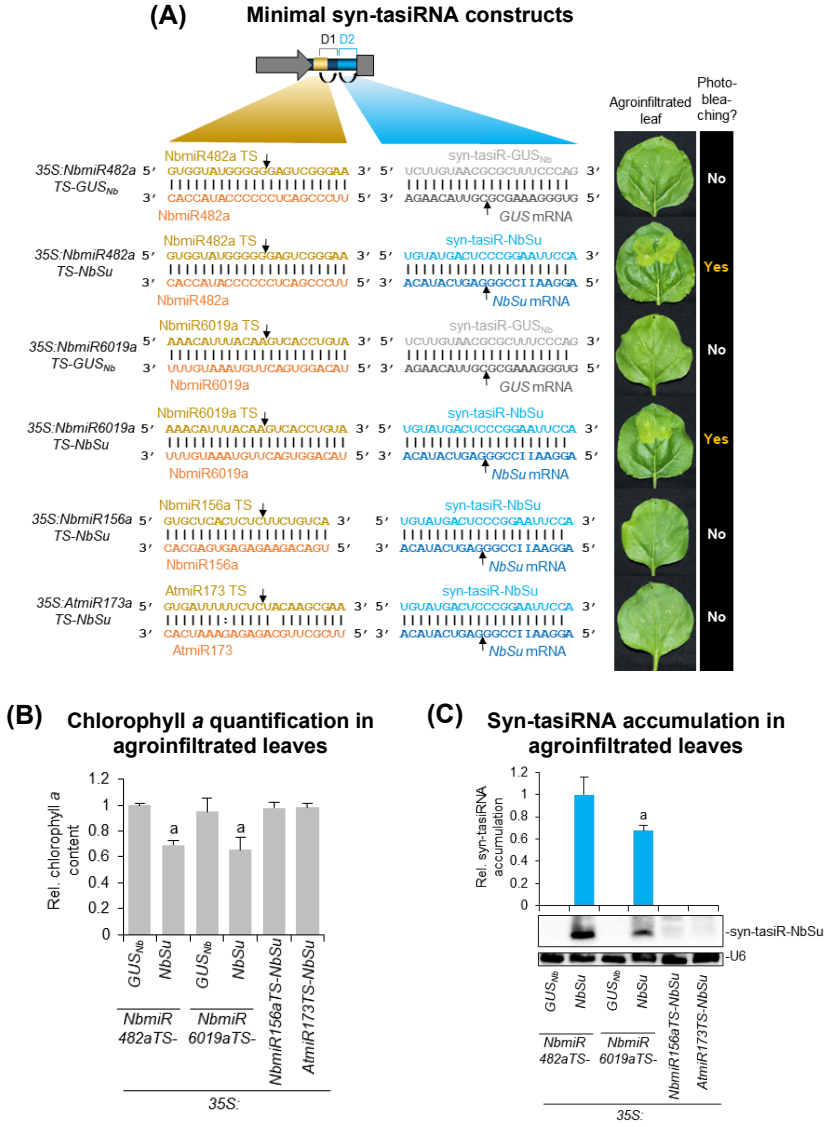

Figure S1. **Functional analysis in *N. benthamiana* leaves of syn-tasiR-NbSu expressed from modified minimal precursors including NbmiR156a or AtmiR173a target site (TS).** (**A**) Diagram of minimal syn-tasiRNA expression constructs. For each construct, nucleotides corresponding to the miRNA and to the TS are represented in orange and yellow, respectively. Other details as in Figure 3A. (**B**) Relative content of chlorophyll *a* in agroinfiltrated patches (control sample *35S:NbmiR482aTS-GUS$_{Nb}$* = 1.0). Other details as in Figure 3B. (**C**) Northern blot detection of syn-tasiR-NbSu (control sample *35S:NbmiR482aTS-NbSu* = 1]. Other details as in Figure 1E.

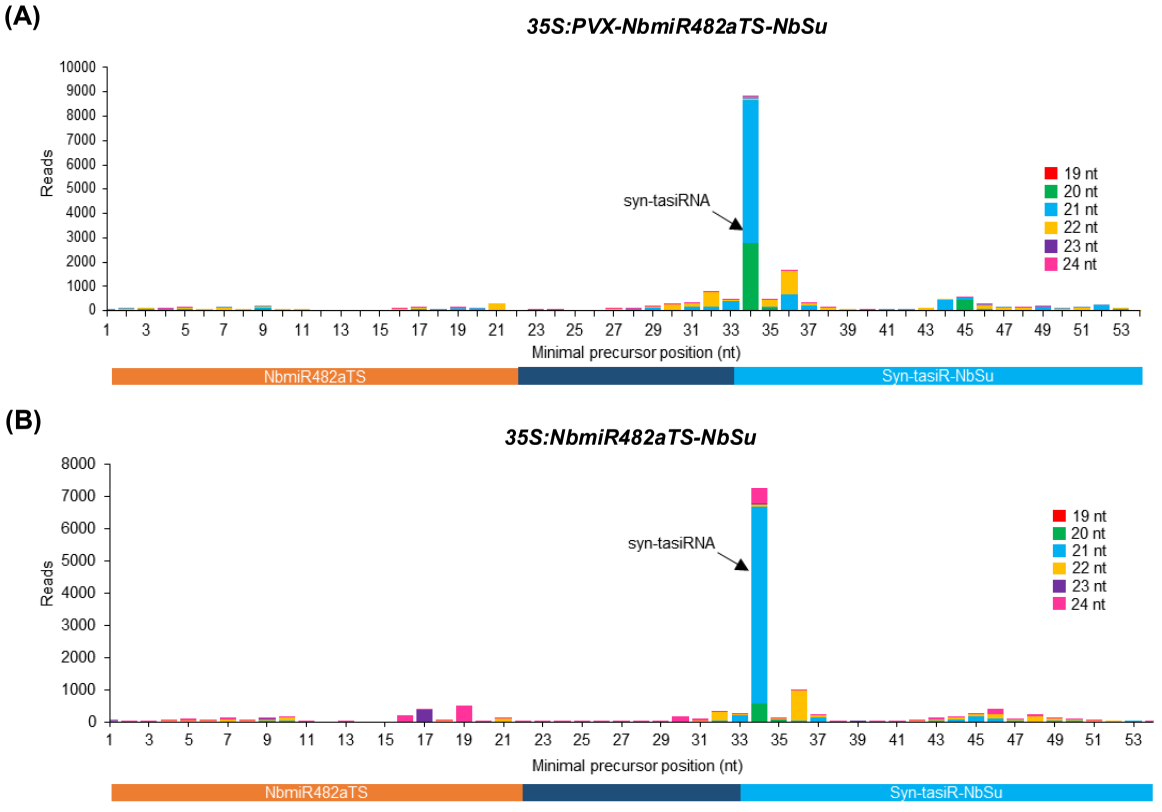

Figure S2. **Syn-tasiRNA processing from *NbmiR482aTS*-based precursors**. sRNA profile of 19-24 nt [+] reads mapping to each of the 54 nucleotidic positions in the *NbmiR482aTS-NbSu* precursor from samples expressing *35S:PVX-NbmiR482aTS-NbSu* (**A**) and *35S:NbmiR482aTS-NbSu* (**B**). Other details as in Figure 5F.

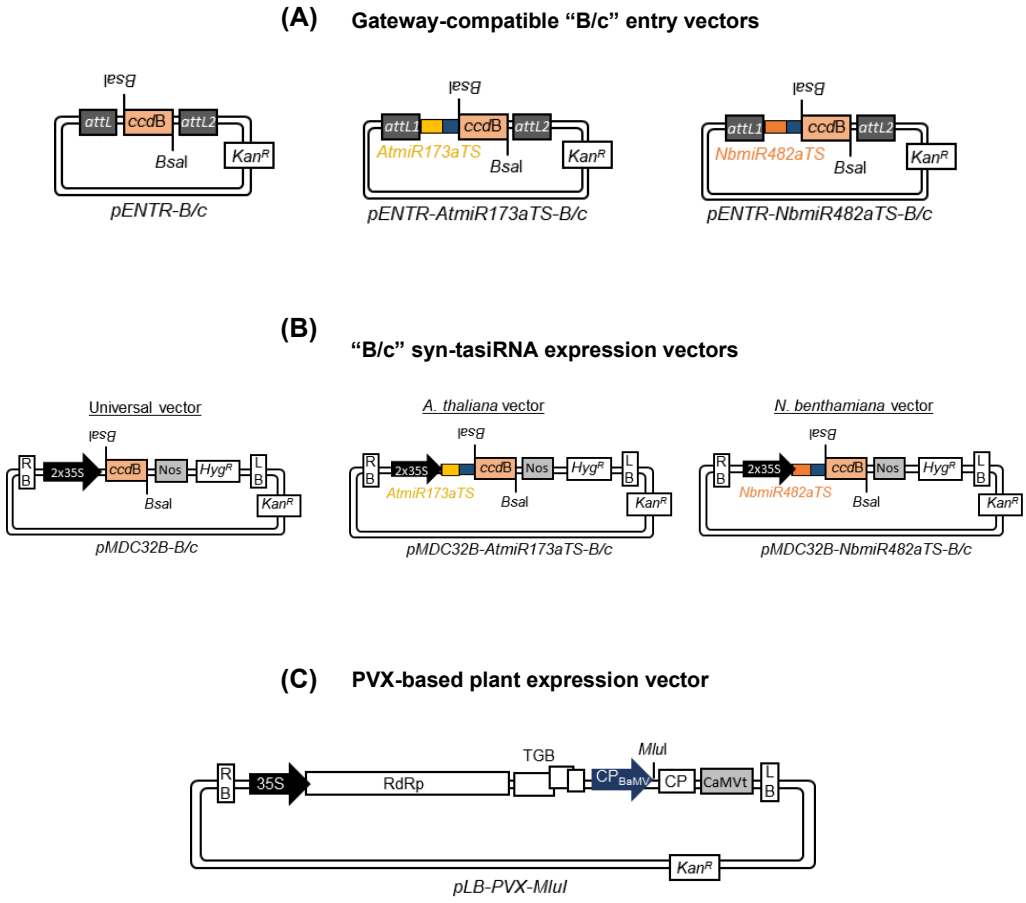

Figure S3. **High-throughput vectors designed for syn-tasiRNA expression from minimal precursors.** (**A**) diagram of the Gateway-compatible entry B/c-based vectors for direct cloning of syn-tasiRNAs. AtmiR173a and NbmiR482a target sites are represented by yellow and orange boxes, respectively. The spacer sequence derived from *AtTAS1c* is in blue. (**B**) Diagram of binary vectors for syn-tasiRNAs expression in plants. Other details as in A. (**C**) Diagram of the PVX-based vector for syn-tasiRNA expression in plants. RB, right border; 35S, Cauliflower mosaic virus promoter; *Bsa*I, *Bsa*I recognition site; *ccd*B, gene encoding the gyrase toxin; LB, left border; attL1 and attL2, GATEWAY recombination sites; KanR, kanamycin resistance gene; HygR, hygromycin resistance gene; Nos, nopaline synthase terminator; CaMVt, cauliflower mosaic virus terminator. Other details as in Figure 5A.

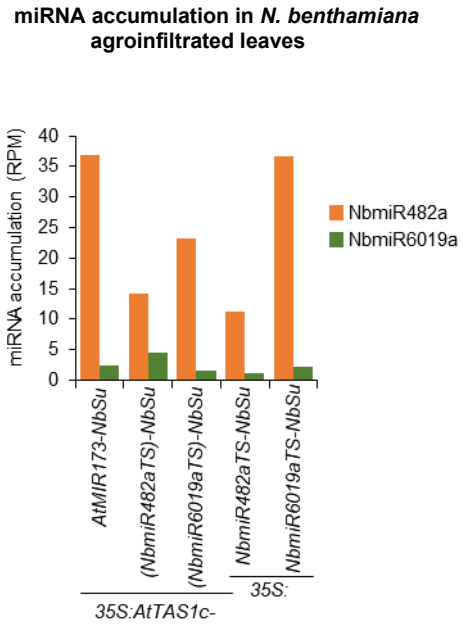

Figure S4. **Accumulation of miR482a and miR6019a/b in *N. benthamiana* agroinfiltrated leaves**. Graph shows the accumulation of NbmiR482a and NbmiR6019a/b in reads per million (RPM) in leaves agroinfiltrated with different constructs containing *AtTAS1c*-based or minimal precursors at 2 dpa.

Table S1. Phenotypic penetrance of syn-tasiRNAs expressed in *A. thaliana* Col-0 T1 transgenic plants for silencing *AtFT*.

Construct	T1 analyzed	Phenotypic penetrance[a]
35S:AtTAS1c-GUS$_{At}$	58	0%
35S:AtTAS1c-AtFT	65	100%
35S:AtmiR173aTS- GUS$_{At}$	53	0%
35S:AtmiR173aTS-AtFT	64	100%

[a] The FT phenotype was defined as a higher 'days to flowering' value when compared to the average 'days to flowering' value of the *35S:AtTAS1c-GUS$_{At}$* and *35S:AtmiR173aTS-GUS$_{At}$* control sets.

Table S2. Phenotypic penetrance of syn-tasiRNAs expressed in *A. thaliana* Col-0 T1 transgenic plants for silencing *AtCH42*.

Construct	T1 analyzed	Phenotypic penetrance[a]
35S:AtTAS1c-GUS$_{At}$	70	0%
35S:AtTAS1c-AtCH42	402	78% 17.9% weak 23.6% intermediate 36.1 % severe
35S:AtmiR173aTS-GUS$_{At}$	134	0%
35S:AtmiR173aTS-AtCH42	389	51% 7.2% weak 19.3% intermediate 24.7 % severe

[a] CH42 phenotype is scored in 10 days-old seedling and is considered 'weak', 'intermediate' or 'severe' if seedlings have >2 leaves, exactly 2 leaves or no leaves (only 2 cotyledons), respectively.

Table S3: Phenotypic penetrance of syn-tasiRNAs expressed in Arabidopsis Col-0 T1 transgenic plants for silencing *AtFT* and *AtTRY*.

Construct	T1 analyzed	Phenotypic penetrance[a]
35S:AtTAS1c-GUS$_{At}$	46	0% FT 0% Trich
35S:AtTAS1c-AtFT-AtTrich	16	100% FT 88% Trich
35S:AtTAS1c-AtTrich-AtFT	16	100% FT 82% Trich
35S:AtmiR173TS-GUS$_{At}$	27	0% FT 0% Trich
35S:AtmiR173TS-AtFT-AtTrich	34	100% FT 80% Trich
35S:AtmiR173TS-AtTrich-AtFT	20	100% FT 72% Trich

[a] The Ft phenotype was defined as a higher 'days to flowering' value when compared to the average 'days to flowering' value of the *35S:AtTAS1c-GUS$_{At}$* control set.
The Trich phenotype was defined as a higher number of trichomes when compared to transformants of the *35S:AtTAS1c-GUS$_{At}$* control set.

DISCUSSION

In this work, we use two different classes of art-sRNAs as biotechnological tools to silence genes of interest. First, we describe the mobility of art-sRNAs to induce silencing in distal parts of the plant and emphasize its possible applications. And second, we engineer previously used art-sRNA precursor molecules to obtain minimal-sized versions, thereby expanding their application as tools for whole-plant gene silencing.

1. Features determining the induction of systemic silencing by mobile art-sRNAs

Over the past two decades, a model has been proposed in which sRNAs act non-cell-autonomously to regulate plant development, growth and defense, functioning as mobile signals. sRNAs can move both short- and long-range distances within the plant. In this model, sRNAs move symplastically to 10-15 neighboring cells through PD from their production site. If sRNAs are produced in, or reach, the phloem companion cells of mature leaves (source tissues), they can be loaded into the phloem sieve elements through PD and move long distances to developing organs (sink tissues) (Y. Yan & Ham, 2022). Once in the sink tissues, sRNAs are unloaded from the vascular system and undergo short-range movement (B.-K. Ham & Lucas, 2017). However, many molecular regulatory mechanisms controlling sRNA-mediated SS remain unknown. Short-range movement of art-sRNAs has previously been studied through their expression from cell-type-specific promoters in transgenic plants (de Felippes et al., 2011; Skopelitis et al., 2018; Slotkin et al., 2009). However, the ability of art-sRNAs to reach the phloem in a non-cell-autonomous manner and move long distances to silence endogenous genes has not been reported yet.

In Chapter 1, we describe the local silencing (LS) and SS induced by two different classes of art-sRNAs of identical sequence, caused by short-range and long-range movement, respectively. Art-sRNA duplexes are generated in infiltrated cells acting as source tissue, moving cell-to-cell through PD until reaching the phloem companion cells. Then, art-sRNAs are loaded into the sieve elements and transported to sink tissues, where they are unloaded from the phloem and move cell-to-cell inducing gene silencing in the 10-15 neighboring cells. Art-sRNAs were designed to target the *NbSu* gene, whose silencing leads to a bleaching phenotype, facilitating the identification and quantification of LS and SS (Koncz et al., 1990). We first analyzed the LS efficiency of both classes of art-sRNAs in *N. benthamiana* leaves via *Agrobacterium*-mediated expression of several art-sRNA constructs. Notably, amiR-NbSu-2 accumulated to significantly higher levels in agroinfiltrated tissues compared to syn-tasiR-NbSu-2. Accumulation differences between amiRNAs and syn-tasiRNAs targeting endogenous

genes have been reported before and may be due to their different biosynthetic pathways (Carbonell et al., 2014; de Felippes et al., 2011). However, the degree of LS, analyzed by *NbSu* mRNA accumulation and phenotype intensity, was not different between tissues expressing the two different classes of art-sRNAs, indicating that lower syn-tasiRNA accumulation does not necessarily correlate with reduced target silencing intensity, as previously proposed (de Felippes et al., 2011).

Interestingly, when expressing amiR-NbSu-2 or syn-tasiRNA-NbSu-2 in areas covering the basal region of the leaf, the first signs of SS appeared in upper non-agroinfiltrated leaves. This finding led us to study the role of the art-sRNA expression region in SS induction. Indeed cell-type dependence has been described as a key element in inducing a systemic response (Ryabov et al., 2004). Specifically, several studies support the idea that miRNA expression in the companion cells of the phloem is required for miRNA movement to distal parts of the plant (Aung et al., 2006; Kawashima et al., 2009; Skopelitis et al., 2018; Tsikou et al., 2018). Our results indicate that art-sRNA expression in cells near the petiole may facilitate their loading into the phloem sieve elements via the companion cells for long-distance movement. The appearance of the systemic signal in young tissues, but not in older leaves, points to a directional source-to-sink movement of art-sRNAs, following a photoassimilate-like directionality (Notaguchi & Okamoto, 2015). The phloem-mediated long-distance movement of art-sRNAs is supported by sRNA detection in the phloem sap (Varkonyi-Gasic et al., 2010; S. Zhang et al., 2009), along with the absence of RNAses (Doering-Saad et al., 2002; Sasaki et al., 1998). The SS detected in upper tissues is characterized by vein-proximal chlorosis, a short-range movement phenotype induced by a silencing signal as previously described (Melnyk et al., 2011; Y. Yan, 2022). Altogether, our results indicate that art-sRNAs are unloaded from the phloem and move to adjacent cells through PD.

Interestingly, under the same experimental conditions, amiR-NbSu-1 did not induce SS, suggesting a sequence specificity of the systemic response. However, previous reports point to a sequence-independent SS induction and emphasize other factors such as silencing signal accumulation, as being more critical for SS induction (Skopelitis et al., 2018). Since amiR-NbSu-2 accumulated to significantly higher levels than amiR-NbSu-1 in infiltrated tissue, we analyzed the influence of amiRNA expression levels on SS induction. Our results showed that increasing the infiltration OD of amiR-NbSu-1 led to the appearance of SS in upper tissues, indicating that amiRNA accumulation levels in agroinfiltrated leaves are crucial for the induction of a systemic response, similar to siRNAs (Kalantidis et al., 2006). Importantly, it has been proposed that amiRNA accumulation levels in source tissues determine the range of the systemic response but not the capacity to move (Skopelitis et al., 2018). Since miRNA loading

into the phloem is considered a highly selective process (Rodriguez-Medina et al., 2011; Skopelitis et al., 2018; Varkonyi-Gasic et al., 2010), it is likely that SS induced by amiRNAs is regulated by multiple factors.

The sRNA biogenesis pathway is another possible element regulating the appearance of SS. Our results show that syn-tasiR-NbSu-2, which has the same sequence than amiR-NbSu-2 induced SS but with less intensity. Interestingly, syn-tasiR-NbSu-2 accumulated to lower levels than amiR-NbSu-2 in agroinfiltrated tissues. As proposed earlier, the reduced amount of syn-tasiR-NbSu-2 in the “source” tissue may have limited the range and intensity of the systemic response. Interestingly, De Felippes et al. reported a higher efficiency in target gene silencing induced by syn-tasiRNAs despite being less accumulated than amiRNAs, atributing this to the generation of secondary sRNAs derived from syn-tasiRNA activity (de Felippes et al., 2011). Indeed, transitivity has been proposed as a requirement for SS induction by miRNAs, facilitating the amplification and spreading of the silencing signal (Skopelitis et al., 2018). In our study, secondary sRNAs were absent in leaves agroinfiltrated with amiR-NbSu-2 or syn-tasiR-NbSu-2, as well as in upper tissues. Interestingly, a 22-nt version of amiR-NbSu-2 induced phased secondary sRNAs generation in agroinfiltrated leaves, but no SS was detected in these plants, likely due to the low local accumulation of both the 22-nt version and the induced secondary sRNAs. In summary, our results indicate that a high accumulation of art-sRNAs in local tissues is critical for SS induction. Moreover, this SS response is transitivity-independent, avoiding the potential risk of having off-target effects caused by the population of unspecific secondary sRNAs generated during transitivity (Senthil-Kumar & Mysore, 2011).

We have discussed the influence that local silencing features have on SS induction; for now focusing on the nature of the mobile signal, which remains to be elucidated. Our results suggest that 21-nt art-sRNA duplexes act as the mobile signal, regardless of their biogenesis pathway. This hypothesis is supported by the identification of siRNA duplexes generated from different precursors and moving long distances in Arabidopsis (Devers et al., 2020), along with the identification of some miRNA and miRNA* strands in Arabidopsis phloem stream (Hsieh et al., 2009). In contrast, only the star strands of some miRNAs have been detected in scions, suggesting that single-stranded sRNAs (ss-sRNAs) may also be the silencing signal moving long distances through the graft junction (Hsieh et al., 2009). Indeed, many ss-sRNAs have been detected in phloem exudates of different species (Yoo et al., 2004). Interestingly, several ss-RNA-binding proteins involved in intercellular and/or systemic movement have been identified in plants, while no dsRNA-binding proteins have been reported to be involved in these processes (B. Ham et al., 2014; Y. Yan, 2022; Y. Yan et al., 2020). It has been suggested that some ss-sRNAs may move through the plant in ribonucleoprotein complexes for increased

stability, while dsRNA may not need to associate with proteins (Y. Yan & Ham, 2022). In any case, our results suggest that sRNAs, and not their precursor molecules, are the mobile silencing signals, as previously proposed (Molnar et al., 2010). Interestingly, some reports indicate that the miRNA precursor typical hairpin structure may facilitate their mobility (Lezzhov et al., 2019; Wang et al., 2021). Therefore, several controversial aspects and unknown features regarding sRNA movement in plants remain and will require further investigation.

2. Applications of mobile art-sRNAs and alternatives to current limitations

As discussed in Chapter 1, the ability to locally express art-sRNAs and cause a systemic response can serve as a powerful tool against viral infections. Importantly, the expression of art-sRNAs targeting exogenous genes could also provide protective treatments against other types of pathogens, such as parasitic plants, since it is known that sRNAs can move between host and parasitic plants through a specific structure called the haustorium (Liu & Chen, 2018). In some parasitic plants like those from the genus *Cuscuta*, the haustorium taps into the phloem and induces the accumulation of many miRNAs when parasitizing Arabidopsis and tobacco (Liu & Chen, 2018; Smith et al., 2001). Therefore, expressing art-sRNAs in the host plant targeting *Cuscuta* vital genes might enhance host resistance due to the trans-species movement of the silencing molecules, as observed with the phloem-specific expression of siRNAs in tobacco plants (Alakonya et al., 2012).

The experimental system described in our study is a powerful tool to decipher some of the many unknown elements participating in sRNA mobility pathway. Grafting experiments have been used to characterize various mobile sRNAs, as well as the genetic requirements for the signal translocation and reception (Y. Yan, 2022). However, grafting techniques have several limitations: (i) they are restricted to specific developmental stages, (ii) there is a delay caused by the formation of a vascular connection between rootstock and scion, which can take a week or more, and (iii) they typically involve the use of transgenic plants (Melnyk, 2017). These limitations are not present in the transient expression of mobile art-sRNAs, making this a promising alternative for studying sRNA mobility. Still, one limitation associated with expressing art-sRNA constructs in plants using *Agrobacterium* is the generation of transgenic tissues, which restricts the biotechnological application of art-sRNAs in regions where GMOs are banned. The exogenous application of art-sRNA precursors offers a non-transgenic alternative, attracting increasing interest for protecting plants against pathogens and regulating endogenous gene(s) expression (Adeyinka et al., 2020; Schwartz et al., 2020). Current studies on the exogenous application of sRNAs use dsRNAs as precursor molecules, hence using art-sRNA precursors would increase target gene specificity with reduced off-target effects, as they

act in a transitivity-independent manner. However, the exogenous delivery of sRNA precursors, as opposed to *Agrobacterium*-mediated expression, might require multiple applications to ensure SS induction, which would increase treatment costs and might be undesirable from a commercial point of view. In any case, further optimization is needed for the cost-effective production of art-sRNA precursors, as well as for identifying suitable alternatives to increase RNA stability (e.g. nanoparticle conjugation) for efficient delivery to plants (Jalaluddin et al., 2023).

One of the primary goals of gene silencing tools is to induce uniform target silencing throughout the entire plant. In our study, the SS phenotype described did not reflect homogeneous silencing of the target gene across the whole leaf surface, likely due to the limited mobility of art-sRNA duplexes once unloaded in apical tissues. An alternative method for silencing endogenous genes at the whole-plant level could be editing endogenous sRNA-generating *loci* to produce art-sRNAs. For example, CRISPR (Clustered Regularly Interspaced Short Palindromic Repeat) technique could be used to replace the endogenous miRNA/miRNA* or tasiRNA sequences within *MIRNA* or *TAS loci* by the desired amiRNA/amiRNA* or syn-tasiRNA(s) sequences, respectively. With this strategy, art-sRNA expression would depend on the expression pattern of the modified *MIRNA* or *TAS* locus, avoiding the risks associated with constitutive expression promoters often used to direct art-sRNA precursor expression. So far CRISPR technology has been applied in plants to generate point mutations in *MIRNA* genes, resulting in either complete knockouts or fine-tuning of miRNA expression (Bravo-Vázquez et al., 2024). Still, the efficiency of gene replacement techniques in plants remains low and involves species-specific and time-consuming protocols, limiting the range of applications (Singh et al., 2023). Finally, another alternative to spread silencing at the whole-plant level without multiple applications is the use of viral vectors to express amiRNAs (amiR-VIGS) or syn-tasiRNAs (syn-tasiR-VIGS). A significant limitation when using viral vectors is insert size, as most have limited cargo capacity, and larger inserts are less stable and typically lost during viral replication. The potential use of this technique to expand the biotechnological tools available for inducing gene silencing at the whole-plant level, led us to study the minimal sequence requirements of art-sRNA precursors for efficient expression from viral vectors.

3. Development of minimal art-sRNA precursors

In this work, we investigated the minimal sequence requirements for generating amiRNAs and syn-tasiRNAs from the *AtMIR390a* and *AtTAS1c* precursors, respectively. Art-sRNAs accumulate to high levels when expressed from these canonical full-length precursors which are accurately processed and have been previously used to express art-sRNAs in model and

non-model species, targeting endogenous genes as well as viral RNAs (Carbonell, 2019; Cisneros et al., 2021). We hypothesized that reducing the size of these art-sRNA precursors would facilitate key aspects of their applicability, such as simplifying the generation of art-sRNA constructs or their expression from viral vectors, while maintaining their silencing efficiency.

In chapter 2 we developed a minimal amiRNA precursor that is efficiently processed and induces high levels of target gene silencing. This 89-nt long minimal precursor was obtained through a systematic functional screening of shortened versions of *AtMIR390a* and is, to our knowledge, the shortest precursor used to express amiRNAs in plants. Our results indicate that deletions in the BS region are critical for amiRNA accumulation, while modifications in the DSL region are better tolerated. This is consistent with the identification of highly conserved BS regions in base-to-loop processed miRNA precursors, particularly in *MIR390* across liverworts and angiosperms (Chorostecki et al., 2017; Xia et al., 2017). For base-to-loop processed precursors, a 15-17 bp double-stranded segment below the miRNA/miRNA* duplex region is required for the correct processing by DCL1 (Mateos et al., 2010; Song et al., 2010; Werner et al., 2010). This segment tolerates minimal changes, such as small unpaired bulges, while maintaining the linear stem structure, since the secondary structure is critical for DCL1-mediated miRNA processing (Wei et al., 2021; Werner et al., 2010). Our results show that amiRNAs can be efficiently produced from a precursor containing the intact BS region, while all deletions tested drastically reduced or abolished amiRNA accumulation. Still, the *AtMIR390a* BS region has some degree of flexibility, as some amiRNA accumulation is detected from the *BS-D7* form. Importantly, point mutations can also completely abolish miRNA precursor processing due to alteration of DCL1, HYL1 or SE recognition sites or the overall precursor secondary structure as previously proposed (Cuperus, Montgomery et al., 2010; Rojas et al., 2020). Likewise, point mutations can also increase miRNA accumulation, as shown by a C-G pair variant in the first DCL1 cleavage site in *AtMIR172a* (Rojas et al., 2020). Therefore, we cannot rule out the possibility that some of these point mutations might recover amiRNA accumulation levels in precursors with less than 15 nt in the BS region, like the *BS-D7* form. In any case, our results indicate that the *AtMIR390a* BS region is sufficient for efficient amiRNA generation and target silencing.

The *AtMIR390a* DSL region showed more flexibility to deletions, as proposed for base-to-loop processed precursors (Bajczyk et al., 2023; Li & Yu, 2021). Specifically, a 13-nt deletion in the canonical DSL region is tolerated with a minor effect on amiRNA accumulation. Previous work reported the successful production of amiRNAs from a chimeric *AtMIR390a-OsDSL* precursor in Arabidopsis (Carbonell et al., 2015). Our results indicate that the *OsDSL* region in the chimeric precursor can be shortened to 12 nt before completely suppressing amiRNA

production. Importantly, in both precursors, deletions compromising the presence of a stem in the DSL region largely affected or abolished amiRNA accumulation. Indeed, the importance of a stem and a loop in the region above the miRNA/miRNA* duplex to ensure DCL1 recognition and cleavage has been highlighted before (Mateos et al., 2010). Interestingly, *AtMIR390a* has recently been described as a bidirectional base-to-loop processed precursor, indicating that, in addition to generating AtmiR390a through base-to-loop processing, abortive products are generated when processed in a loop-to-base manner (X. Yan et al., 2024). The bidirectional processing of some miRNA precursors seems to be triggered by a large internal loop, which, in the case of *AtMIR390a*, is located in the DSL region (X. Yan et al., 2024). In our work, only precursors containing the canonical DSL region maintained the large internal loop. Therefore, it cannot be ruled out that some of the modifications performed in this region may have altered the proposed bidirectional processing of *AtMIR390a,* since the specific features determining the alternative loop-to-base processing of this precursor remain elusive.

In Chapter 3, we describe the development of a minimal syn-tasiRNA precursor from the canonical full-length *AtTAS1c*. Since a 22-nt miRNA TS is sufficient to trigger the formation of phasiRNAs from a given sequence, we evaluated the silencing efficiency of a minimal *AtTAS1c* precursor containing only the triggering AtmiR173 TS and the tasiRNA-yielding region. Previous studies analyzing tasiRNA/syn-tasiRNA generation from shortened *TAS* precursors reported lower accumulation levels compared to full-length precursors (Felippes & Weigel, 2009; Montgomery et al., 2008). Here, we observed a reduction in syn-tasiRNA accumulation levels when produced from the minimal precursor, suggesting the presence of *cis* regulatory elements in the removed sequences of the *AtTAS1c* precursor. TasiRNA precursor processing partially depends on SGS3 aggregation to form siRNA bodies and recruit RDR6, all of which is promoted by ribosome stalling and leads to an increase in tasiRNA accumulation (Iwakawa et al., 2021; Tan et al., 2023). Interestingly, the removed regions of the *AtTAS1c* precursor contain actively translated open reading frames (ORFs) (de Felippes, 2019; Wu et al., 2024). Therefore, it is possible that the differences in syn-tasiRNA accumulation observed in the minimal precursor are due to the lack of ORFs, as reported for tasiRNA precursors containing mutated ORFs (Bazin et al., 2017; Yoshikawa et al., 2016, Zhang et al., 2012). However, more importantly, target mRNA expression levels were not significantly affected in plants expressing syn-tasiRNAs from either full-length or minimal precursors.

To simplify and facilitate syn-tasiRNA expression from *AtTAS1c* in a non-Arabidopsis species, the AtmiR173a TS was substituted by NbmiR482a or NbmiR6019a/b TS. Syn-tasiRNA accumulation and target gene silencing levels were similar in plants expressing the *AtTAS1c* full-length or minimal precursors containing the miRNA TS swap. Interestingly, syn-tasiRNA

accumulated to lower levels when expressed from precursors containing the NbmiR6019a/b TS compared to those containing the NbmiR482a TS, most likely due to the lower expression levels of NbmiR6019a/b observed in *N. benthamiana* leaves when compared to NbmiR482a (Baksa et al., 2015 and Figure S4 from Chapter 3). In any case, regardless of the TS selected, minimal precursors containing a heterologous miRNA TS were correctly processed and efficiently downregulated the target gene. It is important to consider that miRNAs expression patterns change between developmental stages and tissues; therefore, this design allows for tissue- or stage-specific syn-tasiRNA generation (D'Ario et al., 2017; Ma et al., 2022; Y. Yu et al., 2019). In summary the generated 54-nt syn-tasiRNA minimal precursor only contains 22 nt of the miRNA TS, an 11-nt spacer from *AtTAS1c* and 21 nt from the syn-tasiRNA.

4. Biotechnological advantages of minimal art-sRNA precursors

One biotechnological advantage of minimal art-sRNA precursors compared to full-length is the simplification of construct generation. Previous studies have developed fast-forward approaches for art-sRNA cloning (Carbonell et al., 2014; López-Dolz et al., 2020; N. Zhang et al., 2019). In this work, we engineered new vectors for construct generation with our developed minimal art-sRNA precursors, which only require inserts of 56 and 21 bp for amiRNA and syn-tasiRNA cloning, respectively. Therefore, costs are expected to be reduced compared to classic construct generation methods, which often involve PCR amplification, purification and ligation steps. These steps can be simplified here by oligo ordering. Importantly, these sizes fall within the lowest production scale offered by manufacturers, allowing for fast and cost-effective generation of art-sRNA constructs.

One of the most promising applications of gene silencing strategies for crop improvement and protection is the topical delivery of RNA precursor molecules. A major limitation of this approach is the lack of cost-effective methods for large-scale RNA synthesis (Basso et al., 2019). As previously mentioned, one of the expected advantages of using minimal art-sRNA precursors is their increased stability and overall efficiency when expressed from *in vitro* or *in vivo* systems. The *in vitro* production of dsRNA precursor molecules is based on enzymatic transcription or chemical synthesis (Voloudakis et al., 2015). The enzymatic transcription approach is versatile and allows for the synthesis of both long and short RNAs (Melo et al., 2023). However, commercial kits are expensive, and as insert size increases, transcript fidelity decreases, along with cost-effectiveness (Gardner et al., 1997; Pleiss et al., 1998; A.-M. Yu et al., 2020). On the other hand, high yields of dsRNA can be obtained through chemical synthesis, but the prize increases rapidly with insert size (Melo et al., 2023). Therefore, we expect reduced costs and increased yields when generating art-sRNA minimal precursors through *in vitro*

production systems. Regarding *in vivo* production alternatives, fermentation-based production is a cost-effective method for producing large amounts of precursor RNA molecules. Two factors limit yield when producing RNAs from *in vivo* systems: insert length and RNA instability (A.-M. Yu et al., 2020). By using art-sRNA minimal precursors, we expect to overcome the first limitation. Regarding the second limitation, RNA stability can be increased when attached to an RNA scaffold, as demonstrated by the high yields obtained when producing mammalian pre-miRNAs fused to a tRNA scaffold *in bacteria* (Chen et al., 2015; Ho et al., 2018; A.-M. Yu et al., 2020). All these reasons support the cost-effective production of minimal art-sRNA precursors from *in vivo* systems.

So far, only dsRNAs and siRNA duplexes have been exogenously applied to plants, primarily to confer pathogen resistance (Abdellatef et al., 2021; Koeppe et al., 2023). These molecules have been used alone or in conjugation with nanoparticles to increase RNA stability and durability (Jalaluddin et al., 2023; Melo et al., 2023; Vatanparast et al., 2024). The exogenous application of art-sRNA precursors would increase target gene silencing specificity, as off-target effects are minimized. Moreover, the high stability of miRNA precursors increases the likelihood of successful delivery to plant cells. Indeed, the topical delivery of art-sRNA precursors has been proposed as a highly specific and low-toxicity alternative for controlling gene expression in plants and conferring pathogen resistance (Basso et al., 2019). To our knowledge, art-sRNA precursors have never been produced for further exogenous application in plants. We hope that our newly developed art-sRNA minimal precursors lay the foundation for further exciting biotechnological application of new-generation gene silencing tools in a transgene-free manner.

As previously mentioned, minimal art-sRNA precursors represent an advantage over full-length precursors for viral vector-based expression. Cargo capacity and genetic stability are two of the main considerations when using viral vectors. Both features depend on insert size, as larger inserts may not be tolerated due to the limited cargo capacity of viral vectors, and they also tend to accumulate more mutations, becoming unstable within the viral genome (Khakhar & Voytas, 2021). The next section will discuss the expression of art-sRNAs precursors through viral vectors.

5. Expression of minimal art-sRNA precursors from an RNA-based viral vector

VIGS-mediated gene silencing has been extensively used, and many viral vectors are available to apply this technology in a wide variety of species. For example, PVX, a monopartite ssRNA (+) virus of the *Solanaceae* family (Adams et al., 2004; Edwardson & Christie, 1997), has been

extensively used as viral vector for several reasons: (i) its small-sized ssRNA-based genome facilitates construct generation, (ii) it can be inoculated mechanically or via agroinoculation, (iii) there is no risk of foreign DNA insertion, and (iv) it replicates to high levels in plants (Batten et al., 2003; Verchot, 2022). In any case, there are only a few examples of amiR-VIGS (Gu et al., 2014; Jian et al., 2017; Ju et al., 2017; Kuo & Falk, 2022; Y. Tang et al., 2010) while syn-tasiRNA expression using VIGS has not yet been reported. The use of RNA-based viral vectors is more suitable than DNA-based ones due to their wider host range and because their cytoplasmic replication avoids the risk of foreign DNA insertion into the plant genome. However, their application for art-sRNA expression seems to be limited by size constrains (Pasin et al., 2019). Therefore, we hypothesized that the development of minimal art-sRNA precursors would facilitate their expression from RNA-based viral vectors.

In Chapter 2 we analyzed the silencing efficiency of the amiR-VIGS technique using PVX as viral vector. Our results show that only plants infected with PVX-based vector containing the minimal amiRNA precursor began to show symptoms of PVX infection similar to the wild type, accumulated high levels of authentic amiR-NbSu, and displayed an intense bleaching phenotype. These results indicate that insert size is a determining factor for efficiently expressing amiRNAs from RNA-based viral vectors. Importantly, the amiRNA minimal precursor is processed correctly and amiRNAs accumulate as single 21-nt bands, highlighting the processing accuracy. It is important to note that the amiRNA processing pathway takes place in the nucleus, while the PVX infection cycle occurs in the cytoplasm. Therefore, the molecular mechanism behind the accurate amiRNA precursor processing is unknown. Several aspects suggest that DCL4 mediates amiRNA precursor processing from the viral RNA in the cytoplasm, being our most direct evidence that amiRNA accumulation and target mRNA silencing are largely diminished in *DCL4i* knockdown plants, while they remain unaltered in *DCL1i* plants.

It is known that the acquisition of a hairpin-like structure by miRNA precursors determines their recognition and processing. Similarly, minimal amiRNA precursors would need to acquire their correct secondary structure within the viral RNA to be accurately processed, as observed when expressing an amiRNA precursor from a viroid vector (Marquez-Molins et al., 2022). We consider that the amiRNA precursor is more likely to be accurately processed if expressed from a viral subgenomic RNA (sgRNA) rather than embedded in the viral genomic RNA, as in this last scenario amiRNA correct folding could be compromised and negatively affecting viral replication and infectivity. Importantly, the minimal amiRNA precursor is located at the 5’ end of a sgRNA which may facilitate the hairpin structure acquisition necessary for its accurate processing. In summary, authentic and accurately processed amiRNAs are generated from a PVX-based vector containing the minimal precursor. Our results suggest that minimal amiRNA

precursors may be processed by the cytoplasmic DCL4, most likely from a (+) sgRNA generated during the infection.

In Chapter 3 we explored the possibility of using syn-tasiR-VIGS to silence endogenous genes in *N. benthamiana*. Plants expressing PVX containing the minimal syn-tasiRNA precursor accumulated syn-tasiRNAs to high levels and displayed an intense bleaching phenotype. While some degree of bleaching was observed in plants expressing PVX containing the full-length precursor, neither the precursor nor syn-tasiRNAs were detected. sRNA sequencing data indicated that syn-tasiRNAs are being processed correctly, while very few sRNAs are being generated from the rest of the precursor. This suggests that precursor processing is more efficient than siRNA generation from dsRNA intermediates produced during viral replication. The high processing specificity points to DCL4 as the main DCL participating in the generation of syn-tasiRNAs from the viral vector. Moreover, DCL4 is the primary antiviral DCL, particularly during PVX infection in *N. benthamiana* and it mediates the processing of *TAS* precursors in the cytoplasm (Andika et al., 2015; Bouché et al., 2006; Deleris et al., 2006; Gasciolli et al., 2005; Xie et al., 2005). Similar to amiRNA processing from the PVX genome, syn-tasiRNA precursors are most likely being processed from a sgRNA, as the 22-nt miRNA TS would be more accessible when located at the end of a sgRNA rather than in the middle of the viral genome. In summary, here we report the first successful expression of syn-tasiRNAs in plants using VIGS, highlighting the biotechnological relevance of developing minimal precursors.

6. Transgene-free application of amiR-VIGS and syn-tasiR-VIGS: methodology, uses and limitations

GMOs are subject to very strict legislation in certain world regions, such as the European Union, leading to the development of new crop improvement techniques that bypass current limitations. In plants treated with VIGS, transgenic tissues are typically generated since the viral vector construct is agroinfiltrated (Rössner et al., 2022). Here, we developed a common methodology for transgene-free gene silencing mediated by art-sRNAs. Our strategy uses infectious crude extracts generated from upper, non-agroinoculated leaves of previously infected plants containing a PVX-based vector with a minimal art-sRNA precursor. These extracts are used to inoculate new plants, thus avoiding the use of *Agrobacterium*. The crude extract is applied by spraying directly onto the leaves, a fast-forward approach that can potentially be scaled up for application in larger areas such as fields. The transgene-free application of amiR/syn-tasiR-VIGS offers an advantage over the exogenous application of art-sRNA precursors because only

one application is needed to induce whole-plant gene silencing. All in all, this technique could potentially be used to silence endogenous genes in all PVX plant hosts for improving economically relevant traits. Moreover, the specific use of syn-tasiR-VIGS for plant vaccination would be an improvement over previous reports of antiviral resistance through the expression of multiple syn-tasiRNAs, due to the fast-forward application method and the variety of compatible species (Carbonell et al., 2019). Similarly, it could also be used to confer resistance to pathogenic fungi or bacteria.

Despite the above-mentioned potential applications of these techniques, we must also consider some specific limitations. For instance, the generation of syn-tasiRNAs from the syn-tasiR-VIGS approach requires the presence of both the viral vector and the triggering miRNA in the same cell. This may not be ideal considering that miRNA expression is often tissue- or condition-specific. To overcome the miRNA dependency of syn-tasiRNA generation, we propose the tandem expression of an amiRNA and syn-tasiRNA minimal precursors from the same cassette. With this approach, the triggering miRNA and the syn-tasiRNAs would always be expressed in the same cell, avoiding variations associated with the dynamic miRNA expression patterns. In any case, in this work we have developed a novel transgene-free approach to induce the silencing of endogenous genes at the whole-plant level mediated by amiRNAs or syn-tasiRNAs expressed from a PVX-based viral vector. We hope that this biotechnological development facilitates gene function studies as well as crop protection and improvement.

CONCLUSIONS

1. Art-sRNAs can move long distances in plants as 21-nucleotide duplexes, specifically silencing endogenous genes in tissues different from where they are applied.

2. Highly effective and accurately processed amiRNAs can be produced from a minimal *AtMIR390a*-based chimeric precursor of only 89 nucleotides, significantly shorter than the widely used 521-nucleotide *AtMIR390a* precursor. This minimal precursor includes the original 33-nucleotide BS region from the *AtMIR390a*, the 21-nucleotide amiRNA/amiRNA* duplex, and a 14-nucleotide shortened DSL region from the *OsMIR390*.

3. Highly effective and accurately processed syn-tasiRNAs can be produced from a minimal precursor of only 54 nucleotides, significantly shorter than the widely used 1011-nucleotide *AtTAS1c* precursor. This minimal precursor includes a 22-nucleotide miRNA target site and the 21-nucleotide syn-tasiRNA sequence, separated by a spacer region of 11 nucleotides derived from *AtTAS1c*.

4. Authentic amiRNAs and syn-tasiRNAs are generated from minimal precursors, but not from full-length precursors, when expressed from an RNA-based viral vector such as potato virus X.

5. Potato virus X-based viral vectors including minimal art-sRNA precursors can be applied to plants in a non-transgenic manner for inducing whole-plant gene silencing.

REFERENCES

Abdellatef, E., Kamal, N. M., & Tsujimoto, H. (2021). Tuning beforehand: A foresight on rna interference (RNAi) and in vitro-derived dsRNAs to enhance crop resilience to biotic and abiotic stresses. *Int J Mol Sci*, **22**(14).

Adams, M. J., Antoniw, J. F., Bar-Joseph, M., Brunt, A. A., Candresse, T., Foster, G. D., Martelli, G. P., Milne, R. G., Zavriev, S. K., & Fauquet, C. M. (2004). The new plant virus family *Flexiviridae* and assessment of molecular criteria for species demarcation. *Arch Virol*, **149**(5), 1045–1060.

Adeyinka, O. S., Riaz, S., Toufiq, N., Yousaf, I., Bhatti, M. U., Batcho, A., Olajide, A. A., Nasir, I. A., & Tabassum, B. (2020). Advances in exogenous RNA delivery techniques for RNAi-mediated pest control. *Mol Biol Rep*, **47**(8), 6309–6319.

Alakonya, A., Kumar, R., Koenig, D., Kimura, S., Townsley, B., Runo, S., Garces, H. M., Kang, J., Yanez, A., David-Schwartz, R., Machuka, J., & Sinha, N. (2012). Interspecific RNA Interference of *SHOOT MERISTEMLESS-Like* Disrupts *Cuscuta pentagona* Plant Parasitism. *Plant Cell*, **24**(7), 3153–3166.

Allen, E., Xie, Z., Gustafson, A. M., & Carrington, J. C. (2005). microRNA-directed phasing during trans-acting siRNA biogenesis in plants. *Cell*, **121**(2), 207–221.

Alvarez, J. P., Pekker, I., Goldshmidt, A., Blum, E., Amsellem, Z., & Eshed, Y. (2006). Endogenous and Synthetic MicroRNAs Stimulate Simultaneous, Efficient, and Localized Regulation of Multiple Targets in Diverse Species. *Plant Cell*, **18**(5), 1134–1151.

Andika, I. B., Maruyama, K., Sun, L., Kondo, H., Tamada, T., & Suzuki, N. (2015). Differential contributions of plant Dicer-like proteins to antiviral defences against potato virus X in leaves and roots. *Plant Journal*, **81**(5), 781–793.

Aung, K., Lin, S.-I., Wu, C.-C., Huang, Y.-T., Su, C., & Chiou, T.-J. (2006). *pho2* , a Phosphate Overaccumulator, Is Caused by a Nonsense Mutation in a MicroRNA399 Target Gene. *Plant Physiol*, **141**(3), 1000–1011.

Axtell, M. J. (2013). Classification and comparison of small RNAs from plants. *Annu Rev Plant Biol*, **64**, 137–159.

Axtell, M. J., Jan, C., Rajagopalan, R., & Bartel, D. P. (2006). A Two-Hit Trigger for siRNA Biogenesis in Plants. *Cell*, **127**(3), 565–577.

Bajczyk, M., Jarmolowski, A., Jozwiak, M., Pacak, A., Pietrykowska, H., Sierocka, I., Swida-Barteczka, A., Szewc, L., & Szweykowska-Kulinska, Z. (2023). Recent Insights into Plant miRNA Biogenesis: Multiple Layers of miRNA Level Regulation. *Plants*, **12**(2).

Baksa, I., Nagy, T., Barta, E., Havelda, Z., Várallyay, É., Silhavy, D., Burgyán, J., & Szittya, G. (2015). Identification of *Nicotiana benthamiana* microRNAs and their targets using high throughput sequencing and degradome analysis. *BMC Genomics*, **16**(1).

Basso, M. F., Ferreira, P. C. G., Kobayashi, A. K., Harmon, F. G., Nepomuceno, A. L., Molinari, H. B. C., & Grossi-de-Sa, M. F. (2019). MicroRNAs and new biotechnological tools for its modulation and improving stress tolerance in plants. *Plant Biotechnol J*, **17**(8), 1482–1500.

Batten, J. S., Yoshinari, S., & Hemenway, C. (2003). Potato virus X: A model system for virus replication, movement and gene expression. *Mol Plant Pathol*, **4**(2), 125–131.

Baulcombe, D. (2004). RNA silencing in plants. *Nature*, **431**(7006), 356–363.

Bazin, J., Baerenfaller, K., Gosai, S. J., Gregory, B. D., Crespi, M., & Bailey-Serres, J. (2017). Global analysis of ribosome-associated noncoding RNAs unveils new modes of

translational regulation. *Proc Natl Acad Sci U S A*, **114**(46), E10018–E10027.

Becker, A. (2003). The major clades of MADS-box genes and their role in the development and evolution of flowering plants. *Mol Phylogenet Evol*, **29**(3), 464–489.

Berbati, M., Kaldis, A., & Voloudakis, A. (2023). Efficient artificial microRNA-mediated resistance against zucchini yellow mosaic virus in zucchini via agroinfiltration. *J Virol Methods*, **321**(114805).

Betti, F., Ladera-Carmona, M. J., Weits, D. A., Ferri, G., Iacopino, S., Novi, G., Svezia, B., Kunkowska, A. B., Santaniello, A., Piaggesi, A., Loreti, E., & Perata, P. (2021). Exogenous miRNAs induce post-transcriptional gene silencing in plants. *Nat Plants*, **7**(10), 1379–1388.

Bhogale, S., Mahajan, A. S., Natarajan, B., Rajabhoj, M., Thulasiram, H. V., & Banerjee, A. K. (2014). *MicroRNA156*: A Potential Graft-Transmissible MicroRNA That Modulates Plant Architecture and Tuberization in *Solanum tuberosum* ssp. *andigena*. *Plant Physiol*, **164**(2), 1011–1027.

Bologna, N. G., Mateos, J. L., Bresso, E. G., & Palatnik, J. F. (2009). A loop-to-base processing mechanism underlies the biogenesis of plant microRNAs miR319 and miR159. *EMBO J*, **28**(23), 3646–3656.

Bologna, N. G., Schapire, A. L., Zhai, J., Chorostecki, U., Boisbouvier, J., Meyers, B. C., & Palatnik, J. F. (2013). Multiple RNA recognition patterns during microRNA biogenesis in plants. *Genome Res*, **23**(10), 1675–1689.

Bouché, N., Lauressergues, D., Gasciolli, V., & Vaucheret, H. (2006). An antagonistic function for Arabidopsis DCL2 in development and a new function for DCL4 in generating viral siRNAs. *EMBO Journal*, **25**(14), 3347–3356.

Bravo-Vázquez, L. A., Méndez-García, A., Chamu-García, V., Rodríguez, A. L., Bandyopadhyay, A., & Paul, S. (2024). The applications of CRISPR/Cas-mediated microRNA and lncRNA editing in plant biology: shaping the future of plant non-coding RNA research. In *Planta* (Vol. 259, Issue 2). Springer Science and Business Media Deutschland GmbH.

Buhtz, A., Springer, F., Chappell, L., Baulcombe, D. C., & Kehr, J. (2008). Identification and characterization of small RNAs from the phloem of *Brassica napus*. *The Plant Journal*, **53**(5), 739–749.

Carbonell, A. (2017). Artificial small RNA-based strategies for effective and specific gene silencing in plants. In D. Tamas (Ed.), *Plant Gene Silencing: Mechanisms and Applications* (pp. 110–127). CABI Biotechnology Series, CABI Publishing.

Carbonell, A. (2019). Secondary small interfering RNA-based silencing tools in plants: An update. *Front Plant Sci*, **10**, 1–5.

Carbonell, A., & Daròs, J.-A. A. (2017). Artificial microRNAs and synthetic trans-acting small interfering RNAs interfere with viroid infection. *Mol Plant Pathol*, **18**(5), 746–753.

Carbonell, A., Fahlgren, N., Mitchell, S., Cox, K. L., Reilly, K. C., Mockler, T. C., & Carrington, J. C. (2015). Highly specific gene silencing in a monocot species by artificial microRNAs derived from chimeric miRNA precursors. *Plant Journal*, **82**(6), 1061–1075.

Carbonell, A., Lisón, P., & Daròs, J.-A. (2019). Multi-targeting of viral RNAs with synthetic trans-acting small interfering RNAs enhances plant antiviral resistance. *The Plant Journal*, **100**(4), 720–737.

Carbonell, A., Takeda, A., Fahlgren, N., Johnson, S. C., Cuperus, J. T., & Carrington, J. C. (2014). New generation of artificial MicroRNA and synthetic trans-acting small interfering RNA vectors for efficient gene silencing in Arabidopsis. *Plant Physiol*, **165**(1), 15–29.

Carrillo-Tripp, J., Shimada-Beltrán, H., & Rivera-Bustamante, R. (2006). Use of geminiviral vectors for functional genomics. In *Current Opinion in Plant Biology* (Vol. 9, Issue 2, pp. 209–215).

Chen, H. M., Chen, L. T., Patel, K., Li, Y. H., Baulcombe, D. C., & Wu, S. H. (2010). 22-Nucleotide RNAs trigger secondary siRNA

biogenesis in plants. *Proc Natl Acad Sci U S A*, **107**(34), 15269–15274.

Chen, Q. X., Wang, W. P., Zeng, S., Urayama, S., & Yu, A. M. (2015). A general approach to high-yield biosynthesis of chimeric RNAs bearing various types of functional small RNAs for broad applications. *Nucleic Acids Res*, **43**(7), 3857–3869.

Chitwood, D. H., Nogueira, F. T. S., Howell, M. D., Montgomery, T. A., Carrington, J. C., & Timmermans, M. C. P. (2009). Pattern formation via small RNA mobility. *Genes Dev*, **23**(5), 549–554.

Chorostecki, U., Moro, B., Rojas, A. M. L., Debernardi, J. M., Schapire, A. L., Notredame, C., & Palatnik, J. F. (2017). Evolutionary footprints reveal insights into plant microRNA biogenesis. *Plant Cell*, **29**(6), 1248–1261.

Cisneros, A. E., & Carbonell, A. (2020). Artificial small RNA-based silencing tools for antiviral resistance in plants. *Plants*, **9**(6).

Cisneros, A. E., de la Torre-Montaña, A., Martín-García, T., & Carbonell, A. (2021). Artificial Small RNAs for Functional Genomics in Plants. In G. Tang, S. Teotia, X. Tang, & D. Singh (Eds.), *RNA-based Technologies For Functional Genomics in Plants* (pp. 1–29). Springer International Publishing.

Cuperus, J. T., Carbonell, A., Fahlgren, N., Garcia-Ruiz, H., Burke, R. T., Takeda, A., Sullivan, C. M., Gilbert, S. D., Montgomery, T. A., & Carrington, J. C. (2010). Unique functionality of 22-nt miRNAs in triggering RDR6-dependent siRNA biogenesis from target transcripts in Arabidopsis. *Nat Struct Mol Biol*, **17**(8), 997–1003.

Cuperus, J. T., Montgomery, T. A., Fahlgren, N., Burke, R. T., Townsend, T., Sullivan, C. M., & Carrington, J. C. (2010). Identification of MIR390a precursor processing-defective mutants in Arabidopsis by direct genome sequencing. *Proc Natl Acad Sci U S A*, **107**(1), 466–471.

Dadami, E., Dalakouras, A., Zwiebel, M., Krczal, G., & Wassenegger, M. (2014). An endogene-resembling transgene is resistant to DNA methylation and systemic silencing. *RNA Biol*, **11**(7), 934–941.

Dadami, E., Moser, M., Zwiebel, M., Krczal, G., Wassenegger, M., & Dalakouras, A. (2013). An endogene-resembling transgene delays the onset of silencing and limits siRNA accumulation. *FEBS Lett*, **587**(6), 706–710.

Dalakouras, A., Wassenegger, M., Dadami, E., Ganopoulos, I., Pappas, M. L., & Papadopoulou, K. (2020). Genetically modified organism-free RNA interference: Exogenous application of RNA molecules in plants. *Plant Physiol*, **182**(1), 38–50.

D'Ario, M., Griffiths-Jones, S., & Kim, M. (2017). Small RNAs: Big Impact on Plant Development. *Trends Plant Sci*, **22**(12), 1056–1068.

de Felippes, F. F. (2019). Gene Regulation Mediated by microRNA-Triggered Secondary Small RNAs in Plants. *Plants*, **8**(112).

de Felippes, F. F., Ott, F., & Weigel, D. (2011). Comparative analysis of non-autonomous effects of tasiRNAs and miRNAs in *Arabidopsis thaliana*. *Nucleic Acids Res*, **39**(7), 2880–2889.

de Felippes, F. F., Wang, J. W., & Weigel, D. (2012). MIGS: MiRNA-induced gene silencing. *Plant Journal*, **70**(3), 541–547.

de Felippes, F. F., & Waterhouse, P. M. (2020). The Whys and Wherefores of Transitivity in Plants*. In *Frontiers in Plant Science* (Vol. 11). Frontiers Media S.A.

de Felippes, F. F., & Weigel, D. (2009). Triggering the formation of tasiRNAs in *Arabidopsis thaliana*: The role of microRNA miR173. *EMBO Rep*, **10**(3), 264–270.

Deleris, A., Javier Gallego-Bartolome, Jinsong Bao, Kristin D. Kasschau, James C. Carrington, & Olivier Voinnet. (2006). Hierarchical Action and Inhibition of Plant Dicer-Like Proteins in Antiviral Defense. *Science (1979)*, **313**(5783), 68–71.

Deng, P., Muhammad, S., Cao, M., & Wu, L. (2018). Biogenesis and regulatory hierarchy of phased small interfering RNAs in plants. *Plant Biotechnol J*, **16**(5), 965–975.

Devers, E. A., Brosnan, C. A., Sarazin, A., Albertini, D., Amsler, A. C., Brioudes, F., Jullien, P. E., Lim, P., Schott, G., & Voinnet, O. (2020). Movement and differential consumption of short interfering RNA duplexes underlie mobile RNA interference. *Nat Plants*, **6**(7), 789–799.

Ding, N., & Zhang, B. (2023). microRNA production in Arabidopsis. *Front Plant Sci*, **14**.

Doering-Saad, C., Newbury, H. J., Bale, J. S., & Pritchard, J. (2002). Use of aphid stylectomy and RT-PCR for the detection of transporter mRNAs in sieve elements. *J Exp Bot*, **53**(369), 631–637.

Dong, Z., Han, M.-H., & Fedoroff, N. (2008). The RNA-binding proteins HYL1 and SE promote accurate *in vitro* processing of pri-miRNA by DCL1. *Proceedings of the National Academy of Sciences*, **105**(29), 9970–9975.

Dunoyer, P., Himber, C., Ruiz-Ferrer, V., Alioua, A., & Voinnet, O. (2007). Intra- and intercellular RNA interference in Arabidopsis thaliana requires components of the microRNA and heterochromatic silencing pathways. *Nat Genet*, **39**(7), 848–856.

Edwardson, J. R., & Christie, R. G. (1997). *Viruses infecting peppers and other solanaceous crops: Vol. Volume 1*.

Endo, Y., Iwakawa, H., & Tomari, Y. (2013). *Arabidopsis* ARGONAUTE7 selects miR390 through multiple checkpoints during RISC assembly. *EMBO Rep*, **14**(7), 652–658.

Fahim, M., Millar, A. A., Wood, C. C., & Larkin, P. J. (2012). Resistance to Wheat streak mosaic virus generated by expression of an artificial polycistronic microRNA in wheat. *Plant Biotechnol J*, **10**(2), 150–163.

Fahlgren, N., & Carrington, J. C. (2010). miRNA Target Prediction in Plants. In *Methods in molecular biology* (pp. 51–57).

Fahlgren, N., Hill, S. T., Carrington, J. C., & Carbonell, A. (2016). P-SAMS: a web site for plant artificial microRNA and synthetic *trans*-acting small interfering RNA design. *Bioinformatics*, **32**(1), 157–158.

Fahlgren, N., Montgomery, T. A., Howell, M. D., Allen, E., Dvorak, S. K., Alexander, A. L., & Carrington, J. C. (2006). Regulation of AUXIN RESPONSE FACTOR3 by TAS3 ta-siRNA Affects Developmental Timing and Patterning in Arabidopsis. *Current Biology*, **16**(9), 939–944.

Fang, Y., & Spector, D. L. (2007). Identification of Nuclear Dicing Bodies Containing Proteins for MicroRNA Biogenesis in Living Arabidopsis Plants. *Current Biology*, **17**(9), 818–823.

Fei, Q., Xia, R., & Meyers, B. C. (2013). Phased, secondary, small interfering RNAs in posttranscriptional regulatory networks. In *Plant Cell* (Vol. 25, Issue 7, pp. 2400–2415). American Society of Plant Biologists.

Fire, A., Xu, S., Montgomery, M. K., Kostas, S. A., Driver, S. E., & Mello, C. C. (1998). Potent and specific genetic interference by double-stranded RNA in Caenorhabditis elegans. *Nature*, **391**(6669), 806–811.

Gardner, L. P., Mookhtiar, K. A., & Coleman, J. E. (1997). Initiation, Elongation, and Processivity of Carboxyl-Terminal Mutants of T7 RNA Polymerase. *Biochemistry*, **36**(10), 2908–2918.

Gasciolli, V., Mallory, A. C., Bartel, D. P., & Vaucheret, H. (2005). Partially Redundant Functions of Arabidopsis DICER-like Enzymes and a Role for DCL4 in Producing trans-Acting siRNAs. *Current Biology*, **15**(16), 1494–1500.

Gu, Z., Huang, C., Li, F., & Zhou, X. (2014). A versatile system for functional analysis of genes and microRNAs in cotton. *Plant Biotechnol J*, **12**(5), 638–649.

Guan, X., Pang, M., Nah, G., Shi, X., Ye, W., Stelly, D. M., & Chen, Z. J. (2014). miR828 and miR858 regulate homoeologous MYB2 gene functions in Arabidopsis trichome and cotton fibre development. *Nat Commun*, **5**(1), 3050.

Gutiérrez-Nava, M. D. L. L., Aukerman, M. J., Sakai, H., Tingey, S. V., & Williams, R. W. (2008). Artificial trans-acting siRNAs confer consistent and effective gene silencing. *Plant Physiol*, **147**(2), 543–551.

Ham, B., Li, G., Jia, W., Leary, J. A., & Lucas, W. J. (2014). Systemic delivery of si

RNA in pumpkin by a plant PHLOEM SMALL RNA-BINDING PROTEIN 1–ribonucleoprotein complex. *The Plant Journal*, **80**(4), 683–694.

Ham, B.-K., & Lucas, W. J. (2017). Phloem-Mobile RNAs as Systemic Signaling Agents. *Annu. Rev. Plant Biol.*, **68**, 173–195.

Han, M.-H., Goud, S., Song, L., & Fedoroff, N. (2004). The *Arabidopsis* double-stranded RNA-binding protein HYL1 plays a role in microRNA-mediated gene regulation. *Proceedings of the National Academy of Sciences*, **101**(4), 1093–1098.

Hernandez-Pinzon, I., Yelina, N. E., Schwach, F., Studholme, D. J., Baulcombe, D., & Dalmay, T. (2007). SDE5, the putative homologue of a human mRNA export factor, is required for transgene silencing and accumulation of *trans* -acting endogenous siRNA. *The Plant Journal*, **50**(1), 140–148.

Himber, C., Dunoyer, P., Moissiard, G., Ritzenthaler, C., & Voinnet, O. (2003). Transitivity-dependent and -independet cell-to-cell movement of RNA silencing. *EMBO J*, **22**(17), 4523–4533.

Ho, P. Y., Duan, Z., Batra, N., Jilek, J. L., Tu, M. J., Qiu, J. X., Hu, Z., Wun, T., Lara, P. N., DeVere White, R. W., Chen, H. W., & Yu, A. M. (2018). Bioengineered noncoding RNAs selectively change cellular miRNome profiles for cancer therapy. *Journal of Pharmacology and Experimental Therapeutics*, **365**(3), 494–506.

Hsieh, L.-C., Lin, S.-I., Shih, A. C.-C., Chen, J.-W., Lin, W.-Y., Tseng, C.-Y., Li, W.-H., & Chiou, T.-J. (2009). Uncovering Small RNA-Mediated Responses to Phosphate Deficiency in Arabidopsis by Deep Sequencing. *Plant Physiol*, **151**(4), 2120–2132.

Ivo L. Hofacker (2003). Vienna RNA secondary structure server, *Nucleic Acids Res*, **31**(13), 3429–3431.

Iwakawa, H. oki, Lam, A. Y. W., Mine, A., Fujita, T., Kiyokawa, K., Yoshikawa, M., Takeda, A., Iwasaki, S., & Tomari, Y. (2021). Ribosome stalling caused by the Argonaute-microRNA-SGS3 complex regulates the production of secondary siRNAs in plants. *Cell Rep*, **35**(13).

Jalaluddin, N.S.M., Asem, M., Harikrishna, J. A., & Ahmad Fuaad, A. A. H. (2023). Recent Progress on Nanocarriers for Topical-Mediated RNAi Strategies for Crop Protection. *Molecules*, **28**(6).

Jian, C., Han, R., Chi, Q., Wang, S., Ma, M., Liu, X., & Zhao, H. (2017). Virus-based MicroRNA silencing and overexpressing in common wheat (*Triticum aestivum L.*). *Front Plant Sci*, **8**(500).

Jouannet, V., Moreno, A. B., Elmayan, T., Vaucheret, H., Crespi, M. D., & Maizel, A. (2012). Cytoplasmic Arabidopsis AGO7 accumulates in membrane-associated siRNA bodies and is required for ta-siRNA biogenesis. *EMBO Journal*, **31**(7), 1704–1713.

Ju, Z., Cao, D., Gao, C., Zuo, J., Zhai, B., Li, S., Zhu, H., Fu, D., Luo, Y., & Zhu, B. (2017). A viral satellite DNA vector (TYLCCNV) for functional analysis of miRNAs and siRNAs in plants. *Plant Physiol*, **173**(4), 1940–1952.

Kalantidis, K., Tsagris, M., & Tabler, M. (2006). Spontaneous short-range silencing of a GFP transgene in *Nicotiana benthamiana* is possibly mediated by small quantities of siRNA that do not trigger systemic silencing. *Plant Journal*, **45**(6), 1006–1016.

Kamthan, A., Chaudhuri, A., Kamthan, M., & Datta, A. (2015). Small RNAs in plants: Recent development and application for crop improvement. *Front Plant Sci*, **6**(APR).

Kawashima, C. G., Yoshimoto, N., Maruyama-Nakashita, A., Tsuchiya, Y. N., Saito, K., Takahashi, H., & Dalmay, T. (2009). Sulphur starvation induces the expression of microRNA-395 and one of its target genes but in different cell types. *The Plant Journal*, **57**(2), 313–321.

Khakhar, A., & Voytas, D. F. (2021). RNA Viral Vectors for Accelerating Plant Synthetic Biology. *Front Plant Sci*, **12**.

Kobayashi, K., & Zambryski, P. (2007). RNA silencing and its cell-to-cell spread during Arabidopsis embryogenesis. *The Plant Journal*, **50**(4), 597–604.

Koeppe, S., Kawchuk, L., & Kalischuk, M. (2023). RNA Interference Past and Future Applications in Plants. *Int J Mol Sci*, **24**(11).

Koncz, C., Mayerhofer, R., Koncz-Kalman, Z., Nawrath, C., Reiss, B., Redei, G. P., & Schell, J. (1990). Isolation of a gene encoding a novel chloroplast protein by T-DNA tagging in *Arabidopsis thaliana*. *EMBO J*, **9**(5), 1337–1346.

Kuo, Y. W., & Falk, B. W. (2022). Artificial microRNA guide strand selection from duplexes with no mismatches shows a purine-rich preference for virus- and non-virus-based expression vectors in plants. *Plant Biotechnol J*, **20**(6), 1069–1084.

Kuo, Y.-W., & Falk, B. W. (2020). RNA Interference Approaches for Plant Disease Control. *Biotechniques*, **69**(6), 469–477.

Kurihara, Y., Takashi, Y., & Watanabe, Y. (2006). The interaction between DCL1 and HYL1 is important for efficient and precise processing of pri-miRNA in plant microRNA biogenesis. *RNA*, **12**(2), 206–212.

Kurihara, Y., & Watanabe, Y. (2004). *Arabidopsis* micro-RNA biogenesis through Dicer-like 1 protein functions. *Proceedings of the National Academy of Sciences*, **101**(34), 12753–12758.

Lezzhov, A. A., Atabekova, A. K., Tolstyko, E. A., Lazareva, E. A., & Solovyev, A. G. (2019). RNA phloem transport mediated by pre-miRNA and viral tRNA-like structures. *Plant Science*, **284**, 99–107.

Li, J., Yang, Z., Yu, B., Liu, J., & Chen, X. (2005). Methylation Protects miRNAs and siRNAs from a 3′-End Uridylation Activity in Arabidopsis. *Current Biology*, **15**(16), 1501–1507.

Li, M., & Yu, B. (2021). Recent advances in the regulation of plant miRNA biogenesis. *RNA Biol*, **18**(12), 2087–2096.

Li, S., Le, B., Ma, X., Li, S., You, C., Yu, Y., Zhang, B., Liu, L., Gao, L., Shi, T., Zhao, Y., Mo, B., Cao, X., & Chen, X. (2016). Biogenesis of phased siRNAS on membrane-bound polysomes in Arabidopsis. *Elife*, **5**(e22750).

Liang, G., He, H., Li, Y., & Yu, D. (2012). A new strategy for construction of artificial miRNA vectors in Arabidopsis. *Planta*, **235**(6), 1421–1429.

Liu, L., & Chen, X. (2018). Intercellular and systemic trafficking of RNAs in plants. *Nat Plants*, **4**(11), 869–878.

Liu, Q., Wang, F., & Axtell, M. J. (2014). Analysis of Complementarity Requirements for Plant MicroRNA Targeting Using a *Nicotiana benthamiana* Quantitative Transient Assay. *Plant Cell*, **26**(2), 741–753.

Liu, Y., Teng, C., Xia, R., & Meyers, B. C. (2020). PhasiRNAs in Plants: Their Biogenesis, genic sources, and roles in stress responses, development, and reproduction. In *Plant Cell* (Vol. 32, Issue 10, pp. 3059–3080). American Society of Plant Biologists.

Lobbes, D., Rallapalli, G., Schmidt, D. D., Martin, C., & Clarke, J. (2006). SERRATE: a new player on the plant microRNA scene. *EMBO Rep*, **7**(10), 1052–1058.

López-Dolz, L., Spada, M., Daròs, J.-A., & Carbonell, A. (2020). Fine-Tune Control of Targeted RNAi Efficacy by Plant Artificial Small. *Nucleic Acids Res*, **48**(11), 6234–6250.

Lopez-Gomollon, S., & Baulcombe, D. C. (2022). Roles of RNA silencing in viral and non-viral plant immunity and in the crosstalk between disease resistance systems. *Nat Rev Mol Cell Biol*, **23**(10), 645–662.

Lozano-Durán, R. (2016). Geminiviruses for biotechnology: The art of parasite taming. *New Phytologist*, **210**(1), 58–64.

Lunardon, A., Kariuki, S. M., & Axtell, M. J. (2021). aExpression and processing of polycistronic artificial microRNAs and trans-acting siRNAs from transiently introduced transgenes in miRNA *Solanum lycopersicum* and *Nicotiana benthamiana*. *Plant Journal*, **106**(4), 1087–1104.

Lyu, J. (2022). Boost transformation. *Nat Plants*, **8**(6), 601–601.

Ma, X., Zhao, F., & Zhou, B. (2022). The Characters of Non-Coding RNAs and Their Biological Roles in Plant Development and Abiotic Stress Response. In *International*

Journal of Molecular Sciences (Vol. 23, Issue 8). MDPI.

Mahmood, M. A., Naqvi, R. Z., Rahman, S. U., Amin, I., & Mansoor, S. (2023). Plant Virus-Derived Vectors for Plant Genome Engineering. *Viruses*, **15**(2).

Manavella, P. A., Koenig, D., & Weigel, D. (2012). Plant secondary siRNA production determined by microRNA-duplex structure. *Proc Natl Acad Sci U S A*, **109**(7), 2461–2466.

Marquez-Molins, J., Hernandez-Azurdia, A. G., Urrutia-Perez, M., Pallas, V., & Gomez, G. (2022). A circular RNA vector for targeted plant gene silencing based on an asymptomatic viroid. *Plant Journal*, **112**(1), 284–293.

Martin, A., Adam, H., Díaz-Mendoza, M., Żurczak, M., González-Schain, N. D., & Suárez-López, P. (2009). Graft-transmissible induction of potato tuberization by the microRNA *miR172*. *Development*, **136**(17), 2873–2881.

Martínez de Alba, A. E., Elvira-Matelot, E., & Vaucheret, H. (2013). Gene silencing in plants: A diversity of pathways. In *Biochimica et Biophysica Acta - Gene Regulatory Mechanisms* (Vol. 1829, Issue 12, pp. 1300–1308).

Mateos, J. L., Bologna, N. G., Chorostecki, U., & Palatnik, J. F. (2010). Identification of MicroRNA Processing Determinants by Random Mutagenesis of Arabidopsis MIR172a Precursor. *Current Biology*, **20**(1), 49–54.

Melnyk, C. W. (2017). Plant grafting: insights into tissue regeneration. *Regeneration*, **4**(1), 3–14.

Melnyk, C. W., Molnar, A., & Baulcombe, D. C. (2011). Intercellular and systemic movement of RNA silencing signals. *EMBO Journal*, **30**(17), 3553–3563.

Melo, J. R., Mammarella, F., & Ariel, F. (2023). Exogenous RNAs: promising tools for the second green revolution. *J Exp Bot*, **74**(7), 2323–2337.

Mencia, R., Gonzalo, L., Tossolini, I., & Manavella, P. A. (2023). Keeping up with the miRNAs: current paradigms of the biogenesis pathway. *J Exp Bot*, **74**(7), 2213–2227.

Meyers, B. C., Simon, S. A., & Zhai, J. (2010). MicroRNA Processing: Battle of the Bulge. *Current Biology*, **20**(2).

Mickiewicz, A., Rybarczyk, A., Sarzynska, J., Figlerowicz, M., & Blazewicz, J. (2016). AmiRNA Designer - new method of artificial miRNA design. *Acta Biochim Pol*, **63**(1).

Molnár, A., Csorba, T., Lakatos, L., Várallyay, E., Lacomme, C., & Burgyán, J. (2005). Plant Virus-Derived Small Interfering RNAs Originate Predominantly from Highly Structured Single-Stranded Viral RNAs. *J Virol*, **79**(12), 7812–7818.

Molnar, A., Melnyk, C. W., Bassett, A., Hardcastle, T. J., Dunn, R., & Baulcombe, D. C. (2010). Small Silencing RNAs in Plants Are Mobile and Direct Epigenetic Modification in Recipient Cells. *Science (1979)*, **328**(5980), 872–875.

Montgomery, T. A., Howell, M. D., Cuperus, J. T., Li, D., Hansen, J. E., Alexander, A. L., Chapman, E. J., Fahlgren, N., Allen, E., & Carrington, J. C. (2008). Specificity of ARGONAUTE7-miR390 Interaction and Dual Functionality in TAS3 Trans-Acting siRNA Formation. *Cell*, **133**(1), 128–141.

Montgomery, T. A., Yoo, J., Fahlgren, N., Gilbert, S. D., Howell, M. D., Sullivan, C. M., Alexander, A., Nguyen, G., Allen, E., Hoon Ahn, J., & Carrington, J. C. (2008). AGO1-miR173 complex initiates phased siRNA formation in plants. *Proceedings of the National Academy of Sciences*, **105**(51).

Nakazawa, Y., Hiraguri, A., Moriyama, H., & Fukuhara, T. (2007). The dsRNA-binding protein DRB4 interacts with the Dicer-like protein DCL4 in vivo and functions in the trans-acting siRNA pathway. *Plant Mol Biol*, **63**(6), 777–785.

Naveen, A. K., & Sontakke, M. (2024). A review on regulatory aspects, challenges and public perception in acceptance of genetically modified foods. *Food Sci Biotechnol*, **33**, 791–804.

Notaguchi, M., & Okamoto, S. (2015). Dynamics of long-distance signaling via plant vascular tissues. *Front Plant Sci*, **6**(161).

Ossowski, S., Schwab, R., & Weigel, D. (2008). Gene silencing in plants using artificial microRNAs and other small RNAs. *Plant Journal*, **53**(4), 674–690.

Otero, S., Helariutta, Y., & Benitez-Alfonso, Y. (2016). Symplastic communication in organ formation and tissue patterning. *Curr Opin Plant Biol*, **29**, 21–28.

Palauqui, J.-C. (1997). Systemic acquired silencing: transgene-specific post-transcriptional silencing is transmitted by grafting from silenced stocks to non-silenced scions. *EMBO J*, **16**(15), 4738–4745.

Parizotto, E. A., Dunoyer, P., Rahm, N., Himber, C., & Voinnet, O. (2004). *In vivo* investigation of the transcription, processing, endonucleolytic activity, and functional relevance of the spatial distribution of a plant miRNA. *Genes Dev*, **18**(18), 2237–2242.

Park, M. Y., Wu, G., Gonzalez-Sulser, A., Vaucheret, H., & Poethig, R. S. (2005). Nuclear processing and export of microRNAs in *Arabidopsis*. *Proceedings of the National Academy of Sciences*, **102**(10), 3691–3696.

Pasin, F., Menzel, W., & Daròs, J. (2019). Harnessed viruses in the age of metagenomics and synthetic biology: an update on infectious clone assembly and biotechnologies of plant viruses. *Plant Biotechnol J*, **17**(6), 1010–1026.

Pleiss, J. A., Derrick, M. L., & Uhlenbeck, O. C. (1998). T7 RNA polymerase produces 5′ end heterogeneity during in vitro transcription from certain templates. *RNA*, **4**(10), S135583829800106X.

Rajagopalan, R., Vaucheret, H., Trejo, J., & Bartel, D. P. (2006). A diverse and evolutionarily fluid set of microRNAs in *Arabidopsis thaliana*. *Genes Dev*, **20**(24), 3407–3425.

Rodriguez-Medina, C., Atkins, C. A., Mann, A. J., Jordan, M. E., & Smith, P. M. (2011). Macromolecular composition of phloem exudate from white lupin (*Lupinus albusL.*). *BMC Plant Biol*, **11**(1), 36.

Rojas, A. M. L., Drusin, S. I., Chorostecki, U., Mateos, J. L., Moro, B., Bologna, N. G., Bresso, E. G., Schapire, A., Rasia, R. M., Moreno, D. M., & Palatnik, J. F. (2020). Identification of key sequence features required for microRNA biogenesis in plants. *Nat Commun*, **11**(5320).

Rössner, C., Lotz, D., & Becker, A. (2022). VIGS Goes Viral: How VIGS Transforms Our Understanding of Plant Science. *Annu Rev Plant Biol*, **20**(73), 703–728.

Ryabov, E. V., van Wezel, R., Walsh, J., & Hong, Y. (2004). Cell-to-Cell, but Not Long-Distance, Spread of RNA Silencing That Is Induced in Individual Epidermal Cells. *J Virol*, **78**(6), 3149–3154.

Sasaki, T., Chino, M., Hayashi, H., & Fujiwara, T. (1998). Detection of Several mRNA Species in Rice Phloem Sap. *Plant Cell Physiol*, **39**(8), 895–897.

Schwab, R., Ossowski, S., Riester, M., Warthmann, N., & Weigel, D. (2006). Highly Specific Gene Silencing by Artificial MicroRNAs in Arabidopsis. *Plant Cell*, **18**(5), 1121–1133.

Schwartz, S. H., Hendrix, B., Hoffer, P., Sanders, R. A., & Zheng, W. (2020). Carbon dots for efficient small interfering RNA delivery and gene silencing in plants. *Plant Physiol*, **184**(2), 647–657.

Senthil-Kumar, M., & Mysore, K. S. (2011). *Caveat of RNAi in Plants: The Off-Target Effect*. 13–25.

Shi, G., Hao, M., Tian, B., Cao, G., Wei, F., & Xie, Z. (2021). A Methodological Advance of Tobacco Rattle Virus-Induced Gene Silencing for Functional Genomics in Plants. *Front Plant Sci*, **12**.

Shine, M. B., Zhang, K., Liu, H., Lim, G., Xia, F., Yu, K., Hunt, A. G., Kachroo, A., & Kachroo, P. (2022). Phased small RNA-mediated systemic signaling in plants. In *Sci. Adv* (Vol. 8).

Singh, S., Chaudhary, R., Deshmukh, R., & Tiwari, S. (2023). Opportunities and challenges with CRISPR-Cas mediated homologous recombination based precise editing in plants and animals. *Plant Mol Biol*, **111**(1–2), 1–20.

Skopelitis, D. S., Hill, K., Klesen, S., Marco, C. F., von Born, P., Chitwood, D. H., &

Timmermans, M. C. P. (2018). Gating of miRNA movement at defined cell-cell interfaces governs their impact as positional signals. *Nat Commun*, **9**(1).

Slotkin, R. K., Vaughn, M., Borges, F., Tanurdžić, M., Becker, J. D., Feijó, J. A., & Martienssen, R. A. (2009). Epigenetic Reprogramming and Small RNA Silencing of Transposable Elements in Pollen. *Cell*, **136**(3), 461–472.

Smith, D., Barkman, T. J., & dePamphilis, C. W. (2001). Hemiparasitism. In *Encyclopedia of Biodiversity* (pp. 70–78). Elsevier.

Smith, L. M., Pontes, O., Searle, I., Yelina, N., Yousafzai, F. K., Herr, A. J., Pikaard, C. S., & Baulcombe, D. C. (2007). An SNF2 protein associated with nuclear RNA silencing and the spread of a silencing signal between cells in Arabidopsis. *Plant Cell*, **19**(5), 1507–1521.

Song, L., Axtell, M. J., & Fedoroff, N. V. (2010). RNA Secondary Structural Determinants of miRNA Precursor Processing in Arabidopsis. *Current Biology*, **20**(1), 37–41.

Song, X., Li, Y., Cao, X., & Qi, Y. (2019). *MicroRNAs and Their Regulatory Roles in Plant-Environment Interactions*.

Tan, H., Luo, W., Yan, W., Liu, J., Aizezi, Y., Cui, R., Tian, R., Ma, J., & Guo, H. (2023). Phase separation of SGS3 drives siRNA body formation and promotes endogenous gene silencing. *Cell Rep*, **42**(1).

Tang, Y., Wang, F., Zhao, J., Xie, K., Hong, Y., & Liu, Y. (2010). Virus-based microRNA expression for gene functional analysis in plants. *Plant Physiol*, **153**(2), 632–641.

Tiwari, M., Sharma, D., & Trivedi, P. K. (2014). Artificial microRNA mediated gene silencing in plants: Progress and perspectives. *Plant Mol Biol*, **86**, 1–18.

Tsikou, D., Yan, Z., Holt, D. B., Abel, N. B., Reid, D. E., Madsen, L. H., Bhasin, H., Sexauer, M., Stougaard, J., & Markmann, K. (2018). Systemic control of legume susceptibility to rhizobial infection by a mobile microRNA. *Science (1979)*, **362**(6411), 233–236.

Varkonyi-Gasic, E., Gould, N., Sandanayaka, M., Sutherland, P., & MacDiarmid, R. M. (2010). Characterisation of microRNAs from apple (*Malus domestica* 'Royal Gala') vascular tissue and phloem sap. *BMC Plant Biol*, **10**(1), 159.

Vasav, A. P., Meshram, B. G., Pable, A. A., & Barvkar, V. T. (2023). Artificial microRNA mediated silencing of cyclase and aldo–keto reductase genes reveal their involvement in the plumbagin biosynthetic pathway. *J Plant Res*, **136**(1), 47–62.

Vatanparast, M., Merkel, L., & Amari, K. (2024). Exogenous Application of dsRNA in Plant Protection: Efficiency, Safety Concerns and Risk Assessment. *Int J Mol Sci*, **25**(12), 6530.

Vaucheret, H., Béclin, C., & Fagard, M. (2001). Post-transcriptional gene silencing in plants. *J Cell Sci*, **114**(17), 3083–3091.

Vaucheret, H., & Fagard, M. (2001). Transcriptional gene silencing in plants: targets, inducers and regulators. *Trends in Genetics*, **17**(1), 29–35.

Verchot, J. (2022). Potato virus X: A global potato-infecting virus and type member of the Potexvirus genus. *Mol Plant Pathol*, **23**(3), 315–320.

Voinnet, O., & Baulcombe, D. C. (1997). Systemic signalling in gene silencing. *Nature*, **389**(6651), 553–553.

Voloudakis, A. E., Holeva, M. C., Sarin, L. P., Bamford, D. H., Vargas, M., Poranen, M. M., & Tenllado, F. (2015). Efficient Double-Stranded RNA Production Methods for Utilization in Plant Virus Control. In *Methods in Molecular Biology* (Vol. 1236, pp. 255–274).

Wang, T., Li, X., Zhang, X., Wang, Q., Liu, W., Lu, X., Gao, S., Liu, Z., Liu, M., Gao, L., & Zhang, W. (2021). RNA Motifs and Modification Involve in RNA Long-Distance Transport in Plants. *Front Cell Dev Biol*, **9**.

Watson, J. M., Fusaro, A. F., Wang, M. B., & Waterhouse, P. M. (2005). RNA silencing

platforms in plants. In *FEBS Letters* (Vol. 579, Issue 26, pp. 5982–5987).

Wei, X., Ke, H., Wen, A., Gao, B., Shi, J., & Feng, Y. (2021). Structural basis of microRNA processing by Dicer-like 1. *Nat Plants*, **7**(10), 1389–1396.

Werner, S., Wollmann, H., Schneeberger, K., & Weigel, D. (2010). Structure Determinants for Accurate Processing of miR172a in *Arabidopsis thaliana*. *Current Biology*, **20**(1), 42–48.

Wu, H. Y. L., Ai, Q., Teixeira, R. T., Nguyen, P. H. T., Song, G., Montes, C., Elmore, J. M., Walley, J. W., & Hsu, P. Y. (2024). Improved super-resolution ribosome profiling reveals prevalent translation of upstream ORFs and small ORFs in Arabidopsis. *Plant Cell*, **36**(3), 510–539.

www.smallrna.mtu.edu/Tang_Website/submit.htm. (2016). *microRNA Designer*.

Xia, R., Xu, J., & Meyers, B. C. (2017). The Emergence, Evolution, and Diversification of the miR390- *TAS3* - *ARF* Pathway in Land Plants. *Plant Cell*, **29**(6), 1232–1247.

Xie, D., Chen, M., Niu, J., Wang, L., Li, Y., Fang, X., Li, P., & Qi, Y. (2021). Phase separation of SERRATE drives dicing body assembly and promotes miRNA processing in Arabidopsis. *Nat Cell Biol*, **23**(1), 32–39.

Xie, Z., Allen, E., Fahlgren, N., Calamar, A., Givan, S. A., & Carrington, J. C. (2005). Expression of Arabidopsis *MIRNA* Genes. *Plant Physiol*, **138**(4), 2145–2154.

Xie, Z., Allen, E., Wilken, A., & Carrington, J. C. (2005). DICER-LIKE 4 functions in trans-acting small interfering RNA biogenesis and vegetative phase change in *Arabidopsis thaliana*. *Proceedings of the National Academy of Sciences*, **102**(36), 12984–12989.

Xie, Z., Johansen, L. K., Gustafson, A. M., Kasschau, K. D., Lellis, A. D., Zilberman, D., Jacobsen, S. E., & Carrington, J. C. (2004). Genetic and Functional Diversification of Small RNA Pathways in Plants. *PLoS Biol*, **2**(5), 0642–0652.

Yan, H., Shi, S., Ma, N., Cao, X., Zhang, H., Qiu, X., Wang, Q., Jian, H., Zhou, N., Zhang, Z., & Tang, K. (2018). Graft-accelerated virus-induced gene silencing facilitates functional genomics in rose flowers. *J Integr Plant Biol*, **60**(1), 34–44.

Yan, X., Li, C., Liu, K., Zhang, T., Xu, Q., Li, X., Zhu, J., Wang, Z., Yusuf, A., Cao, S., Peng, X., Cai, J. J., & Zhang, X. (2024). Parallel degradome-seq and DMS-MaPseq substantially revise the miRNA biogenesis atlas in Arabidopsis. *Nat Plants*, **10**(7), 1126–1143.

Yan, Y. (2022). Insights into Mobile Small-RNAs Mediated Signaling in Plants. *Plants*, **11**(22).

Yan, Y., & Ham, B. K. (2022). The Mobile Small RNAs: Important Messengers for Long-Distance Communication in Plants. *Front Plant Sci*, **13**.

Yan, Y., Ham, B. K., Chong, Y. H., Yeh, S. D., & Lucas, W. J. (2020). A Plant SMALL RNA-BINDING PROTEIN 1 Family Mediates Cell-to-Cell Trafficking of RNAi Signals. *Mol Plant*, **13**(2), 321–335.

Yong, J., Wu, M., Carroll, B. J., Xu, Z. P., & Zhang, R. (2024). Enhancing plant biotechnology by nanoparticle delivery of nucleic acids. *Trends in Genetics*, **40**(4), 352–363.

Yoo, B. C., Kragler, F., Varkonyi-Gasic, E., Haywood, V., Archer-Evans, S., Lee, Y. M., Lough, T. J., & Lucas, W. J. (2004). A systematic small RNA signaling system in plants. *Plant Cell*, **16**(8), 1979–2000.

Yoshikawa, M., Han, Y.-W., Fujii, H., Aizawa, S., Nishino, T., & Ishikawa, M. (2021). Cooperative recruitment of RDR6 by SGS3 and SDE5 during small interfering RNA amplification in Arabidopsis. *PNAS*, **118**(34).

Yoshikawa, M., Iki, T., Numa, H., Miyashita, K., Meshi, T., & Ishikawa, M. (2016). A short open reading frame encompassing the microRNA173 target site plays a role in trans-acting small interfering RNA biogenesis. *Plant Physiol*, **171**(1), 359–368.

Yoshikawa, M., Iki, T., Tsutsui, Y., Miyashita, K., Scott Poethig, R., Habu, Y., & Ishikawa, M. (2013). 3′ fragment of miR173-

programmed RISC-cleaved RNA is protected from degradation in a complex with RISC and SGS3. *Proc Natl Acad Sci U S A*, **110**(10), 4117–4122.

Yu, A.-M., Batra, N., Tu, M.-J., & Sweeney, C. (2020). Novel approaches for efficient *in vivo* fermentation production of noncoding RNAs. *Appl Microbiol Biotechnol*, **104**(5), 1927–1937.

Yu, B., Yang, Z., Li, J., Minakhina, S., Yang, M., Padgett, R. W., Steward, R., & Chen, X. (2005). Methylation as a Crucial Step in Plant microRNA Biogenesis. *Science (1979)*, **307**(5711), 932–935.

Yu, Y., Zhang, Y., Chen, X., & Chen, Y. (2019). Plant noncoding RNAs: Hidden players in development and stress responses. In *Annual Review of Cell and Developmental Biology* (Vol. 35, pp. 407–431). Annual Reviews Inc.

Zhan, J., & Meyers, B. C. (2023). Plant Small RNAs: Their Biogenesis, Regulatory Roles, and Functions. *Annu Rev Plant Biol*, **74**, 21–51.

Zhang, C., Ng, D. W. K., Lu, J., & Chen, Z. J. (2012). Roles of target site location and sequence complementarity in trans-acting siRNA formation in Arabidopsis. *Plant Journal*, **69**(2), 217–226.

Zhang, N., Zhang, D., Chen, S. L., Gong, B., Guo, Y., & Xu, L. (2019). Engineering Artificial MicroRNAs for Multiplex Gene Silencing and Simplified Transgenic Screen 1. *Int J Mol Sci*, **20**(22), 989–1001.

Zhang, S., Liu, Y., & Yu, B. (2015). New insights into pri-miRNA processing and accumulation in plants. *Wiley Interdiscip Rev RNA*, **6**(5), 533–545.

Zhang, S., Sun, L., & Kragler, F. (2009). The Phloem-Delivered RNA Pool Contains Small Noncoding RNAs and Interferes with Translation. *Plant Physiol*, **150**(1), 378–387.

Zhu, H., Zhou, Y., Castillo-González, C., Lu, A., Ge, C., Zhao, Y. T., Duan, L., Li, Z., Axtell, M. J., Wang, X. J., & Zhang, X. (2013). Bidirectional processing of pri-miRNAs with branched terminal loops by Arabidopsis Dicer-like1. *Nat Struct Mol Biol*, **20**(9), 1106–1115.

Zulfiqar, S., Farooq, M. A., Zhao, T., Wang, P. P., Tabusam, J., Wang, Y., Xuan, S., Zhao, J., Chen, X., Shen, S., & Gu, A. (2023). Virus-Induced Gene Silencing (VIGS): A Powerful Tool for Crop Improvement and Its Advancement towards Epigenetics. *Int J Mol Sci*, **24**(6).

ibmcp

UNIVERSITAT POLITÈCNICA DE VALÈNCIA

CSIC
Consejo Superior de Investigaciones Científicas